UNIVERSITÀ DEGLI STUDI DI PADOVA

Sede Amministrativa: Università degli Studi di Padova

Dipartimento di Geoscienze
Via G. Gradenigo n.6 - 35131- Padova

CORSO DI DOTTORATO DI RICERCA IN SCIENZE DELLA TERRA
CICLO XXIX

LATE NORIAN-RHAETIAN CARBON CYCLE PERTURBATIONS: FROM A TETHYAN TO A GLOBAL PERSPECTIVE

Tesi redatta con il contributo finanziario dell'Università degli Studi di Padova

Coordinatore: Ch.mo Prof. Fabrizio Nestola
Supervisore: Ch.mo Dott. Manuel Rigo
Co-Supervisore: Ch.mo Prof. Claudia Agnini

Dottorando: Mariachiara Zaffani

Ai miei Grandi Giganti Gentili:
Giulio, Giordano e Giancarlo,
modelli ed esempi di professionalità ed umanità, sempre.

CONTENTS

GENERAL INTRODUCTION

We are facing global climate changes driven by increasing concentrations of greenhouse gases in the atmosphere, which are responsible for global warming and possibly detrimental for the biosphere. Earth's climate has significantly and repeatedly changed throughout the geological past, but the recent rate of global warming appears to far exceed any previous episode of extreme climate occurred since now. The Intergovernmental Panel on Climate Change (IPCC) estimates that the present atmospheric concentrations of greenhouse gases, related to human activities, are at unprecedented levels since at least 800,000 years (IPCC, 2014). In particular, carbon dioxide has been increased at the fastest observed rate of change in the last two decades (2.0±0.1 ppm/yr for the 2002–2011 decade; IPCC, 2014), trigging a detectable lowering of the pH values of the ocean surface waters (ocean acidification) and, consequently, a reduction of the $CaCO_3$ saturation state and the shoaling of the CCD. These changes will lead to unpredictable impacts on calcifying organisms, such the aragonitic corals and the calcareous microplankton (e.g., Caldeira and Wickett, 2003; Kleypas et al., 2006; Allen et al., 2009; IPCC, 2014). Observational data on current climate change and models predicting the future evolution of Earth's climate should be integrated with geologic data, which could serve to unveil analogous patterns providing clues onto the future scenarios (Raven et al., 2005; Ruhl; 2009; Hönisch et al., 2012).The study of geological time intervals characterized by carbon emissions comparable to the present-day conditions is crucial for describing their effects on the past carbon cycle and consequently on the ocean geochemistry and marine ecosystem(e.g., Sala et al., 2000).

During the Mesozoic (ca. 252 Ma – 66 Ma), our planet was affected by recurrent carbon cycle perturbations, marked by episodes of climate change and biodiversity loss (e.g., Rampino & Stothers, 1988; Wignall, 2001, Jones and Jenkyns, 2001; Ward et al., 2004; Richoz et al., 2007; Van de Schootbrugge et al., 2008; Jenkyns, 2010; Tanner, 2010; Palfy et al., 2014, Trotter et al., 2015). On this perspective, the Triassic is paradigmatic and it is the System bounded by 2 mass extinctions.

The Triassic (ca. 252-201 Ma) is in fact a key period of the Earth's history, characterized by a supercontinent in which all the land were merged together named Pangaea and later by its the break-up, a variable climate regime (e.g., Preto et al., 2010; Rigo et al., 2012a; Trotter et al., 2015) interrupted by several global geological events, such as humid (e.g., Carnian Pluvial Event-CPE, Late Triassic, Simms and Ruffell, 1989, 1990; Simms et al., 1995) and warm episodes (W1, W2, W3 by Trotter et al., 2015) deeply affecting the Earth biota or extreme volcanic activity likely triggering profound biotic crises (e.g., Raup & Sepkoski, 1982; McElwain et al., 1999; Hallam, 2002; Marzoli et al., 2004; McRoberts et al., 2008; Lucas, 2010; Ogg et al., 2012; Dal Corso et al., 2013, 2014; Trotter et al., 2015). This System is constrained by two of the biggest mass extinctions of the Phanerozoic, the end-Permian mass extinction - the most extensive biotic decimation of the Phanerozoic (e.g., Lucas, 1999; Benton & Twitchett, 2003; Lucas & Orchard, 2004; Erwin, 2006) and the end-Triassic mass extinction, culminating at the Triassic/Jurassic boundary (e.g., Hallam, 2002; Tanner et al., 2004; Richoz et al., 2007).

An important proxy to give essential clues on the evolution of ocean water chemistry, oxygenation, and productivity of past marine environments are represented by the changes in the isotopic composition documented in the sediments. In particular, perturbations observed in $\delta^{13}C$ values are widely applied and interpreted in terms of palaeoclimate and palaeoenvironmental changes (e.g., Hayes et al., 1999; Veizer et al., 1999; Payne et al., 2004; Korte et al., 2005; Lucas, 2010; Muttoni et al., 2004, 2014; Galli et al., 2005, 2007; Mazza et al., 2010; Preto et al., 2012). Indeed, the stable carbon isotope record available for the Triassic gives a general overview of the $\delta^{13}C$ evolution, but its paleoclimatic/paleoocenographic interpretation is somewhat uncertain due to the multiple ecological and geochemical controls driving changes on the carbon isotope system. In a long-term perspective the Triassic $\delta^{13}C$ profile starts with a, pronounced negative excursion coinciding with the Permian-Triassic boundary, this deep perturbation of the global carbon cycle is followed by a strong isotopic instability during the earliest Triassic (e.g., Payne et al., 2004; Lucas, 2010) that eventually lead to a more stable period spanning the Middle-Late Triassic (Julian, early Carnian) (Payne et al., 2004; Tanner, 2010) . This interval is characterized by steadily rising values in $\delta^{13}C$, which is likely related to biotic reassessment in the aftermath of the end-Permian mass extinction and the consequentially enhanced storage of organic carbon in terrestrial environments (e.g., Lucas, 2010). The Late Triassic (ca. 237 Ma - 201.3 Ma) is bracketed by two significant negative carbon isotope shifts, both linked to the emplacement of Large Igneous Provinces (LIPs). The first $\delta^{13}C$ excursion occurred in the middle Carnian is referred to as the Carnian Pluvial Event and it is associated to the emplacement of the Wrangellia igneous province (e.g., Furin et al., 2006; Dal Corso et al., 2014, 2015). The second $\delta^{13}C$ perturbation, recorded at the Triassic-Jurassic transition, is associated with the end-Triassic mass extinction and the emplacement of the Central Atlantic Magmatic Province (CAMP; e.g., Marzoli et al., 2004; Whiteside et al., 2010; Schaller et al., 2012; Dal Corso et al., 2013). The causes of the Triassic carbon isotope excursions remain a topic of much debate, with the most likely trigger mechanisms being related to the greenhouse gases emissions produced by the volcanic activity, with a total estimated amount of CO_2 input in the atmosphere comparable to nowadays anthropogenic carbon dioxide feed in. Alternatively, other processes that can explain the occurrence and magnitude of observed carbon cycle perturbation would be changes in biotic productivity, global ocean anoxia or seafloor methane release (e.g., Richoz et al., 2007; Lucas, 2010). In principle, all these processes are able to perturb the global carbon cycle and cause episodes of biotic crises (e.g., Rampino & Stothers, 1988; Wignall, 2001; Jones and Jenkyns, 2001; Ward et al., 2004; Richoz et al., 2007; van de Schootbrugge et al., 2008; Jenkyns, 2010; Tanner, 2010; Palfy et al., 2014, Trotter et al., 2015). Therefore, a global composite carbon isotope curve for the Triassic would have the potential for global correlations and would provide new insights on how the Earth's dynamics respond to carbon dioxide emissions similar to the ongoing anthropogenic input, hopefully providing useful insight for climate modeling. Muttoni et al. (2014) provide a new almost continuous million-year scale composite $\delta^{13}C_{carb}$ record from the Ladinian (ca. 242 Ma) to Rhaetian (ca. 205.7 Ma), but the construction of an analogous Triassic organic carbon isotope record is not available to date. The published $\delta^{13}C_{org}$ data are especially concentrated on the mass extinction events (i.e., Permian/Triassic boundary, Triassic/Jurassic boundary) and the long-term background conditions are instead little known.

Moreover, data from the Norian (ca. 227.0-205.7 Ma; Diakow et al., 2011, 2012; Maron et al., 2015) of North America seems to indicate rapid oscillations of the $\delta^{13}C_{org}$ that culminate in a positive $\delta^{13}C_{org}$ peak in correspondence to the extinction of the bivalve *Monotis*, around the Norian/Rhaetian boundary (Ward et al., 2004; Wignall et al., 2007; Whiteside & Ward, 2011; Rigo et al., 2015; Bertinelli et al., 2016). This positive excursion has been possibly interpreted as the result of an increased stagnation in ocean circulation (Sephton et al., 2002; Ward et al., 2004). Multiple sections supporting the occurrence of a global carbon isotope perturbation at the Norian/Rhaetian boundary have been investigated for $\delta^{13}C_{carb}$ in the Tethyan area (e.g., Atudorei, 1999; Gawlick et al., 2000; Hauser et al., 2001; Muttoni et al., 2004; Hornung and Brandner, 2005; Korte et al., 2005; Preto et al., 2013), but a complete Norian carbon organic carbon isotope profile is not available yet.

Notably, poor information on $\delta^{13}C_{org}$ are available for the Rhaetian (ca. 205.7-201.3±0.2 Ma; Maron et al., 2015; Schoene et al., 2010; Rigo et al., 2015), a stage marked by significant faunal turnovers both in the marine and continental realms (e.g., ammonites, Guex et al., 2004, Whiteside & Ward, 2011; bivalves, McRoberts and Newton, 1995; radiolarian, Ward et al., 2001; dinoflagellates and foraminifera, Hesselbo et al., 2002; calcareous nannofossil, van de Schootbrugge et al., 2007; Theropod dinosaurs; Olsen et al., 2002; terrestrial plants; McElwain et al., 1999, 2009; Kuerschner et al., 2007; Bonis et al., 2009). Besides the paroxysmal crisis referred to as the end-Triassic mass extinction occurred at the Triassic/Jurassic boundary (TJB), the Rhaetian appears to document a series of biotic crises and turnovers that gradually culminated at the TJB, supporting the hypothesis of a step-like extinction pattern for the end-Triassic mass extinction (e.g., Hallam et al., 2002; Whiteside

& Ward, 2011). Moreover, the latemost Rhaetian appears to be affected by the huge volcanic activity related to the CAMP, which is supposed to be the trigger of three major negative carbon isotope excursions (CIEs): the “main” CIE at the Triassic/Jurassic boundary, preceded by the late Rhaetian “initial” and “precursor” CIEs, commonly associated to two different eruptive phases of the Moroccan CAMP (Marzoli et al., 2004; Hesselbo, et al., 2002; McRoberts & Pálfy, 2007; Deenen et al., 2010; Dal Corso et al., 2014). Many publications focused their attention on $\delta^{13}C$ evolution across the TJB, but little is known about the background carbon isotope conditions during the early-middle Rhaetian and their possible links to the faunal extinction patterns and/or climate events documented at this time. Noteworthy, organic carbon isotopic data from North America display the presence of repeated, apparently chaotic, $\delta^{13}C_{org}$ oscillations associated with low faunal diversity (Whiteside & Ward, 2011), but no data are available for the Tethyan realm to support a global significance of these trends. Thus, at present, we do need further data from different areas to confirm that $\delta^{13}C_{org}$ oscillations have a widespread occurrence of and do not simply reflect a North America local paleoenviromental conditions.

SYNOPSIS

The final aim of this PhD thesis is to produce a Norian/Rhaetian organic carbon isotopes profile from multiple successions and interpret the causes of $\delta^{13}C_{org}$ perturbations, comparing their occurrence at different locations and geological settings trying to verify if a causal link between $\delta^{13}C_{org}$ perturbation and episodes of biotic crises exists. To achieve this goal, the following three areas have been investigated and/or taken into consideration in this project (Fig. 1):

1. The Tethyan realm:

    1.1 the Lagonegro Basin (Apennines, southern Italy), investigated at four localities: Pignola-Abriola, Mt Volturino, Madonna del Sirino, Mt St. Enoc;

    1.2 the Lombardian Basin (southern Alps, northern Italy), investigated at three localities: Mt Albenza, Brumano (Italcementi active quarry) and Malanotte;

    1.3 St Audrie's Bay (UK) (data from Hesselbo et al., 2002; Guex et al., 2004; van de Schootbrugge et al., 2007);

    1.4 the Eiberg Basin (Northern Calcareous Alps, Austria) (data from Kuerschner et al., 2007; Hillebrandt et al., 2007; Ruhl et al., 2009);

    1.5 the Pindos Zone (Peloponnese, Greece), investigated at the Kastelli section.

2. The North American realm:

    2.1 British Columbia Islands (Canada) (data from Ward et al., 2001, 2004, 2007; Sephton et al., 2002; Whiteside & Ward, 2011);

    2.2 Williston Lake (Canada) (data from Wignall et al., 2007).

3. The Southern hemisphere:

    3.1 the Wombat Basin (northwestern Australia), investigated at ODP Site 761.

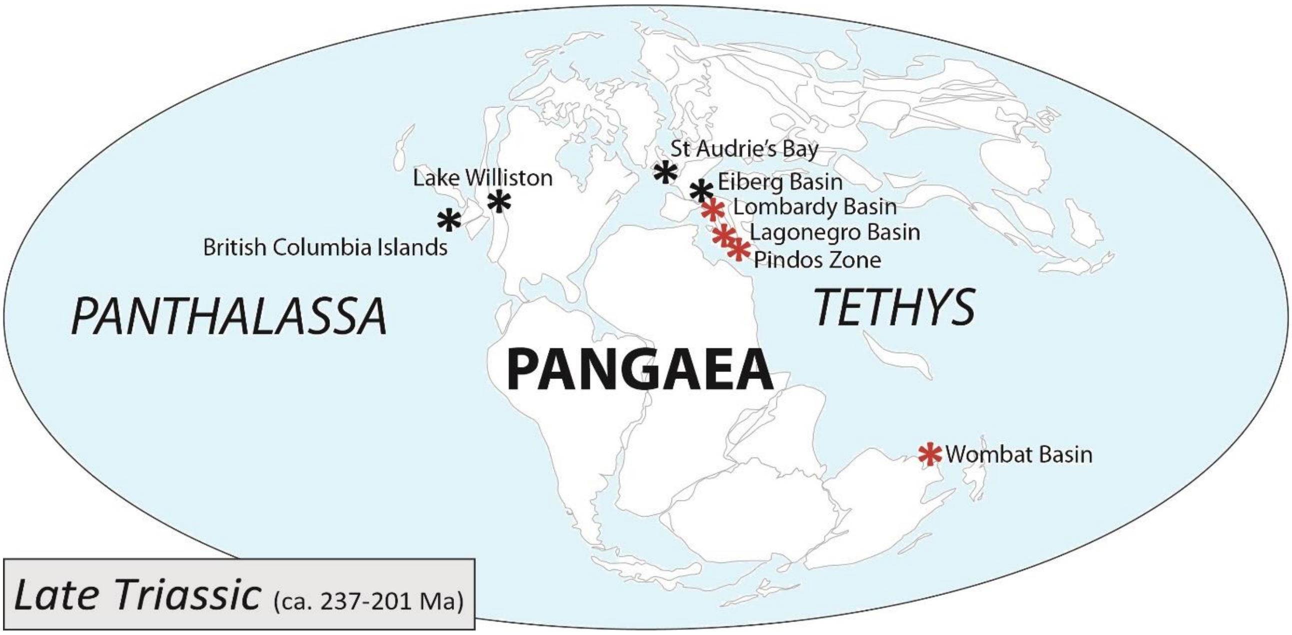

Fig. 1 Continent and ocean distribution during the Late Triassic. Red bold stars = analyzed areas; black bold stars = data from literature (Hesselbo et al., 2002; Wignall et al., 2007; Ruhl et al., 2009; Whiteside and Ward, 2011).

This study presents the chemostratigraphic profiles ($\delta^{13}C_{org}$, $\delta^{13}C_{carb}$, TOC, integrated with $\delta^{15}N$, $^{87}Sr/^{86}Sr$, $\delta^{88/86}Sr$) of several sections located at different locations and in different depositional setting in order to highlight the occurrence of carbon cycle perturbations. The stratigraphic correlations among the geochemical profiles of the different successions are supported by integrated biostratigraphic framework based on conodonts, radiolarian, bivalves and, when possible, ammonoids. As long as the documented interval spans from ca. 220 Ma to 200 Ma, the investigate successions are used to examine the relative timing between the bio-, chemical- and physical- events preceding the end-Triassic biotic turnover and the palaeoenvironmental changes, thus evidencing the high potential of carbon isotopes as high-resolution stratigraphic correlation tool.

This thesis is organized as a collection of published or submitted articles, rearranged respect to the original journal format in order to be suitable for this publication.

The **Methods** chapter describes the sample preparation and the analysis methodologies applied in this work. The choice of using the so-called "rinse" sample-preparation method over other validated techniques (i.e., in situ acidification and fumigation methods) deserves a special attention and has been thus treated in detail within this introductory chapter.

Chapter 1 illustrates the late Norian-early Rhaetian $\delta^{13}C_{org}$ and TOC profiles obtained for three localities (Pignola-Abriola, Mt Volturino and Madonna del Sirino) from the Lagonegro Basin (southern Apennines, Italy). The studied sections show similar trends, depicting a noticeable $\delta^{13}C_{org}$ decrease at the Norian/Rhaetian boundary preceded by other two negative shifts. Intra-basinal $\delta^{13}C_{org}$ correlations rely essentially on an integrated approach in which chemostratigraphy and biostratigraphy (conodonts and radiolarians) are combined together in order to obtain time-constrained successions to be compared. As a result, we suggest the $\delta^{13}C_{org}$ decreases observed across the Norian-Rhaetian transition are a common feature of the Lagonegro Basin during the late Norian. Moreover, the $\delta^{13}C_{org}$ negative trend documented at the Norian/Rhaetian boundary (NRB) at these three localities are correlative with those identified also in the Lombardy Basin (Muttoni et al., 2014) and in the composite record of Korte et al. (2005). Most interestingly, the NRB $\delta^{13}C_{org}$ decrease observed in the Lagonegro Basins sections has been correlated with the NRB $\delta^{13}C_{org}$ decrease recorded in North America successions (Wignall et al., 2007; Whiteside & Ward, 2011), suggesting the likely global extension of this carbon cycle perturbation. Multiple lines of evidence such the duration of the carbon isotope excursion, the oxygen and strontium isotope data, the CO_2 estimations, the Late Triassic climate models, the extinction patterns and the scars on fossil wood have been taken into accont to discuss and possibly explain the trigger mechanism for the NRB CIE, which in fact involves the role played by the emplacement of the Angayucham large igneous province (Alaska) in enhancing the amount of volcanogenic CO_2 in the atmosphere during the late Norian.

For its suitable features, the Pignola-Abriola section has been proposed as the Global Stratigraphic Section and Point (GSSP) of the Rhaetian stage. I curated the Geochemistry section of the GSSP proposal, which has been attached in **Appendix A.**

Chapter 2 describes the $\delta^{13}C_{org}$ record obtained from the Lombardy Basin (southern Alps, northern Italy). This record covers, for the first time, the entire Rhaetian. This profile is perturbed by a series of $\delta^{13}C_{org}$ decreases that might be identified as the “main”, “initial” and “precursor” negative CIEs on the basis of the available stratigraphic constraints. The comparison of our data with the $\delta^{13}C_{org}$ profiles from the St Audrie’s Bay (Hesselbo et al., 2002) and the Eiberg Basin (e.g., Ruhl et al., 2009) permits to better constrain and identify these negative CIEs likely related to the CAMP activity. Using bio-, chemo- and lithostratigraphic correlations, we propose two possible interpretations of the Lombardy Basin $\delta^{13}C_{org}$ CIEs. The first possible interpretation is based on the chemo- and lithostratigraphic correlation with the Eiberg Basin (Austria) and it is in agreement with the previous interpretation of the Mt. Albenza TJB $\delta^{13}C_{org}$ record, which correlates the major $\delta^{13}C_{org}$ decrease at the transition from the Calcari di Zu to the Malanotte Fm. with the "initial" CIE. The second possible interpretation relies on the chemo- and biostratigraphic correlation with the St. Audrie's Bay section (UK), where the "main" and "initial" CIEs were originally defined. On the base of this correlation, the "initial" CIE in the Lombardy Basin seems to occur within the Zu3b submember, and the onset of the "main" CIE at the top of the Zu3b submember. This new interpretation is possible in the light of the complete Rhaetian $\delta^{13}C_{org}$ profile produced for the Lombardy Basin. More pieces of evidence are required in order to trust one interpretation over the other.

Chapter 3 is a summary of unpublished and/or minor works of my PhD project. It contains the low-resolution $\delta^{13}C_{org}$ profiles of Mt St. Enoc section (Lagonegro Basin, southern Apennines, southern Italy) and Kastelli section (Pindos Zone, Peloponnese, Greece). The low resolution of these Tethyan successions is related to the reduced number of samples suitable for $\delta^{13}C_{org}$ analyses, such as dark marls and limestones. In fact, these successions are composed mainly by red radiolarites, which are characterized by an extremely low carbon content. Part of this chapter is dedicated to the $\delta^{15}N$ of the Pignola-Abriola section. A special paragraph is dedicated to the late Norian-early Rhaetian $\delta^{13}C_{org}$ profile obtained from ODP Site 761 from the Wombat Basin (northwestern Australia), the first $\delta^{13}C_{org}$ record covering this time interval in the Southern hemisphere.

Stable carbon isotopes are extremely useful tools for paleoclimate and paleoenvironmental interpretation, as well as for stratigraphic correlations, but more realistic reconstructions can be obtained using and comparing all the available datasets, such as other isotope systems, biostratigraphies, magnetostratigraphy. On this perspective, part of this PhD project has been dedicated to the study and developing of the strontium isotope system. The $^{87}Sr/^{86}Sr$ ratio has been widely applied to different kinds of material, providing information on the contribution of continental weathering and volcanic activity on the global seawater composition (e.g., Palmer and Elderfield, 1985; Faure, 1986; Raymo et al., 1988; Hodell et al., 1989; Palmer and Edmond, 1989; Berner and Rye, 1992; Veizer et al., 1997; Taylor and Lasaga, 1999; Korte et al., 2003). Instead, methodology to measure $\delta^{88/86}Sr$ has been developed in the last decade thanks to the improvement of new spectrometric techniques, such as the double spike method (Krabbenhoft et al., 2009). $\delta^{88/86}Sr$ values are thought to be interpreted in terms of carbonate burial rates, carbonate shelf recrystallization/weathering, carbonate dissolution and ocean anoxia. As part of this PhD project, the double spike method has been applied for the first time to Triassic conodont samples for $\delta^{88/86}Sr$ analyses. **Chapter 4** illustrates the sample preparation methodologies and the data treatment, as well as preliminary results and considerations.

Concluding remarks. The late Norian-early Hettangian time interval appears to be marked by a series of $\delta^{13}C_{org}$ oscillations that provide new clues on the relationship among carbon cycle perturbations, the LIP volcanism and the end-Triassic mass extinction The late Norian $\delta^{13}C_{org}$ record from the Lagonegro Basin (western Tethys) and the chemo- and biostratigraphic correlation with the North America successions allows to interpreted the recurrent $\delta^{13}C_{org}$ decreases to a single global mechanism, the emplacement of the Angayucham large igneous magmatic province, widespread complex ocean plateau originally located on the western margin of North America and today outcropping in Alaska. In addition, the Rhaetian appears to be marked by a series of $\delta^{13}C_{org}$ decreases. In particular, the almost complete $\delta^{13}C_{org}$ record of the Lombardy Basin permits to attribute these $\delta^{13}C_{org}$ disruptions to the late Rhaetian CAMP activity.

The late Norian-early Hettangian $\delta^{13}C_{org}$ profile presented in this PhD thesis improves the Late Triassic organic carbon isotope record and evidenced for the occurrence of a series of decreases/oscillations driven by the emplacement of different LIPs: the late Ladinian - early Norian Wrangellia, the late Norian Angayucham and the late Rhaetian-early Hettangian CAMP. The emplacement of LIPs may have had extreme environmental consequences, potentially associated with changes in primary productivity and/or warming, which could have induced humid conditions and episodes of seawater oxygen depletion, biotic crises and extinctions, writing the complex history of this particular period of time.

References

Allen, M.R., Frame, D.J., Huntingford, C., Jones, C.D., Lowe, J.A., Meinshausen, M., Meinshausen, N., 2009. Warming caused by cumulative carbon emissions towards the trillionth tonne. Nature, 458, 1163-1166.

Atudorei, N.V., 1999, Constraints on the Upper Permian to Upper Triassic marine carbon isotope curve. Case studies from the Tethys. PhD Thesis: Lausanne University, p. 155.

Benton, M. J. and Twitchett, R. J., 2003, How to kill (almost) all life: the end-Permian extinction event: Trends in Ecology and Evolution, v. 18, p. 358–365.

Berner, R.A., and Rye, D.M., 1992, Calculation of the Phanerozoic strontium isortope record of the oceans from a carbon cycle model: American Journal of Science, v. 292, p. 136–148.

Bonis, N.R., Kürschner, W.M. and Krystyn, L., 2009. A detailed palynological study of the Triassic-Jurassic transition in key sections of the Eiberg Basin (Northern Calcareous Alps, Austria). Review of Palaeobotany and Palynology, 156(3-4): 376-400.

Caldeira, K. and Wickett, M.E., 2003. Anthropogenic carbon and ocean pH. Nature, 425,365.

Dal Corso, J., Marzoli, A., Tateo, F., Jenkyns, H.C., Bertrand, H., Youbi, N., Mahmoudi, A., Font, E., Buratti, N., Cirilli, S., 2013, The dawn of CAMP volcanism and its bearing on the end-Triassic carbon cycle disruption: The Geological Society of London, v. 171, p. 153-164.

Dal Corso, J., Mietto, P., Newton, R.J., Pancost, R.D., Preto, N., Roghi, G., Wignall, P.B., 2014, Discovery of a major negative δ13C spike in the Carnian (Late Triassic) linked to the eruption of Wrangellia flood basalts: Geology, v. 40, p. 79–82, doi:10.1130/G32473.1.

Dal Corso, J., Gianolla, P., Newton, R.J., Franceschi, M., Roghi, G., Caggiati, M., Raucsik, B., Budai, T., Haas, J., Preto, N., 2015, Carbon isotope records reveal synchronicity between carbon cycle perturbation and the “Carnian Pluvial Event” in the Tethys realm (Late Triassic): Global and Planetary Change, v. 127 , p. 79-90.

Deenen, M.H.L., Ruhl, M., Bonis, N.R., Krijgsman, W., Kuerschner, W.M., Reitsma. M., van Bergen, M.J., 2010. A new chronology for the end-Triassic mass extinction. Earth and Planetary Science Letters, 291, 113–125.

Diakow, L., Orchard, M.J., and Friedman, R., 2011, Absolute ages for the Norian Stage: a contribution from southern British Columbia, Canada: Canadian Paleontology Conference, Proceedings no. 9, p. 27-28.

Diakow, L., Orchard, M.J., and Friedman, R., 2012, Absolute ages for the Norian Stage: a further contribution from southern British Columbia, Canada: Cordilleran Tectonics Workshop, Geological Association Canada, Pacific Section. Program and Abstracts, 2 p.

Erwin, D. H., 2006, Extinction: How Life on Earth Nearly Ended 250 Million Years Ago: Princeton University Press, Princeton.

Faure, G., 1986, Principles of Isotope Geology: second edition, John Wiley and Sons, New York, p. 589.

Furin, S., Preto, N., Rigo. M., Roghi, G., Gianolla, P., Crowley, J.L. & Bowring, S.A., 2006, High precision U–Pb zircon age from the Triassic of Italy: implications for the Triassic time scale and the Carnian origin of calcareous nannoplankton and dinosaurs: Geology, v. 35, p. 146.

Galli, M.T., Jadoul, F., Bernasconi, S.M., Weissert, H., 2005, Anomalies in global carbon cycling at the Triassic/Jurassic boundary: evidence from a marine C-isotope record: Palaeogeogr. Palaeoclimatol. Palaeoecol., v. 216, p. 203–214.

Galli, M.T., Jadoul, F., Bernasconi, S.M., Cirilli, S., Weissert, H., 2007, Stratigraphy and palaeoenvironmental analysis of the Triassic–Jurassic transition in the western Southern Alps (Northern Italy): Palaeogeogr. Palaeoclimatol. Palaeoecol., v. 244, p. 52–70.

Gawlick, H.J., Bohm, F., 2000, Sequence and isotope stratigraphy of Late Triasic distal periplatform limestones from the Nothern Calcareous Alps (Kälberstein Quarry, Berchtesgaden Hallstatt Zone): Int. J. Earth Sciences, v. 89, p. 108-129.

Guex, J., Bartolini, A., Atudorei, V. and Taylor, D., 2004. High-resolution ammonite and carbon isotope stratigraphy across the Triassic-Jurassic boundary at New York Canyon (Nevada). Earth and Planetary Science Letters, 225(1-2): 29-41.

Hallam, A., 2002, How catastrophic was the end-Triassic mass extinction?: Lethaia, v. 35, p. 147-157.

Hauser, M., Martini, R., Burns, S., Dumitrica, P., Krystyn, L., Matter, A., Peters, T. and Zaninetti, L., 2001, Triassic stratigraphic evolution of the Arabian-Greater India embayment of the southern Tethys margin: Eclogae Geologicae Helvetiae, v. 94, p. 29-62.

Hayes, J.M., Strauss, H., Kaufman, A.J., 1999, The abundance of 13C in marine organic matter and isotopic fractionation in the global biogeochemical cycle of carbon during the past 800 Ma: Chem. Geol., v. 161, p. 103–125.

Hillebrandt, A.V., Krystyn, L. and Kürschner, W.M., 2007. A candidate GSSP for the base of the Jurassic in the Northern Calcareous Alps (Kuhjoch section, Karwendel Mountains, Tyrol, Austria). International Subcommission on Jurassic Stratigraphy Newsletter, 34(1): 2-20.

Hodell, D.A; Mueller, P.A; McKenzie, J.A; Mead, G., 1989, Strontium isotope stratigraphy and geochemistry of the late Neogene ocean: Earth and Planetary Science Letters, v. 92, no. 2, p. 165-178, doi:10.1016/0012-821X(89)90044-7.

Hönisch et al., 2012. The Geological Record of Ocean Acidification. Science, 335, 1058-1063.

Hornung, T., Brandner, R., 2005, Biochronostratigraphy of the Reingraben Turnover (Hallstatt Facies Belt): Local black shale events controlled by regional tectonics, climatic change and plate tectonics: Facies, v. 51, p. 460-479.

IPCC, 2014: Climate Change 2014: Synthesis Report. Contribution of Working Groups I, II and III to the Fifth Assessment Report of the Intergovernmental Panel on Climate Change [Core Writing Team, R.K. Pachauri and L.A. Meyer (eds.)]. IPCC, Geneva, Switzerland, 151 pp.

Jenkyns, H.C., 2010, Geochemistry of oceanic anoxic events: Geochemistry Geophysics Geosystems, v. 11, p. 1-30.

Jones, C.E. and Jenkyns, H.C., 2001, Seawater strontium isotopes, oceanic anoxic events, and seafloor hydrothermal activity in the Jurassic and Cretaceous: Am. J. Sci., v. 301, p. 112–149.

Kleypas. J.A., Feely, R.A., Langdon, C., Sabine, C.L., Robbins, L.L., 2006. Impacts of Ocean Acidification on Coral Reefs and Other Marine Calcifiers: A Guide for Future Research, report of a workshop held 18-20 April 2005, St. Petersburg, FL, sponsored by NSF, NOAA, and the U.S. Geological Survey, 88pp.

Korte, C., Kozur, H.W., Bruckschen, P. & Veizer, J., 2003, Strontium isotope evolution of Late Permian and Triassic seawater: Geochemica et Cosmochimica Acta, v. 67, p. 47–62.

Korte, C., Kozur, H.W., Veizer, J., 2005, 13C and 18O values of Triassic brachiopods and carbonate rocks as proxies for coeval seawater and palaeotemperature: Palaeogeography, Palaeoclimatology, Palaeoecology, v. 226, p. 287–306.

Krabbenhoft A., Fietzke J., Eisenhauer A., Liebetrau V., Bohm F. and Vollstaedt H. (2009) Determination of radiogenic and stable strontium isotope ratios (87Sr/86Sr; d88/86Sr) by thermal ionization mass spectrometry applying an 87Sr/84Sr double spike. J. Anal. At. Spectrom. 24, 1267–1271.

Kuerschner, W.M., Bonis, N.R. and Krystyn, L., 2007. Carbon-isotope stratigraphy and palynostratigraphy of the Triassic-Jurassic transition in the Tiefengraben section - Northern Calcareous Alps (Austria). Palaeogeography, Palaeoclimatology, Palaeoecology, 244(1-4): 257-280.

Lucas, S. G., 1999, The epicontinental Triassic, an overview: Zentralblatt fur Geologie und Palaontologie Teil I, 1998, p. 475–496.

Lucas, S. G. & Orchard, M. J., 2004, Triassic. In: Selley, R. C., Cocks, L. M. R. & Plimer, I. R. (eds) Encyclopedia of Geology. Elsevier, Amsterdam, p. 344–351.

Lucas, S.G., 2010, The Triassic Timescale. Geological Society, London, special publication, v. 334, p. 103-118.

Maron, M., Rigo, M., Bertinelli, A., Katz, M.E., Godfrey, L., Zaffani, M., and Muttoni, G., 2015, Magnetostratigraphy, biostratigraphy and chemostratigraphy of the Pignola-Abriola section: New constraints for the Norian-Rhaetian boundary: Geological Society of America Bulletin, v. 127, p. 962-974, doi:10.1130/B31106.1.

Marzoli, A., Bertrand, H., Knight, K.B., Cirilli, S., Buratti, N., Vérati, C., Nomade, S., Renne, P.R., Youb,i N., Martini, R., Allenbach, K., Neuwerth, R., Rapaille, C., Zaninetti, L., Bellieni, G., 2004, Synchrony of the Central Atlantic magmatic province and the Triassic-Jurassic boundary climatic and biotic crisis: Geology, v. 32, p. 973–976.

Mazza, M., Furin, S., Spötl, C., Rigo, M., 2010, Generic turnovers of Carnian/Norian conodonts: climatic control or competition?: Palaeogeogr. Palaeoclimatol. Palaeoecol., v. 290, p. 120–137.

McElwain J.C., Beerling D.J., Woodward F.I., 1999, Fossil plants and global warming at the Triassic-Jurassic boundary: Science, v. 285, p. 1386-1390.

McElwain, J.C., Wagner, P.J. and Hesselbo, S.P., 2009. Fossil Plant Relative Abundances Indicate Sudden Loss of Late Triassic Biodiversity in East Greenland. Science, 324: 1554-1556.

McRoberts, C.A. and Newton, C.R., 1995. Selective extinction among end-Triassic European bivalves. Geology, 23(2): 102-104.

McRoberts, C.A., Krystyn, L. & Shea, A., 2008, Rhaetian (Late Triassic) Monotis (Bivalvia: Pectinoida) from the eastern Northern Calcareous Alps (Austria) and the end-Norian crisis in pelagic faunas: Palaeontology, v. 51, p. 721–735.

Muttoni, G., Kent, D.V., Olsen, P., Di Stefano, P., Lowrie, W., Bernasconi, S., Martin Hernandez, F., 2004, Tethyan magnetostratigraphy from Pizzo Mondello (Sicily) and correlation to the Late Triassic astrochronological polarity time scale: Geol. Soc. Am. Bull., v. 116, p. 1043-1058.

Muttoni, G., Mazza, M., Mosher, D., Katz, M.E., Kent, D.V., Balini, M., 2014, A Middle–Late Triassic (Ladinian–Rhaetian) carbon and oxygen isotope record from the Tethyan Ocean: Palaeogeography, Palaeoclimatology, Palaeoecology, v. 399, p. 246-259.

Ogg, J.G., 2012. Triassic. In: Gradstein, F.M., Ogg, J.G., Schmitz, M.D., and Ogg, G.M., (eds) The Geologic Time Scale. Elsevier Publ., p. 681-730.

Olsen, P.E., Kent, D.V., Sues, H.-D., Koeberl, C., Huber, H., Montanari, A., Rainforth, E.C., Fowell, S.J., Szajna, M.J., Hartline, B.W., 2002. Ascent of Dinosaurs Linked to an Iridium Anomaly at the Triassic-Jurassic Boundary. Science, 296: 1305-1307.

Pálfy, J., Kocsis, A.T., 2014, Volcanism of the Central Atlantic magmatic province as the trigger of environmental and biotic changes around the Triassic-Jurassic boundary: Geological Society of America Special Papers, v. 505, p. SPE505-12.

Palmer, M.R. & Elderfield, H., 1985, Sr isotope composition of sea water over the past 75 Myr: Nature, v. 314, p. 526-528.

Palmer, M.R. and Edmond, J.M., 1989, The Strontium Isotope Budget of the Modern Ocean: Earth and Planetary Science Letters, v. 92, no. 1, p. 11-26, doi: 10.1016/0012-821X(89)90017-4.

Payne, J.L., Lehrmann, D.J., Wei, J., Orchard, M.J., Schrag, D.P., Knoll, A.H., 2004, Large perturbations of the carbon cycle during recovery from the end-Permian extinction: Nature, v. 305, p. 506–509.

Preto, N., Kustatscher, E., and Wignall, P.B., 2010. Triassic climates—State of the art and perspectives. Palaeogeography, Palaeoclimatology, Palaeoecology, 290, 1–10, doi:10.1016/j.palaeo.2010.03.015.

Preto, N., Rigo, M., Agnini, C., Bertinelli, A., Guaiumi, C., Borello, S.,Westphal, H., 2012, Triassic and Jurassic calcareous nannofossils of the Pizzo Mondello section: a SEM study: Riv. Ital. Paleontol. Stratigr., v. 118, no. 1, p. 131–141.

Preto, N., Agnini, C., Rigo, M., Sprovieri, M., Westphal, H., 2013, The calcareous nannofossil Prinsiosphaera achieved rock-forming abundances in the latest Triassic of western Tethys: consequences for the $\delta^{13}C$ of bulk carbonate: Biogeosciences, v. 10, p. 6053-6068.

Rampino, M.R., and R.B. Stothers, 1988, Flood basalt volcanism during the past 250 million years: Science, v. 241, p. 663-668, doi:10.1126/science.241.4866.663.

Raven, J., Caldeira, K., Elderfield, H., Hoegh- Guldberg, O., Liss, P., Riebesell, U., Shepherd, J., Turley, C., Watson, A., 2005. Ocean acidification due to increasing atmospheric carbon dioxide, Policy Doc. 12/05, 60 pp., R. Soc., London.

Raup, D.M. and Sepkoski, J.J., 1982, Mass extinction in the fossil record: Science, v. 215, p. 1501–1503.

Raymo, M.E., Ruddiman, W.F., Froelich, P.N., 1988, Influence of late Cenozoic mountain building on ocean geochemical cycles: Geology, v. 16, p. 649– 653, doi: 10.1130/0091-7613(1988)016<0649:IOLCMB>2.3.CO;2.

Richoz, S., Krystyn, L., Spotl, C., 2007, Towards a carbon isotope reference curve of the Upper Triassic: New Mexico Museum of Natural History and Science Bulletin, v. 41, p. 366-367.

Rigo, M., Trotter, J.A., Preto, N., Williams, I.S., 2012. Oxygen isotopic evidence for Late Triassic monsoonal upwelling in the northwestern Tethys, Geology, v. 40; no. 6, p. 515–518, DOI: 10.1130/G32792.1.

Ruhl, M., 2009. Carbon cycle changes during the Triassic-Jurassic transition. PhD thesis.

Sala, O.E., Chapin, F.S., III, Armesto, J.J., Berlow, E., Bloomfield, J., Dirzo, R., Huber-Sanwald, E., Huenneke, L.F., Jackson, R.B., Kinzig, A.,Leemans, R., Lodge, D.M., Mooney, H.A., Oesterheld, M., Poff, N.L., Sykes, M.T., Walker, B.H., Walker, M., Wall, D.H., 2000. Global Biodiversity Scenarios for the Year 2100. Science, 287(5459), 1770-1774.

Schaller, M.F., Wright, J.D., Kent, D.V., Olsen, P.E., 2012, Rapid emplacement of the Central Atlantic Magmatic Province as a net sink for CO2: Earth and Planetary Science Letters, v. 323–324, p. 27–39.

Schoene, B., Guex, J., Bartolini, A., Schaltegger, U. & Blackburn, T.J., 2010, A correlation between the Triassic-Jurassic boundary mass extinction and flood basalt eruption at the 100-ka level using ID-TIMS U/Pb zircon geochronology: Geology, v. 38, p. 387–390.

Sephton, M.A., Amor, K., Franchi, I.A., Wignall, P.B., Newton, R., Zonneveld, J.P., 2002, Carbon and nitrogen isotope disturbances and an end-Norian (Late Triassic) extinction event: Geology, v. 30, p. 1119-1122.

Simms, M.J., Ruffell, A.H., 1989, Synchroneity of climatic change and extinctions in the Late Triassic: Geology, v. 17, p. 265–268.

Simms, M.J., Ruffell, A.H., 1990, Climatic and biotic change in the late Triassic: J. Geol. Soc. (Lond.) v. 147, p. 321–327.

Simms, M.J., Ruffell, A.H., Johnson, A.L.A., 1995, Biotic and climatic changes in the Carnian (Triassic) of Europe and adjacent areas. In: Fraser, N.C., Sues, H.D. (Eds.), In the Shadow of the Dinosaurs. Early Mesozoic Tetrapods. Cambridge Univ. Press p. 352–365.

Tanner, L.H., Lucas, S.G., Chapman, M.G., 2004, Assessing the record and causes of Late Triassic extinction: Earth Sciences Reviews, v. 65, p. 103-139.

Tanner, L.H., 2010, The Triassic isotope record. In: Lucas, S.G. (ed.) The Triassic Timescale. Geological Society, London, special publication, v. 334, p. 103-118.

Taylor, A.S., Lasaga, A.C., 1999, The role of basalt weathering in the Sr isotope budget of the oceans: Chemical Geology, v. 161, no. 1-3, p. 199-214, doi: 10.1016/S0009-2541(99)00087-X.

Trotter, A.J., Williams, S.I., Nicora, A., Mazza, M. and Rigo, M., 2015, Long-term cycles of Triassic climate change: a new d^{18}O record from conodont apatite: Earth and Planetary Science Letters, v. 415, p. 165–174.

van de Schootbrugge, B., Payne, J.L., Tomasovych, A., Pross, J., Fiebig, J., Benbrahim, M., Follmi, K.B., Quan, T.M,. 2008, Carbon cycle perturbation and stabilization in the wake of the Triassic-Jurassic boundary mass extinction event: Geochemistry Geophysics Geosystems, v. 9, p. 1-16.

Veizer, J., Buhl, D., Diener, A., Ebneth, S., Podlaha, O.G., Bruckschen, P., Jasper, T., Korte, C., Schaaf, M., Ala, D., Azmy, K., 1997, Strontium isotope stratigraphy: potential resolution and event correlation: Paleogeogr., Paleoclimatol., Paleoecol., v. 132, p. 65–77.

Veizer, J., Ala, K., Azmy, K., Bruckschen, P., Buhl, D., Bruhn, F., Carden, G.A.F., Diener, A., Ebneth, S., Godderis, Y., Jasper, T., Korte, C., Pawellek, F., Podlaha, O.G., Strauss, H., 1999, 87Sr/86Sr, δ13C and δ18O evolution of Phanerozoic seawater: Chem. Geol., v. 161, p. 59–88.

Ward, P.D., Haggart, J.W., Carter, E.S., Wilbur, D., Tipper, H.W., Evans, T., 2001. Sudden productivity collapse associated with the Triassic-Jurassic boundary mass extinction. Science, 292(5519): 1148-1151.

Ward, P.D., Garrison, G.H., Haggart, J.W., Kring, D.A., Beattie, M.J., 2004, Isotopic evidence bearing on Late Triassic extinction events, Queen Charlotte Islands, British Columbia, and implications for the duration and cause of the Triassic/Jurassic mass extinction: Earth and Planetary Science Letters, v. 224, p. 589-600.

Whiteside, J.H., Olsen, P.E., Eglinton, T., Brookfield, M.E., and Sambrotto, R.N., 2010, Compound-specific carbon isotopes from Earth's largest flood basalt eruptions directly linked to the end-Triassic mass extinction: PNAS, v. 107, p. 6721–6725.

Whiteside, J.H., Ward, P.D., 2011, Ammonoid diversity and disparity track episodes of chaotic carbon cycling during the early Mesozoic: Geology, v. 39, p. 99-102.

Wignall, P.B., 2001, Large igneous provinces and mass extinctions: Earth-Science Reviews, v. 53, p. 1–33.

Wignall, P.B., Zonneveld, J.-P., Newton, R.J., Amor, K., Sephton, M.A. & Hartley, S., 2007, The end Triassic mass extinction record of Williston Lake, British Columbia: Palaeogeogr. Palaeoclimatol. Paleoecol., v. 253, p. 385–406.

METHODS

$\delta^{13}C_{org}$ AND TOC SAMPLE PREPARATION METHODS: WHICH ONE?

More than one sample preparation method exist for organic carbon analyses, as a consequence it is crucial to assess the validated methodologies in order to obtain the most trustable results.

Nowadays, the most commonly applied methods are based on the removal of inorganic carbon through an acid, usually hydrochloric acid (HCl) or orthophosphoric acid (H_3PO_4). Three different acidification methods are common: the in-situ acidification, the fumigation and the so called "rinse method" (Konitzer et al., 2012).

With the in-situ acidification, the powdered material contained into a silver capsule is placed on a hot plate. Drops of acid are added gradually and evaporated, paying attention to avoid spilling of the solution during the reaction and/or the damage of the capsule (to avoid the latter, some laboratories uses to wrap silver capsules in tin capsules for better combustion). With the fumigation method, samples are exposed to acid vapors in a desiccator until the total removal of carbonates (usually one or more than one day). The "rinse method" requires the repeated reaction of powdered samples in acid, followed by the discarding of the solution and rinsing in deionized water. The repeated discarding of the supernatant containing acid soluble organic matter could potentially involves the loss of variable proportion of the latter. In fact, some studies suggest underestimation of TOC (Total Organic Carbon) likely related to these discarding steps: the estimated loss of organic matter ranges between negligible values (e.g., Midwood and Boutton, 1998), 14-19% (Galy et al., 2007), to 44% (Roberts et al., 1973; Froelich, 1980). As a consequence, the artificial concentration of the more acid-resistant fraction of organic matter could result in a depletion of the $\delta^{13}C_{org}$ (Fernandes and Krull, 2008; Brodie et al., 2011a), even if some studies demonstrates that it remains relatively unchanged (Midwood and Boutton, 1998; Schubert and Nielsen, 2000; Konitzer et al., 2012). In theory, in situ acidification and fumigation could minimize the loss of organic material, but recent studies highlight issues with samples characterized by high carbonate content (Konitzer et al., 2012). Moreover, with the in situ acidification method, the solution within the capsule is prone to spill during the reaction and it has been showed that CO_2 bubbles tend to protect carbonate from dissolution (Brodie et al., 2011b; Konitzer et al., 2012). In addition, in situ acidification of carbonate produces hygroscopic salts (e.g., calcium chloride), which are problematic for mass balance calculations of total carbon (TC)and represent a potential hazard to the elemental analyzer over prolonged periods (Schubert and

Nielsen, 2000; Fernandes and Krull, 2008; Larson et al., 2008; Konitzer et al., 2012). Some concerning issues involves also the fumigation method, in which the vapor may not attack all of the carbonate, resulting in higher TOC and $\delta^{13}C_{org}$ (Brodie et al., 2011a).

Konitzer et al. (2012) evaluated all the pro and cons of these three different methods and undertook a series of tests on different lithologies to provide a trustable preparation procedure. They showed that 5-10% HCl seems to be the most efficient reagent in removing carbonates (accordingly also to Kennedy et al., 2005; Fernandes and Krull, 2008). It is crucial to ensure an excess of acid respect to the amount of carbonate and leave the sample into acid for a reasonable amount of time (at least 12h), in order to fully remove calcium carbonate. Mg and Fe carbonates, such as dolomite and siderite, can be eliminated through treatment with 20% HCl (van Kaam-Peters et al., 1997) or with low acid concentration (5-10%) at high temperatures (Huon et al., 2002). Therefore, accordingly to Konitzer et al. (2012), by following these procedures it is possible to obtain the best approximation of bulk $\delta^{13}C_{org}$ and TOC in fine-grained sedimentary rocks.

For this reason we decided to applied the "rinse method" for our $\delta^{13}C_{org}$ sample preparation, undertaken at the Department of Geosciences, University of Padova (Italy).

PROTOCOL FOR $\delta^{13}C_{org}$ ANALYSES SAMPLE PREPARATION

Prior to acidification, all samples are washed in high-purity water and selected to avoid sampling of unrepresentative portions (*e.g.*, fracture-filling mineralization, bioturbation, diagenetic alteration). A few grams of each sample were reduced to a fine powder using a Retsch RM0 grinder or manually using an agate mortar and dried overnight at 40°C. Then, all the pulverized rock samples are acid-washed with 10% HCl overnight (at least 12h). Successively, the solution is discarded after centrifuging. Then samples are neutralized in deionized water, dried at 40°C overnight and wrapped in tin capsules.

The $\delta^{13}C_{org}$ analyses has been undertaken using a Delta V Advantage mass spectrometer connected to a Flash HT Elemental Analyzer. For every set of analysis, multiple blank capsules and isotope standards (IAEA CH-6 = -10.45‰, IAEA CH-7 = -32.15‰, Coplen et al., 2006) has been included. The standard deviation of the in-house standard ($\delta^{13}C_{org}$ = -26.00‰) during the period of analyses was better than 0.2‰.

Raw data were corrected for the blank contribution (i.e., $\delta^{13}C_{org}$ of the tin capsule), by subtracting the mean of the blank measurements from the unknown samples in order to calculates the $\delta^{13}C_{org}$ of the sample. Fort the blank correction, the following equation was applied:

$$raw\ \delta 13\mathrm{Corg}_{\ sample} = \frac{\left(A45_{sample} * \delta 13\mathrm{Corg}_{sample}\right) - \left(A45_{blank} * \delta 13\mathrm{Corg}_{blank}\right)}{\left(A45_{sample} - A45_{blank}\right)}$$

with A45 = area of the peak measured on the 45 cup.

The obtained raw $\delta^{13}C_{org}$ were calibrated against IAEA CH-6 ($\delta^{13}C_{org}$=-10.45‰) and IAEA CH-7 ($\delta^{13}C_{org}$=-32.15‰) following the two-point calibration method. This technique relies on the ordinary least squares method and the linear regression model, which are applied to obtain the slope (m) and the intercept (q) of the regression line based on the measured and nominal $\delta^{13}C_{org}$ values of the standards (CH-6 and CH-7). The equation of the regression line was then applied to obtain the calibrated $\delta^{13}C_{org}$ values of the samples:

$$calibrated\ \delta 13\mathrm{Corg}_{sample} = m * \left(raw\ \delta 13\mathrm{Corg}_{sample}\right) + q$$

PROTOCOL FOR TOC ANALYSES SAMPLE PREPARATION

The TOC investigations were conducted at the Department of Agronomy, Food, Natural Resources, Animals and the Environment (DAFNAE), University of Padova (Italy), following the in situ acidification technique. The powders are treated with a 10% HCl solution in silver capsules wrapped into tin capsules to remove inorganic carbon (i.e., carbonate component). Drops of acid are added progressively till the decarbonating reaction is concluded (i.e., no more effervescence). Successively, they are dried on a hot plate at 50°C. An amount of tungsten trioxide (WO_3) equal to the sample weight is added to the dried sample. The WO_3 prevents the formation of alkaline sulfates, which are difficult to combust in the Elemental Analyzer, and safeguard the fused-quartz column of the Elemental Analyzer. Eventually, samples are analyzed using a Vario Macro CNS Elemental Analyzer. Results are calibrated against Sulfanilamide standard (N=16.25%; C=41.81%; S=18.62%; H=4.65%). The analytical uncertainty of the instrument, expressed as relative standard deviation, is σ=0.5%.

In collaboration with Prof. Concheri (DAFNAE, University of Padova), we tested an alternative sample preparation technique for TOC analyses, avoiding the use of acids. It is called the "*muffola*" (= high-temperature oven) method. It requires the preparation of two aliquots of pulverized sample:

the first aliquote is added to WO_3 and wrapped in tin capsule and analyzed directly at the Elemental Analyzer, in order to obtain the TC (Total Carbon) content of the sample. The second aliquot contained in a silver capsule is treated in the high-temperature oven: when the temperature reaches 550°C, all the organic carbon components (exception made for coal) are removed. Successively, WO_3 is added and the sample is analyzed to obtain the TIC (Total Inorganic Carbon). The difference between the TC and the TIC gives the TOC. We tested this method on different lithologies: marls, shales, limestones, dolostones, for a total of 97 samples. Each sample has been analyzed five times for both methods: the in situ acidification and the "*muffola*". The comparison between the two methods reveals an average coefficient of determination R^2 equals to 0.934 and a Pearson coefficient ρ higher than 0.7 ($\rho = 0.967$), confirming the validity of the "*muffola*" method.

However, since the "*muffola*" is an experimental method that has not been validated officially yet, we decided to present in this thesis only the TOC results obtained from the validated acidification technique. More information about the "*muffola*" method, raw data, results and statistics can be found in Zaffani master thesis (2013).

Focus on: ***WHY COEVAL SHIFT COULD SHOW DIFFERENT $\delta^{13}C_{org}$ AMPLITUDE?***

$\delta^{13}C_{org}$ analyses (if is not specified differently) refers to the $\delta^{13}C$ composition of *bulk* organic matter. Organic matter can be constituted by a number of components, such as bacteria, phytoplankton, zooplankton, pollens and/or other terrestrial biomass and so on. Each of these components is characterized by a peculiar value of $\delta^{13}C_{org}$. This means that changes in relative contributions of these components could affect the $\delta^{13}C_{org}$ record, without necessarily requiring changes in the isotope composition of the ocean and/or the atmosphere (van de Schootbrugge et al., 2008; Fio et al., 2010, Bartolini et al., 2012). Nevertheless, if similar trends are found to occur in the same time interval and in different and likely distant locations, the robust correlation between excursions of the $\delta^{13}C_{org}$ record can argue for a regional or, if more extended, global interpretation. In fact, as discussed above, the amplitude and absolute values of coeval $\delta^{13}C_{org}$ changes might be amplified or hindered by local environmental conditions and source control, i.e., the contribution of marine relative to terrestrial organic matter, and profound changes in the composition of standing biomass, i.e., terrestrial floras or phytoplankton communities (van de Schootbrugge et al., 2008). However, the similarity between two or more shapes of the $\delta^{13}C_{org}$ profile likely traces a regional or global history (Bartolini et al., 2012).

References

Bartolini, A., J. Guex, J. E. Spangenberg, B. Schoene, D. G. Taylor, U. Schaltegger, and V. Atudorei, 2012. Disentangling the Hettangian carbon isotope record: Implications for the aftermath of the end- Triassic mass extinction. Geochem. Geophys. Geosyst., 13, Q01007, doi:10.1029/2011GC003807.

Brodie, C.R., Leng, M.J. Casford, J.S.L., Kendrick, C.P., Lloyd, J.M., Yongqiang, Z., Bird M.I., 2011a. Evidence for bias in C and N concentrations and d13C composition of terrestrial and aquatic organic materials due to pre-analysis acid preparation methods. Chem. Geol., 282, 67–83, doi:10.1016/j.chemgeo.2011.01.007.

Brodie, C. R., J. S. L. Casford, J. M. Lloyd, M. J. Leng, T. H. E. Heaton, C. P. Kendrick, and Z. Yongqiang, 2011b. Evidence for bias in C/N, d13C and d15N values of bulk organic matter, and on environmental interpretation, from a lake sedimentary sequence by pre-analysis acid treatment methods. Quat. Sci. Rev., 30, 3076–3087, doi:10.1016/j.quascirev.2011.07.003.

Coplen, T.B., Brand, W.A., Gehre, M., Groning, M., Meijer, H.A.J., Toman, B. and Verkouteren, R.M., 2006. New guidelines for $d^{13}C$ measures. Analytical Chemistry, 78, 2439–2441.

Fernandes, M., and Krull E., 2008. How does acid treatment to remove carbonates affect the isotopic and elemental composition of soils and sediments?. Environ. Chem., 5, 33–39, doi:10.1071/EN07070.

Fio, K., J. E. Spangenberg, I. Vlahović, J. Sremac, I. Velić, and E. Mrinjek, 2010. Stable isotope and trace element stratigraphy across the Permian–Triassic transition: A redefinition of the boundary in the Velebit Mountain, Croatia. Chem. Geol., 278, 38–57, doi:10.1016/j.chemgeo.2010.09.001.

Froelich, P. N., 1980. Analysis of organic carbon in marine sediments. Limnol. Oceanogr., 25, 564–572, doi:10.4319/lo.1980.25.3.0564.

Galy, V., J. Bouchez, and C. France-Lanord, 2007. Determination of total organic carbon content and d13C in carbonaterich detrital sediments. Geostand. Geoanal. Res., 31, 199–207, doi:10.1111/j.1751-908X.2007.00864.x.

Huon, S., F. E. Grousset, D. Burdloff, G. Bardoux, and A. Mariotti, 2002. Sources of fine-sized organic matter in North Atlantic Heinrich layers: d13C and d15N tracers, Geochim. Cosmochim. Acta, 66, 223–239, doi:10.1016/S0016-7037(01)00776-1.

Kennedy, P., H. Kennedy, and S. Papadimitriou, 2005. The effect of acidification on the determination of organic carbon, total nitrogen and their stable isotopic composition in algae and marine sediment. Rapid Commun. Mass Spectrom., 19, 1063–1068, doi:10.1002/rcm.1889.

Konitzer, S.F., Leng, M.J., Davies, S.J., Stephenson, M.H., 2012. An assessment of geochemical preparation methods prior to organic carbon concentration and carbon isotope ratio analyses of fine-grained sedimentary rocks. Geochem., Geophys., Geosys., 13, 1-12, doi:10.1029/2012GC004094.

Larson, T. E., J. M. Heikoop, G. Perkins, S. J. Chipera, and M. A. Hess, 2008. Pretreatment technique for siderite removal for organic carbon isotope and C:N ratio analysis in geological samples. Rapid Commun. Mass Spectrom., 22, 865–872, doi:10.1002/rcm.3432.

Midwood, A.J., and Boutton, T.W., 1998. Soil carbonate decomposition by acid has little effect on d13C of organic matter.Soil Biol. Biochem., 30, 1301–1307, doi:10.1016/S0038-0717(98)00030-3.

Roberts, A. A., J. G. Palacas, and I. C. Frost, 1973. Determination of organic carbon in modern carbonate sediments. J. Sediment. Res., 43, 1157–1159.

Schubert, C.J., and Nielsen, B., 2000. Effects of decarbonation treatments on d13C values in marine sediments.Mar. Chem., 72, 55–59, doi:10.1016/S0304-4203(00)00066-9.

Van de Schootbrugge, B., Payne, J.L., Tomasovych, A., Pross, J., Fiebig, J., Benbrahim, M., Follmi, K.B., Quan, T.M,. 2008. Carbon cycle perturbation and stabilization in the wake of the Triassic-Jurassic boundary mass extinction event. Geochemistry Geophysics Geosystems, 9, 1-16.

van Kaam-Peters, H. M. E., S. Schouten, J. W. de Leeuw, and J. S. Sinninghe Damsté, 1997. A molecular and carbon isotope biogeochemical study of biomarkers and kerogen prolysates of the Kimmeridge Clay Facies: Palaeoenvironmental implications. Org. Geochem., 27, 399–422, doi:10.1016/S0146-6380(97)00084-3.

CHAPTER 1:

The Norian "chaotic carbon interval": new clues from the $\delta^{13}C_{org}$ record of the Lagonegro Basin (southern Italy)

Mariachiara Zaffani[1], Claudia Agnini[1,5], Giuseppe Concheri[2], Linda Godfrey[3], Miriam Katz[4], Matteo Maron[1], Manuel Rigo[1,5]

[1] Department of Geosciences, University of Padova, via Gradenigo 6, 35131 Padova, Italy
[2] Department of Agronomy, Food, Natural Resources, Animals and the Environment – DAFNAE, University of Padova, Viale dell'Università 16, 35020 Legnaro (PD), Italy
[3] Department of Earth and Planetary Sciences, Rutgers University, Piscataway, NJ, 08854, USA
[4] Department of Earth and Environmental Sciences, Rensselaer Polytechnic Institute, 110 8th St., Troy, NY, 12180, USA
[5] Institute of Geosciences and Earth Resources - CNR, Via G. Gradenigo 6, 35131 Padova, Italy

ABSTRACT

A global carbon isotope curve for the Late Triassic has the potential for global correlations and new insights on the complex and extreme environmental changes that took place in this time interval. We reconstruct the global $\delta^{13}C_{org}$ profile for the late Norian, improving on sparse published data from North American successions that depict a "chaotic carbon isotope interval" with rapid oscillations. In this context, we studied three sections outcropping in the Lagonegro Basin (southern Italy), originally located in the western Tethys. The carbon isotope profiles show four negative excursions correlatable within the Lagonegro Basin. In particular, a negative shift close to the Norian/Rhaetian boundary appears to correlate with that observed in the North American $\delta^{13}C_{org}$ record, documenting the widespread occurrence of this carbon cycle perturbation. $^{87}Sr/^{86}Sr$ and $^{187}Os/^{188}Os$ profiles suggest that this negative shift was possibly caused by emplacement of a Large Igneous Province (LIP). The release of greenhouse gases (CO_2) to the atmosphere-ocean system is supported by the ^{12}C enrichment observed, as well as by the increase of atmospheric pCO_2 inferred by different models for the Norian-Rhaetian interval. The trigger of this strongly perturbed interval could thus be enhanced magmatic activity that can be ascribed to the Angayucham province (Alaska, North America), a large oceanic plateau active ca. 214±7 Ma, which has an estimated volume comparable to the Wrangellia and the CAMP LIPs. In fact, these three Late Triassic igneous provinces may have caused extreme environmental and climate changes during the Late Triassic.

INTRODUCTION

The Triassic is a key period of the Earth's history, characterized by the break-up of the supercontinent Pangaea, episodes of biotic crises and climate fluctuations (e.g., Ogg et al., 2012). This period is constrained by two of the biggest mass extinctions of the Phanerozoic: 1) the end-Permian mass extinction - the most extensive biotic decimation of the Phanerozoic (e.g., Lucas, 1999; Benton & Twitchett, 2003; Lucas & Orchard, 2004; Erwin, 2006); and 2) the end-Triassic mass extinction (e.g., Hallam, 2002; Tanner et al., 2004; Richoz et al., 2007). The Triassic is also characterized by a dynamic climate regime (e.g., Preto et al., 2010; Rigo et al., 2012b; Trotter et al., 2015) and widespread geological and paleontological events, including humid and warm episodes (e.g., Carnian Pluvial Event, Upper Triassic, Simms and Ruffell, 1989, 1990; Simms et al., 1995; Ruffell et al., 2015), volcanism, and changes in the biosphere (e.g., Raup & Sepkoski, 1982; McElwain et al., 1999; Hallam, 2002; Marzoli et al., 2004; McRoberts et al., 2008; Lucas, 2010; Dal Corso et al., 2013, 2014; Rigo & Joachimski, 2010; Rigo et al., 2012b; Trotter et al., 2015). Stable isotopes play a critical role in biogeochemical cycles and therefore can provide important clues of ocean water chemistry, oxygenation, and productivity of marine environments during the Triassic. Among these tools, one of the most widely applied is $\delta^{13}C_{org}$. This isotopic system varies in time as a function of productivity, organic carbon burial and C assimilation pathway (C3 or C4). Therefore, $\delta^{13}C_{org}$ can provide essential clues on the evolution of ocean water chemistry, oxygenation, and productivity of past marine environments (e.g., Hayes et al., 1999; Veizer et al., 1999; Payne et al., 2004; Korte et al., 2005; Lucas, 2010; Preto et al., 2012). In particular, excursions in marine $\delta^{13}C_{org}$ records that can be correlated globally are often thought to be related to global changes in the carbon cycle, such as those induced by marine and terrestrial extinction episodes (Berner, 2002; Galli et al., 2005; Payne and Kump, 2007; Korte and Kozur, 2010), which are often marked by negative $\delta^{13}C_{org}$ anomalies.

The carbon isotope record of the Triassic has been studied in some detail, but its interpretation is complex because of the multiple ecological and geochemical controls on this proxy (e.g., Hayes et al., 1999; Veizer et al., 1999; Payne et al., 2004; Korte et al., 2005; Lucas, 2010; Muttoni et al., 2004, 2014; Galli et al., 2005, 2007; Mazza et al., 2010; Preto et al., 2012). A pronounced negative excursion is recorded at the Permian-Triassic boundary with repercussions in the lowermost Triassic, which is characterized by strong isotopic instability (e.g., Payne et al., 2004; Lucas, 2010). This is followed by a more stable period represented by the Middle Triassic (Payne et al., 2004; Tanner, 2010) and early Late Triassic (Julian, lower Carnian), with steadily rising values of $\delta^{13}C_{org,\ carb}$ likely related to environmental recovery after the Late Permian mass extinction and increasing storage of organic carbon in terrestrial environments (e.g., Lucas, 2010). The Late Triassic is bracketed by two significant negative shifts, both linked to a Large Igneous Province (LIP). The first occurred in the Carnian and it is associated with the Carnian Pluvial Event and the emplacement of the Wrangellia igneous province (e.g., Furin et al., 2006; Dal Corso et al., 2014, 2015). The second is at the Triassic-Jurassic transition associated with the end-Triassic mass extinction and emplacement of the Central American magmatic province (CAMP) (e.g., Marzoli et al., 2004; Whiteside et al., 2010; Schaller et al., 2012; Dal Corso et al., 2013). The causes of the Triassic carbon isotope excursions remain a topic of much debate, with the most likely trigger mechanisms being outgassing during volcanic activity, changes in productivity, ocean anoxia and seafloor methane release (e.g., Richoz et al., 2007; Lucas, 2010). These processes evidently perturbed the global carbon cycle and caused episodes of biotic crises (e.g., Rampino & Stothers, 1988; Wignall, 2001, Jones and Jenkyns, 2001; Ward et al., 2004; Richoz et al., 2007; Van de Schootbrugge et al., 2008; Jenkyns, 2010; Tanner, 2010; Palfy et al., 2014, Trotter et al., 2015). Therefore, a global carbon isotope curve for the Triassic would have the potential for global correlation and would provide new insights on the environmental changes that took place in this period. Muttoni et al. (2014) provides a composite $\delta^{13}C_{carb}$ record from the Ladinian (ca. 242 Ma) to present, but the construction of a Triassic organic carbon isotope record is still in progress. The published $\delta^{13}C_{org}$ data are especially focused on the mass extinction events (i.e., Permian/Triassic boundary, Triassic/Jurassic boundary) and the long-term background conditions are instead largely understudied. For instance, few carbon isotope data are available for the Late Triassic, which seems to be characterized by significant $\delta^{13}C_{org}$ excursions associated with important episodes of faunal turnovers. In particular, data from the Norian (ca. 227.0-205.7 Ma; Diakow et al., 2011, 2012; Maron et al., 2015) of North America seems to indicate rapid oscillations of $\delta^{13}C_{org}$ that culminate in a positive $\delta^{13}C_{org}$ excursion that corresponds to the extinction of the bivalve *Monotis*, at the Norian/Rhaetian boundary (Ward et al., 2004; Wignall et al., 2007; Whiteside & Ward, 2011). This positive excursion is interpreted as the result of an increased stagnation in ocean circulation (Sephton et al., 2002; Ward et al., 2004). Tethyan sections have been investigated for $\delta^{13}C_{carb}$ at the Norian/Rhaetian boundary (e.g., Atudorei, 1999; Gawlick et al., 2000; Hauser et al., 2001; Muttoni et al., 2004; Hornung and Brandner, 2005; Korte et al., 2005; Preto et al., 2013; Rigo et al., 2016; Bertinelli et al., 2016), but a complete Norian organic carbon isotope profile is not available yet.

Therefore, the aim of this study is to verify the occurrence and to understand the causes of the Norian organic carbon isotope perturbations in the Tethyan realm, in particular in the Lagonegro Basin (southern Italy), as a contribution to the construction of a more complete global C_{org} isotope curve for the Late Triassic. For this purpose, we investigated three geological sections, representing intermediate to distal basinal pelagic successions, for the concentration of total organic carbon (TOC) and organic carbon isotopes ($\delta^{13}C_{org}$).

GEOLOGICAL SETTING

The Lagonegro Basin is located in the Southern Apennines (Italy) and is interpreted as part of the Ionian Sea, a branch of the western Tethys Ocean (Sengor et al., 1984; Catalano et al., 1991; Stampfli & Marchant, 1995; Ciarapica & Passeri, 1998, 2002; Stampfli et al., 2003). The Lagonegro Basin is interpreted as an oceanic basin based on the available seismic lines and magnetic anomaly pattern of the Ionian Sea, which show that the sedimentary succession of this area lies upon oceanic crust (e.g., Finetti, 1982; Finetti et al., 1996; Catalano et al., 2001; Argnani, 2005; Rigo et al., 2007; 2012a; Speranza et al., 2012). It consists of shallow to deep basinal pelagic successions, Permian to Miocene in age (Scandone 1967, Rigo et al. 2005, 2012; 2012a; Giordano et al., 2010). The Lagonegro sequence is subdivided into many tectonic units, accumulated between the Apenninic and Apulian carbonate platforms (Mostardini & Merlini, 1986) during the Apenninic orogenesis and formation of a part of the Southern Apennines chain (southern Italy). The Upper Triassic in the Lagonegro Basin is represented by the Calcari con Selce and the Scisti Silicei (Formations). The Calcari con Selce consists of calcilutites bearing conodonts, radiolarians and thin-shelled bivalves (e.g., genus *Halobia*), intercalated with marls, siltstones and calcarenites (Rigo et al., 2005, 2012a; Giordano et al., 2010). Nodules and layers of chert are present throughout this unit and limestones might show varying degrees of dolomitization. The Scisti Silicei is characterized by centimeter-thick multicolored cherts, radiolarites and often siliceous shales (Amodeo, 1999; Bertinelli et al., 2005a; Giordano et al., 2010). This formation represents the beginning of the biosiliceous sedimentation within the Lagonegro Basin, occurring from the uppermost Norian to lower Hettangian, thus the base of the Scisti Silicei is considered diachronous (Bertinelli et al., 2005a; Reggiani et al., 2005; Giordano et al., 2010, 2011; Casacci et al., 2016). The gradual passage between the Calcari con Selce and the Scisti Silicei is represented by the so-called “transitional interval” (Miconnet, 1982; Amodeo & Baumgartner, 1994; Amodeo, 1999; Bertinelli, 2003; Rigo et al., 2005, 2012a; Giordano et al., 2010). Going upward, the “transitional interval” shows a gradual decrease in carbonates in favor of clay and siliceous components. Silicification of the carbonates also increases upward (Amodeo, 1999; Rigo et al., 2005; Giordano et al., 2010). The base of this “transitional interval” is marked by a meter-thick level of red shales (Amodeo, 1999; Bertinelli et al., 2005a; Rigo et al., 2005, 2012a; Giordano et al., 2010), which is conventionally used as a regional lithomarker within the Lagonegro Basin. This red shale level approximates the base of the *Mockina bidentata* Zone (*sensu* Kozur & Mock, 1991), Sevatian 1 in age (ca. 216-210.5 Ma; Rigo et al., 2005, 2012a; Maron et al., 2015). The Triassic and Jurassic successions of the Lagonegro Basin (i.e., Calcari con Selce and Scisti Silicei) can be differentiated in proximal, intermediate and distal facies (Scandone, 1967), depending on thickness of the formations and on the amount of resedimented calcarenites and calcirudites coming from the adjacent carbonate platforms. The proximal facies in the Calcari con Selce persisted from Upper Triassic to Middle Jurassic (Selli, 1962; Scandone, 1967; Bertinelli et al., 2005a; Passeri et al., 2005; Rigo et al., 2005; Giordano et al., 2010). Instead, the distal facies, which are characterized by the transition from the carbonate sedimentation of the Calcari con Selce to the siliceous deposition of Scisti Silicei, occurred with different patterns between the uppermost Triassic and the lowermost Jurassic (Scandone, 1967; Rigo et al., 2005, 2012a; Giordano et al., 2010).

The Lagonegro Basin has been investigated at three localities, where the Norian-Rhaetian interval is well documented: the Pignola-Abriola, Mt Volturino and Madonna del Sirino sections (Fig. 1.1). These successions belong to the Calcari con Selce and Scisti Silicei and generally display good exposure and continuity in the field.

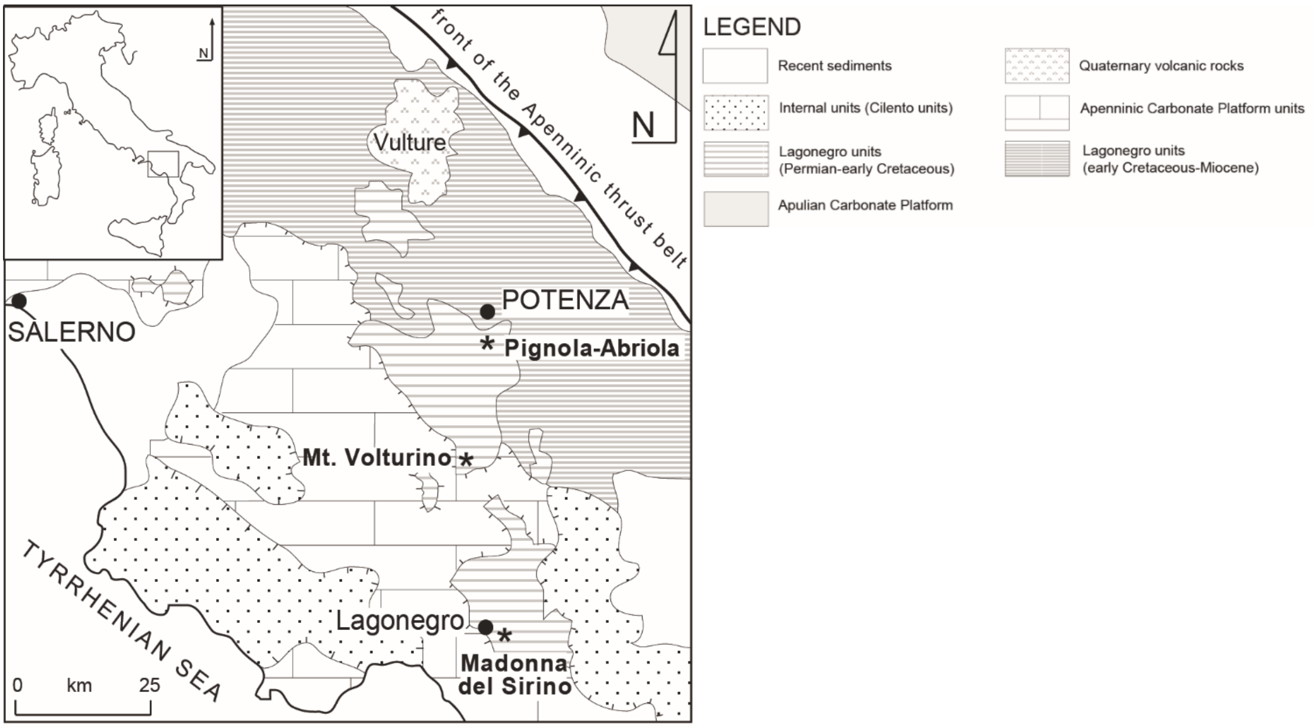

Fig. 1.1 Structural map showing the tectonic units of the Lagonegro Basin. The outcrops of the studied sections are marked by black solid stars. Modified from Bertinelli et al. (2005b).

Pignola-Abriola section

The Pignola-Abriola section crops out along the road between the villages of Pignola and Abriola (Potenza province, southern Italy) on the mountainside of Mt Crocetta (Geographic coordinate system, datum WGS 84: 40° 330 23.50″ N, 15° 470 1.71″ E). This section spans from the upper part of the Calcari con Selce, where the Norian-Rhaetian transition is documented (Amodeo, 1999;

Bazzucchi et al., 2005; Rigo et al., 2005, 2016; Tanner et al., 2006; Giordano et al., 2010), to the lowermost part of the Scisti Silicei. The Pignola-Abriola section lacks the red shales level of the "transitional interval" that conventionally marks the uppermost portion of Calcari con Selce. The basal part (from 0 to 13 m) of the Pignola-Abriola section consists of thin-bedded cherty limestones, sometimes dolomitized, shales and rare thin layers of calcarenites with platform-derived bioclasts. The overlying 37 meters consist of alternations of dark grey shales, thin beds of limestones and black cherty layers. This part of the section is characterized by a progressive decrease in the relative abundance of carbonates in favor of the cherty and siliceous components (Amodeo, 1999; Bazzucchi et al., 2005; Rigo et al., 2005; Tanner et al., 2006; Giordano et al., 2010). Repeated thin and well laminated interbeds of black shales with the shaly interval across and above the NRB suggest a transient period between suboxic/anoxic to more oxic conditions (Casacci et al., 2016). The observed sedimentation pattern suggests that the Pignola-Abriola section belongs to the intermediate facies association (Scandone, 1967; Rigo et al., 2005; Giordano et al., 2010; Casacci et al., 2016).

The Pignola-Abriola section yields rich assemblages of conodonts and pyritized radiolarians (Bazzucchi et al., 2005; Rigo et al., 2005, 2016; Bertinelli et al., 2016), which were used to construct a biostratigraphic framework for the section (Fig. 1.2), following the conodont and radiolarian biozonations proposed respectively by Kozur & Mock (1991) and Carter (1993) and summarized in Rigo et al. (2016) and Bertinelli et al. (2016). The conodont alteration index (CAI) of the Pignola-Abriola specimens is ≤1.5 (Giordano et al., 2010). *Mockina zapfei* and *Mockina slovakensis* are present from the base of the section (Giordano et al., 2010). *Mockina bidentata* is recovered from ca. 7 m, defining the base of the *M. bidentata* Zone (Kozur & Mock, 1991; Giordano et al., 2010). The Lowest Occurence (LO) of the conodont *Misikella hernsteini* marks the base of the *M. hernsteini – P. andrusovi* Zone (Kozur & Mock, 1991), at meter 21.4 (Giordano et al., 2010). *Misikella hernsteini* occurs with *Norigondolella steinbergensis* and *Parvigondolella andrusovi.* At ca. 32 m, the first occurrence of *M. hernsteini/Misikella posthernsteini* transitional form is observed. At 44.9 m *Misikella koessenensis* and *M. posthernsteini* appear. The First Appearance Datum (FAD) of *M. posthernsteini* delineates the base of the Rhaetian stage and defines the base of the eponymous conodont biozone (Kozur & Mock, 1991; Giordano et al., 2010). *Misikella ultima* appears at ca. 54.2 m with *Misikella kovacsi*.

The radiolarians are generally pyritized and not well preserved, but are still useful in allowing the recognition of two assemblage zone boundaries: the base of the *Betraccium deweveri* Assemblage Zone (Carter, 1993) at ca. 22 m (late Norian in age), and the base of the *Proparvicingula moniliformis* Assemblage Zone at 41 m.

Mt Volturino section

The Mt Volturino section is located along the southern slope of Mt Volturino (Geographical coordinate system, datum WGS 84: 40°24013.46″ N; 15°4902.25″ E). This succession can be ascribed to the Calcari con Selce and the Scisti Silicei. The basal part of the section is characterized by red shales ascribed to the "transitional interval" (Giordano et al., 2010, 2011). The overlying 56 meters consists of cherty limestones with red shale intercalations, red cherts, radiolarites, black siliceous shales and silicified calcarenites rich in organic matter (Giordano et al., 2010, 2011; Rigo et al., 2016). This section belongs to the intermediate facies association (Scandone, 1967; Giordano et al., 2010, 2011).

The "transitional interval" is characterized by a rich assemblage of conodonts and several pyritized radiolarians, unlike the Scisti Silicei that provides a good assemblage of radiolarians but few conodonts (Fig. 1.2). The CAI of the Mt Volturino specimens is 3 (Giordano et al., 2010, 2011). *Parvigondolella lata*, *M. bidentata* and *P. andrusovi* first occur at ca. 12 m. The FO (First Occurrence) of *M. hernsteini*, which defines the base of the *M. hernsteini – P. andrusovi* Zone (Kozur & Mock, 1991; Giordano et al., 2010, 2011), occurs at ca. 18 m along with *Parvigondolella vrielyncki*. At ca. 39 m, *M. hernsteini/M. posthernsteini* transitional form (Giordano *et al*., 2010, 2011) first occurs. Unfortunately, radiolarians from the "transitional interval" are very poorly preserved (Giordano et al., 2010). The base of the *B. deweveri* Assemblage Zone (Carter, 1993) occurs at 41 m. The base of the *P. moniliformis* Zone occurs at 45 m, while the base of the *Globolaxtorum tozeri* Zone is at 51 m (Giordano et al., 2010, 2011). The Rhaetian/Hettangian boundary is approximately located in the upper portion of the section, within the Nevera Member of the Scisti Silicei (Fig. 1.2; Bertinelli, 2003).

Madonna del Sirino section

The section of Madonna del Sirino is located on the western flank of Mt Sirino, along the trail connecting the Madonna del Brusco Sanctuary to the Madonna del Sirino Sanctuary (Geographic coordinate system, datum WGS 84. 40°07′ N; 15°48′ E). The upper part of the Calcari con Selce and the Scisti Silicei are exposed in this section. The Calcari con Selce consists of well-bedded micritic limestones, commonly with cherty nodules. The red horizon distinctive of the "transitional interval" lies in the upper part of Calcari con Selce exposed at this section (Reggiani et al., 2005; Tanner et al., 2007). This interval consists of siliceous shale and scattered radiolarites (Passeri et al., 2005). The overlying sediments belonging to Scisti Silicei are made up of red and green radiolarian-bearing siliceous shales and cherts with minor calcarenites (Reggiani et al., 2005; Tanner et al., 2007). The

Madonna del Sirino section is characterized by small amount of platform-derived carbonates and slumps and by a reduced thickness of Scisti Silicei, thus it belongs to the distal facies association (Scandone, 1967; Miconnet, 1982; Rigo et al., 2005).

Conodont occurrences are scattered (Fig. 1.2), with a CAI of 3 (Reggiani et al., 2005). In contrast, radiolarians are abundant. *M. bidentata* first occurs at the base of the section, while *P. andrusovi* and *M. hernsteini* appear at ca. 12 m. The FO of *M. hernsteini* marks the base of the *M. hernsteini – P. andrusovi* Zone (Kozur & Mock, 1991). At ca. 25 m, the rich radiolarian assemblages permit the identification of the base of the *P. moniliformis* Zone (Carter, 1993). The base of the *G. tozeri* Zone occurs at ca. 33 m. The Rhaetian/Hettangian boundary is approximately located in the upper portion of the section, within the Nevera Member (Fig. 1.2), between the last occurrence of Rhaetian radiolarians and the first occurrence of Jurassic radiolarians (Reggiani et al., 2005).

Fig. 1.2 Lithostratigraphy, conodont and radiolarian biostratigraphy, TOC and $\delta^{13}C_{org}$ of the Lagonegro sections. Biostratigraphy is based on, and integrated from, the work of Giordano et al. (2010). Three $\delta^{13}C_{org}$ decreases (S1, S2 and S3, grey bars) are correlated using biostratigraphy. These $\delta^{13}C_{org}$ events show similar magnitude (3-5‰). Their duration have been established using the age model of Pignola-Abriola section provided by Maron et al. (2015): S1=ca. 0.7 My, S2=ca. 1.32 My, S3=ca. 1 My. In particular, the S3 decrease culminated at the Norian/Rhaetian boundary. TOC roughly doubles within S3 at Pignola-Abriola, and begins to increase by the Norian/Rhaetian boundary at the other 2 sections.

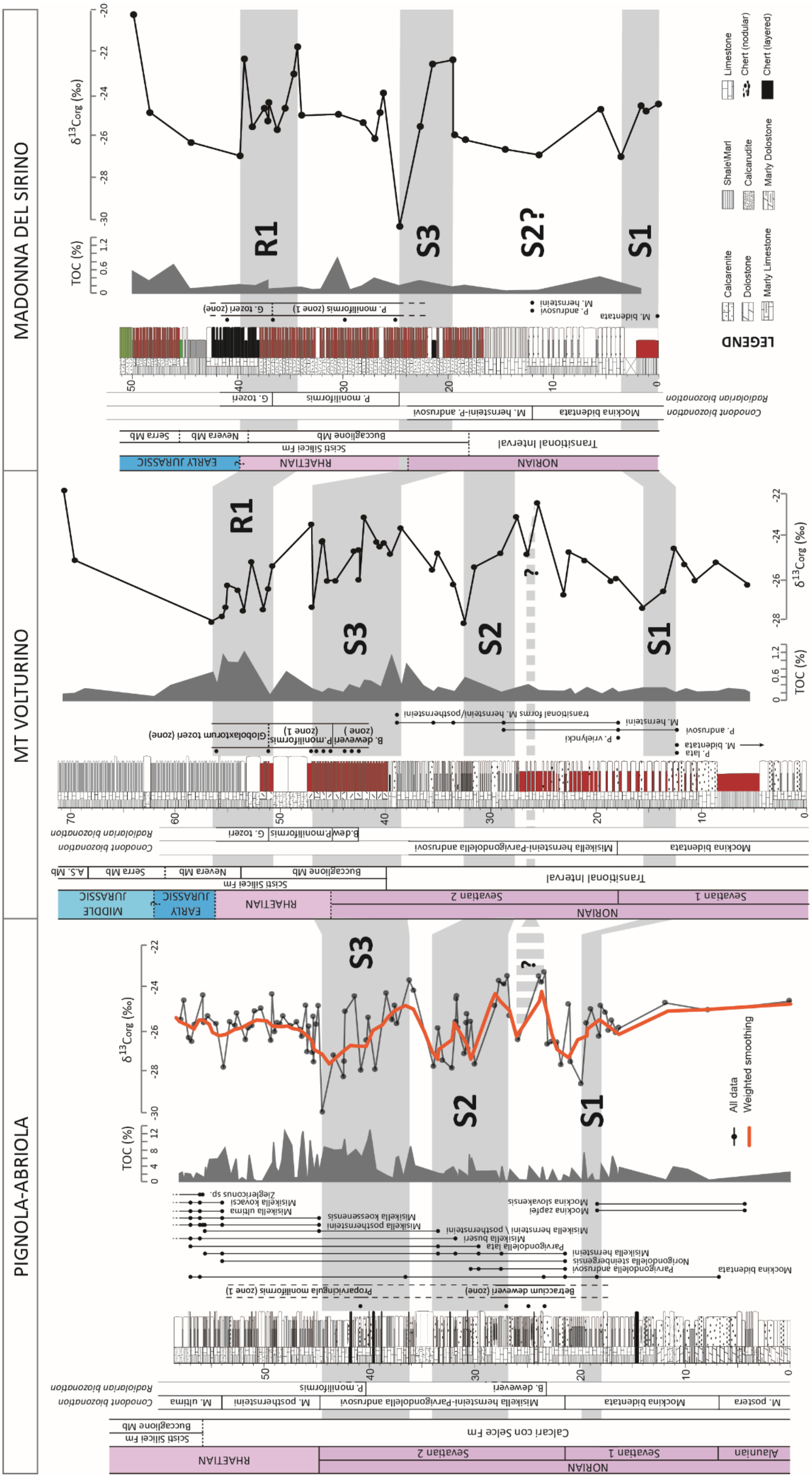

PIGNOLA-ABRIOLA
MT VOLTURINO
MADONNA DEL SIRINO
NORIAN
RHAETIAN
EARLY JURASSIC
MIDDLE JURASSIC
Alaunian
Sevatian 1
Sevatian 2
Calcari con Selce Fm
Scisti Silicei Fm
Buccaglione Mb
Nevera Mb
Serra Mb
Transitional Interval
Conodont biozonation
Radiolarian biozonation
Mockina bidentata
Misikella hernsteini-Parvigondolella andrusovi
M. posthernsteini
M. ultima
M. posterna
B. deweveri
P. moniliformis
G. tozeri
TOC (%)
δ13Corg (‰)
S1
S2
S2?
S3
R1
All data
Weighted smoothing
LEGEND
Calcarenite
Dolostone
Marly Limestone
Shale\Marl
Calcarudite
Marly Dolostone
Limestone
Chert (nodular)
Chert (layered)

METHODS

The Lagonegro Basin has been investigated for Total Organic Carbon (TOC) content and organic carbon isotopes ($\delta^{13}C_{org}$). For the TOC analyses, we analyzed 101 rock samples from the Pignola-Abriola section, 80 samples from the Mt Volturino section and 47 samples from the Madonna del Sirino section. For the $\delta^{13}C_{org}$ analyses, we analyzed 96 samples from the Pignola-Abriola section, 50 samples from the Mt Volturino section and 31 samples from the Madonna del Sirino section (see **Appendix B**). All samples were washed in high-purity water and selected to avoid sampling unrepresentative portions (*e.g.*, fracture-filling mineralization, bioturbation, diagenetic alteration). A few grams of each sample were reduced to a fine powder using a Retsch RM0 grinder and dried overnight at 40°C.

The TOC investigations were conducted at the University of Padova. The powders were treated with a 10% HCl solution in silver capsules to remove inorganic carbon (i.e., carbonate component). Successively, they were dried on a hot plate at 50°C and analyzed using a Vario Macro CNS Elemental Analyzer. Results were calibrated against Sulfanilamide standard (N=16.25%; C=41.81%; S=18.62%; H=4.65%). The analytical uncertainty of the instrument, expressed as relative standard deviation, is σ=0.5%.

For the $\delta^{13}C_{org}$ measurements, all the pulverized rock samples were acid-washed with 10% HCl for at least three hours, usually overnight. Successively, the samples were neutralized in deionized water, dried at 40°C overnight and wrapped in tin capsules. Forty-one samples from the Pignola-Abriola section were analyzed using a GVI Isoprime CF-IRMS mass spectrometer at Rutgers University: multiple blank capsules and certified isotope standards (IAEA N-1 = 0.43‰, IAEA N-3 = 4.72 ‰, NBS 22 = -30.03‰; Coplen et al., 2006) and an in-house sediment standard were added for every batch of isotopic analysis. The standard deviation of the in-house standards during the period of analyses was better than 0.2‰. The other sixty samples from the Pignola-Abriola section and the samples from all the other sections were analyzed using a Delta V Advantage mass spectrometer connected to a Flash HT Elemental Analyzer at the University of Padova. For every set of analysis, multiple blank capsules and isotope standards (IAEA CH-6 = -10.45‰, IAEA CH-7 = -32.15‰, Coplen et al., 2006) were included. The standard deviation of the in-house standard during the period of analyses was better than 0.3‰.

Duration of isotopic excursions has been calculated by applying the age model proposed by Maron et al. (2015) on the Pignola-Abriola section (see **Appendix B**). This model is based on the magnetostratigraphic correlation with the Newark APTS (Maron et al., 2015).

RESULTS

We construct late Norian global $\delta^{13}C_{org}$ records for three sections outcropping in the Lagonegro Basin (southern Italy). Several lines of evidence indicate that our $\delta^{13}C_{org}$ data record a pristine signal. First, the conodont alteration index (CAI) of specimens recovered in the Lagonegro Basin ranges between ≤1.5 (Pignola-Abriola; Giordano et al., 2010) and 3 (Mt Volturino and Madonna del Sirino; Bazzucchi et al., 2005; Reggiani et al., 2005; Rigo et al., 2005, 2012a), suggesting that the burial temperatures never exceeded 100°C (Epstein et al., 1977; Di Leo et al., 2003) and 200°C (Epstein et al., 1977; Bazzucchi et al., 2005; Reggiani et al., 2005; Rigo et al., 2005, 2012a), respectively. The effect of these temperatures is negligible on the $\delta^{13}C_{org}$ signal, because temperatures approaching those of oil generation are required to significantly alter the $\delta^{13}C_{org}$ primary signal (Cramer and Saltzman, 2007). Second, the Pignola-Abriola $\delta^{13}C_{org}$ trend is consistent with (and adds significant detail to) the $\delta^{13}C_{carb}$ profile illustrated in Preto et al. (2013) for the Norian-Rhaetian interval (S3 in Fig. 1.3).

The Pignola-Abriola $\delta^{13}C_{org}$ profile shows greater detail than the Mt Volturino and Madonna del Sirino profiles. This different resolution is mainly related to the greater abundance of organic matter in the samples (see the TOC content in Fig. 1.2) of the Pignola-Abriola section, which allows us greater density of $\delta^{13}C_{org}$ analyses. They also contain a higher siliciclastic component (i.e., dark shales and marls) and this lithological feature is likely related to the more proximal position of the Pignola-Abriola section within the Lagonegro Basin (Scandone, 1967; Amodeo, 1999; Bertinelli et al., 2005b; Rigo et al., 2005, 2016; Giordano et al., 2010, 2011).

The Pignola-Abriola $\delta^{13}C_{org}$ profile depicts three decreases (S1, S2, S3) followed by a recovery phase toward background values (Fig. 1.2). Using the age model for the Pignola-Abriola section of Maron et al. (2015), it is possible to propose durations for these isotopic excursions.

The first $\delta^{13}C_{org}$ decrease (S1) has an amplitude of ca. 4‰ and occurs within the *Mockina bidentata* Zone, upper Sevatian 1. The recovery phase toward higher values is recorded above the *M. bidentata* and *M. hernsteini – P. andrusovi* Zones, in the Sevatian 2. The duration of S1 is ca. 0.70 My.

The second decrease (S2) predates the first appearance of the *M. hernsteini/posthernsteini* transitional forms (*sensu* Giordano et al., 2010, 2011) and shows an amplitude of ca. 4‰ and lasts for ca. 1.00 My.

The third decrease (S3) in the carbon isotope profile culminates at the Norian/Rhaetian boundary, over the *M. hernsteini – P. andrusovi* and *M. posthernsteini* Zones and within the base of the radiolarian *P. moniliformis* Zone. This decrease reaches the lowest $\delta^{13}C_{org}$ value at the Norian/Rhaetian boundary (*sensu* Maron et al., 2015; Rigo et al., 2016), almost in correspondence to the FAD of the conodont *M. posthernsteini*. It shows the highest amplitude (ca. 6‰) and lasts for ca. 1.33 My. The recovery phase occurs within the *M. posthernsteini* Zone. The return to background $\delta^{13}C_{org}$ values is associated with persistent high TOC content, a feature that is not evident in the recovery phases of S1 and S2.

Using biostratigraphy (conodont and radiolarian biozonations), we try to correlate these three $\delta^{13}C_{org}$ decreases (S1, S2 and S3) with the Mt Volturino and Madonna del Sirino $\delta^{13}C_{org}$ profiles, as shown in Fig. 1.2. In Mt Volturino and Madonna del Sirino, a ca. 4‰ decrease occurs within the *Mockina bidentata* Zone (Fig. 1.2), which has been identified as S1. Within the *M. hernsteini – P. andrusovi* Zone, a ca. 4.5‰ decrease is recorded in the Mt Volturino section, which we correlate with S2. Apparently, S2 is not recorded in Madonna del Sirino, but this could be an artifact due to the low-resolution sampling and the poor biostratigraphic resolution of the section. Notably, S2 is preceded by a ca. 2‰ negative peak (dashed in Fig. 1.2) in both the Pignola-Abriola and Mt Volturino sections, supporting our correlations. However, because this negative peak is constrained by few data and is not documented in Madonna del Sirino section, we conservatively do not use this negative peak for correlations outside the Lagonegro Basin. S3 seems easily correlatable within the Lagonegro Basin: in Mt Volturino and Madonna del Sirino, it reaches its minimum within the base of the radiolarian *P. moniliformis* Zone, depicting an amplitude of ca. 4 and 6‰ respectively (Fig. 1.2). Notably, in Mt Volturino and Madonna del Sirino sections S1-S3 do not show the high-frequency fluctuations that marked the Pignola-Abriola $\delta^{13}C_{org}$ decreases (Fig. 1.2). These high-frequency fluctuations could be explained simply by the different sampling resolution of the study sections, but they could be also the result of a variable mixing of carbon with different isotopic composition, provenance and source in the Pignola-Abriola section, especially if we recall that this is the most proximal site (e.g., Holmden et al., 1998; Veizer et al., 1999; Immenhauser et al., 2003; Swart and Eberli, 2005; Swart, 2008; Muttoni et al., 2014).

In the Madonna del Sirino and Mt Volturino sections, a fourth $\delta^{13}C_{org}$ decrease is recorded in the upper Rhaetian (R1, Fig. 1.2), just below the Rhaetian/Hettangian boundary (201.3 ±0.2; Schoene et al., 2010), within the radiolarian *G. tozeri* Assemblage Zone. The R1 $\delta^{13}C_{org}$ decrease has an amplitude of 5-6‰ and is not documented in the Pignola-Abriola section because this succession terminated before the Triassic/Jurassic boundary (Fig. 1.2).

DISCUSSION

Correlations with published records

The detailed comparison of the studied sections indicates that the carbon isotope records are correlatable within the Lagonegro Basin, especially for S3, suggesting that these recurrent decreases in $\delta^{13}C_{org}$ are likely a common feature within the Basin. The correlation among the studied sections cannot be considered an artifact of the lithostratigraphy, because the base of the Scisti Silicei has been shown to be diachronous within the basin (Giordano et al., 2010, 2011). Moreover, based on chemostratigraphy integrated with biostratigraphy, the isotopic trend appears unrelated to the lithological facies; in fact, coeval shifts are observed in different lithological units (Fig. 1.2).

Only a few other Norian sections have been investigated for the organic carbon isotope record. Wignall et al. (2007) observed a ca. 3‰ negative $\delta^{13}C_{org}$ shift at the Norian/Rhaetian boundary in the composite Lake Williston record (British Columbia, Canada), likely correlatable with our S3 event (Fig. 1.3), based on biostratigraphic constraints. Specifically, the extinction of the large forms of bivalve *Monotis*, the FAD of the conodont *Misikella posthernsteini* and the base of the radiolarian *Proparvicingula moniliformis* Zone are considered virtually coeval biohorizons (Rigo et al., 2016) and have been suggested in fact to be used to approximate the base of the Rhaetian stage (Ogg in Gradstein et al., 2012; Rigo et al., 2016; Bertinelli et al., 2016). Notably, S3 in Lake Williston is not characterized by a highly noisy record as in Pignola-Abriola (Fig. 1.3), where the high-frequency fluctuations are probably due, as discussed above, either to the higher sampling resolution or to mixed carbon sources.

In the Kennecott Point section (Queen Charlotte Islands, British Columbia, Canada), Ward et al. (2004) recognized a positive $\delta^{13}C_{org}$ excursion corresponding with the extinction of the bivalve *Monotis*, at the Norian/Rhaetian boundary, which is interpreted as resulting from enhanced stagnation due to subdued ocean circulation (Sephton et al., 2002; Ward et al., 2004). This result conflicts with the negative $\delta^{13}C_{org}$ shift recorded at the Norian/Rhaetian boundary in the Lagonegro Basin (Maron et al., 2015; Rigo et al., 2016; this work). In fact, Ward et al. (2004) and subsequently Whiteside and Ward (2011) establish the base of the Rhaetian stage at the last occurrence of the bivalve *Monotis*. In their work, Ward et al. (2004) noticed a reduction in maximum *Monotis* shell-size approaching the final extinction. The presence of dwarfed forms has been observed also by McRoberts et al. (2008) and explained as a peculiar feature of *Monotis* around the Norian/Rhaetian boundary in response to stressed environments and/or during recovery phases following mass extinction events. Therefore, the $\delta^{13}C_{org}$ negative peak ($\delta^{13}C_{org}$ = -30.5‰) occurring ca. 10 m below the positive $\delta^{13}C_{org}$ excursion recorded in Kennecott Point section and coinciding with the last occurrence of the large-sized *Monotis* (i.e., ca. 8 cm, Ward et al., 2004) could be correlated with the minimum $\delta^{13}C_{org}$ value reached in S3 in the Lagonegro Basin (Fig. 1.3). Whiteside and Ward (2011) implemented the Kennecott Point $\delta^{13}C_{org}$ record with new data from Frederick Islands (Queen Charlotte Islands, British Columbia, Canada), offering an almost complete Norian organic carbon isotope stratigraphy for the Queen Charlotte Islands. The North American Norian $\delta^{13}C_{org}$ record is characterized by rapid oscillations associated with relatively low faunal generic diversity (Whiteside & Ward, 2011). These carbon cycle perturbations are referred to as a "chaotic carbon interval", which is in contrast to stable carbon isotope intervals characterized by high-richness faunas (Whiteside & Ward, 2011). Using the biostratigraphic constraints proposed by Rigo et al. (2016), the conodont and radiolarian biozones recognized in the Lagonegro Basin can be correlated to the ammonoid biozones of the North America realm. Specifically, the ammonoid *Gnomohalorites cordilleranus* Zone coincides with the conodont *Mockina bidentata* Zone and *Parvigondolella andrusovi-Misikella hernsteini* Zone, while the *Paracochloceras amoenum* Zone corresponds to the conodont *M. posthernsteini* Zone and radiolarian *Proparvicingula moniliformis* Zone (Orchard, 1991; Carter, 1993; Dagys & Dagys, 1994; McRoberts et al., 2008). Therefore, we tentatively correlated S1 and S2 with the two Norian decreases recorded at Queen Charlotte Islands as shown in Fig. 1.3. In agreement with the biostratigraphic correlations summarized in Rigo et al. (2016), S1 and S2 should occur within the base of the ammonoid *G. cordilleranus* Zone, while S3 should reach its minimum close both to the base of the ammonoid *P. amoenum* Zone and the disappearance of large forms of bivalve *Monotis*. As already demonstrated, a significant negative peak occurred in correspondence to the extinction of the Norian *Monotis* forms, which we correlated to the S3 minimum. According to this correlation, the observed $\delta^{13}C$ perturbations can be traced over wide areas (i.e., North America and Tethys domains): in fact, the Lagonegro Basin was located on the eastern side of the supercontinent Pangaea while the Queen Charlotte Islands were positioned on the other side of the Panthalassa Ocean during the Norian (Fig. 1.3). These results consequently suggest a global significance of the $\delta^{13}C$ perturbations and, in turn, of the mechanisms affecting the organic carbon record during the late Norian.

Causes of carbon cycle perturbations

The multiple $\delta^{13}C_{org}$ events documented in the Norian were likely caused by retention of ^{12}C or the release of isotopically light carbon into the atmosphere-ocean system. This relative increase in ^{12}C can originate from different mechanisms, such as the isolation of an epeiric sea, a decrease in primary productivity, or input of ^{12}C from a comet impact, methane hydrate dissociation, peatland thermal decomposition and/or enhanced magmatic activity (e.g., Kent et al., 2003; Hesselbo et al., 2004;

Higgins and Schrag, 2006; Jenkyns, 2010; Tanner, 2010; Meyers, 2014; Schaller et al., 2016). S1 and S2 are recognizable at least at a basinal level, while S3 seems to have a more convincing global occurrence (Rigo et al., 2016). Therefore, since S1-S2 and S3, are likely different in nature, different causative mechanisms should be invoked to explain these perturbations in the $\delta^{13}C_{org}$ curve.

S1 and S2 require some local mechanism(s) affecting the Lagonegro Basin during the late Norian. These two decreases might be explained as the result of changes in relative contributions of $\delta^{13}C_{org}$ components. Organic matter present in sediments can be constituted by a number of different components, such as bacteria, phytoplankton, zooplankton, pollen and/or other terrestrial biomass. Each of these components is characterized by a specific value of $\delta^{13}C_{org}$. This means that changes in relative contributions of these components could affect the bulk $\delta^{13}C_{org}$ record, without necessarily requiring changes in the global isotope composition of the ocean and/or the atmosphere (van de Schootbrugge et al., 2008; Fio et al., 2010, Bartolini et al., 2012), which instead would be reflected as global $\delta^{13}C_{org}$ variations.

The interpretation of S3 requires a more comprehensive discussion. Because this $\delta^{13}C_{org}$ decrease has been clearly recognized on both sides of the supercontinent Pangaea, we should consider only those mechanisms able to affect the global carbon cycle. Therefore, we can exclude some of the above-listed hypotheses. First, it is well established that the Lagonegro Basin was a branch of the western Tethys, not an epeiric sea (Sengor et al., 1984; Stampfli et al., 1991; Catalano et al., 1991; Stampfli & Marchant, 1995; Stampfli et al., 1998; Ciarapica & Passeri, 1998, 2002; Stampfli et al., 2003; Speranza et al., 2012). Second, the decrease in primary productivity, as explanation for $\delta^{13}C_{org}$ decrease, should result in a TOC decrease; instead, TOC maintains almost constant values throughout the Lagonegro Basin record and even increases in the Pignola-Abriola S3, where it roughly doubles (Fig. 1.2). Third, a comet impact can release ca. 10^2 to 10^3 Gt of light carbon ($\delta^{13}C$ = -45‰) depending on its size (Greenberg, 1998), producing a rapid (less than 1 kyr) negative shift in the $\delta^{13}C$ values of ca 0.2-1.6‰ (Kaiho et al., 2009; Kent et al. 2003). A comet impact is thus able to cause sudden and short-lived decreases in the $\delta^{13}C$ record, which contrasts with the gradual and relatively slow decreases over S3 of the studied $\delta^{13}C_{org}$ profiles. Moreover, the only impact structure crater documented in the upper Norian is the Manicougan crater, which has a radiometric age of ca. 214.5 (214.5±0.5 Ma with $^{40}Ar/^{39}Ar$ and 214.56±0.05 Ma with U/Pb dating, Ramezani et al., 2005), ca. 3 Myr before S1, discarding the idea of a comet as the main trigger for S3.

Among the remaining hypotheses, the most plausible mechanism able to introduce isotopically light carbon into the atmosphere-ocean system throughout the latest Norian is the injection of volcanogenic greenhouse gases. The Rhaetian $\delta^{13}C_{org}$ decrease (R1) might instead be correlated with the negative organic carbon isotope excursion recognized worldwide just before the Triassic/Jurassic boundary, the so-called initial negative Carbon Isotope Excursion (CIE) (McElwain et al., 1999; Palfy et al., 2001, 2007; Hesselbo et al., 2002; Dal Corso et al., 2013). The initial CIE is proposed as a prelude phase of the main CAMP activity (e.g., Hesselbo et al., 2002; Guex et al., 2004; Whiteside et al., 2010; Ruhl et al., 2011; Dal Corso et al., 2013). If this is true, the Norian organic carbon isotope perturbations recorded in the Lagonegro Basin could be interpreted as pulsed pre-CAMP volcanic activity and S3 might have been caused by a separate input of volcanogenic CO_2 to the atmosphere-ocean system. We cannot exclude a priori that S1 and S2 also might be the result of inputs of volcanogenic CO_2. In fact, the recurrent $\delta^{13}C_{org}$ decreases (S1, S2, S3) during the Norian could be interpreted as representing the typical pulsing behavior of magmatic activity (e.g., Tolan et al., 1989; Saunders et al., 1997; Courtillot & Renne, 2003; Jerram & Widdowson, 2005; Ernst et al., 2008; Greene et al., 2012). We cannot exclude that S1 and S2 might occur at global scale, but we were not able to recognize them in the North American Lake Williston section as this succession covers a limited interval across only the Norian/Rhaetian boundary $\delta^{13}C_{org}$. Moreover, the correlation with the composite British Columbia Islands succession is not straightforward because of a gap immediately below the Norian/Rhaetian boundary (see *Discussion - Correlations with published records*). Nevertheless, in order to take into consideration on one hand results and on the other hand the reliability of proposed correlations, the following interpretations can be considered pertinent for S3 and hypothetical for S1 and S2.

These volcanic emissions would have enhanced chemical weathering via acceleration of the hydrological cycle and increased nutrient discharge (e.g., nitrates and phosphates) to the ocean, driving increased biological productivity (e.g., Jones and Jenkyns, 2001; Jenkyns, 2010; Pogge Von Strandmann et al., 2013) and resulting in high TOC content, which is observed in the case of the Pignola-Abriola S3 event.

These recurrent inputs of isotopically light carbon are recorded also in the Norian-Rhaetian composite $\delta^{13}C_{carb}$ profile constructed by Muttoni et al. (2014) (Fig. 1.3). This composite $\delta^{13}C_{carb}$ curve depicts three negative peaks at ca. 212, 206 and 202 Ma, correlatable with the dating of the minimum $\delta^{13}C_{org}$ values of S1, S3 and R1 respectively (ca. 211.5, 206 and 201 Ma; Fig. 1.3). Unfortunately, this $\delta^{13}C_{carb}$ curve (Muttoni et al., 2014) has a gap exactly in the interval between 209 and 207 Ma, when S2 may have occurred. To further support the global significance of S3 we also compare our data with the $\delta^{13}C_{carb}$ profile of Korte et al. (2005), which displays a minimum value of the $\delta^{13}C_{carb}$ at ca. 206 Ma, correlatable with the S3 negative $\delta^{13}C_{org}$ peak at Pignola-Abriola (Fig. 1.3). This line of evidence further highlights the global meaning of the Norian/Rhaetian boundary carbon cycle perturbation (i.e., S3).

The occurrence of Norian volcanic activity is also supported by an increase of surface water temperature of the Tethyan subtropics of ca. 6°C (~1.5‰), recorded in the $\delta^{18}O_{phos}$ curve from biogenic apatite (labeled "W3" in Trotter et al., 2015). The W3 warming phase is documented in the Norian and is correlatable with S1, S2 and S3 $\delta^{13}C_{org}$ decreases (Fig. 1.3). A late Norian warming is further supported by paleobotanical and pedogenic evidence, which estimate an increase of atmospheric CO_2 from 600 to 2100-2400 ppm and 2000-3000 ppm, corresponding to a warming of ca. 3-4°C and 7-10°C, respectively (McElwain et al., 1999; Cleveland et al., 2008). The proposed scenario is hence in agreement with estimates based on numerical coupled ocean-atmospheric climate models performed for the Upper Triassic (Huynh and Poulsen, 2005).

An additional piece of evidence supporting the hypothesis of a magmatic activity as the source of isotopically light carbon in the system is the $^{87}Sr/^{86}Sr$ record (Callegaro et al., 2012). Because the residence time of strontium is longer (ca. 2.4 My; Jones and Jenkyns, 2001) than the mixing time of the ocean (ca. 1-2 ky; e.g., Broecker and Li, 1970; Gordon, 1973; Hodell et al., 1990; Garret and Laurent, 2002), the $^{87}Sr/^{86}Sr$ curve is representative of the global seawater composition (Veizer et al., 1997; Korte et al., 2003). The $^{87}Sr/^{86}Sr$ composition of seawater is controlled by two major fluxes: the riverine flux, whose $^{87}Sr/^{86}Sr$ depends on the balance between the weathering of highly radiogenic old sialic crust and less radiogenic young basalts (average $^{87}Sr/^{86}Sr$=ca. 0.710) and the hydrothermal flux, sourced from the mantle ^{86}Sr (average $^{87}Sr/^{86}Sr$=ca. 0.703 (e.g., Faure, 1986; Palmer and Edmond, 1989; Veizer et al., 1997; Taylor and Lasaga, 1999). Therefore, increases of seawater $^{87}Sr/^{86}Sr$ are commonly interpreted as increased continental weathering of highly radiogenic old sialic crust and/or denudation rates, which in turn could be driven by humid climate and/or tectonics (Palmer and Elderfield, 1985; Raymo et al., 1988; Hodell et al., 1989), whereas negative shifts are usually linked to weathering of young basalts (which implies the emplacement of some kind of volcanic activity) and/or increased rate of seafloor spreading (Berner and Rye, 1992; Jones and Jenkyns, 2001). The $^{87}Sr/^{86}Sr$ profile (Callegaro et al., 2012) depicts three negative excursions correlatable with the $\delta^{13}C_{org}$ decreases recognized throughout the late Norian in the Lagonegro Basin, Queen Charlotte Islands and Lake Williston sections (Fig. 1.3). However, at the base of the Rhaetian stage, the $^{87}Sr/^{86}Sr$ curve shows an opposite trend compared to the $\delta^{13}C_{org}$ record: in fact, while the $\delta^{13}C_{org}$ returns to background values, the $^{87}Sr/^{86}Sr$ profile keeps decreasing, suggesting two possible scenarios: 1) a lag in response time of the $^{87}Sr/^{86}Sr$ system due to its longer seawater residence time; or 2) persistent magmatic activity and/or weathering of volcanic rocks, coupled with increase of primary productivity and/or inhibition of the organic matter oxidation processes (increasing $\delta^{13}C_{org}$). The decrease in efficiency of organic matter recycling mechanisms may be related to oxygen-depleted conditions, which is supported by the high TOC content (Fig. 1.2, see TOC content after S3 in Pignola-Abriola). Moreover, the Rhaetian $\delta^{13}C_{org}$ profile is mimicked by the $^{187}Os/^{188}Os$ curve recorded in Japan (Kuroda et al., 2010) and in the UK (Cohen & Coe, 2007), suggesting that an abrupt and intense large-scale event affected multiple isotopic systems during the Late Triassic, causing large perturbations in the $\delta^{13}C_{org}$, $\delta^{13}C_{carb}$, $^{87}Sr/^{86}Sr$ and $^{187}Os/^{188}Os$ recordsSeawater $^{187}Os/^{188}Os$, like $^{87}Sr/^{86}Sr$, is controlled by two major fluxes: i) weathering of continental crust (average $^{188}Os/^{187}Os$ = ca. 1.3); and ii) mantle/extraterrestrial inputs (average $^{188}Os/^{187}Os$ =ca. 0.13) (e.g., Shirey and Walker, 1998; Peucker-Ehrenbrink and Ravizza, 2000; Cohen & Coe, 2007; Kuroda et al., 2010). In particular, young, mantle-derived basalts could release large amounts of unradiogenic Os. Based on this rationale, Os isotopes are used to identify the initiation of major flood basalt volcanism (e.g., Cohen and Coe, 2002; Ravizza and Peucker-Ehrenbrink, 2003; Turgeon and Creaser, 2008; Tejada et al., 2009; Kuroda et al., 2010).

The late Norian volcanic activity seems to resemble the best-known Mesozoic LIPs, such as the Wrangellia (estimated duration: late Ladinian-early Norian, U-Pb zircon dating from a gabbro sill: 232.2±1.0 Ma, Mortensen and Hulbert, 1991), the CAMP (estimated duration: late Rhaetian-early Hettangian, U-Pb zircon dating of the North Mountain basalt: 201.56±0.01/0.22 Ma, e.g. Marzoli et al., 2006a, 2006b; Blackburn et al., 2013) and the Karoo-Ferrar (Toarcian, 183.1 Ma, e.g., Bomfleur et al., 2014; Sell et al., 2014). The emplacement of all these LIPs coincides with episodes of significant biotic crises, suggesting that a causal relationship might exist with eruptions and climate change (e.g., Rampino & Stothers, 1988; Furin et al., 2006; Rigo et al., 2007, 2010, 2012a). With respect to the tempo, the estimated duration of the Norian activity is very similar to those inferred for the CAMP and the Wrangellia. The main phase of CAMP volcanism lasted less than 1.6-2 My, a comparable duration of 2 My has been proposed for the Wrangellia phase (Greene et al., 2009, 2012). These durations are consistent with those estimated in the Pignola-Abriola section, where the $\delta^{13}C_{org}$ decreases last between 0.7-1.3 My. The total duration of the late Norian volcanic activity, from S1 to S3, is ca. 7 My, if the age model of Maron et al. (2015) is adopted; this is consistent with the total duration of the Karoo-Ferrar event (ca. 8-10 My; Jourdan et al., 2007; Hastie et al., 2014) and of each major pulse of the Karoo-Ferrar LIP, which lasts from ca. 0.8 to 3-4.5 My (Jourdan et al., 2007). All these estimated durations are comparable to those observed in the Pignola-Abriola section during the late Norian (ca. 1.3 My for each decrease).

The sparse and rare outcrops of Norian successions limit the recognition of volcanic deposits associated with the emplacement of a LIP during the late Norian, which is identifiable so far only by its geochemical signatures. Volcanic deposits linked to this event could have undergone subduction, accretion as allochtonous terranes or collision. Nevertheless, recent dating of the Late Triassic Angayucham large igneous province (Alaska, Pallister et al., 1989) gives an estimated age of 214±7 Ma (Ernst and Buchan, 2001; Prokoph et al., 2013). This datum is consistent with both the Norian age of the $^{87}Sr/^{86}Sr$ and $\delta^{13}C_{org}$ decreases (from ca. 214 to 206 Ma: Maron et al., 2015) and distinguishable from those of Wrangellia (late Ladinian-early Norian, Mortensen and Hulbert, 1991) and CAMP activities (late Rhaetian-early Hettangian, e.g. Marzoli et al., 2006a, 2006b; Blackburn et al., 2013). The total volume of the Angayucham oceanic plateau has been evaluated from the areal extent of outcropping ophiolites, and the most recent estimates range between 225 and 450 10^3 km^3 (Ernst and Buchan, 2001; Prokoph et al., 2013). This volume is not dissimilar from that of the Wrangellia oceanic plateau (ca. 500-1000 10^3 km^3; Lassiter et al., 1995; Ernst and Buchan, 2001; Prokoph et al., 2008), although it is one order of magnitude smaller than the volume estimated for the CAMP deposits (ca. 2500 10^3 km^3) and the Karoo-Ferrar continental flood basalts (ca. 5000 10^3 km^3) (Ernst and Buchan, 2011; Prokoph et al., 2008). Even if LIPs are assumed to outgas SO_2 and CO_2 at significant rates (e.g., the CAMP is thought to outgas SO_2 and CO_2 at rates of at most 1 Gt per year; Self et al., 2005), CO_2 emissions alone may not be sufficient to account for the significant magnitude of the Norian LIP $\delta^{13}C_{org}$ decreases (e.g., even up to 6‰ for Pignola-Abriola S3, this work). Therefore, some other mechanism(s) might further contribute to the effects of the Norian LIP emissions on the carbon isotopic system. For instance, fire scars left on fossil tree trunks from the Petrified Forest Member of the Upper Triassic Chinle Formation (Arizona, US) provide evidence of widespread peatland fires throughout the Norian and likely throughout the whole Late Triassic (Byers et al., 2014). The age of these wildfires ranges from 213.1 to 209 Ma (Ramezani et al., 2011; Byers et al., 2014), within the estimated duration of the Norian LIP activity ("Wildfires" in Fig. 1.3). The carbon isotopic composition of land-plant organic matter can reach values up to ca. -35‰ (e.g., Meyers, 2014). As a consequence, these wildfires could play a role in explaining the large magnitude of the Norian $\delta^{13}C_{org}$ decreases. Finally, the intense warming indicated by the oxygen isotopic record (Trotter et al, 2015) which could have occurred due to the emplacement of a Norian LIP with its associated CO_2 flux (see different CO_2 models above), might have destabilized methane hydrate reservoirs ($\delta^{13}C$=−60‰), which could have further increased the amplitude of the observed carbon isotope excursions. This mechanism has already been proposed to explain short-term changes during the Karoo-Ferrar carbon isotope excursion (Kemp et al., 2005). Therefore, wildfires and clathrate dissociation may account for the minor negative peaks, the high-frequency fluctuations and the total amplitude of changes recognized along the $\delta^{13}C_{org}$ profiles with higher resolution datasets (Fig. 1.3). It is also worth noting that the estimated durations for the secondary and short-lived $\delta^{13}C_{org}$ peaks in the Pignola-Abriola section range between ca. 10 and 100 kyr according to the age model of Maron et al. (2015), which essentially means that each single peak might represent an input of ^{12}C-rich carbon in the ocean-atmosphere system due to a combination of possible sources which include volcanogenic gases, methane-release and wildfires. Whereas wildfires and methane hydrate dissociation contributed to the magnitude of the Norian $\delta^{13}C_{org}$ decreases, they have to be considered as possible amplification factors of the magmatic activity, which we propose as the trigger mechanism of the Norian carbon cycle perturbations.

Fig. 1.3 Correlation of the Lagonegro $\delta^{13}C_{org}$ profiles with other records from literature. Isotopic profiles from: i) Kennecott Point section, Queen Charlotte Islands, British Columbia, Canada (Whiteside et al., 2010); ii) $\delta^{13}C_{org}$ and $\delta^{13}C_{carb}$ of Pignola-Abriola section, Lagonegro Basin, Italy (this work, chronology by Maron et al., 2015; $\delta^{13}C_{carb}$ record modified from Preto et al., 2013); iii) composite $\delta^{13}C_{carb}$ record from Muttoni et al. (2014): Pizzo Mondello (southern Italy, from ca. 215 to ca. 209 Ma) + Brumano (northern Italy, from ca. 206 to ca. 202 Ma) + Italcementi Quarry (northern Italy, dashed line); iv) composite $\delta^{13}C_{carb}$ record from Korte et al. (2005); v) Mt Volturino section, Lagonegro Basin, Italy (this work); vi) Madonna del Sirino section, Lagonegro Basin, Italy (this work); vii) composite profile for Queen Charlotte Islands: Kennecott Point (from 0 to 120 m) + Frederick Islands (from -215 to -135m) (Whiteside and Ward, 2011); viii) Lake Williston, British Columbia, Canada (Wignall et al., 2007); ix) $^{87}Sr/^{86}Sr$ profile from Callegaro et al. (2010). $\delta^{13}C_{org}$ correlations rely on chemostratigraphy and biostratigraphy. Biostratigraphic correlations between ammonoid and conodont biozones are based on Rigo et al. (2015). The carbon isotope stratigraphy of the North America and Tethys realms depicts three decreases of similar magnitude (3-5‰) and duration (ca. 1.3 My) throughout the late Norian (S1, S2 and S3, highlighted by grey bars). They correlate with the decreases in the $^{87}Sr/^{86}Sr$ record (Callegaro et al., 2010). All these oscillations occur within the W3 warming interval (sensu Trotter et al., 2015; blue and red bar). Fire scars (red bar) left on petrified trunks, indicating wildfires, show similar age (Norian) (Byers et al., 2014). The the Late Triassic Angayucham large igneous province (Alaska) paleogeographic position (Sussman and Weil, 2004) is shown as a red dotted circle on the map; the age of the Angayucham LIP is 214±7 Ma (Ernst and Buchan, 2001; Prokoph et al., 2013), compatible with the Norian carbon and strontium decreases. The late Rhaetian-early Hettangian $\delta^{13}C_{org}$ signature of the CAMP is highlighted by R1 grey bar. Its original areal extent (Marzoli et al., 1999) is shown on the map as a grey dotted area. All the discussed sections are shown on the map: 1) British Columbia Islands (Canada); 2) Lake Williston (Canada); and 3) Lagonegro Basin (Italy).

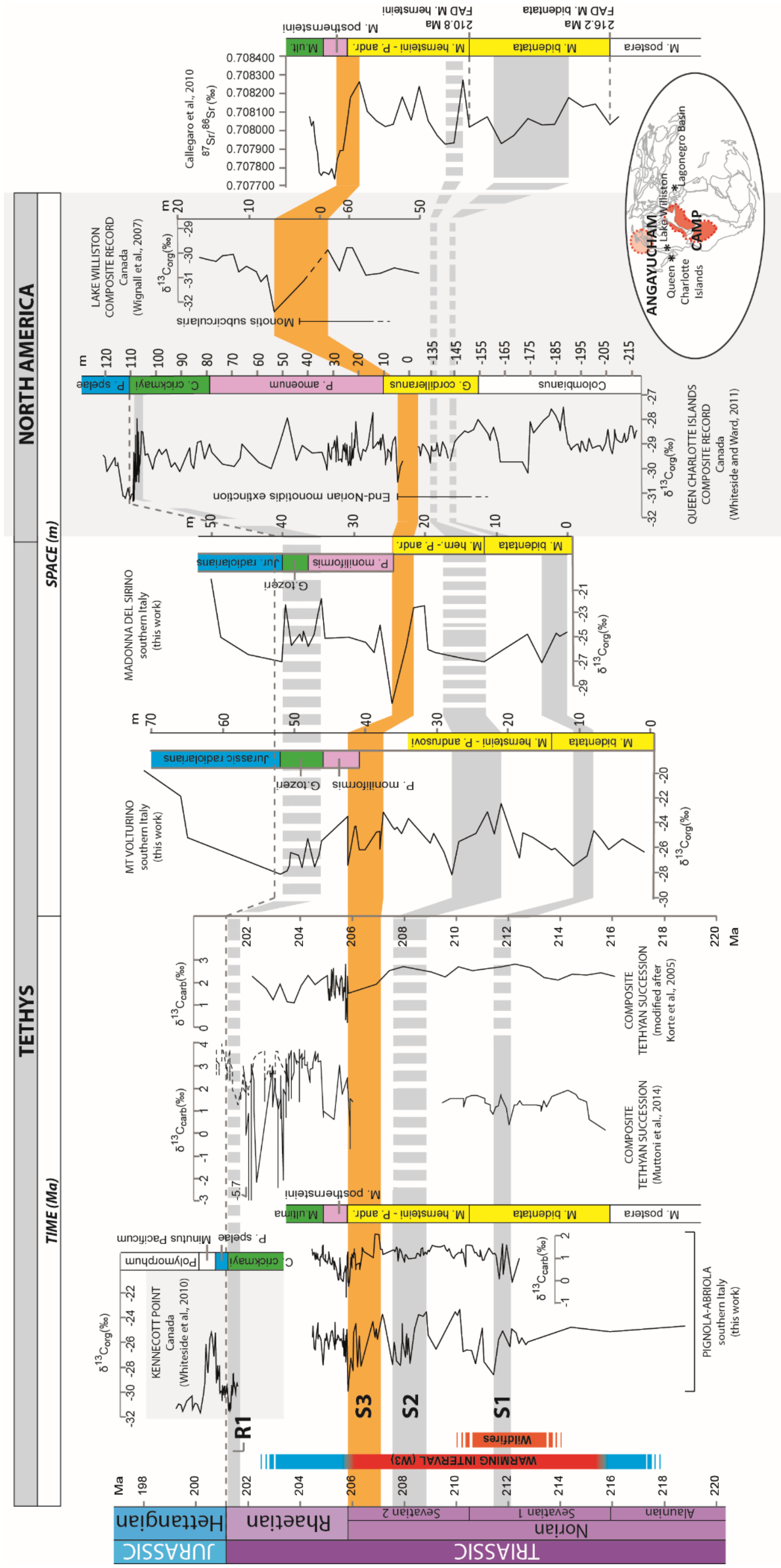

NORTH AMERICA
TETHYS
TIME (Ma)
SPACE (m)
JURASSIC
TRIASSIC
Hettangian
Rhaetian
Norian
Sevatian 2
Sevatian 1
Alaunian
WARMING INTERVAL (W3)
Wildfires
R1
S3
S2
S1
KENNECOTT POINT
Canada
(Whiteside et al., 2010)
PIGNOLA-ABRIOLA
southern Italy
(this work)
COMPOSITE TETHYAN SUCCESSION
(Muttoni et al., 2014)
COMPOSITE TETHYAN SUCCESSION
(modified after Korte et al., 2005)
MT VOLTURINO
southern Italy
(this work)
MADONNA DEL SIRINO
southern Italy
(this work)
QUEEN CHARLOTTE ISLANDS COMPOSITE RECORD
Canada
(Whiteside and Ward, 2011)
LAKE WILLISTON COMPOSITE RECORD
Canada
(Wignall et al., 2007)
Callegaro et al., 2010
End-Norian monotidis extinction
Monotis subcircularis
M. posthernsteini
M. hernsteini - P. andr.
M. bidentata
M. postera
M. ultima
FAD M. hernsteini
210.8 Ma
FAD M. bidentata
216.2 Ma
P. moniliformis
G.tozeri
Jurassic radiolarians
Jur. radiolarians
C. crickmayi
P. spelae
Polymorphum
Minutus Pacificum
P. ammoenum
G. cordilleranus
Colombianus
ANGAYUCHAM
CAMP
Queen Charlotte Islands
Lake Williston
Lagonegro Basin

CONCLUSIONS

The organic carbon isotope record of the Lagonegro Basin (Western Tethys) shows the occurrence of a ca. 5‰ negative shift close to the Norian-Rhaetian transition, preceded by two additional $\delta^{13}C_{org}$ decreases of similar magnitude (3-5‰), correlatable within the Lagonegro Basin. Moreover, the carbon isotope perturbation close to the Norian/Rhaetian boundary is correlatable (using biostratigraphy) with that recognized in the North America realm, supporting the idea that the lateest Norian carbon cycle was affected at a global scale. We propose that the trigger mechanism for the input of isotopically light carbon in the ocean-atmosphere system was the emplacement of a large igneous province, possibly amplified by consequent feedbacks. The $\delta^{18}O_{phos}$ profile, the $^{87}Sr/^{86}Sr$ curve, and increase in the pCO_2 values strongly support this scenario. This suggested late Norian volcanic activity was thought to be active between 214-206 Ma, and is tentatively attributed to the Angayucham province, a complex ocean plateau originally located on the western margin of North America and today outcropping in Alaska. The late Norian $\delta^{13}C_{org}$ records presented here improve the Late Triassic organic carbon isotope record, which displays a series of decreases we link to the emplacement of different LIPs: the late Ladinian-early Norian Wrangellia, the late Norian Angayucham and the late Rhaetian-early Hettangian CAMP. These events may have had extreme environmental consequences,such as a decrease in primary productivity and/or a warming phase, which could have favored the establishment of humid conditions and episodes of seawater oxygen depletion, biotic crises and extinctions, contributing to the complex history of this particular period of time.

ACKNOWLEDGEMENTS

This study was supported by the grant EX60% 60A05-7013/15 to Manuel Rigo and by the University of Padova, CPDA152211/15 (P.I. Manuel Rigo) and CPDA121100/12 (P.I. Nereo Preto). Stable isotope analyses were supported by National Science Foundation grant EAR 0844252 to Linda Godfrey. Acknowledgment is made to the donors of the American Chemical Society Petroleum Research Fund for partial support of this research to Miriam E. Katz (grant 49637-DN18).

References

Amodeo, F., Baumgartner, P.O., 1994, Stratigraphic revision of the Scisti Silicei Formation (Upper Triassic-Upper Jurassic), Lagonegro Basin, southern Italy. Preliminary report: Paleopelagos, v. 4, p. 35-46.

Amodeo, F., 1999, Il Triassico terminale–Giurassico del Bacino Lagonegrese. Studi stratigrafici sugli Scisti Silicei della Basilicata (Italia meridionale): Memoires de Geologie (Lausanne), v. 33, p. 1–123.

Argnani, A., 2005, Possible record of a Triassic ocean in the Southern Apennines: Boll. Soc. Geol. Ital., v. 124, p. 109–121.

Atudorei, N.V., 1999, Constraints on the Upper Permian to Upper Triassic marine carbon isotope curve. Case studies from the Tethys. PhD Thesis: Lausanne University, p. 155.

Bazzucchi, P., Bertinelli, A., Ciarapica, G., Marcucci, M., Passeri, L., Rigo, M. and Roghi, G., 2005, The Late Triassic–Jurassic stratigraphic succession of Pignola (Lagonegro-Molise Basin, Southern Apennines, Italy): Bollettino Società Geologica Italiana, v. 124, p. 143–153.

Benton, M. J. and Twitchett, R. J., 2003, How to kill (almost) all life: the end-Permian extinction event: Trends in Ecology and Evolution, v. 18, p. 358–365.

Berner, R.A., 1982, Burial of organic carbon and pyrite sulfur in the modern ocean: its geochemical and environmental significance: Am. J. Sci., v. 282, p. 451–473.

Berner, R.A., Lasaga, A.C., Garrels, R.M., 1983, The carbonate–silicate geochemical cycle and its effect on atmospheric carbon dioxide over the last 100 million years: Am. J. Sci., v. 283, p. 641–683.

Berner, R.A., and Rye, D.M., 1992, Calculation of the Phanerozoic strontium isortope record of the oceans from a carbon cycle model: American Journal of Science, v. 292, p. 136–148.

Berner, R.A., 1994, GEOCARB II: a revised model of atmospheric CO2 over Phanerozoic time: Am. J. Sci., v. 294, p. 56–91.

Bertinelli, A., 2003, Il Bacino Lagonegrese-Molisano nel contesto della Tetide occidentale durante il Triassico superiore-Giurassico. PhD thesis: Università degli Studi di Perugia, p. 215.

Bertinelli, A., Ciarapica, G. and Passeri, L., 2005a, Late Triassic-Jurassic basinal successions in Molise and northern Basilicata: the northernmost witness of the Lagonegro domain: Bollettino Società Geologica Italiana, v. 124, p. 177–188.

Bertinelli, A., Ciarapica, G., De Zanche, V., Marcucci, M., Mietto, P., Passeri, L., Rigo, M. and Roghi, G., 2005b, Stratigraphic evolution of the Triassic–Jurassic Sasso di Castalda succession (Lagonegro basin, Southern Apennines, Italy): Bollettino Società Geologica Italiana, v. 124, p. 161–175.

Bertinelli, A., Casacci, M., Concheri, G., Gattolin, G., Godfrey, L., Katz, M.E., Maron, M., Mazza, M., Mietto, P., Muttoni, G., Rigo, M., Sprovieri, M., Stellin, F., Zaffani, M., 2016, The Norian/Rhaetian boundary interval at Pignola-Abriola section (southern Apennines, Italy) as a GSSP candidate for the Rhaetian stage: an update: Albertiana, v. 43, p. 6-19.

Blackburn, T.J., Olsen, P.E., Bowring, S.A., McLean, N.M., Kent, D.V., Puffer, J., McHone, G., Rasbury, E.T., Et-Touhami, M., 2013, Zircon U-Pb Geochronology Links the End-Triassic Extinction with the Central Atlantic Magmatic Province: Science, v. 340, p. 941.

Bomfleur, B., Schöner, R., Schneider, J.W., Viereck, L., Kerp, H., McKellar, J.L., 2014, From the Transantarctic Basin to the Ferrar Large Igneous Province-New palynostratigraphic age constraints for Triassic–Jurassic sedimentation and magmatism in East Antarctica: Review of Palaeobotany and Palynology, v. 207, p. 18–37.

Broecker, W.S., Li, Y.H., 1970, Interchange of water between the major oceans: Journal of Geophysical Research, v. 75, p. 3545-3552.

Byers, B.A., Ash, S.R., Chaney, D., DeSoto, L., 2014, First known fire scar on a fossil tree trunk provides evidence of Late Triassic wildfire: Palaeogeography, Palaeoclimatology, Palaeoecology, v. 411, p. 180-187.

Callegaro, S., Rigo, M., Chiaradia, M. & Marzoli, A., 2012, Latest Triassic marine Sr isotopic variations, possible causes and implications: Terra Nova, v. 24, p. 130–135.

Carter, E.S., 1993, Biochronology and Paleontology of uppermost Triassic (Rhaetian) radiolarians, Queen Charlotte Islands, British Columbia, Canada: Memoires de Geologie (Lausanne), v. 11, p. 1–176.

Casacci, M., Bertinelli, A., Algeo, T.J., Rigo, M., 2016, Carbonate to biosilica transition at the Norian-Rhaetian boundary controlled by rift-related subsidence in the western Tethyan

Lagonegro Basin (southern Italy): Palaeogeography, Palaeoclimatology, Palaeoecology, http://dx.doi.org/10.1016/j.palaeo.2016.05.007.

Catalano, R., Doglioni, C. and Merlini, S., 1991, On the Mesozoic Ionian basin: Geophysical Journal International, v. 144, p. 49–64.

Ciarapica, G. and Passeri, L., 1998, Evoluzione paleogeografica degli Appennini: Atti Tic. Sc. Terra, v. 40; p. 233-29.

Ciarapica, G. and Passeri, L., 2002, The palaeogeographic duplicity of the Apennines: Bollettino Della Società Geologica Italiana, v. 121, p. 67–75.

Cleveland, D.M., Nordt, L.C., Dworkin, S.I., Atchley, S.C., 2008, Pedogenic carbonate isotopes as evidence for extreme climatic events preceding the Triassic-Jurassic boundary: implications for the biotic crisis?: Geological Society of America Bullettin, v. 120, p. 1408-1415.

Cohen, A. S., Coe, A. L., 2007, The impact of the Central Atlantic Magmatic Province on climate and on the Sr- and Os-isotope evolution of seawater: Palaeogeogr. Palaeoclimatol. Paleoecol., v. 244, p. 374–390.

Coplen, T.B., Brand, W.A., Gehre, M., Groning, M., Meijer, H.A.J., Toman, B. and Verkouteren, R.M., 2006, New guidelines for $d^{13}C$ measures: Analytical Chemistry, v. 78, p. 2439–2441.

Courtillot, V.E., Renne, P.R., 2003, On the ages of flood basalt events: Geoscience, v. 335, p. 113–140.

Cramer, B.D., Saltzman, M.R., 2007, Early Silurian paired $d^{13}C_{carb}$ and $d^{13}C_{org}$ analyses from the Midcontinent of North America: Implications for paleoceanography and paleoclimate: Palaeogeography, Palaeoclimatology, Palaeoecology, v. 256, p. 195-203.

Dal Corso, J., Marzoli, A., Tateo, F., Jenkyns, H.C., Bertrand, H., Youbi, N., Mahmoudi, A., Font, E., Buratti, N., Cirilli, S., 2013, The dawn of CAMP volcanism and its bearing on the end-Triassic carbon cycle disruption: The Geological Society of London, v. 171, p. 153-164.

Dal Corso, J., Mietto, P., Newton, R.J., Pancost, R.D., Preto, N., Roghi, G., Wignall, P.B., 2014, Discovery of a major negative δ13C spike in the Carnian (Late Triassic) linked to the eruption of Wrangellia flood basalts: Geology, v. 40, p. 79–82, doi:10.1130/G32473.1.

Dal Corso, J., Gianolla, P., Newton, R.J., Franceschi, M., Roghi, G., Caggiati, M., Raucsik, B., Budai, T., Haas, J., Preto, N., 2015, Carbon isotope records reveal synchronicity between carbon cycle perturbation and the “Carnian Pluvial Event” in the Tethys realm (Late Triassic): Global and Planetary Change, v. 127 , p. 79-90.

Dagys, A.S. and Dagys, A.A., 1994, Global correlation of the terminal Triassic. In: Guex, J., Baud, A. (eds): Recent Developments on Triassic Stratigraphy. Memoires de Geologie, Lausanne, v. 22, p. 25–34.

Diakow, L., Orchard, M.J., and Friedman, R., 2011, Absolute ages for the Norian Stage: a contribution from southern British Columbia, Canada: Canadian Paleontology Conference, Proceedings no. 9, p. 27-28.

Diakow, L., Orchard, M.J., and Friedman, R., 2012, Absolute ages for the Norian Stage: a further contribution from southern British Columbia, Canada: Cordilleran Tectonics Workshop, Geological Association Canada, Pacific Section. Program and Abstracts, 2 p.

Ernst, R.E., Buchan, K.L., 2001, Large mafic magmatic events through time and links to mantle-plume heads: Geological Society of America Special Paper, v. 352, p. 483-575.

Ernst, R.E., Wingate, M.T.D., Buchan, K.L., Li, Z.X.., 2008, Global record of 1600–700 Ma Large Igneous Provinces (LIPs): Implications for the reconstruction of the proposed Nuna (Columbia) and Rodinia supercontinents: Precambrian Research, v. 160, p. 159–178, doi: 10.1016/j.precamres.2007.04.019.

Erwin, D. H., 2006, Extinction: How Life on Earth Nearly Ended 250 Million Years Ago: Princeton University Press, Princeton.

Faure, G., 1986, Principles of Isotope Geology: second edition, John Wiley and Sons, New York, p. 589.

Finetti, I., 1982, Structure, stratigraphy and evolution of central Mediterranean: Boll. Geofis. Teor. Appl., v. 24, p. 247–315.

Finetti, I., Lentini, F., Carbone, S., Catalano, S., Del Ben, A., 1996, Il sistema Appennino Meridionale-Arco Calabro-Sicilia nel Mediterraneo Centrale: studio geologico-geofisico: Boll. Soc. Geol. Ital., v. 115, p. 529–559.

Furin, S., Preto, N., Rigo. M., Roghi, G., Gianolla, P., Crowley, J.L. & Bowring, S.A., 2006, High precision U–Pb zircon age from the Triassic of Italy: implications for the Triassic time scale and the Carnian origin of calcareous nannoplankton and dinosaurs: Geology, v. 35, p. 146.

Galli, M.T., Jadoul, F., Bernasconi, S.M., Weissert, H., 2005, Anomalies in global carbon cycling at the Triassic/Jurassic boundary: evidence from a marine C-isotope record: Palaeogeogr. Palaeoclimatol. Palaeoecol., v. 216, p. 203–214.

Galli, M.T., Jadoul, F., Bernasconi, S.M., Cirilli, S., Weissert, H., 2007, Stratigraphy and palaeoenvironmental analysis of the Triassic–Jurassic transition in the western Southern Alps (Northern Italy): Palaeogeogr. Palaeoclimatol. Palaeoecol., v. 244, p. 52–70.

Garrett, C., St. Laurent, L., 2002, Aspects of deep ocean mixing: Journal of Oceanography, v. 58, p. 11-24.

Gawlick, H.J., Bohm, F., 2000, Sequence and isotope stratigraphy of Late Triasic distal periplatform limestones from the Nothern Calcareous Alps (Kälberstein Quarry, Berchtesgaden Hallstatt Zone): Int. J. Earth Sciences, v. 89, p. 108-129.

Giordano, N., Rigo, M., Ciarapica, G. & Bertinelli, A., 2010, New biostratigraphical constraints for the Norian/Rhaetian boundary: data from Lagonegro Basin, Southern Apennines, Italy: Lethaia, v. 43, p. 573–586.

Giordano, N., Ciarapica, G., Bertinelli, A. & Rigo, M., 2011, The Norian-Rhaetian interval in two sections of the Lagonegro area: the transition from carbonate to siliceous deposition: Italian Journal of Geoscience, v. 130, p. 380–393.

Gordon, A. L., 1973, Physical Oceanography Antarctic: Journal of the United States, v. 8, p. 61-69.

Gradstein, F.M., Ogg, J.G., Schmitz, M.D. and Ogg, G.M., eds, 2012, The Geological Time Scale 2012: Amsterdam, Elsevier, 2 vols., 1144 pp.

Greenberg, J.M., 1998, Making a comet nucleus: Astronomy and Astrophysics, v. 330, p. 375–380.

Greene, S.E., Bottjer, D.J., Corsetti, F.A., Berelson, W.M., Zonneveld, J.P., 2010, Might ocean acidification leave a diagenetic record?: Geological Society of America Abstracts with Programs, 42 (5), 437.

Greene, S.E., Martindale, R.C., Ritterbush, K.A., Bottjer, D.J., Corsetti, F.A., Berelson, W.M., 2012, Recognizing ocean acidification in deep time: An evaluation of the evidence for acidification across the Triassic-Jurassic boundary: Earth-Science Reviews, v. 113, p. 72-93.

Guex, J., Bartolini, A., Atudorei, V. & Taylor, D., 2004, High-resolution ammonite and carbon isotope stratigraphy across the Triassic–Jurassic boundary at New York Canyon (Nevada): Earth and Planetary Science Letters, v. 225, p. 29–41.

Hallam, A., 2002, How catastrophic was the end-Triassic mass extinction?: Lethaia, v. 35, p. 147-157.

Hastie, W.W., Watkeys, M.K., Aubourg, C., 2014, Magma flow in dyke swarms of the Karoo LIP: Implications for the mantle plume hypothesis: Gondwana Research, v. 25, p. 736–755.

Hauser, M., Martini, R., Burns, S., Dumitrica, P., Krystyn, L., Matter, A., Peters, T. and Zaninetti, L., 2001, Triassic stratigraphic evolution of the Arabian-Greater India embayment of the southern Tethys margin: Eclogae Geologicae Helvetiae, v. 94, p. 29-62.

Hayes, J.M., Strauss, H., Kaufman, A.J., 1999, The abundance of 13C in marine organic matter and isotopic fractionation in the global biogeochemical cycle of carbon during the past 800 Ma: Chem. Geol., v. 161, p. 103–125.

Hesselbo, S.P., Robinson, S.A., Surlyk, F. & Piasecki, S., 2002, Terrestrial and marine extinction at the Triassic-Jurassic boundary synchronized with major carbon- cycle perturbation: a link to initiation of massive volcanism?: Geology, v. 30, p. 251–254.

Higgins, J.A. & Schrag, D.P., 2006, Beyond methane: towards a theory for the Paleocene–Eocene thermal maximum: Earth Planetary Science Letters, v. 245, p. 523–537.

Hodell, D.A; Mueller, P.A; McKenzie, J.A; Mead, G., 1989, Strontium isotope stratigraphy and geochemistry of the late Neogene ocean: Earth and Planetary Science Letters, v. 92, no. 2, p. 165-178, doi:10.1016/0012-821X(89)90044-7.

Hodell, D.A, Mead, G., Mueller, P.A., 1990, Variation in the strontium isotopic composition of seawater (8 Ma to present); implications for chemical weathering rates and dissolved fluxes to the oceans: Chemical Geology, v. 80, no. 4, p. 291-307, doi:10.1016/0168-9622(90)90011-Z.

Holmden, C., Creaser, R.A., Muehlenbachs, K., Leslie, S.A., Bergstrom, S.M., 1998, Isotopic evidence for geochemical decoupling between ancient epeiric seas and bordering oceans: Implications for secular curves: Geology, v. 26, p. 567–570.

Hornung, T., Brandner, R., 2005, Biochronostratigraphy of the Reingraben Turnover (Hallstatt Facies Belt): Local black shale events controlled by regional tectonics, climatic change and plate tectonics: Facies, v. 51, p. 460-479.

Huynh, T.T., Poulsen, C.J., 2005, Rising atmospheric CO2 as a possible trigger for the end-Triassic mass extinction: Palaeogeography, Palaeoclimatology, Palaeoecology, v. 217, p. 223-242.

Immenhauser, A., Della Porta, G., Kenter, J.A.M., Bahamonde, J.R., 2003, An alternative model for positive shifts in shallow-marine carbonate d13C and d18O: Sedimentology, v. 50, p. 953–959.

Jenkyns, H.C., 2010, Geochemistry of oceanic anoxic events: Geochemistry Geophysics Geosystems, v. 11, p. 1-30.

Jerram, D.A., Widdowson, M., 2005, The anatomy of continental flood basalt provinces. Geological constraints on the processes and products of flood volcanism: Lithos, v. 79, p. 385–405, doi: 10.1016/j.lithos.2004.09.009.

Jones, C.E. and Jenkyns, H.C., 2001, Seawater strontium isotopes, oceanic anoxic events, and seafloor hydrothermal activity in the Jurassic and Cretaceous: Am. J. Sci., v. 301, p. 112–149.

Jourdan, F., Féraud, G., Bertrand, H., Watkeys, M.K., Renne, P.R., 2007, Distinct brief major events in the Karoo large igneous province clarified by new $^{40}Ar/^{39}Ar$ ages on the Lesotho basalts: Lithos, v. 98, p. 195–209.

Kaiho, K., Chen, Z.Q., Sawada, K., 2009, Possible causes for a negative shift in the stable carbon isotope ratio before, during and after the end-Permian mass extinction in Meishan, South China: Australian Journal of Earth Sciences, v. 56, p. 799–808.

Kemp, D.B., Coe, A.L., Cohen, A.S., Schwark, L., 2005, Astronomical pacing of methane release in the early Jurassic period: Nature, v. 437, p. 396‑399.

Korte, C., Kozur, H.W., Bruckschen, P. & Veizer, J., 2003, Strontium isotope evolution of Late Permian and Triassic seawater: Geochemica et Cosmochimica Acta, v. 67, p. 47–62.

Korte, C., Kozur, H.W., Veizer, J., 2005, 13C and 18O values of Triassic brachiopods and carbonate rocks as proxies for coeval seawater and palaeotemperature: Palaeogeography, Palaeoclimatology, Palaeoecology, v. 226, p. 287–306.

Kozur, H. & Mock, R., 1991, New Middle Carnian and Rhaetian conodonts from Hungary and the Alps, stratigraphic importance and tectonic implications for the Buda Mountains and adjacent areas: Jahrbuch der Geologischen Bundesanstalt, v. 134, p. 271–297.

Krystyn, L., 2010, Decision report on the defining event for the base of the Rhaetian stage: Albertiana, v. 38, p. 11–12.

Kump, L.R., Arthur, M.A., 1999, Interpreting carbon-isotope excursions: carbonates and organic matter: Chemical Geology, v. 161, p. 181-198.

Kuroda, J., Hori, R.S., Suzuki, K., Grocke, D.R., Ohkouchi, N., 2010, Marine osmium isotope record across the Triassic-Jurassic boundary from a Pacific pelagic site: Geology, v. 38, p. 1095–1098.

Lucas, S. G., 1999, The epicontinental Triassic, an overview: Zentralblatt fur Geologie und Palaontologie Teil I, 1998, p. 475–496.

Lucas, S. G. & Orchard, M. J., 2004, Triassic. In: Selley, R. C., Cocks, L. M. R. & Plimer, I. R. (eds) Encyclopedia of Geology. Elsevier, Amsterdam, p. 344–351.

Lucas, S.G., 2010, The Triassic Timescale. Geological Society, London, special publication, v. 334, p. 103-118.

Maron, M., Rigo, M., Bertinelli, A., Katz, M.E., Godfrey, L., Zaffani, M., and Muttoni, G., 2015, Magnetostratigraphy, biostratigraphy and chemostratigraphy of the Pignola-Abriola section: New constraints for the Norian-Rhaetian boundary: Geological Society of America Bulletin, v. 127, p. 962-974, doi:10.1130/B31106.1.

Marzoli, A., Bertrand, H., Knight, K.B., Cirilli, S., Buratti, N., Vérati, C., Nomade, S., Renne, P.R., Youb,i N., Martini, R., Allenbach, K., Neuwerth, R., Rapaille, C., Zaninetti, L., Bellieni, G., 2004, Synchrony of the Central Atlantic magmatic province and the Triassic-Jurassic boundary climatic and biotic crisis: Geology, v. 32, p. 973–976.

Marzoli A., Bertrand, H., Chiaradia, M., Fontignie, D., Youbi, N., Bellieni, G., 2006°, The genesis of CAMP basalts (Morocco) from enriched lithosphere to late asthenosphere mantle sources: Geochimica et Cosmochimica Acta, v. 70, p. 396, doi: 10.1016/j.gca.2006.06.799.

Marzoli, A., Rapaille, C., Reisberg, L., Bertrand, H., 2006b, Trace element and Sr-Nd-Pb-Os evidence for a lithospheric mantle source for the European CAMP basalts: Geochimica et Cosmochimica Acta, v. 70, p. 397.

Mazza, M., Furin, S., Spötl, C., Rigo, M., 2010, Generic turnovers of Carnian/Norian conodonts: climatic control or competition?: Palaeogeogr. Palaeoclimatol. Palaeoecol., v. 290, p. 120–137.

McElwain J.C., Beerling D.J., Woodward F.I., 1999, Fossil plants and global warming at the Triassic-Jurassic boundary: Science, v. 285, p. 1386-1390.

McRoberts, C.A., Krystyn, L. & Shea, A., 2008, Rhaetian (Late Triassic) Monotis (Bivalvia: Pectinoida) from the eastern Northern Calcareous Alps (Austria) and the end-Norian crisis in pelagic faunas: Palaeontology, v. 51, p. 721–735.

Meyers, P.A., 2014, Why are the $d^{13}C_{org}$ values in Phanerozoic black shales more negative than in modern marine organic matter?: Geochemistry, Geophysiscs, Geosystems, doi: 10.1002/2014GC005305.

Miconnet, P., 1982, Precisions stratigraphiques et tectoniques dans un secteur du Lagonegro (Italie meridionale) : Annales de la Societe Geologique du Nord, v. 102, p. 17–24.

Mortensen, J.K and Hulbert, L.J., 1991, A U-Pb zircon age for a Maple Creek gabbro sill, Tatamagouche Creek area, southwest Yukon Territory. In: Radiogenic age and isotopic studies, Report 5, Geological Survey of Canada, Paper 91-2, p. 175-179.

Mostardini, F. and Merlini, S., 1986, Appennino centro-meridionale. Sezioni geologiche e proposta di modello strutturale: Memorie Società Geologica Italiana, v. 35, p. 177–202.

Muttoni, G., Kent, D.V., Olsen, P., Di Stefano, P., Lowrie, W., Bernasconi, S., Martin Hernandez, F., 2004, Tethyan magnetostratigraphy from Pizzo Mondello (Sicily) and correlation to the Late Triassic astrochronological polarity time scale: Geol. Soc. Am. Bull., v. 116, p. 1043-1058.

Muttoni, G., Mazza, M., Mosher, D., Katz, M.E., Kent, D.V., Balini, M., 2014, A Middle–Late Triassic (Ladinian–Rhaetian) carbon and oxygen isotope record from the Tethyan Ocean: Palaeogeography, Palaeoclimatology, Palaeoecology, v. 399, p. 246-259.

Ogg, J.G., 2012. Triassic. In: Gradstein, F.M., Ogg, J.G., Schmitz, M.D., and Ogg, G.M., (eds) The Geologic Time Scale. Elsevier Publ., p. 681-730.

Orchard, M.J,. 1991, Upper Triassic conodont biochronology and new index species from the Canadian Cordillera: Geological Survey of Canada Bulletin, v. 417, p. 299–335.

Palfy, J., Demeny, A., Haas, J., Hetenyi, M., Orchard, M.J., Veto, I., 2001, Carbon isotope anomaly and other geochemical changes at the Triassic-Jurassic boundary from a marine section in Hungary: Geology, v. 29, p. 1047-1050.

Palfy, J., Demeny, A., Haas, J., Carter, E.S., Gorog, A., Halasz, D., Oravecz-Scheffer, A., Hetenyi, M., Marton, E., Orchard, M.J., Ozsvart, P., Veto, I., Zaizon, N., 2007, Triassic-Jurassic boundary events inferred from integrated stratigraphy of the Csovar section, Hungary: Palaeogeography, Palaeoclimatology, Palaeoecology, v. 224, p. 11-33.

Pálfy, J., Kocsis, A.T., 2014, Volcanism of the Central Atlantic magmatic province as the trigger of environmental and biotic changes around the Triassic-Jurassic boundary: Geological Society of America Special Papers, v. 505, p. SPE505-12.

Pallister, J.S., Budahn, J.R., Murchey, B.L., 1989, Pillow basalts of the Angayucham Terrane: Oceanic Plateau and Island Crust Accreted to the Brooks Range: Journal of Geophysical Research, v. 94, p. 15901-15923.

Palmer, M.R. & Elderfield, H., 1985, Sr isotope composition of sea water over the past 75 Myr: Nature, v. 314, p. 526-528.

Palmer, M.R. and Edmond, J.M., 1989, The Strontium Isotope Budget of the Modern Ocean: Earth and Planetary Science Letters, v. 92, no. 1, p. 11-26, doi: 10.1016/0012-821X(89)90017-4.

Passeri, L., Bertinelli, A. and Ciarapica, G., 2005, Palaeogeographic meaning of the late Triassic–Early Jurassic Lagonegro units: Bollettino Società Geologica Italiana, v. 124, p. 231–245.

Payne, J.L., Lehrmann, D.J., Wei, J., Orchard, M.J., Schrag, D.P., Knoll, A.H., 2004, Large perturbations of the carbon cycle during recovery from the end-Permian extinction: Nature, v. 305, p. 506–509.

Pogge von Strandmann, P.A.E., Jenkyns, H.C., Woodfine, R.G., 2013, Lithium isotope evidence for enhanced weathering during Oceanic Anoxic Event 2: Nature Geoscience, v. 6, no. 8, p. 668-672, doi:10.1038/ngeo1875.

Preto, N., Kustatscher, E., and Wignall, P.B., 2010, Triassic climates—State of the art and perspectives: Palaeogeography, Palaeoclimatology, Palaeoecology, v. 290, p. 1–10, doi:10.1016/j.palaeo.2010.03.015.

Preto, N., Rigo, M., Agnini, C., Bertinelli, A., Guaiumi, C., Borello, S.,Westphal, H., 2012, Triassic and Jurassic calcareous nannofossils of the Pizzo Mondello section: a SEM study: Riv. Ital. Paleontol. Stratigr., v. 118, no. 1, p. 131–141.

Preto, N., Agnini, C., Rigo, M., Sprovieri, M., Westphal, H., 2013, The calcareous nannofossil Prinsiosphaera achieved rock-forming abundances in the latest Triassic of western Tethys: consequences for the $\delta^{13}C$ of bulk carbonate: Biogeosciences, v. 10, p. 6053-6068.

Prokoph, A., El Bilali, H., Ernst, R., 2013, Periodicities in the emplacement of large igneous provinces through the Phanerozoic: Relations to ocean chemistry and marine biodiversity evolution: Geoscience Frontiers, v. 4, p. 263-276.

Ramezani, J., Bowring, S.A., Pringle, M.S., Winslow III, F.D., Rasbury, E.T., 2005, The Manicouagan impact melt rock: a proposed standard for the intercalibration of U–Pb and 40Ar/39Ar isotopic systems: Geochim. Cosmochim. Acta Suppl., v. 69, p. A321.

Ramezani, J., Hoke, G.D., Fastovsky, D.E., Bowring, S.A., Therrien, F., Dworkin, S.I., Atchley, S.C., Nordt, L.C., 2011, High precision U-Pb zircon geochronology of the Late Triassic Chinle Formation, Petrified Forest National Park (Arizona, USA): temporal constraints on the early evolution of dinosaurs: Geol. Soc. Am. Bull., v. 123, p. 2142-2159.

Rampino, M.R., and R.B. Stothers, 1988, Flood basalt volcanism during the past 250 million years: Science, v. 241, p. 663-668, doi:10.1126/science.241.4866.663.

Raymo, M.E., Ruddiman, W.F., Froelich, P.N., 1988, Influence of late Cenozoic mountain building on ocean geochemical cycles: Geology, v. 16, p. 649– 653, doi: 10.1130/0091-7613(1988)016<0649:IOLCMB>2.3.CO;2.

Raup, D.M. and Sepkoski, J.J., 1982, Mass extinction in the fossil record: Science, v. 215, p. 1501–1503.

Reggiani, L., Bertinelli, A., Ciarapica, G., Marcucci, M., Passeri, L., Ricci, C. & Rigo, M., 2005, Triassic-Jurassic stratigraphy of the Madonna del Sirino succession (Lagonegro basin, Southern Apennines, Italy): Bollettino Società Geologica Italiana, v. 124, p. 281–291.

Richoz, S., Krystyn, L., Spotl, C., 2007, Towards a carbon isotope reference curve of the Upper Triassic: New Mexico Museum of Natural History and Science Bulletin, v. 41, p. 366-367.

Rigo, M., De Zanche, V., Mietto, P., Preto, N. and Roghi, G., 2005, Biostratigraphy of the Calcari con Selce formation: Bollettino Società Geologica Italiana, v. 124, p. 293–300.

Rigo, M., Preto, N., Roghi, G., Tateo, F. and Mietto, P., 2007, A CCD rise in the Carnian (Upper Triassic) of western Tethys, deep-water equivalent of the Carnian Pluvial Event: Palaeogeography, Palaeoclimatology, Palaeoecology, v. 246, p. 31–182.

Rigo, M. and Joachimski, M.M., 2010, Palaeoecology of Late Triassic conodonts: Constraints from oxygen isotopes in biogenic apatite: Acta Palaeontologica Polonica, v. 55, no. 3, p. 471–478.

Rigo, M., Trotter, J.A., Preto, N., Williams, I.S. 2012, Oxygen isotopic evidence for Late Triassic monsoonal upwelling in the northwestern Tethys: Geology, v. 40; no. 6, p. 515–518, DOI: 10.1130/G32792.1.

Rigo, M., Preto, N., Franceschi, M. and Guaiumi, C., 2012b, Stratigraphy of the Carnian-Norian Calcari con Selce Formation in the Lagonegro Basin, Southern Apennines: Rivista Italiana di Paleontologia e Stratigrafia, v. 118, p. 143–154.

Rigo, M., Bertinelli, A., Concheri, G., Gattolin, G., Godfrey, L., Katz, M.E., Maron, M., Muttoni, G., Sprovieri, M., Stellin, F., Zaffani, M., 2015, The Pignola-Abriola section (southern Apennines, Italy): a new GSSP candidate for the base of the Rhaetian Stage: Lethaia, doi: 10.1111/let.12145.

Ruhl, M., Kurschner, W.M., 2011, Multiple phases of carbon cycle disturbance from large igneous province formation at the Triassic-Jurassic transition: Geology, v. 39, p. 431-434.

Saunders, A.D., Fitton, J.G., Kerr, A.C., Norry, M.J., and Kent, R.W., 1997, The North Atlantic Igneous Province. In: Mahoney, J.J., and Coffin, M.F. (eds.). Large igneous provinces: Continental, oceanic, and planetary flood volcanism. American Geophysical Union Geophysical Monograph, v. 100, p. 45–93.

Scandone, P., 1967, Studi di geologia lucana: la serie calcareo-silicomarnosa: Bollettino Società Naturalisti Napoli, v. 76, p. 1–175.

Schaller, M.F., Wright, J.D., Kent, D.V., Olsen, P.E., 2012, Rapid emplacement of the Central Atlantic Magmatic Province as a net sink for CO2: Earth and Planetary Science Letters, v. 323–324, p. 27–39.

Self, S., Thordarson, T., Widdowson, M., 2005, Gas fluxes from flood basalt eruptions: Elements, v. 1, p. 283-287.

Sell, B., Ovtcharova, M., Guex, J., Bartolini, A., Jourdan, F., Spangenberg, J.E., Vicente, J.C., Schaltegger, U., 2014, Evaluating the temporal link between the Karoo LIP and climatic–biologic events of the Toarcian Stage with high-precision U–Pb geochronology: Earth and Planetary Science Letters, v. 408, p. 48–56.

Selli, R., 1962, Il Paleogene nel quadro della Geologia dell’Italia Meridionale: Memorie Società Geologica Italiana, v. 3, p. 737–790.

Sengor, A.M.C., Yilmaz, Y. & Sungurlu, O., 1984, Tectonics of the Mediterranean Cimmerides: nature and evolution of the western termination of Palaeo-Tethys: Geological Society, London, Special Publications, v. 17, p. 77–112.

Sephton, M.A., Amor, K., Franchi, I.A., Wignall, P.B., Newton, R., Zonneveld, J.P., 2002, Carbon and nitrogen isotope disturbances and an end-Norian (Late Triassic) extinction event: Geology, v. 30, p. 1119-1122.

Schoene, B., Guex, J., Bartolini, A., Schaltegger, U. & Blackburn, T.J., 2010, A correlation between the Triassic-Jurassic boundary mass extinction and flood basalt eruption at the 100-ka level using ID-TIMS U/Pb zircon geochronology: Geology, v. 38, p. 387–390.

Simms, M.J., Ruffell, A.H., 1989, Synchroneity of climatic change and extinctions in the Late Triassic: Geology, v. 17, p. 265–268.

Simms, M.J., Ruffell, A.H., 1990, Climatic and biotic change in the late Triassic: J. Geol. Soc. (Lond.) v. 147, p. 321–327.

Simms, M.J., Ruffell, A.H., Johnson, A.L.A., 1995, Biotic and climatic changes in the Carnian (Triassic) of Europe and adjacent areas. In: Fraser, N.C., Sues, H.D. (Eds.), In the Shadow of the Dinosaurs. Early Mesozoic Tetrapods. Cambridge Univ. Press p. 352–365.

Speranza, F., Minelli, L., Pignatelli, A., Chiappini, M., 2012, The Ionian Sea: the oldest in situ ocean fragment of the world?: Journal of Geophysical Research, v. 117, p. B12101. 1-13., doi:10.1029/2012JB009475

Stampfli, G., Marcoux, J. & Baud, A., 1991, Tethyan margins in space and time: Palaeogeography, Palaeoclimatology, Palaeoecology, v. 87, p. 373–409.

Stampfli, G.M. & Marchant, R.H., 1995, Plate configuration and kinematics in the Alpine region: Accademia Nazionale Delle Scienze, Scritti e Documenti, v. 14, p. 147–166.

Stampfli, G.M., Mosar, J., De Bono, A., Vavassis, I., 1998, Late Paleozoic, early Mesozoic plate tectonics of the western Tethys: Bullettin od the Geological Society of Greece, v. 32, p. 113-120.

Stampfli, G.M., Vavassis, I., De Bono, A., Rosselet, F., Matti, B. & Bellini, M., 2003, Remnants of the Paleotethys oceanic suture-zone in the western Tethys area: Bollettino della Società Geologica Italiana, Special Volume, no. 2, p. 1-23.

Swart, P.K., Eberli, G.P., 2005, The nature of the d13C of periplatform sediments: Implications for stratigraphy and the global carbon cycle: Sedimen Geol, v. 175, p. 115–130.

Swart, P.K., 2008, Global synchronous changes in the carbon isotopic composition of carbonate sediments unrelated to changes in the global carbon cycle: Proc. Natl. Acad. Sci., v. 105, no. 37, p. 13741–13745.

Tanner, L.H., Lucas, S.G., Chapman, M.G., 2004, Assessing the record and causes of Late Triassic extinction: Earth Sciences Reviews, v. 65, p. 103-139.

Tanner, L.H., Schiattarella, M. and Di Leo, P., 2006, Carbon isotope record of Upper Triassic strata of the Lagonegro Basin, Southern Apennines, Italy: preliminary results: Mexico Museum of Natural History and Science Bulletin, v. 37, p. 23–28.

Tanner L.H., Ciarapica G., Reggiani L., Atudorei V., 2007, Upper Triassic carbon isotope stratigraphy of the Lagonegro Succession, Southern Apennines, Italy: New Mexico Natural History and Science Bullettin, v. 41, p. 406-410.

Tanner, L.H., 2010, The Triassic isotope record. In: Lucas, S.G. (ed.) The Triassic Timescale. Geological Society, London, special publication, v. 334, p. 103-118.

Taylor, A.S., Lasaga, A.C., 1999, The role of basalt weathering in the Sr isotope budget of the oceans: Chemical Geology, v. 161, no. 1-3, p. 199-214, doi: 10.1016/S0009-2541(99)00087-X.

Trotter, A.J., Williams, S.I., Nicora, A., Mazza, M. and Rigo, M., 2015, Long-term cycles of Triassic climate change: a new $d^{18}O$ record from conodont apatite: Earth and Planetary Science Letters, v. 415, p. 165–174.

Tolan, T.L., Reidel, S.P., Beeson, M.H., Anderson, J.L., Fecht, K.R., and Swanson, D.A., 1989, Revisions to the estimates of the areal extent and volume of the Columbia River Basalt Group. In: S. Reidel, P. and P. Hooper, R. (eds.). Volcanism and tectonism in the Columbia River flood-basalt province. Geological Society of America, Boulder, p. 1-20.

Van de Schootbrugge, B., Payne, J.L., Tomasovych, A., Pross, J., Fiebig, J., Benbrahim, M., Follmi, K.B., Quan, T.M,. 2008, Carbon cycle perturbation and stabilization in the wake of the Triassic-Jurassic boundary mass extinction event: Geochemistry Geophysics Geosystems, v. 9, p. 1-16.

Veizer, J., Buhl, D., Diener, A., Ebneth, S., Podlaha, O.G., Bruckschen, P., Jasper, T., Korte, C., Schaaf, M., Ala, D., Azmy, K., 1997, Strontium isotope stratigraphy: potential resolution and event correlation: Paleogeogr., Paleoclimatol., Paleoecol., v. 132, p. 65–77.

Veizer, J., Ala, K., Azmy, K., Bruckschen, P., Buhl, D., Bruhn, F., Carden, G.A.F., Diener, A., Ebneth, S., Godderis, Y., Jasper, T., Korte, C., Pawellek, F., Podlaha, O.G., Strauss, H., 1999, 87Sr/86Sr, δ13C and δ18O evolution of Phanerozoic seawater: Chem. Geol., v. 161, p. 59–88.

Ward, P.D., Garrison, G.H., Haggart, J.W., Kring, D.A., Beattie, M.J., 2004, Isotopic evidence bearing on Late Triassic extinction events, Queen Charlotte Islands, British Columbia, and implications for the duration and cause of the Triassic/Jurassic mass extinction: Earth and Planetary Science Letters, v. 224, p. 589-600.

Whiteside, J.H., Olsen, P.E., Eglinton, T., Brookfield, M.E., and Sambrotto, R.N., 2010, Compound-specific carbon isotopes from Earth's largest flood basalt eruptions directly linked to the end-Triassic mass extinction: PNAS, v. 107, p. 6721–6725.

Whiteside, J.H., Ward, P.D., 2011, Ammonoid diversity and disparity track episodes of chaotic carbon cycling during the early Mesozoic: Geology, v. 39, p. 99-102.

Wignall, P.B., 2001, Large igneous provinces and mass extinctions: Earth-Science Reviews, v. 53, p. 1–33.

Wignall, P.B., Zonneveld, J.-P., Newton, R.J., Amor, K., Sephton, M.A. & Hartley, S., 2007, The end Triassic mass extinction record of Williston Lake, British Columbia: Palaeogeogr. Palaeoclimatol. Paleoecol., v. 253, p. 385–406.

CHAPTER 2:

Through a complete Rhaetian $\delta^{13}C_{org}$ record: carbon cycle disturbances, volcanism, end-Triassic mass extinction. A composite succession from the Lombardy Basin (N Italy)

Mariachiara Zaffani[1], Flavio Jadoul[2], Manuel Rigo[1,3]

[1] *Department of Geosciences, Università degli Studi di Padova, 35131 Padova, Italy.*
[2] *Department of Earth Sciences, Università degli Studi di Milano, 20133 Milan, Italy.*
[3] *IGG - CNR, Via G. Gradenigo 6, 35131 Padova, Italy*

ABSTRACT

The Lombardy Basin offers an almost continuous stratigraphic record of the Late Triassic. Several studies had focused their attention on the Triassic/Jurassic boundary, analyzing the $\delta^{13}C_{org}$ of the latemost Rhaetian. This work covers, for the first time, the entire Rhaetian – starting from the presumed latemost Norian to the earliest Hettangian. The obtained profile appears perturbed by a series of $\delta^{13}C_{org}$ decreases: three of them might be identified as the "main", "initial" and "precursor" negative CIEs on the basis of the available stratigraphic constraints. The comparison of our data with the $\delta^{13}C_{org}$ profiles from the St Audrie's Bay and the Eiberg Basin permits to better constrain and identify these negative CIEs likely related to the CAMP activity. Using bio-, chemo- and lithostratigraphic correlations, we propose two possible interpretations of the Lombardy Basin $\delta^{13}C_{org}$ CIEs.

INTRODUCTION

The Late Triassic (ca. 237-201 Ma) was a period of intense climate, environmental and biological changes. It was characterized by pivotal events like the break-up of the supercontinent Pangaea, the transition from arid to humid conditions and the occurrence of dramatic extinction episodes, such as the end-Triassic mass extinction, one of the five largest and most discussed events of the Phanerozoic (e.g., Sepkoski, 1996). In fact, the timing and causes of the end-Triassic mass extinction are still the subject of controversial discussion (e.g., Hallam, 2002): massive volcanism in the Central Atlantic Magmatic Province (CAMP) (Marzoli et al., 1999, 2004; Wignall, 2001; Hesselbo et al., 2002) and/or a bolide impact event (Olsen et al., 2002; Simms, 2003) are included in the possible causes. The CAMP activity is thought to have triggered also a methane release and a sea-level change, involving ocean anoxia, which might have contributed to the end-Triassic biotic crises (Hallam and Wignall, 1999; Palfy et al., 2001). Notably, the end-Triassic mass extinction seems to be associated with significant perturbations of the global carbon cycle (Ward et al., 2004; Richoz et al., 2007; Van de Schootbrugge et al., 2008; Tanner, 2010; Zaffani et al., submitted). In particular, negative carbon isotope excursions (CIEs) have been worldwide recognized at the Rhaetian/Hettangian boundary (McElwain et al., 1999; Palfy et al., 2001; Hesselbo et al., 2002; Richoz et al., 2007), specifically distinguished in three CIEs, referred as the "main" CIE at the Triassic/Jurassic boundary (T/J), preceded by an "initial" and a "precursor" CIE, commonly associated to different eruptive phases of the Moroccan CAMP commenced during the Late Triassic (Marzoli et al., 2004; Hesselbo, McRoberts & Pálfy, 2007; Dal Corso et al., 2014). Recently, the occurrence of another carbon isotope perturbation at the Norian/Rhaetian boundary has been documented (Ward et al., 2001, 2004; Sephton et al., 2002; Whiteside & Ward; 2011; Maron et al., 2015; Rigo et al., 2015; Zaffani et al., submitted) and likely associated to the Angayucham activity (Zaffani et al., submitted), a late Norian Large Igneous Province (LIP). From this point of view, the Rhaetian carbon isotope record seems to be marked by the outgassing and eruptive activity of two of the bigger Mesozoic LIPs, at least at its stage boundaries. The Rhaetian seems to be characterized also by significant faunal turnovers, both in the marine and continental realms (e.g., Tanner et al., 2004; Trotter et al., 2015). In fact, besides the paroxysmal crises of the end-Triassic mass extinction at the T/J, the Rhaetian appears to be marked by a series of biotic crises and faunal turnovers that gradually culminated at the T/J, supporting the hypothesis of a step-like extinction pattern (e.g., Hallam et al., 2002; Tanner et al., 2004; Whiteside & Ward, 2011). Carbon isotope analyses could represent a useful tool in the evaluation of palaeoenvironmental changes during these biotic crises. In fact, such perturbations in the Earth's carbon cycle associated to faunal turnovers have a worldwide occurrence and can potentially be observed in a variety of facies, both marine and continental (Kump&Arthur, 1999; Beerling&Berner, 2002; Korte et al., 2005; Deenen et al., 2010; Whiteside et al., 2010). Carbon isotopes may also provide new clues on the extinction timing, helping to clarify the nature of the crisis (McRoberts & Newton, 1995; McElwain, Beerling & Woodward, 1999; Sephton et al. 2002; Ward et al. 2001, 2004; McElwain et al. 2007; McElwain, Wagner & Hesselbo, 2009; Deenen et al. 2010; Whiteside et al. 2010). Therefore, a detailed investigation of the Rhaetian (ca. 205.7-201.3±0.2 Ma; Maron et al., 2015; Rigo et al. 2015) could provide useful information on the events that affected the global carbon cycle during this peculiar time interval of the Late Triassic.

Hence, the aim of this work is to provide a complete organic carbon isotope record for the Rhaetian, in order to cast light on the series of events affecting the global carbon cycle that eventually culminated in the T/J mass extinction. We analyzed a composite succession easily correlating three stratigraphic sections belonging to the Lombardy Basin, cropping out in less than 5 km: Brumano, the freshly-caved Italcementi active quarry and Malanotte, displaying good exposure and an almost continuous record from the late Norian to the early Hettangian. The Lombardy Basin have been previously partially studied for $\delta^{13}C$ purposes, especially at the T/J. These studies highlight the occurrence of the "initial" CIE at the T/J both in the $\delta^{13}C_{carb}$ (Muttoni et al., 2010; 2014; Bachan et al., 2012) and $\delta^{13}C_{org}$ records (Galli et al., 2005; 2007; Bachan et al., 2012; Bottini et al., submitted), followed by the positive Hettangian CIE (Galli et al., 2005; 2007; Muttoni et al., 2010; Bachan et al., 2012; Bottini et al., submitted). Bottini et al. (submitted) showed also the occurrence of the "precursor" and "main" CIEs in the late Rhaetian and early Hettangian respectively. Here we propose an almost complete $\delta^{13}C_{org}$ record for the entire Rhaetian, starting from the late Norian to the early Hettangian, suggesting alternative correlations of the three CIEs characterising the latemost Triassic.

GEOLOGICAL SETTING

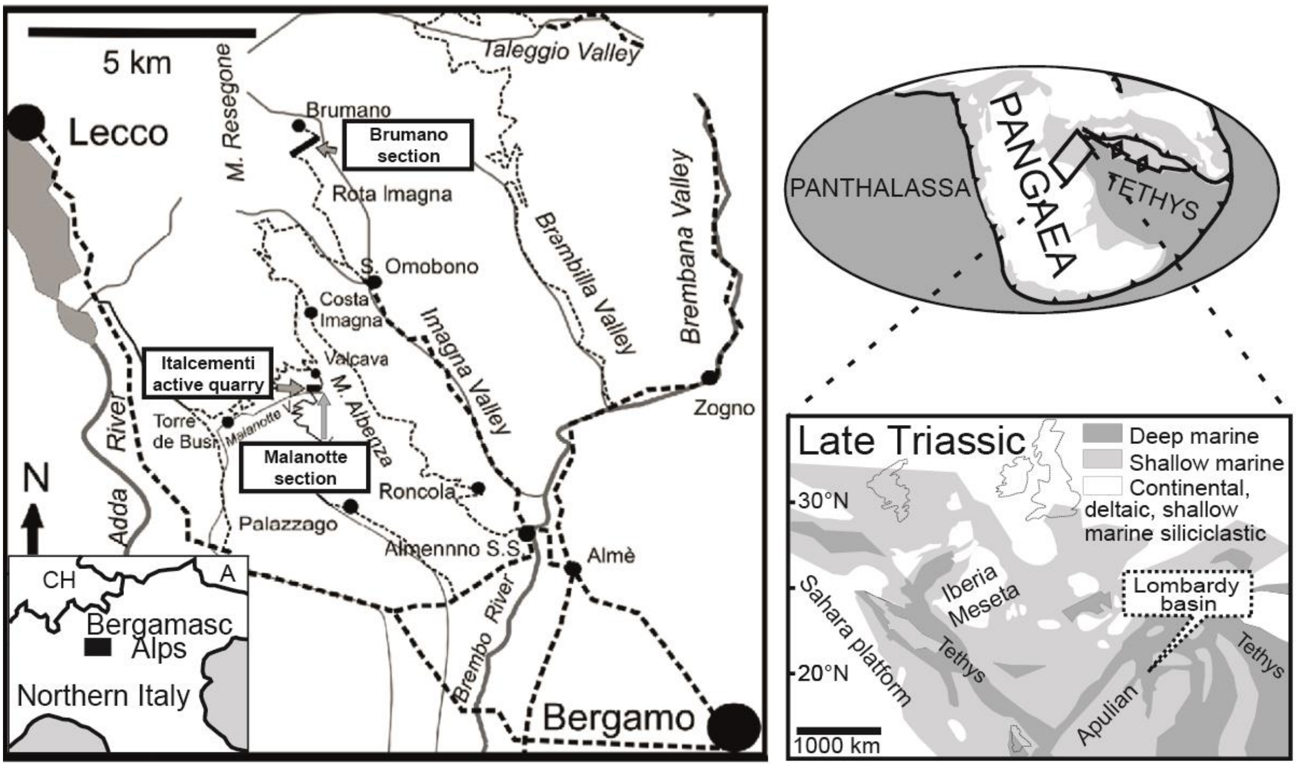

Fig. 2.1 Location map of the studied area and palaeogeography of the Lombardy Basin (modified from Muttoni et al., 2010; Galli et al., 2005).

The Brumano, Italcementi and Malanotte sections are located in the Bergamasc Alps (southern Alps, northern Italy; Fig. 2.1) and belong to the Lombardy Basin, a north-western gulf of the Tethys Ocean (Galli et al., 2005, 2007; Jadoul and Galli, 2008; Muttoni et al., 2010; Bottini et al., submitted), late Norian to early Hettangian in age. The studied successions expose the Calcari di Zu and Malanotte Formations. The Calcari di Zu Fm is made up of a cyclic alternation of shallow-water carbonates and shales, deposited at subtropical palaeolatitudes in the Tethys Ocean (e.g., Kent and Muttoni, 2003; Muttoni et al., 2010) (Fig. 2.1), and is subdivided into thee Members, named Zu1, Zu2 and Zu3 (Galli et al., 2007; Jadoul and Galli, 2008) (Fig. 2.2). The overlying Malanotte Fm consists of micritic limestones, marls and biocalcarenites (Cirilli et al., 2000; Galli, 2002; Jadoul et al., 2004). In particular, the Brumano section is ca. 200 km thick and exposes the Zu1, Zu2 and Zu3 Mbs. The Zu1 Member (first 50 meters circa) is composed by a monotonous alternation of dark-grey marls and marly limestone intercalated with micritic limestones arranged in decameter-scale cycles. The marls of the uppermost Zu1 contains large bivalves (Homomia sp., Cardita sp., Trigonia sp.) and a typical late Norian palynologic association that suggests the proximity to the Norian-Rhaetian transition (Carnisporites sp., Lundbladispora lundbladii, Ricciisporites tuberculatus and other Norian taxa; Fig. 2.2) (Jadoul et al., 2004). The overlying bioturbated limestones yield corals, brachiopods, crinoids and foraminifers, phosphate and quartz grains (Jadoul et al., 2004). The Zu2 member (from ca. 50 m to ca. 130 m) is composed of decameter scale carbonate cycles of bioturbated and fossiliferous dark-grey wackestones. Compared to Zu1, it is characterized by a decreased siliciclastic content. The base of this Zu2 Member consists of mudstones-wackestones and associated Retiophyllia spp. patch reefs, with sponges, echinoids, Microtubus sp., Porostromata and foraminifers. Within the base of Zu2 the turnover from the palynological phase II and III is recorded (palynological phases according to Shuurman, 1979) (Jadoul et al., 2004). In particular, the transition from a late Norian (Carnisporites sp., Lundbladispora lundbladii, Ricciisporites tuberculatus, Gliscopollis meyeriana, Ovalipollis pseudoalatus, Microreticulatisporites fuscus, Granuloperculatipollis rudis, Classopollis torosus, Todisporites spp., Calamospora mesozoica) to early Rhaetian pollen assemblage (Rhaetipollis germanicus, C. torosus, Zaebrasporites laevigatus, M. fuscus, Acanthotriletes spp., L. lundblandii, Tsugaepollenites pseudomassulae, Uvaesporites argenteaeformis, O. pseudoalatus, Dapcodinium priscum) is observed (Fig. 2.2; Jadoul et al., 2004). The middle and upper portions of Zu2 is made of bioclastic packstones and grainstones bearing brachiopods (Rhaetina gregaria) and associated Porostromata colonies. The top of Zu2 is partially dolomitized. The Zu3 member encompasses three subunits (Zu3a–c), but only Zu3a is exposed in the Brumano section. It consists of thick marl and micritic limestone cycles, with a rich fauna and microflora. Benthic foraminifera dominated by Triasina hantkeni (Majzon, 1954) are associated with corals, calcareous sponges, encrusting organisms, and megalodontids (Lakew, 1990) (Fig. 2.2). The Italcementi active quarry section is ca. 130 m thick and shows the Zu3b and Zu3c subunits (Fig. 2.2). They consist of ca. 120 m thick bioturbated and fossiliferous wackestones and packstones. The Zu3b is characterized by grey marly-limestones and marls bearing Rhaetavicula contorta and Bactrillum. The top of the Zu3b is marked by a carniole-type marly limestone with evaporate molds, and black shale intercalations (Jadoul et al., 2004). The Zu3c is characterized by an increase of biogenic packstones-grainstones, bearing foraminifers, corals (e.g., Thecosmilia sp.), sponges and Megalodontids. In some successions of the Lombard Basin, the top of the Zu3 member is marked by a paraconformity that is interpreted as a regional drowning unconformity (Schlager, 1989), and is characterized by the disappearance of benthic foraminifera and reef communities, justified as an evidence of the end-Triassic mass extinction event (Wood, 1999; Galli et al., 2005). Our studied succession shows a continue record for the Zu3 member without unconformities. The disappearance of these marine Triassic taxa precedes the T/J change in the palynological assemblages, which occurs within the base of the Malanotte Fm. The Zu3c contains evidence of the uppermost part of the nannofossil Zone NT2b (Prinsiosphaera triassica, Eoconusphaera zamblachensis and Crucirhabdus minutes, see Fig. 2.2) of late Rhaetian age (Bottini et al., submitted). This interval contains also other Late Triassic taxa, such as Tetralithus pseudotrifidus, Tetralithus cassianus, Hayococcus floralis (Bottini et al., submitted).

The Zu3 Member is overlain by the Malanotte Formation, ca. 12 m thick, composed of thinly bedded micritic limestones and marls with rare thin-shelled bivalves and crinoids (Fig. 2.2). Within the Lombardy Basin, the base of the Malanotte Fm is commonly marked by a meter-thick marly/silty horizon, comparable with the T/J boundary beds of the Schattwald Shale in western Austria (McRoberts et al., 1997; Galli et al., 2005). The Malanotte Formation contains palynological evidence of the Triassic/Jurassic boundary, such as the disappearance of Rhaetipollis germanicus and an acme of Kraeuselisporites reissingeri, a diagnostic Hettangian pollen associated with other typical species of the Malanotte Formation (i.e., Classopollis torosus, Gliscopollis meyeriana, Microreticulatisporites fuscus, Retitriletes austroclavatidites, R. clavatoides, Tsugapollenites pseudomassulae; Galli et al., 2005; 2007; Muttoni et al., 2010). The Malanotte Fm provides scarce specimens of Schizosphaerella sp. and Conusphaera sp., and very rare specimens of C. minutes, indicating the nannofossil Zone NJT1 of early Hettangian age (Bottini et al., submitted). In the Italcementi section, the NT2b and NJT1 nannofossil zones are separated by a barren interval (Bottini et al., submitted).

Besides the Hettangian pollen association and the nannofossil distribution at the Zu3c-Malanotte transition, the studied sections do not provide any other paleontological evidence useful for the identification of stage boundaries and/or biostratigraphic correlations, such as conodonts or ammonoids. Nevertheless, the Costa Imagna section (Fig. 2.1), coeval to Brumano, contains specimens of the conodont Misikella posthernsteini (Muttoni et al., 2010), a common biomarker for the base of the Rhaetian stage in the Tethyan area (e.g., Krystyn, 2010; Rigo et al., 2015; Bertinelli et al., 2016). In Costa Imagna, M. posthernsteini appears in the uppermost portion of Zu1, just below the Zu1/Zu2 boundary (Fig. 2.3; revised after Muttoni et al., 2010; see also Giordano et al., 2010; Maron et al., 2015). Therefore, on lithostratigraphic basis, it is possible to approximately place the appearance of M. posthernsteini around the Zu1-Zu2 transition in the Brumano section (Fig. 2.3). However, the peculiar negative $\delta^{13}C_{org}$ shift recognizable at the Norian/Rhaetian boundary just below the first occurrence of M. posthernsteini, suggested as an useful physical marker base of the Rhaetian because of its globally occurrence (Maron et al., 2015; Rigo et al., 2015), has not been documented at the Brumano section.

Fig. 2.2 Lithostratigraphy, biostratigraphy, $\delta^{13}C_{org}$ and TOC profiles of the Lombardy Basin composite succession. Biostratigraphy from Jadoul et al. (2004), Muttoni et al. (2010) and Bottini et al. (2016). We labelled the $\delta^{13}C_{org}$ decreases as E1, E2, E3, E4 and E5, and highlighted the peaks of the uppermost Calcari di Zu Fm (peak 5, peak 6 and peak 7).

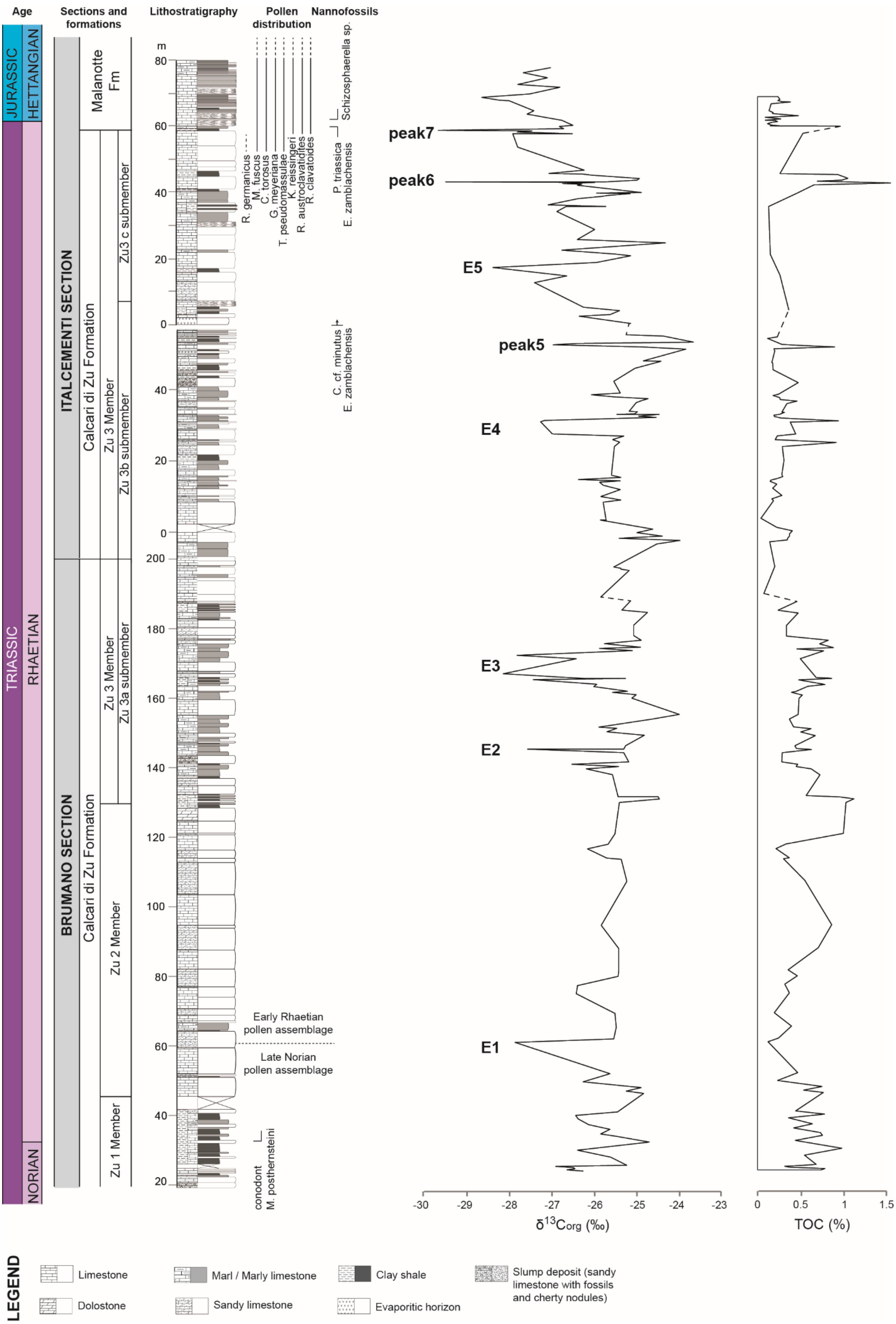

Age
Sections and formations
Lithostratigraphy
Pollen distribution
Nannofossils
JURASSIC
HETTANGIAN
TRIASSIC
RHAETIAN
NORIAN
ITALCEMENTI SECTION
BRUMANO SECTION
Malanotte Fm
Calcari di Zu Formation
Zu 3 Member
Zu 2 Member
Zu 1 Member
Zu3 c submember
Zu 3b submember
Zu 3a submember
R. germanicus
M. fuscus
C. torosus
G. meyeriana
T. pseudomassulae
K. reissingeri
R. austroclavatidites
R. clavatoides
P. triassica
E. zamblachensis
Schizosphaerella sp.
C. cf. minutus
E. zamblachensis
Early Rhaetian pollen assemblage
Late Norian pollen assemblage
conodont
M. posthernsteini
peak7
peak6
E5
peak5
E4
E3
E2
E1
δ13Corg (‰)
TOC (%)
LEGEND
Limestone
Dolostone
Marl / Marly limestone
Sandy limestone
Clay shale
Evaporitic horizon
Slump deposit (sandy limestone with fossils and cherty nodules)

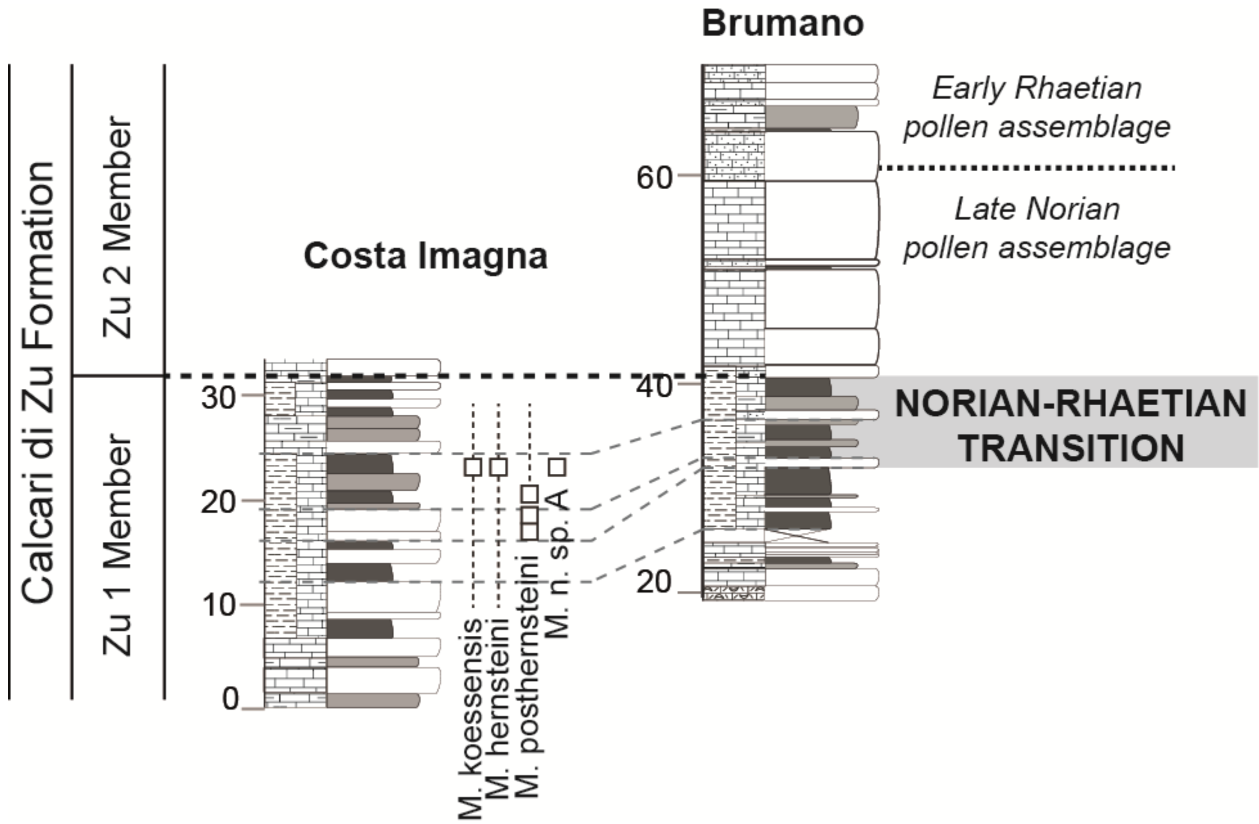

Fig. 2.3 Lithostratigraphic correlation between the Costa Imagna and Brumano section. Through this correlation, it is possible to approximate the position of the first occurrence of the conodont Misikella posthernsteini in the Brumano section, which can be used as a physical proxy to place the Norian/Rhaetian boundary. Conodont distribution of the Brumano section from Muttoni et al. (2010).

METHODS

A total of 187 samples from the Lombardy Basin were collected for TOC analyses and $\delta^{13}C_{org}$ (see **Appendix C**). All samples were washed in deionized water, dried overnight and reduced to a fine powder using an agate mortar. For the TOC analyses, the powdered samples were divided into two aliquots: 1) ca. 100 mg of sample were added to ca. 100 mg of WO3 and wrapped in tin capsules for Total Carbon (TC) analyses; 2) ca. 100 mg of sample were added to ca. 100 mg of WO3, wrapped in silver capsules and heated at 550°C in order to remove organic compounds for Total Inorganic Carbon (TIC) analyses. The difference between the TC and TIC provided the TOC of each sample. The analyses were performed at the DAFNAE (Department of Agronomy, Food, Natural resources, Animals and Environment), University of Padova (Italy), using a Vario Macro CNS Elemental Analyzer. Results were calibrated against Sulfanilamide standard (N=16.25%; C=41.81%; S=18.62%; H=4.65%). The analytical uncertainty of the instrument, expressed as relative standard deviation, is σ=0.5%.

The $\delta^{13}C_{org}$ analysis was performed through a Delta V Advantage mass spectrometer connected to a Flash HT Elemental Analyzer via CONFLO at the Department of Geosciences, University of Padova (Italy). A couple of grams of powder for each sample were dissolved in 25 cl of 3M HCl for at least 4 hours. The solution was then neutralized with 20 cl of deionized water and discarded after centrifuging. After that, the residue was dissolved in 25 cl of 3M HCl at 70°C for at least 4 hours, and successively neutralized as before. We repeated the reaction with HCl in hot water bath for at least three times per sample, in order to remove possible insoluble carbonate phases (e.g., dolomite, siderite) of the residue. Eventually, the samples were neutralized in deionized water, dried at 40°C overnight, wrapped in tin capsules and analyzed along with multiple blank capsules and isotope standards (IAEA CH-6 = -10.45‰, IAEA CH-7 = -32.15‰, Coplen et al., 2006). The standard deviation of the in-house standard during the period of analyses was better than σ=0.2‰.

RESULTS

The obtained $\delta^{13}C_{org}$ profile shows a background value of ca. -25.70‰, ranging between a minimum of ca. -28.75‰ and a maximum of ca. -23.68‰ (Fig. 2.2).

Notably, the $\delta^{13}C_{org}$ profile depicts a series of significant $\delta^{13}C_{org}$ decreases. The first decrease (E1) occurs at the base of the Brumano section, reaching its miminum of -27.86‰ within the base of the Zu2 Mb (at 61 m, Fig. 2.2), and is followed by a sharp return to background values. Another significant negative peak (E2) occurs in the Brumano section within the base of the Zu3a submember, at 145.3 m ($\delta^{13}C_{org}$ = -27.55‰), immediately followed by the third important negative excursion (E3) between ca. 160-180 m (minimum of -28.13‰ at 166 m; Fig. 2.2). The fourth negative peak of -27.27‰ (E4) occurs in the Italcementi section, within the Zu3b submember, between ca. 27-32 m. From the top of Zu3b to the top of the Italcementi section (Malanotte Fm), the $\delta^{13}C_{org}$ profile depicts a decreasing trend from ca. -23.68‰ to ca. -28.63‰. This negative trend is marked by three sharp negative peaks occurring in the Zu3b and in the Malanotte Fm at meter 52.6, 43.5 and 57, called peak5, peak6 and peak7 respectively ($\delta^{13}C_{org}$ = -26.98‰, -29.45‰ and -29.62‰ respectively; Fig. 2.2) and by an excursion that we called E5 (Fig. 2.2).

The TOC profile depicts a series of increased-value intervals that seems to be correlated with the $\delta^{13}C_{org}$ decreases. The TOC values range between a maximum of 1.52%, reached in correspondence of peak 6, and a minimum of 0.1%, with an average of ca. 0.42%. The marly horizon at the base of the Malanotte Formation records TOC values of up to 0.88%, in agreement with previous results (Galli et al., 2005).

DISCUSSION

The obtained $\delta^{13}C_{org}$ data offer an almost continuous curve from the latest Norian to the early Hettangian, covering the entire Rhaetian interval. Such a continuous record is available only for one other Rhaetian succession, the British Columbia Islands (Canada, Whiteside & Ward, 2011).

Around the Triassic/Jurassic boundary, the “main” and “initial” CIEs are expected to be found, but their identification is not so straightforward. These two isotope excursions have been defined for the first time by Hesselbo et al. (2002) in St Audrie’s Bay (UK): the “initial” was defined as a ca. 5‰ negative excursion, which minimum occurs almost in correspondence of the transition from the Triassic pollen assemblage of the Rhaetipollis germanicus Zone to the Jurassic assemblage of the Heliosporites reissingeri Zone; the turnover from the Triassic dinoflagellate Rhaetogonyaulax rhaetica Zone and the Jurassic Dapcodinium priscum Zone; and the turnover from the foraminifera Glomospira/Glomospirella assemblage to the Eoguttulina liassica assemblage (Hounslow et al., 2004) (Fig. 2.4). The “initial” CIE is followed by the ca. 3.5‰ “main” CIE, which spans a broad interval in which ammonoid Psiloceras species appears (specifically, Psiloceras planorbis; Hesselbo et al., 2002). Between the “initial” and the “main” CIEs, within an interval of more positive $\delta^{13}C_{org}$ values, conodonts disappear (Hesselbo et al., 2002) (Fig. 2.4). In St Audrie’s Bay, van de Schootbrugge et al. (2007) noticed the occurrence of bio-calcification crises expressed as the extinction and malformation of calcareous nannofossils contemporaneous to a bloom of organic-walled algal species (that they defined “disaster” species, i.e., prasinophytes and acritarchs). These bio-calcification crises occurred at the onset and within the “main” CIE, close to the first appearance of the ammonoid Psiloceras planorbis (Fig. 2.4, 2.6).

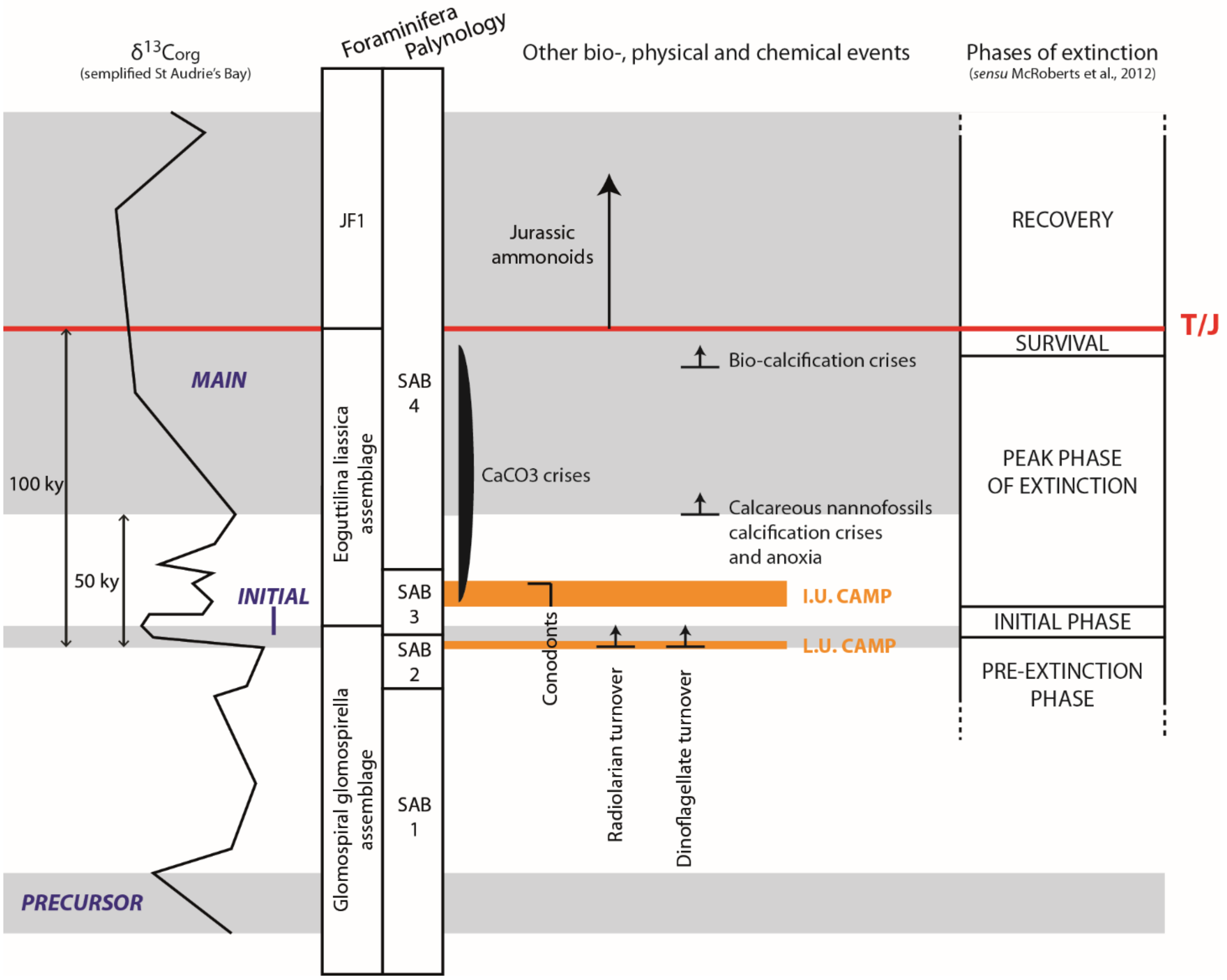

Fig. 2.4 Sketch summarizing the major geochemical, biotic and environmental events at the Rhaetian-Hettangian transition. Modified and integrated from Deenen et al. (2010) and McRoberts et al. (2012).

Correlations based on $\delta^{13}C_{org}$ within the Tethyan area revealed a better constrained chronology for the major (bio-) events, characterizing the "initial" and "main" CIEs. In particular, the correlation with the Austrian sections of the Eiberg Basin, in the Northern Calcareous Alps (Kuerschner et al., 2007; Ruhl et al., 2009), highlighted the easiest identification and correlation of the "initial" CIE respect to the "main" CIE. In fact, in the Austrian sections the "initial" CIE is expressed as a sharp ca. 6‰ negative peak occurring at the transition between the limestones of the Eiberg Member and the marly siltstones of the overlying grey Teifengraben Member (e.g., Ruhl et al., 2009) (Fig. 2.5). The "initial" CIE in the Northern Calcareous Alps is slightly preceded by the disappearance of conodonts and the ammonoid Choristoceras marshi (e.g., Ruhl et al., 2009), thus highlighting a first discrepancy with the St Audrie's Bay record, where conodonts disappeared between the "initial" and the "main" CIEs (Hesselbo et al., 2002). The "main" CIE is recorded only in some Austrian sections

(Kuhjoch/Ochsentaljoch, Kueschner et al., 2007; Hochalplgraben, Kendlbach, Restentalgraben, Schlossgraben, Ruhl et al., 2009) and is represented by a ca. 2-3.5‰ decrease. It encompasses the appearance of the ammonoid Psiloceras spelae and Psiloceras spelae tirolicum; it approximately co-occurred with the base of the Jurassic pollen Cerebropollenites thiergartii; and it is almost in correspondence to the turnover from the Triassic calcareous nannofossil Prinsiosphaera triassica and the Jurassic Schizosphaerella punctuata (to be more precise, S. punctuata occurs ca. 2.5 m below the TJB; Hillebrandt et al., 2007; Bonis et al., 2009a, 2009b; Ruhl et al., 2009). The appearance of the ammonoid P. spelae tirolicum (close to the appearance of P. spelae) has been approved as the bio-event marking the base of the Jurassic (Hillebrandt et al., 2013), as a consequence, the "main" CIE appears to start in the latemost Rhaetian to continue during the early Hettangian, while the "initial" CIE appears to be late Rhaetian in age. Deenen et al. (2010) associated the "initial" CIE with the emplacement of the Lower Unit (L.U.) of Argana Basalts, the ancient CAMP basalts of the Moroccan outcrop, which is supposed to be responsible for the turnover from the Triassic radiolarian assemblage and the Hettangian Canopum merum radiolarian zone (Ward et al., 2001; Williford et al., 2007; Crne et al., 2014). The Intermediate Unit (I.U.), which corresponds to the second lava pulse of CAMP in Morocco (Knight et al., 2004; Deenen et al., 2010), occurs ca. 20 ky after the L.U. and it coincides with the turnover of palynomoph (Hesselbo et al., 2002) and foraminifera assemblages (Hounslow et al., 2004); the disappearance of conodonts; the calcification crises of calcareous nannofossils (Deenen et al., 2010); and marine anoxia (Wignall and Bond, 2008) (Fig. 2.4). The emplacement of the I.U. does not coincide with the onset of the "main" CIE, which therefore appears to be unrelated to the emplacement of the CAMP basalts (Deenen et al., 2010). Evaluation of the timing between the $\delta^{13}C_{org}$ perturbations and the extinction events has been provided by McRoberts et al. (2012) from the Koessen Basin (Northern Calcareous Alps, Austria), where the first appearance of Psiloceras species (approximating the Triassic/Jurassic boundary) occurs ca. 100 ky after the "initial" CIE (Deenen et al., 2010) (Fig. 2.4). They defined the interval below the "initial" CIE (at the top of the limestones of the Eiberg Member) as the "pre-extinction phase", characterized by an "equilibrium fauna" composed of ammonoids (Choristoceras marshi) and bivalves (Oxytoma, Cassianella, Pinna) for deeper water environments, and bivalves (Rhaetavicula, Lyriochlamys, Palaeocardita, Actinostreon, and Palaeonucula), hypercalcifying megalodonts, scleractinian corals, sponges, echinoids, brachiopods and a rich microfauna and microflora for the basin margin environments. These paleocommunities exhibit trophic complexity and dominant stenohaline elements (McRoberts et al., 2012). The "initial" CIE marks the extinction phase, which seems to last for the entire interval comprised between the "initial" and the "main" CIEs and is subdivided into an "initial phase" and a "peak phase" (McRoberts et al., 2012). The "initial extinction phase", coinciding with the minimum of the "initial" CIE, is marked by a significant loss of calcareous nannofossils, an increase in conifer (Cheirolepidiaceae) pollen, Classopollis spores, rare calcareous benthic foraminifera and sporadic bivalves (infaunal heterodont Cardinia hybrida, epibyssate pectinoids Agerchlamys textoria, Pseudolima cf. hettangiensis, epibyssate species of the pterioid Meleagrinella) (Hillebrandt et al., 2007; Boniset al., 2010a; Clemence et al., 2010, McRoberts et al., 2012). The “peak phase” of extinction was particularly severe and no fossils were recovered from this interval, except for some specimens of Cardinia hybrida (McRoberts et al., 2012) (Fig. 2.4). The recovery from the marine extinction seems to coincide with the first appearance of Jurassic ammonoids, in the marly siltstones of the Teifengraben Member, where a paleofauna similar to that of the “pre-extinction phase” has been found (McRoberts et al., 2012).

The transition from the Zu3c submember (Zu Limestones Fm) and the Malanotte Formation of our studied succession bears great similarity with the Austrian sections: the meter-thick marly silty horizon marking the base of the Malanotte Formation seems comparable to the base of the Schattwald Beds, the marly unit at the base of the Teifengraben Member (McRoberts et al., 1997; Galli et al., 2005). This marly horizon in the Malanotte Formation is followed by laminated mudstones and wackestones similar to the lithology of the Teifengraben Member. If this lithostratigraphic correlation is accepted, the “initial” CIE is expected to occur at the base of the Malanotte Fm, as previously confirmed by the work of Galli et al. (2005, 2007), Muttoni et al. (2010) and Bottini et al. (submitted). Moreover, the top of the Zu3c is characterized by the disappearance of benthic foraminifera and reef communities, likely related to a drowning event linked to the end-Triassic mass extinction (Galli et al., 2005) that could be linked to the “initial phase of extinction” described by McRoberts et al. (2012). Nevertheless, there are some inconsistencies. First of all, considering the works of Galli et al. (2005, 2007) and Muttoni et al. (2010), the $\delta^{13}C_{carb}$ negative excursion that they linked to the “initial” CIE is preceded by the marine extinction phase, not followed by as for the Northern Calcareous Alps sections (McRoberts et al., 2012). It can be debated that the stratigraphic position of the “initial” CIE respect to the biotic events could vary as a function of the different sample resolutions of the sections, but the extremely detailed litho-, cyclo- and biostratigraphic study of the Lombard and Austrian successions excluded this option (Jadoul and Gnaccolini, 1992; Jadoul et al., 2004; Galli et al., 2005, 2007; Krystyn et al., 2005, 2007; Kurschner et al., 2007; Hillebrandt et al., 2007, 2009; Jadoul and Galli, 2008; Rigo et al., 2009; Ruhl et al., 2009). Moreover, the published records from all the other Tethyan sections (Palfy et al., 2001, 2007; Hesselbo et al., 2002; Kuerschner et al., 2007; Ruhl et al., 2009; McRoberts et al., 2012) demonstrated that the biotic crises started with the “initial” CIE, and not before. Furthermore, in the Lombard succession, the turnover from the Triassic calcareous nannofossil Prinsiosphaera triassica and the Jurassic Schizosphaerella punctuata (which occurs within the "main" CIE in the Austrian sections) occurs at the base of the Malanotte Formation (Bottini et al., submitted) (Fig. 2.5), suggesting that the $\delta^{13}C$ record of the base of the Malanotte Formation should be marked by the "main" CIE. As a consequence, the $\delta^{13}C_{carb}$ negative excursion recognized by Galli et al. (2005, 2007) and Muttoni et al. (2010), could not correlate to the "initial" CIE, but more likely to a peak of the "main" CIE or at least of the ca. 50 ky interval between the "initial" and the "main" CIEs. Moreover, following McRoberts et al. (2012) chronology, the marine extinction should occur between the "initial" and the "main" CIEs, thus suggesting that the disappearance of benthic foraminifera and reef communities at the top of the Zu3c (Galli et al., 2005) should lie between these two CIEs.

Our work offers for the first time an almost complete $\delta^{13}C_{org}$ record for the whole Rhaetian, providing the opportunity to better investigate and understand the relationship between the trend of the $\delta^{13}C_{org}$ record and the major bio- and lithostratigraphic changes.

Basing on all these information, we propose two possible interpretations for our Rhaetian-Hettangian $\delta^{13}C_{org}$ record: one following the previous studies on the Lombardy Basin (that we called "option 1 - confirmed previous interpretation"), and one considering the new complete $\delta^{13}C_{org}$ record ("option 2 - possible new interpretation").

OPTION 1

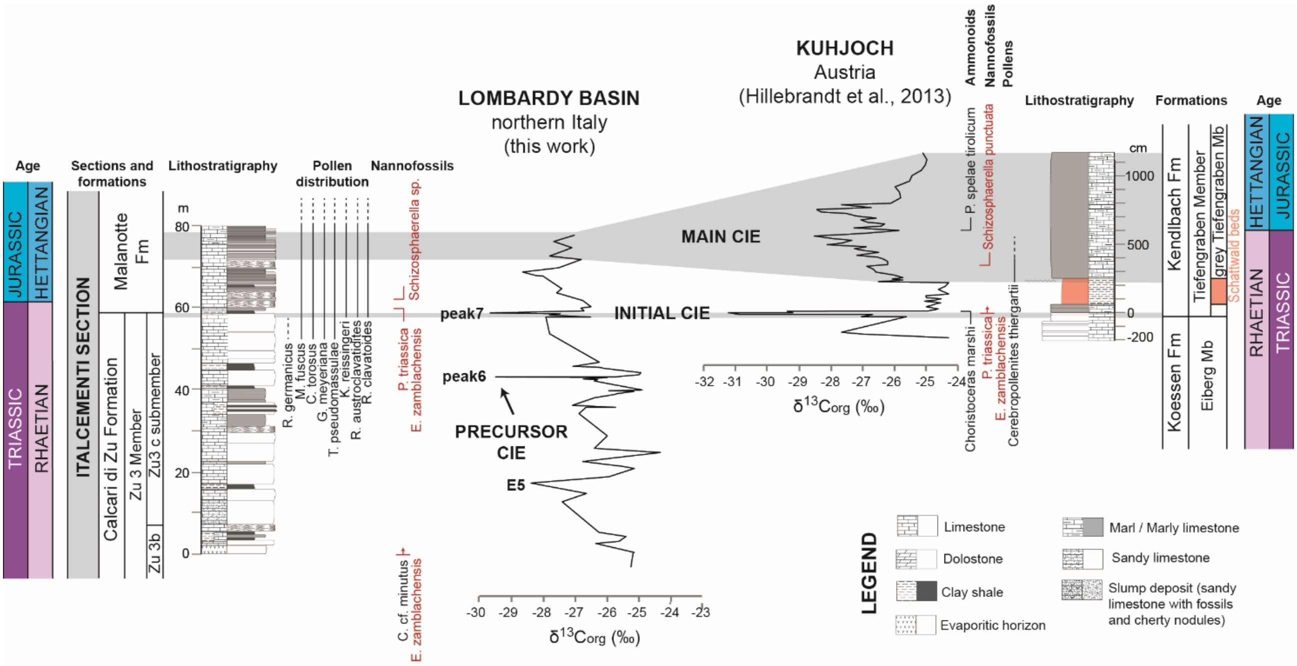

Fig. 2.5 Option 1 – Correlation between the composite succession of the Lombardy Basin (this work) and the Kuhjoch section (Hillebrandt et al., 2013).

Our first interpretation follows the version proposed by Bottini et al. (submitted): peak 7, at the base of the Malanotte Formation, could be interpreted as the “initial” CIE, preceding the bio-calcification crises recorded between the disappearance of the nannofossils P. triassica and E. zamblachensis and the first appearance of Schizosphaerella sp. (Fig. 2.5). As a consequence, peak 6 could be recognized as the “precursor” CIE (Fig. 2.5). The “main” CIE is not clearly identified and its onset is approximately placed after the first appearance of Schizosphaerella sp. (Fig. 2.5). The “initial” and the “main” CIEs are separated by a ca. 10 m interval at the base of the Malanotte Formation: considering an average sedimentation rate of the basin of ca. 100-150 m/Ma (Galli et al., 2005), this interval seems to last for ca. 100-66 ky.

This interpretation is in agreement with the works of Galli et al. (2005, 2007) and Muttoni et al. (2010) that interpreted the $\delta^{13}C_{carb}$ negative peak at the base of the Malanotte Formation as the “initial” CIE. In our studied section, the “initial” occurs within a marly horizon marking the base of the Malanotte Formation (Fig. 2.2, 2.5): this marly horizon is lithostratigraphically correlatable with the Schattwald Beds, the marly unit at the base of the Teifengraben Member in the Eiberg Basin (McRoberts et al., 1997; Galli et al., 2005). In the Eiberg Basin, the “initial” CIE occurs within the Schattwald Beds (Kuerschner et al., 2007; Ruhl et al., 2009), thus supporting option-1 interpretation.

Nevertheless, basing on the GSSP proposal of Hillebrandt et al. (2013) and on the work of van de Schootbrugge et al. (2007), the first appearance of Schizosphaerella sp. should occur within the “main” CIE, in disagreement with option 1.

If we accept option 1 interpretation, E1, E2, E3, E4, peak 5 and E5 appear to be new significant perturbations of the Rhaetian $\delta^{13}C_{org}$ record of the Tethys realm. We thus try to correlate the Rhaetian organic carbon isotope record of the Lombardy Basin with the only other available Rhaetian $\delta^{13}C_{org}$ profile, the British Columbia Islands (Canada, Whiteside & Ward, 2011) (Fig. 2.6) that is a composite $\delta^{13}C_{org}$ profile. This composite profile belongs to the North America realm and it was located on the eastern side of the Panthalassa ocean, on the opposite margin of the supercontinent Pangaea respect to the Lombardy Basin during the Late Triassic (Fig. 2.6). The correlation between these two successions can rely only on the carbon chemostratigraphy, since the Lombardy Basin lacks of a biostratigraphy (or other constraints) useful for global correlations, such as ammonoid or conodont distributions. Therefore, from a chemostratigraphic point of view, we tentatively correlated these two successions as illustrated in Fig. 2.6. Overall, the trends of these two Rhaetian $\delta^{13}C_{org}$ profiles are quite dissimilar, and only some decreases could be tentatively correlated (Fig. 2.6). In particular, the British Columbia Islands profile depicts a wide interval of chaotic oscillations (grey dashed area in Fig. 2.6) that cannot be recognized in our Lombardy Basin record. The dissimilarity between the two successions could be related to the different sampling resolution. On the other hand, it is possible that the accidents of the two compared $\delta^{13}C_{org}$ profiles depend on local factors rather than global causes.

Fig. 2.6 Chemostratigraphic correlation of the Lombardy Basin with other late Rhaetian-early Hettangian sections based on option 1.

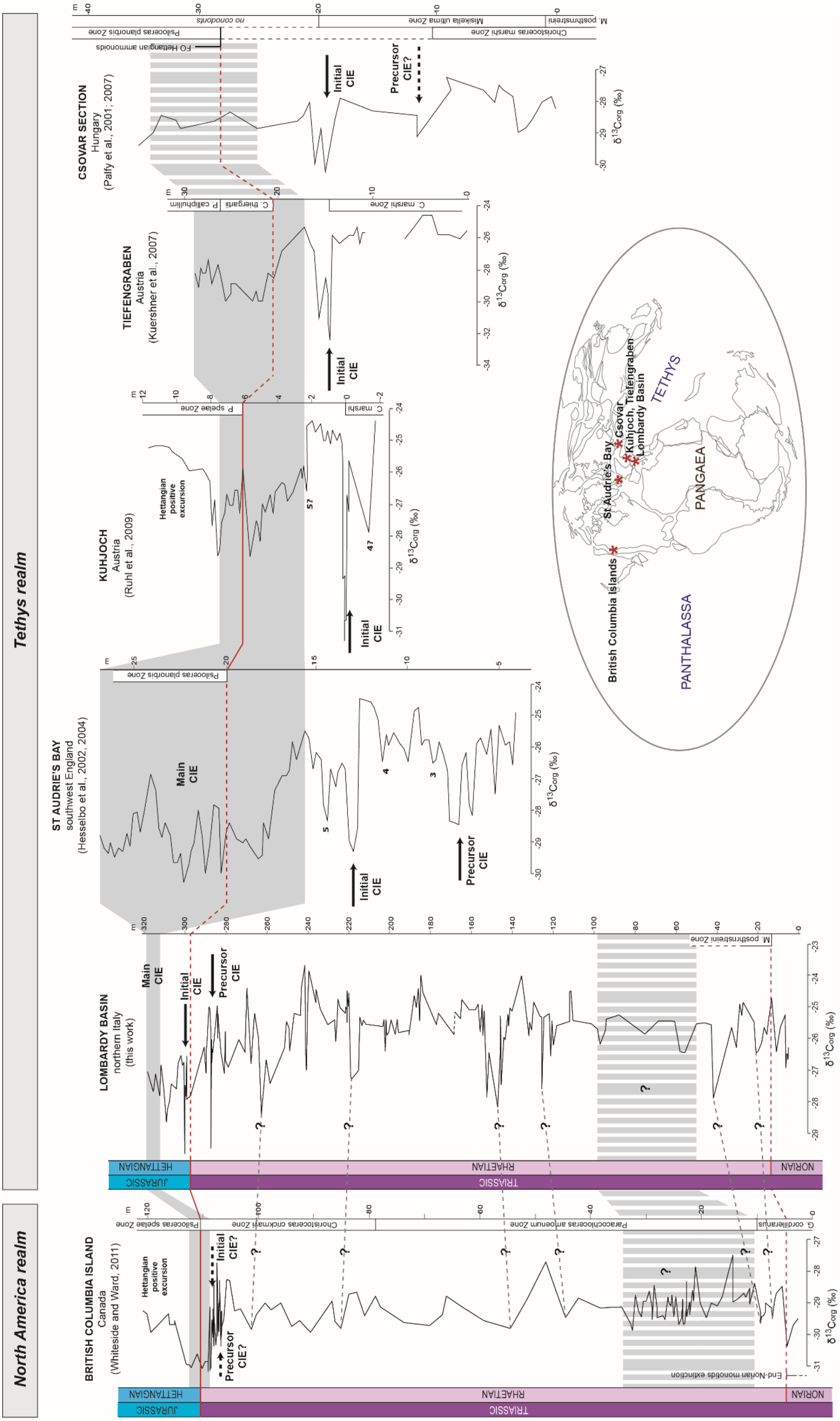

North America realm
Tethys realm
BRITISH COLUMBIA ISLAND
Canada
(Whiteside and Ward, 2011)
LOMBARDY BASIN
northern Italy
(this work)
ST AUDRIE'S BAY
southwest England
(Hesselbo et al., 2002, 2004)
KUHJOCH
Austria
(Ruhl et al., 2009)
TIEFENGRABEN
Austria
(Kuershner et al., 2007)
CSOVAR SECTION
Hungary
(Palfy et al., 2001; 2007)
Hettangian positive excursion
Main CIE
Initial CIE
Precursor CIE
Initial CIE?
Precursor CIE?
JURASSIC
TRIASSIC
HETTANGIAN
RHAETIAN
NORIAN
Psiloceras spelae Zone
Choristoceras crickmayi Zone
Paracochloceras amoenum Zone
G. cordilleranus
End-Norian monotids extinction
M. posthernsteini Zone
Psiloceras planorbis Zone
P. spelae Zone
C. marshi
C. marshi Zone
C. thiergarti
P. calliphyllum
FO Hettangian ammonoids
no conodonts
Misikella ultima Zone
Choristoceras marshi Zone
M. posthernsteini
δ13Corg (‰)
British Columbia Islands
St Audrie's Bay
Csovar
Kuhjoch, Tiefengraben
Lombardy Basin
TETHYS
PANGAEA
PANTHALASSA

OPTION 2

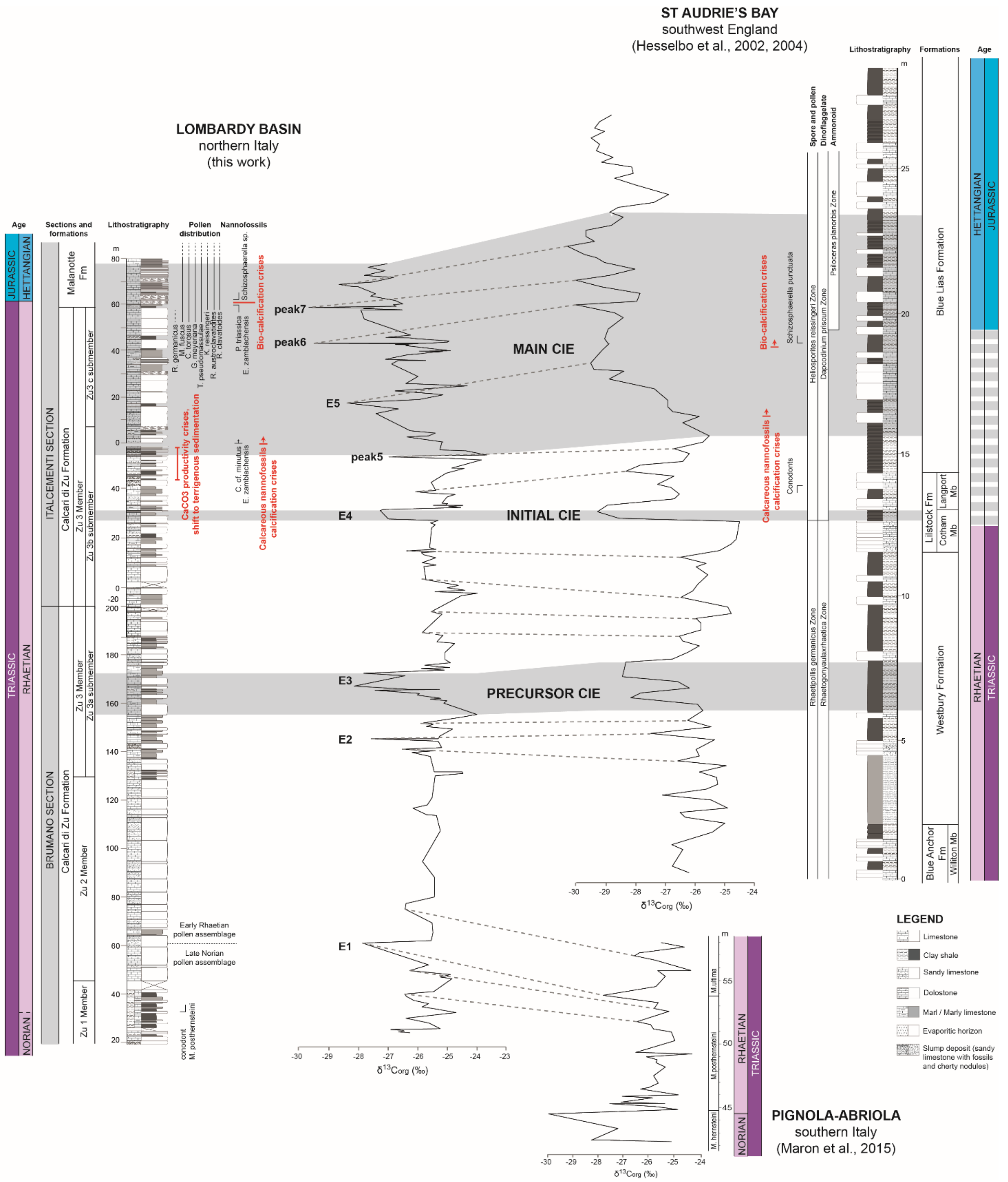

Fig. 2.7 Option 2 – Correlation between the composite succession of the Lombardy Basin (this work) and the St Audrie's Bay section (Hesselbo et al., 2002, 2004).

The Lombardy Basin $\delta^{13}C_{org}$ profile bears great similarity with the St Audrie's Bay $\delta^{13}C_{org}$ record illustrated by Hesselbo et al. (2002) (Fig. 2.7), where the "main" and the "initial" CIEs have been defined for the first time. Therefore, it is possible to correlate not only the "main", "initial" and “precursor” CIEs, but also some single $\delta^{13}C_{org}$ peaks (Fig. 2.7). This interpretation is supported also by the strong correlation between the occurrences of the bio-calcification crises described by van de Schootbrugge et al. (2007) in St Audrie’s Bay and those recognized by Bottini et al. (submitted) in the Lombardy Basin (Fig. 2.7). In fact, in St Audrie’s Bay these calcification crises seem to start at the onset of and during the “main” CIE and are characterized by extremely rare, poorly preserved and smaller-than-average specimens of calcareous nannofossils (van de Schootbrugge et al., 2007). Accordingly, Bottini et al. (submitted) described the calcareous nannofossils from the topmost Zu3b submember to the Malanotte Fm of the Lombardy Basin as rare and poorly to moderately preserved, with overgrowth and showing a decreasing-size trend approaching the T/J. This similarity between the calcareous nannofossils of the St Audrie’s Bay and Lombardy Basin further support option-2 interpretation. Moreover, differently from the option 1, in option 2 the first appearance of Schizosphaerella sp. in the Lombardy Basin occurs within the “main” CIE, in agreement with Hillebrandt et al. (2013) and van de Schootbrugge et al. (2007). Furthermore, if we accepted this new possible interpretation, the interval between the “initial” and the “main” CIEs appears to be characterized by an increase in the terrigenous input, frequent bioturbation and iron-oxide microbial crusts surfaces (hardgrounds), recording a crises of the carbonate productivity (Jadoul et al., 2004), in agreement with McRoberts et al. (2012), who highlighted the occurrence of a carbonate crises (that they referred as “CaCO3 undersaturated ocean”) between the “initial” and the “main” CIEs in the Austrian sections (see also Fig. 2.4). Considering an average sedimentation rate of the basin of ca. 100-150 m/Ma (Galli et al., 2005), the interval between the “initial” and the “main” CIEs seems to last for ca. 200-133 ky, a considerable higher amount of time compared to the ca. 50 ky evaluated by Deenen et al. (2010).

Basing on this interpretation, E2 can be associated to those negative peaks of the St Audrie’s Bay $\delta^{13}C_{org}$ profile (Fig. 2.7) that Dal Corso et al. (2014) suggested to be related to the CAMP volcanism, which is proposed to be started even before the “precursor” CIE (Dal Corso et al., 2012). If we accept this new possible interpretation, all the biotic crises recorded at the top of the Calcari di Zu Fm could be linked to the CAMP activity. On the other hand, E1 appears to occur just above the Norian/Rhaetian boundary (considering the first appearance of conodont Misikella posthernsteini as the bioevent defining the base of the Rhaetian) and could be correlated with the negative peak coinciding with the first appearance of conodont Misikella ultima of the Pignola-Abriola section (southern Italy, Maron et al., 2015; Rigo et al., 2015; Zaffani et al., submitted) (Fig. 2.7).

The “main”, “initial” and “precursor” CIEs are easily recognizable in a number of marine and continental successions worldwide, such as the marine sections of British Columbia Islands (Canada, Whiteside & Ward, 2011), Lake Williston (Canada, Wignall et al., 2007), Newark-Hartford (United States, Whiteside et al., 2010), Ferguson Hill (United States, Ward et al., 2007), New York Canyon (United States, Guex et al., 2004), St Audrie's Bay (UK, Hesselbo et al., 2002), Csovar (Hungary, Palfy et al., 2007), Kuhjoch (Austria, Ruhl et al., 2009), Tiefengraben (Austria, Kuershner et al., 2007); and in the continental section of Astartekloft (Greenland, Hesselbo et al., 2002) (Fig. 2.8). Notably, there is an appreciable similarity among the "main" CIE of the Lombardy Basin composite section, St Audrie's Bay and the Queen Charlotte Islands composite section (see "Close-up of the Main CIE" in Fig. 2.8). The distant palaeogeographic position of these three geological successions during the Late Triassic (planisphere in Fig. 2.8) and the similarity between their $\delta^{13}C_{org}$ records suggest that the "main" CIE has a global occurrence and was likely triggered by a common cause(s) (e.g., CAMP activity, methane release, bolide impacts, Hallam and Wignall, 1999; Palfy et al., 2001; Wignall, 2001; Hesselbo et al., 2002; Olsen et al., 2002; Simms, 2003).

Fig. 2.8 Chemostratigraphic correlation of the Lombardy Basin with other late Rhaetian-early Hettangian sections distributed worldwide based on option 2. In the grey box, a close-up of the chemostratigraphic correlation of the "main" CIE.

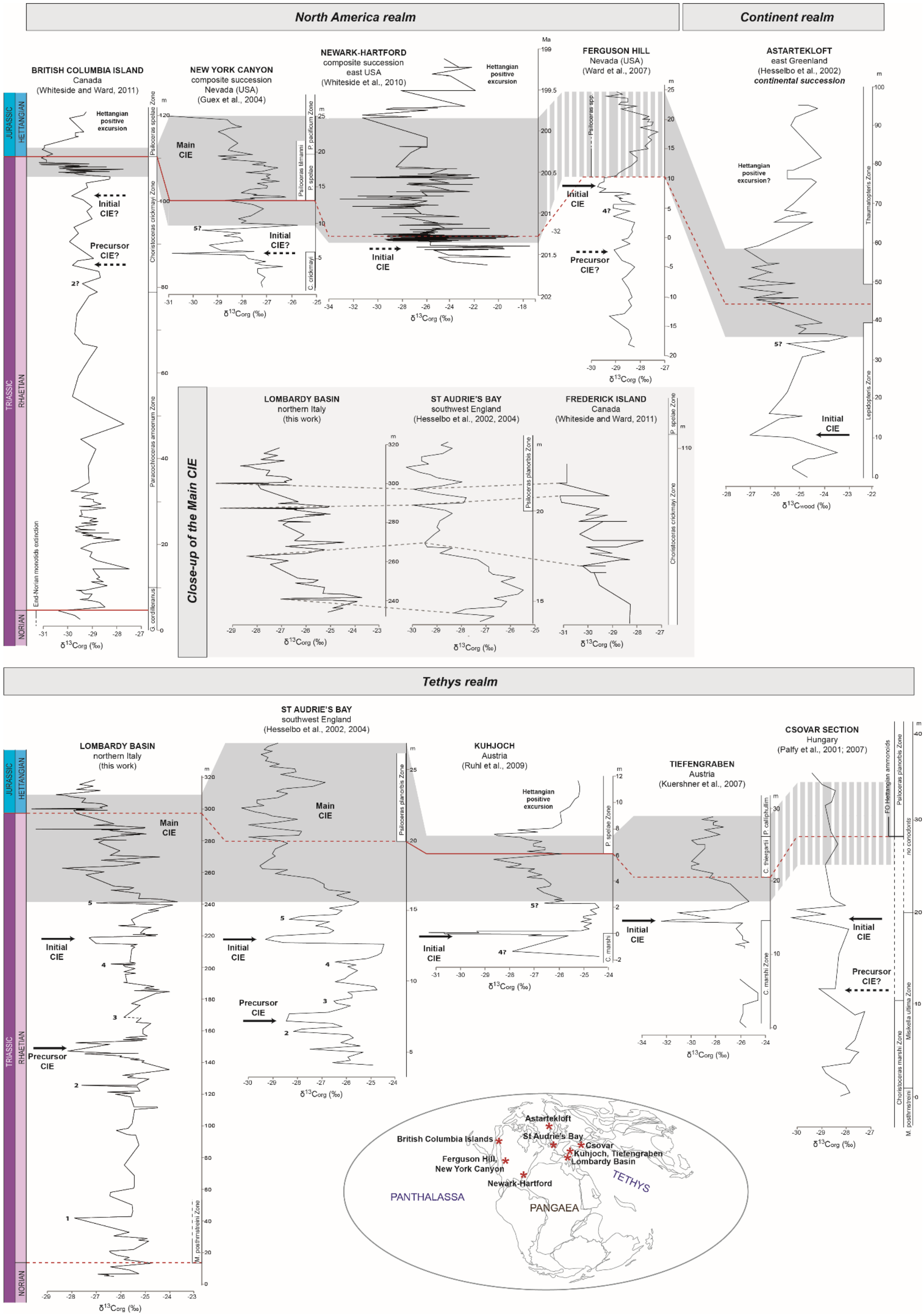
North America realm
Continent realm
BRITISH COLUMBIA ISLAND
Canada
(Whiteside and Ward, 2011)
NEW YORK CANYON
composite succession
Nevada (USA)
(Guex et al., 2004)
NEWARK-HARTFORD
composite succession
east USA
(Whiteside et al., 2010)
FERGUSON HILL
Nevada (USA)
(Ward et al., 2007)
ASTARTEKLOFT
east Greenland
(Hesselbo et al., 2002)
continental succession
Hettangian positive excursion
Hettangian positive excursion?
Main CIE
Initial CIE
Initial CIE?
Precursor CIE?
End-Norian monotids extinction
JURASSIC
HETTANGIAN
TRIASSIC
RHAETIAN
NORIAN
Close-up of the Main CIE
LOMBARDY BASIN
northern Italy
(this work)
ST AUDRIE'S BAY
southwest England
(Hesselbo et al., 2002, 2004)
FREDERICK ISLAND
Canada
(Whiteside and Ward, 2011)
Tethys realm
KUHJOCH
Austria
(Ruhl et al., 2009)
TIEFENGRABEN
Austria
(Kuershner et al., 2007)
CSOVAR SECTION
Hungary
(Palfy et al., 2001; 2007)
Precursor CIE
$\delta^{13}C_{org}$ (‰)
$\delta^{13}C_{wood}$ (‰)
Astartekloft
British Columbia Islands
St Audrie's Bay
Csovar
Kuhjoch, Tiefengraben
Lombardy Basin
Ferguson Hill, New York Canyon
Newark-Hartford
PANTHALASSA
TETHYS
PANGAEA

CONCLUSION

The late Norian-early Hettangian organic carbon isotope record of the Lombardy Basin reveal a series of $\delta^{13}C_{org}$ decreases that provides a new possible interpretation of the relationship between carbon cycle disruption, CAMP volcanism and end-Triassic mass extinction for the Lombardy Basin area. In fact, previous works (here referred as "option 1") recognized the "initial" CIE as the sharp negative $\delta^{13}C_{org}$ peak at the base of the Malanotte Formation and the "precursor" as the negative shift at the top of the Zu3c submember, while the "main" has never been clearly identified. Our complete Rhaetian $\delta^{13}C_{org}$ profile shows a great similarity with the St Audrie's Bay $\delta^{13}C_{org}$ record, where the "main", "initial" and "precursor" negative carbon isotope excursions were defined for the first time. Therefore, through these new chemostratigraphic correlations ("option 2") it is possible to reconsider the previous interpretation of the Lombardy Basin $\delta^{13}C_{org}$ disruptions (option 1). In fact, the correlation with the St Audrie's Bay section permits to identify the "initial" CIE with the pronounced and sharp negative peak within the Zu3b submember, ca. 90 m below the base of the Malanotte Formation. In light of the complete Rhaetian $\delta^{13}C_{org}$ profile of the Lombardy Basin and considering the correlation with the St Audrie's Bay section, it is possible to place the onset of the "main" CIE at the top of the Zu3b submember. The "main" CIE thus appears to encompass the Zu3c submember and the Malanotte Fm. With option 2, the "precursor" has been identified in the Zu3a submember. These negative carbon isotope excursions have been linked by several Authors to the CAMP volcanism: as a consequence, all the biotic crises recorded at the top of the Calcari di Zu Formation could be ascribed to this large igneous province activity. This new interpretation (option 2) of the Lombardy Basin organic carbon isotope record seems to be in agreement with the relative timing of the major end-Triassic events, that are the carbonate productivity crises, at least two bio-calcification crises, the first appearance of calcareous nannofossil Schizosphaerella sp. and the age of the "main" negative carbon isotope excursion. Nevertheless, option 2 fails to account for the lithostratigraphic correlation between the Malanotte Fm and the Tiefengraben Member, which was considered a major constraints of the previous interpretation of the $\delta^{13}C_{org}$ profile of the Lombardy Basin (option 1). Moreover, with option 2 the estimated duration of the interval between the "initial" and the "main" CIEs almost doubles that evaluated by previous works. On the other hand, option 1 shows inconsistencies between the occurrence of the $\delta^{13}C_{org}$ excursions and the timing of the major biotic events. Therefore, basing on the available data, we cannot exclude one interpretation for the other. Further biostratigraphic analyses (especially of fossils useful for the identification of stage boundaries and/or biostratigraphic correlations, such as conodonts or ammonoids) are required in order to constrain the timing and the cause-and-effects relationship of the Rhaetian organic carbon isotope record of the Lombardy Basin.

References

Bachan, A., van de Schootbrugge, B., Fiebig, J., McRoberts, C.A., Ciarapica, G. and Payne, J.L., 2012. Carbon cycle dynamics following the end-Triassic mass extinction: Constraints from paired d13Ccarb and d13Corg records. Geochem. Geophys. Geosyst., 13, Q09008, doi:10.1029/2012GC004150.

Beerling, D.J., Berner, R.A., 2002. Biogeochemical constraints on the Triassic–Jurassic boundary carbon cycle event. Glob. Biogeochem. Cycles, 16, 1 –13.

Cirilli, S., Galli, M.T., Jadoul, F., Rettori, R., Spina, A., 2000. Implicazioni stratigrafico-paleoclimatiche ed evoluzione paleogeografica della successione Retico-Hettangiana del Monte Albenza (Prealpi Bergamasche). In: A. Cherchi and C. Corradini (eds), Crisi biologiche, radiazioni adattative e dinamica delle piattaforme carbonatiche.

Cirilli, S., Marzoli, A., Tanner, L., Bertrand, H., Buratti, N., Jourdan, F., Bellieni, G., Kontak, D., Renne, P.R., 2009. Latest Triassic onset of the Central Atlantic Magmatic Province (CAMP) volcanism in the Fundy Basin (Nova Scotia): New stratigraphic constraints. Earth and Planetary Science Letters 286 (3–4), 514–525.

Coplen, T.B., Brand, W.A., Gehre, M., Groning, M., Meijer, H.A.J., Toman, B. & Verkouteren, R.M., 2006. New guidelines for $d^{13}C$ measures. Analytical Chemistry, 78, 2439–2441.

Dal Corso, J., Mietto, P., Newton, R.J., Pancost, R.D., Preto, N., Roghi, G., Wignall, P.B., 2014. Discovery of a major negative δ13C spike in the Carnian (Late Triassic) linked to the eruption of Wrangellia flood basalts. Geology, 40, 79–82; doi:10.1130/G32473.1.

Deenen, M.H.L., Ruhl, M., Bonis, N.R., Krijgsman, W., Kuerschner, W.M., Reitsma. M., van Bergen, M.J., 2010. A new chronology for the end-Triassic mass extinction. Earth and Planetary Science Letters, 291, 113–125.

Galli, M.T., 2002. Il limite Triassico-Giurassico neele Prealpi Bergamasche: un approccio stratigrafico integrato. PhD tesi, University of Milan.

Galli, M. T., Jadoul, F., Bernasconi, S. M. and Weissert, H., 2005. Anomalies in global carbon cycling and extinction at the Triassic/Jurassic boundary: Evidence from a marine C-isotope record. Palaeogeogr. Palaeoclimatol. Palaeoecol., 216, 203–214.

Galli, M. T., Jadoul, F., Bernasconi, S. M., Cirilli, S., and Weissert H., 2007. Stratigraphy and palaeoenvironmental analysis of the Triassic-Jurassic transition in the western southern Alps (northern Italy). Palaeogeogr. Palaeoclimatol. Palaeoecol., 244, 52–70.

Giordano, N., Rigo, M., Ciarapica, G. & Bertinelli, A., 2010. New biostratigraphical constraints for the Norian/Rhaetian boundary: data from Lagonegro Basin, Southern Apennines, Italy. Lethaia, 43, 573–586.

Greene, S.E., Martindale, R.C., Ritterbush, K.A., Bottjer, D.J., Corsetti, F.A., Berelson, W.M., 2012. Recognizing ocean acidification in deep time: An evaluation of the evidence for acidification across the Triassic-Jurassic boundary. Earth-Science Reviews, 113, 72-93.

Guex, J., Bartolini, A., Atudorei, V., Taylor, D., 2004. High resolution ammonite and carbon isotope stratigraphy across the Triassic–Jurassic boundary at New York Canyon (Nevada). Earth Planet. Sci. Lett. 225, 29–41.

Hallam, A.,2002. How catastrophic was the end-Triassic mass extinction? Lethaia, 35, 147-157.

Hallam, A., Wignall, P.B., 1999. Mass extinction and sea level change. Earth-Science Review, 48, 217– 258.

Hames, W.E., Renne, P.R., Ruppel, C., 2000. New evidence for geologically instantaneous emplacement of earliest Jurassic Central Atlantic magmatic province basalts on the North American margin. Geology 28, 859–862.

Hesselbo, S.P., Robinson, S.A., Surlyk, F. & Piasecki, S., 2002. Terrestrial and marine extinction at the Triassic-Jurassic boundary synchronized with major carbon- cycle perturbation: a link to initiation of massive volcanism? Geology, 30, 251–254.

Hesselbo, S. P., McRoberts, C. A., and Pálfy, J., eds., 2007. Special Issue: Triassic-Jurassic Boundary Events: Palaeogeography, Palaeoclimatology, Palaeoecology, v. 244. 423 p.

Hounslow, M.W., Posen, P.E., Warrington, G., 2004. Magnetostratigraphy and biostratigraphy of the Upper Triassic and lowermost Jurassic succession, St. Audrie's Bay, UK. Palaeogeogr. Palaeoclimatol. Palaeoecol., 213, 331–358.

Jadoul, F, Gnaccolini, M., 1992. Sedimentazione ciclica nel Trias Lombardo: osservazioni e prospettive. Rivista Italiana di Paleontologia e Stratigrafia, 97, 307-328.

Jadoul, F., Galli, M.T., Berra, F., Cirilli, S., Ronchi, P., Paganoni, A., 2004. The Late Triassic–Early Jurassic of the Lombardy Basin: stratigraphy, palaeogeography and palaeontology. 32nd International Geological Congress, Field Trip Guide Book, P68, 6, 36 pp.

Jadoul, F., and Galli, M. T., 2008. The Hettangian shallow water carbonates after the Triassic/Jurassic biocalcification crisis: The Albenza formation in the western Southern Alps. Riv. Ital. Paleontol. Stratigr., 114, 453–470.

Kent, D.V., and Muttoni, G., 2003. Mobility of Pangea: Implications for Late Paleozoic and early Mesozoic paleoclimate. P.M. Letourneau, P.E. Olsen, Editors, The Great Rift Valleys of Pangea in Eastern North America. Tectonics, Structure, and Volcanism. Volume 1, 12-20, Columbia University Press.

Kent, D.V., Olsen, P.E., 2008. Early Jurassic magnetostratigraphy and paleolatitudes from the Hartford continental rift basin (eastern North America): Testing for polarity bias and abrupt polar wander in association with the central Atlantic magmatic province. Journal of Geophysical Research B: Solid Earth 113 (6), 1–24.

Korte, C., Kozur, H.W., Veizer, J., 2005. 13C and 18O values of Triassic brachiopods and carbonate rocks as proxies for coeval seawater and palaeotemperature. Palaeogeography, Palaeoclimatology, Palaeoecology, 226, 287–306.

Krystyn, L., Boehm, F., Kürschner, W.M. and Delecat, S., 2005. The Triassic-Jurassic boundary in the Northern Calcareous Alps. In: Palfy J. and Oszvart P. (Eds), Program, Abstracts and Field Guide. 5th Field Workshop of IGCP 458 Project (Tata and Hallein, September 2005).

Krystyn, L., Richoz, S., Gallet, Y., Bouquerel, H., Kürschner, W.M., Spotl, C., 2007. Updated bio- and magnetostratigraphy from Steinbergkogel (Austria), candidate GSSP for the base of the Rhaetian stage. Albertiana, 36: 164-173.

Krystyn, L., 2010. Decision report on the defining event for the base of the Rhaetian stage. Albertiana, 38: 11–12.

Kump, L.R., Arthur, M.A., 1999. Interpreting carbon-isotope excursions: carbonates and organic matter. Chemical Geology, 161, 181-198.

Kürschner, W.M., Bonis, N.R. and Krystyn, L., 2007. Carbon-isotope stratigraphy and palynostratigraphy of the Triassic-Jurassic transition in the Tiefengraben section - Northern

Calcareous Alps (Austria). Palaeogeography, Palaeoclimatology, Palaeoecology, 244(1-4): 257-280.

Lakew, T., 1990. Microfacies and cyclic sedimentation of the Upper Triassic (Rhaetian) Calcare di Zu (Southern Alps). Facies, 22, 187–232.

Maron, M., Rigo, M., Bertinelli, A., Katz, M.E., Godfrey, L., Zaffani, M., and Muttoni, G., 2015. Magnetostratigraphy, biostratigraphy and chemostratigraphy of the Pignola-Abriola section: New constraints for the Norian-Rhaetian boundary. Geological Society of America Bulletin, 127, 962-974. doi:10.1130/B31106.1.

Marzoli, Andrea, Renne, P.R., Piccirillo, E.M., Ernesto, M., Bellieni, G., and De Min, A., 1999. Extensive 200 Million-Year-Old Continental Flood Basalts of the Central Atlantic Magmatic Province, *Science*, 284, 616-618.

Marzoli, A., Bertrand, H., Knight, K.B., Cirilli, S., Buratti, N., Vérati, C., Nomade, S., Renne, P.R., Youb,i N., Martini, R., Allenbach, K., Neuwerth, R., Rapaille, C., Zaninetti, L., Bellieni, G., 2004. Synchrony of the Central Atlantic magmatic province and the Triassic-Jurassic boundary climatic and biotic crisis. Geology, 32, 973–976.

Majzon, L., 1954. Contributions to the stratigraphy of the Dachstein-Limestone. Budapest Acta Geol. Acad. Sci. Hongrie, 2, 243–249.

McElwain J.C., Beerling D.J., Woodward F.I., 1999. Fossil plants and global warming at the Triassic-Jurassic boundary. Science, 285, 1386-1390.

McElwain, J.C., Popa, M.E,. Hesselbo, S.P., Haworth, M., Surlyk, F., 2007. Macroecological responses of terrestrial vegetation to climatic and atmospheric change across the Triassic/Jurassic boundary in East Greenland. Paleobiology, 33, 547–573.

McElwain, J.C., Wagner, P.J., Hesselbo, S.P., 2009. Fossil plant relative abundances indicate sudden loss of late Triassic biodiversity in East Greenland. Science, 324, 1554–1556.

McRoberts, C.A., Newton, C.R., 1995. Selective extinction among end-Triassic European bivalves. Geology, 23, 102-104.

McRoberts, C.A., Furrer, H., Jones, D.S., 1997. Palaeoenvironmental interpretation of a Triassic–Jurassic boundary section from Western Austria based on palaeoecological and geochemical data. Palaeogeogr. Palaeoclimatol. Palaeoecol., 136, 79– 95.

Muttoni, G., Kent, D.V., Jadoul, F., Olsen, P.E., Rigo, M., Galli, M.T., Nicora, A., 2010. Rhaetian magneto-biostratigraphy from the Southern Alps (Italy): Constraints on Triassic chronology. Palaeogeography, Palaeoclimatology, Palaeoecology, 285, 1–16.

Muttoni, G., Mazza, M., Mosher, D., Katz, M.E., Kent, D.V., Balini, M., 2014. A Middle–Late Triassic (Ladinian–Rhaetian) carbon and oxygen isotope record from the Tethyan Ocean. Palaeogeography, Palaeoclimatology, Palaeoecology, 399, 246-259.

Nomade, S., Knight, K.B., Beutel, E., Renne, P.R., Verati, C., Féraud, G., Marzoli, A., Youbi, N., Bertrand, H., 2007. Chronology of the Central Atlantic Magmatic Province: Implications for the Central Atlantic rifting processes and the Triassic-Jurassic biotic crisis. Palaeogeography, Palaeoclimatology, Palaeoecology, 244 (1–4), 326–344.

Olsen, P. E., Kent, D. V., Sues, H.-D., Koeberl, C., Huber, H., Montanari, A., Rainforth, E. C., Fowell, S. J., Szajna, M. J., Hartline, B. W., 2002. Ascent of Dinosaurs Linked to an Iridium Anomaly at the Triassic-Jurassic Boundary. Science, 296, 1305-1307.

Palfy, J., Demeny, A., Haas, J., Hetenyi, M., Orchard, M.J., Vetl, I., 2001. Carbon isotope anomaly and other geochemical changes at the Triassic–Jurassic boundary from a marine section in Hungary. Geology, 29, 1047–1050.

Palfy, J., Demeny, A., Haas, J., Carter, E.S., Gorog, A., Halasz, D., Oravecz-Scheffer, A., Hetenyi, M., Marton, E., Orchard, M.J., Ozsvart, P., Veto, I., Zaizon, N., 2007. Triassic-Jurassic boundary events inferred from integrated stratigraphy of the Csovar section, Hungary. Palaeogeography, Palaeoclimatology, Palaeoecology, 224, 11-33.

Richoz, S., Krystyn, L., Spotl, C., 2007. Towards a carbon isotope reference curve of the Upper Triassic. New Mexico Museum of Natural History and Science Bulletin, 41, 366-367.

Rigo, M., Galli, M.T., Jadoul, F., 2009. Late Triassic biostratigraphic constraints in the Imagna Valley (western Bergamasc Alps, Italy). Albertiana, 37, 39-42.

Rigo, M., Bertinelli, A., Concheri, G., Gattolin, G., Godfrey, L., Katz, M.E., Maron, M., Muttoni, G., Sprovieri, M., Stellin, F., Zaffani, M., 2015. The Pignola-Abriola section (southern Apennines, Italy): a new GSSP candidate for the base of the Rhaetian Stage. Lethaia, doi: 10.1111/let.12145.

Ruhl, M., Kürschner, W.M., Krystyn, L.,(2009. Triassic-Jurassic organic carbon isotope stratigraphy of key sections in the western Tethys realm (Austria). Earth and Planetary Science Letters, 281 (3-4). 169-187.

Schaller,M.F.,Wright, J.D., Kent,D.V., 2011.Atmospheric pCO2 Perturbations Associated with the Central Atlantic Magmatic Province. Science 331 (6023), 1404–1409.

Schlager, W., 1989. Drowning unconformities on carbonate platforms. Spec. Publ.-SEPM 44, 15–25.

Schoene, B., Guex, J., Bartolini, A., Schaltegger, U., Blackburn, T.J., 2010. Correlating the end-Triassic mass extinction and flood basalt volcanism at the 100 ka level. Geology, 38, 387–390.

Sepkoski, J.J., Jr., 1996. Competition in macroevolution: the double wedge revisited. In E*volutionary Paleobiology* (D. Jablonski, D.H. Erwin and J.H. Lipps, eds), pp. 211–255. Chicago, IL: University of Chicago Press.

Sephton, M.A., Amor, K., Franchi, I.A., Wignall, P.B., Newton, R., Zonneveld, J.P., 2002. Carbon and nitrogen isotope disturbances and an end-Norian (Late Triassic) extinction event. Geology, 30, 1119-1122.

Schuurman, W.M.L., 1979. Aspects of Late Triassic palynology. 3 Palynology of latest Triassic and earliest Jurassic deposits of the northern Limestone Alps in Austria and southern Germany, characterization of the Rhaetian stage in Europe. Review Palaeobotany, Palynology, 27, 29-54.

Simms, M.J., 2003. Uniquely extensive seismite from the latest Triassic of the United Kingdom: Evidence for bolide impact? Geology, 31, 557-560.

Tanner, L.H., 2010. The Triassic isotope record. In: Lucas, S.G. (ed.) The Triassic Timescale. Geological Society, London, special publication, 334, 103-118.

Van de Schootbrugge, B., Payne, J.L., Tomasovych, A., Pross, J., Fiebig, J., Benbrahim, M., Follmi, K.B., Quan, T.M,. 2008. Carbon cycle perturbation and stabilization in the wake of the Triassic-Jurassic boundary mass extinction event. Geochemistry Geophysics Geosystems, 9, 1-16.

Ward PD, Haggart JW, Carter ES, Wilbur D, Tipper HW, Evans T., 2001. Sudden productivity collapse associated with the Triassic-Jurassic boundary mass extinction. Science, 292, 1148-1151.

Ward, P.D., Garrison, G.H., Haggart, J.W., Kring, D.A., Beattie, M.J., 2004. Isotopic evidence bearing on Late Triassic extinction events, Queen Charlotte Islands, British Columbia, and implications for the duration and cause of the Triassic/Jurassic mass extinction. Earth and Planetary Science Letters, 224, 589-600.

Ward, P., Garrison, G., Williford, K.. Kring, D., Goodwin, D., Beattie, M., and McRoberts, C., 2007. The organic carbon isotopic and paleontologicalrecord across the Triassic-Jurassic boundary at the candidate GSSP section at Ferguson Hill, Muller Canyon, Nevada,USA. Palaeogeography, Palaeoclimatology, Palaeoecology, 244 (1-4), 281-289.

Whiteside, J.H., Olsen, P.E., Eglinton, T., Brookfield, M.E., and Sambrotto, R.N., 2010. Compound-specific carbon isotopes from Earth's largest flood basalt eruptions directly linked to the end-Triassic mass extinction. PNAS, 107, 6721–6725.

Whiteside, J.H., Ward, P.D., 2011. Ammonoid diversity and disparity track episodes of chaotic carbon cycling during the early Mesozoic. Geology, 39, 99-102.

Wignall, P.B., 2001. Large igneous provinces and mass extinctions. Earth-Science Reviews, 53, 1–33.

Wignall, P.B., Zonneveld, J.-P., Newton, R.J., Amor, K., Sephton, M.A. & Hartley, S., 2007. The end Triassic mass extinction record of Williston Lake, British Columbia. Palaeogeogr. Palaeoclimatol. Paleoecol., 253, 385–406.

Wood, R., 1999. Reef Evolution. Oxford University Press. 414 pp.

CHAPTER 3

Unpublished data and minor works

MT. S. ENOC SECTION (LAGONEGRO BASIN, SOUTHERN ITALY)

This geological section belongs to the Lagonegro Basin (southern Apennines, southern Italy) and was analyzed for $\delta^{13}C_{org}$ and TOC purposes along with the Pignola-Abriola, Mt. Volturino and Madonna del Sirino sections (Fig. 3.1). Compared to all the other Lagonegro sections, the Mt. S. Enoc succession consists of more frequent and thicker beds of cherty limestone, often red in color, characterized by low organic carbon content. As a consequence, the scarcity of samples suitable for $\delta^{13}C_{org}$ and TOC analyses (i.e., enriched in organic matter, such as dark limestones, marls and shales) is reflected in the low-resolution profiles of this section.

Lithostratigraphy

The Mt. S. Enoc section crops out close to Viggiano village, on the right bank of the Alli river (Val d'Agri) (Fig. 3.1). This succession displays the topmost portion of the Calcari con Selce Fm (i.e., the so-called "transitional interval"; Miconnet, 1982) and the Scisti Silicei Fm. The base of the section is characterized by 2,5 m of "transitional interval", which shows a gradual decrease in carbonate accompanied by a gradual increase in the clay and siliceous components through the top of the interval. Silicification of the carbonates also increases upward (Amodeo, 1999; Rigo et al., 2005; Giordano et al., 2010). The "transitional interval" is followed by 20 m of cherty limestones (sometimes nodular) alternated to thin silicified calcarenites with red and green clayey intercalations belonging to the Scisti Silicei Fm (Giordano et al., 2011). The rest of the succession consists of thick cherty limestones (mostly silicified), in alternation with clayey shales and thin cherty limestones (Giordano et al., 2010, 2011). Considering the transition from the carbonate sedimentation of the "transitional interval" to the siliceous deposition of Scisti Silicei Fm, the Mt. S. Enoc section may be considered an intermediate-distal facies-association of the Lagonegro Triassic-Jurassic successions (*sensu* Scandone, 1967; see also Giordano et al., 2010, 2011).

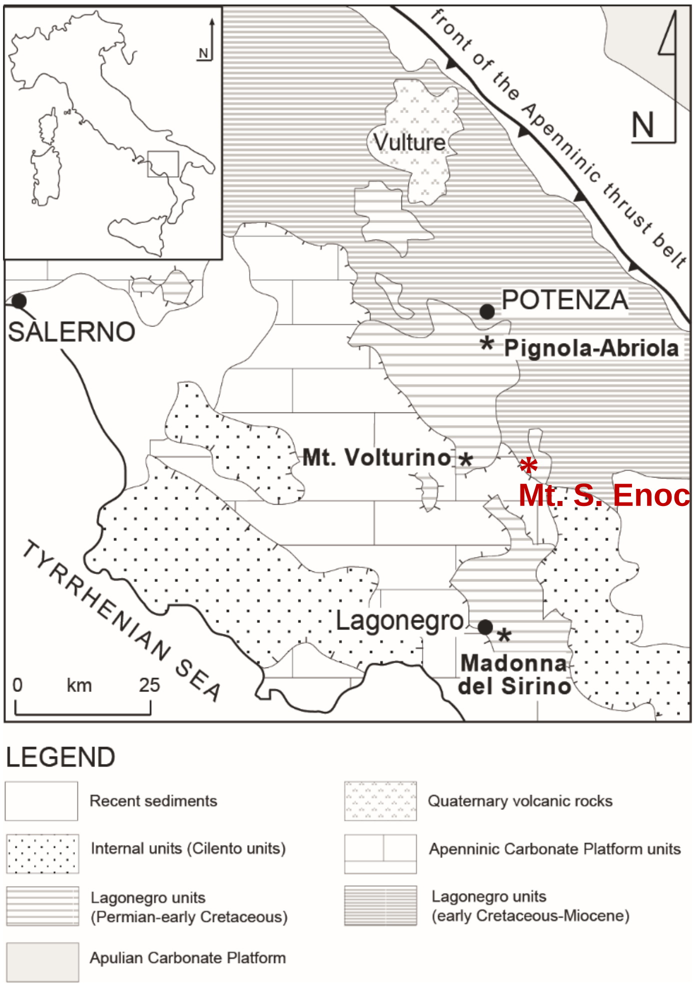

Fig. 3.1 Structural map showing the tectonic units of the Lagonegro Basin. The outcrops of the studied sections are marked by black solid stars. Mt. S. Enoc position is highlighted by the red bold star. Modified from Bertinelli et al. (2005b).

Biostratigraphy

The distribution of the most important conodonts and radiolarians is shown in Fig. 3.2. The biozonations are those proposed by Kozur & Mock (1991) and Carter (1993). At the base of the section, *Mockina bidentata*, *Parvigondolella lata* and *Parvigondolella andrusovi* occur, the latter defining the base of the *Misikella hernsteini – P. andrusovi* Zone (Kozur & Mock, 1991; Giordano et al., 2010, 2011). *Parvigondolella vrielyncki* occurs only at ca. 18 m. *Misikella hernsteini* appears with the first specimen of *Misikella hernsteini/Misikella posthernsteini* transitional form (Kozur & Mock, 1991; Giordano et al., 2010, 2011) at 43 m. *M. hernsteini/M. posthernsteini* transitional forms are supposed to represent the phylogenetic evolution of *M. hernsteini*: for this reason, the first occurrence of *M. hernsteini* is supposed to occur at a lower stratigraphic level than the transitional forms (Fig. 3.2). *M. posthernsteini* occurs at 52 m, marking the base of the *M. posthernsteini* zone (Kozur & Mock, 1991; Giordano et al., 2010). The poor preservation of the pyritized radiolarians recovered at ca. 44 m prevents their specific determination (Giordano et al., 2010). The CAI of the samples collected in the Mt. S. Enoc section corresponds to 3, which indicates that the temperature never exceeded 200°C (Epstein et al., 1977; Bazzucchi et al., 2005; Reggiani et al., 2005; Rigo et al., 2005, 2012). The effect of these temperature are negligible on the $\delta^{13}C_{org}$ signal, since temperatures approaching those of oil generation are required to significantly alter the $\delta^{13}C_{org}$ primary signal (Hayes et al., 1999; Cramer & Saltzman, 2007).

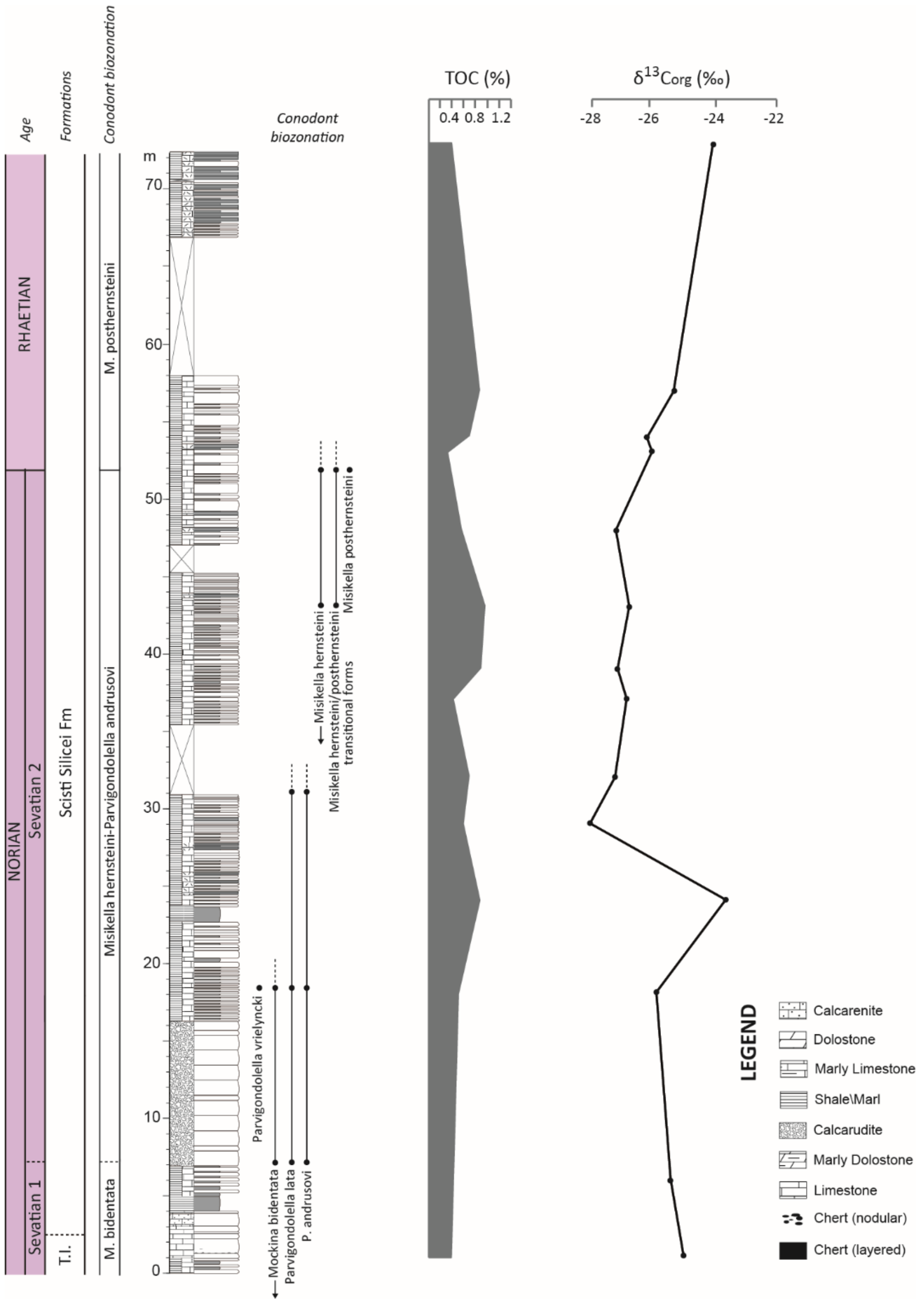

Figure 3.2 Lithostratigraphy, conodont biostratigraphy, TOC and $\delta^{13}C_{org}$ of the Mt. S. Enoc section. Biostratigraphy is based on the work of Giordano et al. (2010).

Chemostratigraphy

The TOC content and the $\delta^{13}C_{org}$ variations are shown in Fig. 3.2. The organic carbon curve shows a minimum of -28.01‰ and a maximum of –23.64‰, with an average value of ca. -26.04‰. Compared to the other Lagonegro sections (Pignola-Abriola, Mt. Volturino, Madonna del Sirino, see **Chapter 1**), Mt. S. Enoc $\delta^{13}C_{org}$ profile appears less detailed and almost flat. This is related to the reduced number of samples suitable for organic carbon analyses, such as marls and dark shales. In fact, clear to reddish silicified cherty limestones are the most abundant lithotypes, which are characterized by a poor content of organic matter. Nevertheless, some trends could be recognized. The first 25 m of the section show a slight decrease of the $\delta^{13}C_{org}$, followed by a prominent increase up to -23.64‰ at 24 m. Successively, the curve steeply decreases to a minimum of -28.01‰, measured at 29 m. After that, the $\delta^{13}C_{org}$ gently increases till the top of the section.

The low resolution of this dataset and the poor biostratigraphy of the Mt. S. Enoc section prevent any possible correlation with the other Lagonegro sections.

The TOC composition of the Mt S. Enoc section ranges between 0.310% and 0.988%, with an average value of ca. 0.606%. The TOC profile displays an alteration of maxima and minima, which apparently does not correlate with the $\delta^{13}C_{org}$ curve (Fig. 3.2).

KASTELLI SECTION (Pindos Zone, Peloponnese, Greece)

This geological section belongs to the Pindos Zone (Peloponnese, Greece) (Fig. 3.3) and was analyzed in order to check the correlability of S1, S2 and S3 (see Chapter 1) within the Tethyan area. The abundance of reddish radiolarites and the occurrence of thick slump deposits is reflected in the poorly detailed $\delta^{13}C_{org}$ profile (Fig. 3.3). This is related to the low organic matter content of the samples: as a matter of fact, only a few samples provided TOC values noticeably different from the noise of the Elemental Analyzer.

Lithostratigraphy

The Pindos Zone belongs to a series of sub-parallel, north-south-trending tectono-stratigraphic terranes of the Hellenides (Brunn, 1956), stretched through the Peloponnese and continental Greece into Albania (Degnan and Robertson, 1998; Kafousia et al., 2012). In particular, the Pindos Zone is piled between the Apulia to the west and the Pelagonia terranes to the east (Degnan and Robertson, 1998) (Fig. 1). The Kastelli section is located about 200 m westwards of the junction of the Kalavrita–Klitoria and Kalavrita–Aroania roads (Fig. 3.3). This section can be ascribed to the Drimos Formation (Fig. 3.3), late Carnian to Early Jurassic in age based on conodonts, foraminifera and calcareous algae (Flament, 1973; Fleury, 1980). The first 17 m of the Kastelli section consist of limestones bearing thin-shelled bivalves (belonging to genus *Halobia*; Degnan and Robertson, 1998) and cherts nodules, alternated with shales. Pyrite cubes are present in several beds (Degnan and Robertson, 1998). The overlain 15 m are characterized by calcirudites and redeposited limestones, likely derived from the Gavrovo-Tripolitza carbonate shelf (Degnan and Robertson, 1998The succession finishes with ca. 10 m of radiolarian chert and radiolarites *sensu stricto*, sometimes intercalated with thin argillaceous limestones (Kafousia et al., 2012).

Biostratigraphy

Conodont residues were obtained from a total of 16 samples. Few kilograms of rock were reduced to powder and dissolved in 6-7% formic acid, dried and sifted at 104-825 μm. All residues were analyzed at the microscope for conodont picking. The conodont biostratigraphy is shown in Fig. 3.3. At 3.50 m, *Mockina bidentata* occurs, defining the base of the *Mockina bidentata* Zone (following the biozonations proposed by Kozur & Mock, 1991). At 11.60 m, sample KA 11.60 provides the first specimens of *Misikella hernsteini*, together with ramiforms and toothfish specimens. The occurrence of *M. hernsteini* defines the base of the *M. hernsteini–Parvigondolella andrusovi* Zone (*sensu* Kozur & Mock, 1991). Sample KA 20.45 contains *M. hernsteini* and ramiforms. At 22.60 m, the only specimen of *Misikella posthernsteini* marks the base of the *M. posthernsteini* Zone, which is one of the physical marker proposed for the definition of the Rhaetian stage (Gradstein et al., 2012).

Geochemical analyses

A total of 99 samples from the Kastelli section and 187 samples from the Lombard Basin were collected for TOC analyses and $\delta^{13}C_{org}$ (see Data Repository). All samples were washed in deionized water, dried overnight and reduced to a fine powder using an agate mortar. Powdered samples were divided into two aliquots: 1) ca. 100 mg of sample were added to ca. 100 mg of WO3 and wrapped in tin capsules for Total Carbon (TC) analyses; 2) ca. 100 mg of sample were added to ca. 100 mg of WO3, wrapped in silver capsules and heated at 550°C in order to remove organic compounds for Total Inorganic Carbon (TIC) analyses. The difference between the TC and TIC provided the TOC of each sample. The analyses were performed at the DAFNAE (Department of Agronomy, Food, Natural resources, Animals and Environment), University of Padova (Italy), using a Vario Macro CNS Elemental Analyzer. Results were calibrated against Sulfanilamide standard (N=16.25%; C=41.81%; S=18.62%; H=4.65%). The analytical uncertainty of the instrument, expressed as relative standard deviation, is σ=0.5%.

The $\delta^{13}C_{org}$ analysis was performed through a Delta V Advantage mass spectrometer connected to a Flash HT Elemental Analyzer at the Department of Geosciences, University of Padova (Italy). A couple of grams of powder were treated with 10% HCl overnight, neutralized with deionized water and dried. Few milligrams of powder were wrapped in tin capsules and analyzed along with multiple blank capsules and isotope standards (IAEA CH-6 = -10.45‰, IAEA CH-7 = -32.15‰, Coplen et al., 2006). The standard deviation of the in-house standard during the period of analyses was better than σ=0.2‰.

Only 30 samples have provided a $\delta^{13}C_{org}$ signal, in fact the carbon content of the remaining samples was too low for carbon isotope analyses. Therefore, the resolution of the obtained $\delta^{13}C_{org}$ profile is lower than expected, but some trends can be outlined. The $\delta^{13}C_{org}$ curve depicts two significant decreases, called K1 and K2 (Fig. 3.3). K1 shows a ca. 4‰ decrease and occurs over the conodont Mockina bidentata Zone and Misikella hernsteini Zone. K2 has an amplitude of ca. 6‰ and occurs within the conodont Misikella posthernsteini Zone.

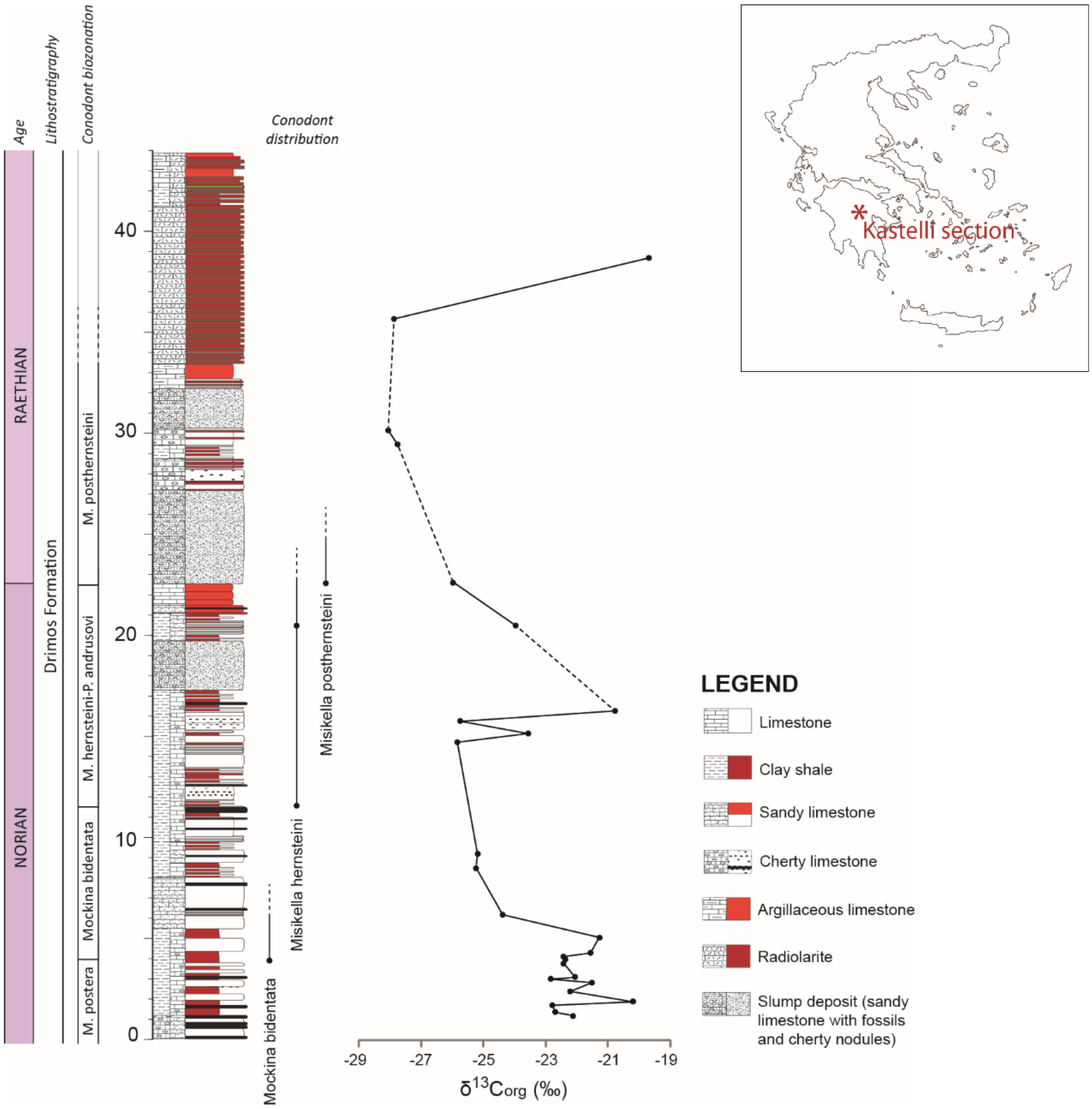

Fig. 3.3 Location, lithostratigraphy, conodont biostratigraphy, TOC and $\delta^{13}C_{org}$ of the Kastelli section. Dashed lines in the $\delta^{13}C_{org}$ profile coincide with the slump deposits of the geological succession, which can be considered as sudden and instantaneous events of the geological record (*i.e.*, negligible in terms of time).

δ^{15}N OF THE PIGNOLA-ABRIOLA SECTION (Lagonegro Basin, southern Italy)

In the view of a multidisciplinary approach, we decided to analyze the $\delta^{15}N$ of the Pignola-Abriola section, in order to investigate the geochemical state of the water column at the Norian-Rhaetian boundary (NRB). In fact, the co-occurrence of a significant decrease of the $\delta^{13}C_{org}$, increased TOC, black shales depositions and poorly preserved microfossils at the Norian-Rhaetian transition in the Pignola-Abriola section could be indicative of sub-oxygenated – likely anoxic – conditions. From this point of view, nitrogen isotopes could provide useful clues on the possible occurrence of denitrification processes and euxinic conditions.

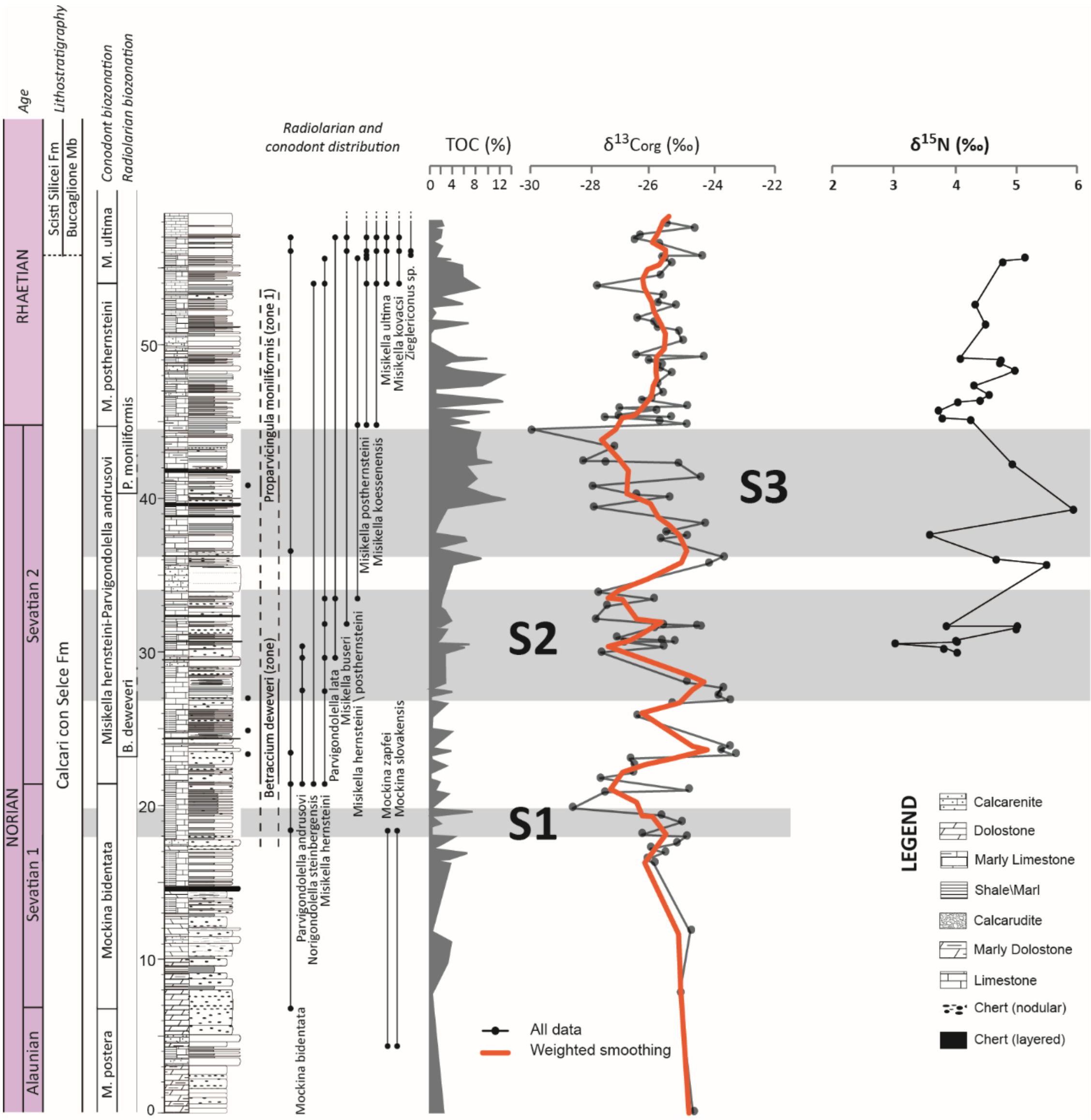

Fig. 3.4 Lithostratigraphy, conodont and radiolarian biostratigraphy, TOC and $\delta^{13}C_{org}$, $\delta^{15}N$ of the Pignola-Abriola section. Grey bars highlight the occurrence of the $\delta^{13}C_{org}$ decreases (S1, S2 and S3) that have been linked -through the comparison with other geochemical proxies and physical pieces of evidence- to the greenhouse gases emissions of the Angayucham large igneous province (see Chapter 1).

Methods

For the analysis of the nitrogen isotope composition, the samples showing higher organic matter content (i.e., TOC) were selected. Rock samples were washed in distilled water, dried in oven at 40°C overnight and then powdered in an agate mortar. $\delta^{15}N$ analysis were performed in collaboration with Dr. Linda Godfrey (Department of Earth and Planet Science, Rutgers University, Piscataway, NJ, USA) and Dr. Miriam Katz (Department of Earth and Enviromental Science, Rensselaer Polytechnic Institute, Troy, NY, USA) at the Rutgers University (USA). Powdered samples were weighted, wrapped in tin capsules and analyzed through a GVI Isoprime CF-IRMS, using an askerite trap to remove CO_2 evolved from carbonate. Multiple blank capsules and isotope standards (IAEA N-1 = 0.43‰, IAEA N-3 = 4.72 ‰, NBS 22 = -30.03‰; Coplen et al., 2006) were included in every sequence for isotope analyses. The blanks and standards were spaced between blocks of no more than 6 samples throughout the entire run. An in-house sediment standard (Ordovician marine shale) and a modern marine sediment, B2151, were also analyzed. The standard deviations for $\delta^{15}N$ of the in-house standard over the period of analysis was better than 0.2‰.

Results

The obtained $\delta^{15}N$ values range between a minimum of 3.04‰ to a maximum of 5,91‰, with an average of value of ca. 4,42‰. From the base up to 35.70 m, the curve shows an increasing trend from 3.04‰ to 5.50‰, followed by a return to less positive values, reaching a negative peak of 3.59‰ at 37.73 m. This negative peak is immediately followed by a positive peak of 5.91‰ at 39.35 m. From this point up to the end the curve, $\delta^{15}N$ profile stabilize around the average value of ca. 4.50‰ (Fig. 3.4).

Discussion

Nitrogen isotopes are particularly sensitive to the redox state of the water column and $\delta^{15}N$ could provide useful information about the continental input into the basin, the equilibrium between the atmospheric and oceanic reservoirs, the equilibrium among different trophic-level groups of the planktic population and the occurrence of particular geochemical state in the water column (e.g., denitrification, euxinification). Nitrogen can reach the oceanic reservoir following three possible pathways: i) through direct exchange with the atmospheric reservoir, which involves only the atmosphere-ocean interface and therefore it is not recorded in the sedimentary record; ii) through fluvial input, especially in case of increased continental weathering; and iii) through denitrification and/or anammox processes that could take place from the middle to the bottom water column (e.g., Kuypers et al., 2005; Thamdrup et al., 2006; Ward et al., 2009; Jenkyns, 2010). The last two processes may involve the activity of N-fixing bacterial groups, which could prevail among the planktonic population in case of intensified oxygen minimum zone, such as during under-oxygenated and euxinic conditions. In fact, these anaerobic bacterial groups are able to introduce significant amount of dinitrogen and/or nitrous oxide into the ocean through the anammox process: nitrate replaces oxygen as prime oxidant for falling organic matter and anaerobic oxidation of ammonium by nitrite takes place (e.g., Kuypers et al., 2005; Thamdrup et al., 2006; Ward et al., 2009; Jenkyns, 2010). These phenomena result in a relative isotopic enrichment of the dissolved residual nitrate that, when upwelled into the photic zone, is relayed to the planktonic population, to ultimately become part of the sedimentary record. Since this chain of events usually takes place in under-oxygenated conditions, increased organic carbon burial commonly accompanied these phenomena. As a consequence, a positive correlation between organic carbon values (TOC) and nitrogen isotope ratios is usually appreciable: this is the case of the Pignola-Abriola NRB record. This relationship is typical of oceanic anoxic events (OAE): in fact, it has been documented for the black shales of the Toarcian and the Cenomanian/Turonian OAEs in Europe and elsewhere (Jenkyns et al., 2001, 2007, 2010; Kuypers et al., 2004; Ohkouchi et al., 2006; Dumitrescu e Brassell, 2006; Junium e Arthur, 2007; Kashiyama et al., 2008).

The denitrification process results also in the production of nitrous oxide: the warming power of this greenhouse gas is thought to be ca. 200 times higher than carbon dioxide (Lashof and Ahuja, 1990; Jenkyns, 2010). Therefore, widespread denitrification could have the potential for enhanced global warming. Interestingly, the Norian-Rhaetian transition – where the Pignola-Abriola $\delta^{15}N$ enrichment occurs – seems to be affected by rising temperatures and warming conditions (Trotter et al., 2015), which could support the hypothesis of increased greenhouse gas concentrations during this time interval, likely due to volcanic activity as well as denitrification processes.

Overall, available data from the Pignola-Abriola section ($\delta^{13}C_{org}$, TOC, $\delta^{15}N$, black shale deposition, poorly preserved microfossils) seem to support the hypothesis of under-oxygenated (anoxic?) conditions at the Norian-Rhaetian boundary. If these conditions will be demonstrated to be widespread at global scale, they would be indicative of an oceanic anoxic event.

ODP SITE 761C FROM THE WOMBAT BASIN (northwestern Australia)

This ODP site was analyzed in order to check the occurrence of S1, S2 and S3 even in the southern margin of the Tethys ocean, in the southern hemisphere. This area has been drilled at 6 sites, progressively named from 759 to 764. In particular, site 761 seems to cover the Norian-Rhaetian transition and is characterized by the alternation of dark limestones and shales: for these reasons, it has been chosen for $\delta^{13}C_{org}$ analysis.

Lithostratigraphy and biostratigraphy

Site 761 is located in the northern Wombat Basin, 16°44.23'S, 115°32.10'E, at a water depth of ca. 2167.9 m. It records an almost continue Late Triassic to Quaternary interval. The Triassic sequence of Hole 761C is dominated by layers of calcareous sediments and can be subdivided on the basis of its microfossil content, which in turn reflects a series of environmental changes (Fig. 3.6). The lowermost interval (core 33R) consists of clayey siltstone and on the base of its fossil content (dinoflagellate cysts *Heibergella balme*i and nannofossils) can be ascribed to a late Norian age. The overlying interval (cores 32R up to 30R) is characterized by an upward increase of the carbonate accompanied by a decrease in plant debris, suggesting the occurrence of a major facies change. This change is reflected also in various fossil groups, which appear characterized by different occurrences. The nannofossil sub-assemblage *Thoracosphaera geometrica* and the occurrence of the foraminifera taxon *Triasina oberhauseri* points to a Norian age for this interval (Bralower et al., 1992; Zaninetti et al., 1992). On the other hand, the co-occurrence of the ostracode *Ogmoconcha owthorpensis* with the dinoflagellate cyst *Rhaetogonyaulax rhaetica* suggest a Rhaetian age (Dépëche and Crasquin-Soleau, 1992; Brenner, 1992), raising difficulties in the age determination of the 32R-30R interval. The interval from 29R to 27R is poorly fossiliferous and depicts only few specimens of ostracodes and foraminifera that are not age-diagnostic. The lack of figured organic material (dinoflagellate cysts, spores, pollen and plant debris) could be indicative of highly oxidized conditions. The overlying section (up to 26R) consists of dark limestones interbedded with calcareous claystones, bearing rich microfossil assemblages. Ostracodes, nannofossils and palynomorphs suggest a Rhaetian age, whereas the foraminifera seem to indicate a transitional Norian to Rhaetian age based on the absence of *Triasina hantkeni*. The uppermost Triassic cores of Hole 761C contains only foraminifera of Rhaetian age (Fig. 3.6).

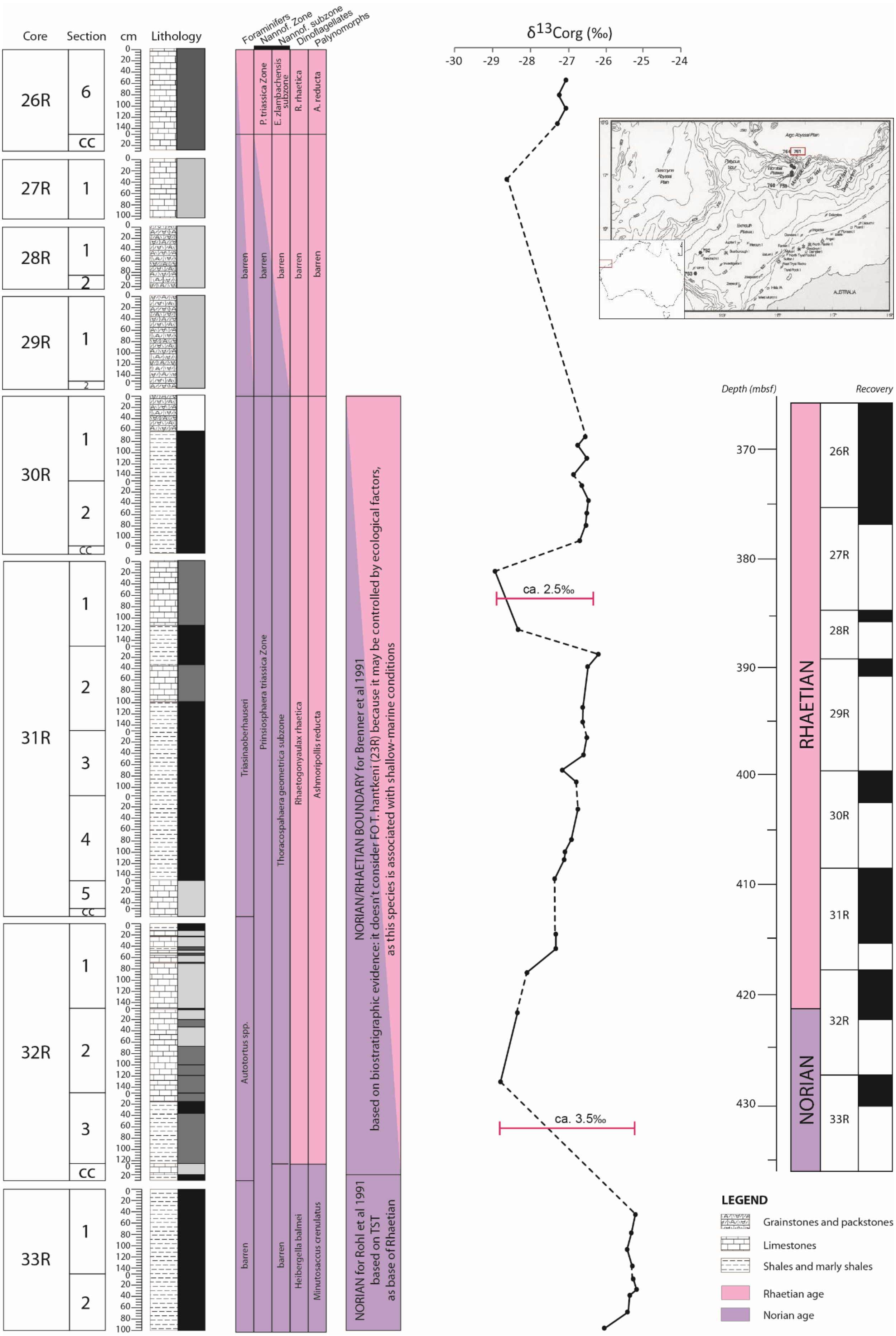
Core
Section
cm
Lithology
Foraminifers
Nannof. Zone
Nannof. subzone
Dinoflagellates
Palynomorphs
δ13Corg (‰)
-30
-29
-28
-27
-26
-25
-24
26R
27R
28R
29R
30R
31R
32R
33R
CC
P. triassica Zone
E. zlambachensis subzone
R. rhaetica
A. reducta
barren
Triasinaoberhauseri
Prinsiosphaera triassica Zone
Thoracospahaera geometrica subzone
Rhaetogonyaulax rhaetica
Ashmoripollis reducta
Autotortus spp.
Heibergella balmei
Minutosaccus crenulatus
NORIAN/RHAETIAN BOUNDARY for Brenner et al 1991
based on biostratigraphic evidence: it doesn't consider FOT. hantkeni (23R) because it may be controlled by ecological factors,
as this species is associated with shallow-marine conditions
NORIAN for Rohl et al 1991
based on TST
as base of Rhaetian
ca. 2.5‰
ca. 3.5‰
Depth (mbsf)
Recovery
370
380
390
400
410
420
430
RHAETIAN
NORIAN
LEGEND
Grainstones and packstones
Limestones
Shales and marly shales
Rhaetian age
Norian age

Fig. 3.6 On the right side: Location map of the ODP sites in the Wombat Basin (modified from Rohl et al., 1991). The studied site (Site 761, hole C) is highlighted by a red box. Norian-Rhaetian interval in site 761C: depth (mbsf), core succession and recovery. On the left side: Core reconstruction, lithostratigraphy, biostratigraphy (foraminifera, nannofossils, dinoflagellates, palynomorphs), chemostratigraphy of Site 761C. Dashed lines in $\delta^{13}C_{org}$ coincide to gaps in core recovery.

Geochemical analyses

The $\delta^{13}C_{org}$ profile of the Wombat Basin appears quite flat, with average value of ca. -26.83‰, exception made for two significant decreases of ca. 3.5‰ and 2.5‰ at the Norian-Rhaetian transition based on dinoflagellate biostratigraphy and on nannofossil assemblages respectively. The absence of other age-diagnostic proxy and the discontinued recovery of the core prevents any further interpretation.

CHAPTER 4

Strontium isotopes:

$\delta^{88/86}$Sr and ^{87}Sr/^{86}Sr from Triassic conodonts

INTRODUCTION

Strontium isotope stratigraphy is widely used as a high-resolution tool in geochronology and chemostratigraphy (Burke et al., 1982; De Paolo and Ingram, 1985; Elderfield, 1986; McArthur, 1994; Smalley et al., 1994; Veizer et al., 1997), but it represents also a potential tool for palaeoenvironmental, palaeoclimatic and palaeotectonic reconstructions, especially if combined with other geochemical proxies, such as carbon isotopes (e.g., Miller et al., 1988; Barrera et al., 1993; Chaisi and Schmitz, 1995; Jacobsen and Kaufman, 1999; Montanez et al., 2000; McArthur et al., 2004; Nogueira et al., 2007; Frei et al., 2011, 2013; Huck et al., 2011; Kakizaki et al., 2013; Ramkumar, 2015). The simultaneous utilization of fluctuations of the ^{87}Sr/^{86}Sr ratios and those of δ^{13}C, which are independent from the former, has been proven to be ideal in high-resolution stratigraphic studies (Ramkumar, 2015). In fact, the strontium-isotope record can offer insights into the relative timing and magnitude of changing global weathering rates and mid-ocean ridge activity (e.g. DePaolo,1986; Hodell et al.,1989; Jones et al.,1994), while carbon isotopes can provide useful information regarding past productivity variability that can be related to various climatic factors and climate-dependent parameters, such as burial and re-oxidation of organic matter, bio-productivity, tectonic activity or changing oceanic circulation patterns (e.g., Shackleton, 1977; Schidlowski and Aharon, 1992; Grossman, 1994; Ferreri et al., 1997; Kump and Arthur, 1999; Saltzman and Thomas, 2012; Ramkumar, 2015).

More precisely, the ^{87}Sr/^{86}Sr composition of seawater (^{87}Sr/^{86}Sr$_{sw}$) reflects imbalances between two major Sr fluxes and their isotope ratios: riverine input of radiogenic Sr linked to continental weathering (average ^{87}Sr/^{86}Sr = ca. 0.710‰), and hydrothermal circulation at mid-ocean ridges, which introduces mantle-derived ^{86}Sr into seawater (average ^{87}Sr/^{86}Sr = ca. 0.703‰) (Faure, 1986; Palmer and Edmond, 1989; Taylor and Lasaga, 1999). The residence time of strontium is longer (ca. 2.4 My; Jones and Jenkyns, 2001) than the mixing time of the ocean (ca. 1-2 ky; e.g., Broecker and Li, 1970; Gordon, 1973; Hodell et al., 1990; Garret and Laurent, 2002), suggesting that Sr is isotopically homogeneous at the global scale (e.g., Peterman et al., 1970; Brass, 1976; Burke et al., 1982; Elderfield, 1986; Clemens et al., 1993; Smalley et al., 1994; Veizer et al., 1974, 1997; Veizer and Compston, 1989; Korte et al., 2003). Therefore, positive shifts of marine $^{87}Sr/^{86}Sr$ are commonly related to increased continental weathering and/or denudation rates, which in turn may be driven by humid climate and/or tectonics (Palmer and Elderfield, 1985; Raymo et al., 1988; Hodell et al., 1989). Instead, negative shifts of $^{87}Sr/^{86}Sr_{sw}$ may be linked to volcanic activity (Berner and Rye, 1992; Jones and Jenkyns, 2001; Young et al., 2009). A reference $^{87}Sr/^{86}Sr$ curve for the entire Phanerozoic has been proposed by Burke et al. (1982), then integered by successive works (e.g., Veizer et al., 1999; Korte et al. 2003; Frija and Parente, 2008; McArthur et al., 2012; Vollstaed et al., 2014; Tackett et al., 2014).

Recent studies suggest that also the stable strontium isotope ratio ($^{88}Sr/^{86}Sr$) varies significantly in different geological bodies (e.g., Halicz et al., 2008; de Souza et al., 2010; Krabbenhoft et al., 2010; Bohm et al., 2012; JinLong et al., 2013; Vollstaed et al., 2014; Andrews et al., 2016). For instance, the $\delta^{88/86}Sr$ composition of modern seawater is +0.38‰ to +0.39‰ (Fietzke and Eisenhauer, 2006; Halicz et al., 2008; Liebetrau et al., 2009; Krabbenhoft et al., de Souza et al., 2010), silicate rocks has an average value of +0.25‰ (Ohno and Hirata, 2007; Halicz et al., 2008; Krabbenhoft et al., 2010; de Souza et al., 2010), marine carbonates are +0.23‰ (Fietzke & Eisenhauer, 2006; Ohno and Hirata, 2007; Halicz et al., 2008; Krabbenhoft et al., 2009; de Souza et al., 2010), whereas meteorites depict a very large range between -1.73‰ and +0.66‰ (Moynier et al., 2010).

Different hypotheses have been proposed regarding the potential causative mechanisms for the observed $\delta^{88/86}Sr$ variations. Since strontium is an isomorphic substitute of calcium in carbonates, $\delta^{88/86}Sr$ studies might be combined $\delta^{44/40}Ca$ and Sr/Ca analyses. Isotopic studies on corals showed the dependence of $\delta^{88/86}Sr$ on temperature, highlighting the potential of this proxy as a palaeothermometer, especially if paired with $\delta^{44/40}Ca$ (Fietzke and Eisenhauer, 2006; Halicz et al., 2008; Ruggeberg et al., 2008) which is useful to identify the fluid sources involved in calcium carbonate precipitation as well as examining biomineralization processes (Fietzke and Eisenhauer, 2006). Krabbenhoft et al. (2010) proposed that, on glacial/interglacial time scales, continental weathering and related riverine inputs into the ocean may play a major role on $\delta^{88/86}Sr$, introducing short-term disequilibria between Sr inputs and outputs, as previously suggested by Stoll et al. (1999). Based on the difference between $\delta^{88/86}Sr$ of modern seawater (ca. +0.39‰) and marine carbonates (ca. +0.23‰), Vollstaed et al. (2014) deduced that variations of $\delta^{88/86}Sr$ of seawater depend on changes in Sr sources as well as on carbonate burial rate, the latter being a main Sr output flux. In fact, the Phanerozoic $\delta^{88/86}Sr$ record of Vollstaed et al. (2014) appears positively correlated with the $\delta^{44/40}Ca$ record, but not with the $^{87}Sr/^{86}Sr$ profile. On shorter time scales, these authors proposed that

$\delta^{88/86}$Sr is significantly influenced by carbonate burial, carbonate shelf recrystallization/weathering, carbonate dissolution, and ocean anoxia. For instance, the high $\delta^{88/86}$Sr values recorded at the Permian-Triassic transition was suggested to be a consequence of increased carbonate alkalinity via bacterial sulfate reduction in deep anoxic waters and sediments in a stratified ocean (Vollstaed et al., 2014).

Recent $\delta^{88/86}$Sr studies have focused on corals, brachiopods, belemnites and inorganic carbonate sediments. Carbonates are conducive to strontium isotope analysis given their relatively high strontium content, but their importance as age-diagnostic stratigraphic tools can be limited. To overcome this issue, fossils that offer good chronological control were investigated. Conodont microfossils are important biostratigraphic indicators and are also ubiquitous throughout marine sequences. However, conodonts are carbonate fluorapatite biominerals, and so are considered more resistant to diagenesis than carbonates (e.g., Pietzner et al., 1968; Kovach, 1980, 1981; Ericson, 1985; Nelson et al., 1986; Austine, 1987; Burnett and Hall, 1992; Aldridge and Purnell, 1996; Holmden et al., 1996; Iacumin et al., 1996; Barrick, 1998; Trotter et al., 1999; 2006, 2007; Barrat et al., 2000). The ^{87}Sr/^{86}Sr compositions of conodonts have been widely analysed for chronostratigraphic and oceanographic studies (Kovach, 1980, 1981; Kuerschner et al., 1992), however few $\delta^{88/86}$Sr analyses have been reported in the literature.

In this study we describe both 87Sr/86Sr and $\delta^{88/86}$Sr analyses of conodonts extracted from latest Permian through Triassic marine sequences.

METHODS: TEST AND EVALUATION OF A PROTOCOL FOR SAMPLE PREPARATION PROCEDURE PRIOR TO $\delta^{88/86}$Sr ANALYSES

In order to test the validity of our sample preparation protocol, several tests on international standards (SRM987, Jcp-1) and in-house standard (biogenic apatite from a whale tooth and a shark tooth) were performed. Due to its similarity to conodont bio-fluorapatite, biogenic apatite from a whale tooth and a shark tooth have been selected for simulation tests. International and in-house standards were weighted in order to obtain ca. 80 ng Sr per sample. This threshold-value of strontium has been evaluated as the minimum concentration of strontium available for 40 μg of Triassic conodonts: in fact, considering that the average Sr concentration for Triassic conodonts is ca. 2000 ppm, then ca. 40 μg of sample contain ca. 80 ng Sr. 40 μg of sample corresponds to ca. 2-5 conodont specimens, depending on their size. This restrained number of specimens facilitates the picking of the same conodont-species for each single $\delta^{88/86}Sr$ analysis, preventing the risk of cross contamination related to possible differences of $\delta^{88/86}Sr$ signature due to species-related effects. The standard materials prepared through our developed procedure provided the same results as the standards directly analyzed at the spectrometer (see Table 4.1). Therefore, we applied the following procedure for the Triassic conodont samples.

	SRM 987 *(treated with our developed protocol for sample preparation)*	
	$\Delta^{88/86}$Sr‰	**^{87}Sr/^{86}Sr**
	-0,010	0,710281
	-0,030	0,710261
	-0,037	0,710271
	0,022	0,710271
	0,048	0,710253
	0,017	0,710259
	0,011	0,710258
	0,024	0,710257
	-0,016	0,710237
	-0,029	0,710266
	-0,001	0,710267
	-0,009	0,710249
	-0,004	0,710248
	0,015	0,710238
	-0,001	0,710240
Mean	**0,000**	**0,710257**
St. dev.	**0,023**	**0,000013**

Table 4.1 $\Delta^{88/86}$Sr and 87/86Sr results for SRM 987 treated with our developed protocol for sample preparations. $\Delta^{88/86}Sr = \delta 8^{8/86}Sr_{SRM987} - \delta^{88/86}Sr_{SRM987meas}$. Mean $\Delta^{88/86}$Sr is 0‰, as expected. Mean 87/86Sr is 0.710257±13, which is in agreement with the reference value proposed by McArthur et al. (2012), i.e., 0.710248.

For this study we selected the best-preserved conodonts (e.g., low Color Alteration Index, avoiding recrystallized specimens, avoiding specimens with extraneous material on conodont surface or in the basal cavity) from our samples. Conodont apatite is rich in Sr and resistant to diagenesis (e.g., Trotter et al., 2015), giving us confidence that our microfossils preserved (near) pristine isotope signature. We weighted at least 40 μg of conodonts per sample using a Mettler ME30 balance: considering that the average Sr concentration for Triassic conodonts is ca. 2000 ppm, then ca. 40 μg of sample contain ca. 80 ng Sr. To remove organic coatings and eventual dirt on the surface, conodonts were leached in 1N acetic acid for at least 30 min (depending on the size of the specimens) and then washed at least three times in Millipore water. Basal cavities were removed in case they contained extraneous materials. All samples were dissolved in one drop of 68% HNO_3. The drops were then evaporated at 150°C and samples heated three times in one drop of 68% HNO_3 at 220°C to dissolve and oxidize organic components. Samples were then dissolved in 800 µl of 8N HNO_3. Small aliquots of solutions were spiked with a combined $^{42\text{-}43}$Ca and $^{84\text{-}87}$Sr tracer (95.6 ppm Ca, 0.49 ppm Sr) for the Sr/Ca and δ44/40Ca analyses; 300 µl of solutions were spiked with a $^{84\text{-}87}$Sr tracer (1 ppm Sr) for the double-spiked measurements (Heuser et al., 2002; Krabbenhoft et al., 2009); the remnant were used for the unspiked measurements. Spiked and unspiked aliquots contained at least 30 ng Sr each; Sr/Ca aliquots contained ca. 10-30 ng Sr and ca. 2-5 µg Ca each. Ion chromatography was performed on Sr-spiked and unspiked solutions; Sr-Ca-spiked solutions were dried down and loaded directly on rhenium filaments and analyzed at the TIMS.

Ion chromatography was performed with home-made prototype columns obtained from BIO-RAD 1 ml pipet tips, filled with 100 µl of Eichrom's Sr resin SRB25 A (100-150 µm mesh). Columns have been tested in order to check and guarantee a complete strontium recovery. Resin was washed several times in MQ water in order to remove floating particles. Resin was then conditioned with 0.6 ml of 8N HNO_3 before the loading of sample solutions. Samples were eluted in 1 ml of 8N HNO_3 to remove the sample-matrix, then in 2 ml of MQ water to collect the Sr fraction. The solutions were dried, refluxed in aqua regia (3 HNO_3 + HCl) to remove organic components and dried again. Samples were loaded in 2% HNO_3 acid on rhenium ribbon single filaments with a Ta_2O_5-activator to stabilize signal intensity, following the procedure proposed by Krabbenhoft et al. (2009). Specific attention was paid in loading sample solutions in a max 1 mm-diameter spot at the center of the filaments, in order to concentrate all the available Sr in a single spot and guarantee the best measurement at the TIMS ("filament reservoir effects", Lehn et al., 2013; Lehn and Jacobson, 2015). For this reason, samples were constraint between parafilm "dams", preventing the spread on the filament's surface. Samples were heated on filaments at 0.7 A to dryness, then slowly heated to 2 A till reaching an intense red glow (glowing phase). After keeping the filaments glowing for about 10 seconds, current was turned off and filaments were mounted onto the sample wheel.

The spike and unspiked Sr analyses were then performed using a Thermofisher TRITON TIMS at the Ocean Institute Laboratory of the School of Earth and Environment, University of Western Australia (Perth, WA). During the period of study, the reproducibility (2 s.d.) of the SRM 987 standard during the period of analyses was better than 0.000034‰. The measurements of both spiked and unspiked samples started when mass ^{88}Sr achieved at least 2 V of signal intensity, for a total of 120 cycles. Ion beams were collected in static mode. The total analysis time, including filament warm-up, was about 1 hour per sample. Runs were monitored to ensure: i) that ^{87}Rb ion beam did not isobarically interfere with ^{87}Sr (by checking ^{85}Rb ion beam); ii) a steady or increasing ^{88}Sr beam; iii) a slightly increasing raw 88/86 ratio fractionation pattern; iv) an increasing raw 86/84 ratio fractionation pattern; v) the absence of filament reservoir effects.

For the $\delta^{88/86}$Sr investigation, we decided to apply the iterative correction algorithm proposed by Krabbenhoft et al. (2009), which assumes an exponential law for the mass fractionation correction and provide simultaneous determination of $\delta^{88/86}$Sr and ^{87}Sr/^{86}Sr. Sample 87/86Sr values were normalized to 86/88Sr ratio of 0.1194 (Nier, 1938) and corrected for the offset between the measured SRM 987 87/86Sr-ratio and the accepted value of 0.710248 (McArthur et al., 2012). The analytical blank has a 87/86Sr ratio of 0.7092±0.0006 and for the entire procedure was less than 34 ρg Sr, which is <0.1% of the Sr amount in our samples and therefore is not expected to influence the 87/86Sr of our samples. $\delta^{88/86}$Sr values of SRM 987 changed though the period of study, suggesting that $\delta^{88/86}$Sr of conodont samples were likely affected by a drift during measurements as well. To correct this drift, we measured both samples and standards for each session of analysis: the session offset was then calculated as the difference between the mean $\delta^{88/86}$Sr value of SRM 987 and its accepted value, i.e., 0‰.

PRELIMINARY RESULTS

The obtained profiles (Fig. 4.1) are composite records obtained from conodont samples hailing from different localities and geological settings (Table 4.2). Permian/Triassic boundary samples come from the geological section of Meishan (China), a carbonate ramp located on the eastern side of the Tethys sea. Carnian samples come from Pignola 2 and Pizzo Mondello (southern Italy), two sections representing open marine settings from western Tethys. Norian and Rhaetian samples were collected from Pizzo Mondello and Pignola-Abriola (southern Italy), another basinal succession from western Tethys. All the analyzed samples come from the Tethys area. Nevertheless, the obtained data are thought to represent the global isotopic composition of Triassic seawater, in fact strontium has been proved to be isotopically homogeneous at global scale (e.g., Broecker and Li, 1970; Gordon, 1973; Hodell et al., 1990; Veizer et al., 1997; Jones and Jenkyns, 2001; Garret and Laurent, 2002; Korte et al., 2003). However, in order to avoid any possible misinterpretation of the data, we compared and integer our results with data from literature (Korte et al., 2003; Callegaro et al., 2012; Tackett et al., 2014; Vollstaedt et al., 2014; Fig. 4.1).

Sample	**Locality**	**Age**		**87/86Sr$_{raw}$**	**2σ**	**87/86Sr**	**$\Delta^{88/86}$Sr‰**
090717-23	Meishan	Permian	253,18	0,707159	0,000007	0,707141	0,239
MS-14	Meishan	Permian	252,94				
MS-32	Meishan	Permian	252,46	0,707131	0,00001	0,707113	0,111
080826-33	Meishan	Permian	252,22	0,707281	0,000014	0,707263	
080826-37	Meishan	Permian	252	0,707406	0,000016	0,707388	
080827-77	Meishan	Permian	251	0,707419	0,000006	0,707401	0,192
P4	Pignola 2	Carnian - Julian	234,29	0,707732	0,000006	0,707714	
P8 Gladi	Pignola 2	Carnian - Julian	233,57	0,707872	0,000005	0,707854	0,350
P15	Pignola 2	Carnian - Tuvalian	232,31	0,707840	0,000002	0,707822	0,131

P19	Pignola 2	Carnian - Tuvalian	231,68	0,707910	0,000005	0,707892	
NA19	Pizzo Mondello	Carnian - Tuvalian	230,15	0,707712	0,000011	0,707694	0,284
NA21	Pizzo Mondello	Carnian - Tuvalian	229,43	0,707710	0,000009	0,707692	0,263
P35	Pizzo Mondello	Carnian - Tuvalian	229,07				
P39	Pizzo Mondello	Carnian - Tuvalian	228,71	0,707941	0,000018	0,707923	
NA35	Pizzo Mondello	Carnian - Tuvalian	227,32				
NA36	Pizzo Mondello	Norian - Lacian	226,33	0,707724	0,000011	0,707706	0,279
NA39	Pizzo Mondello	Norian - Lacian	225,34	0,707726	0,000005	0,707708	0,272
NA42	Pizzo Mondello	Norian - Lacian	224,35	0,707728	0,000011	0,707711	0,243
NA44A	Pizzo Mondello	Norian - Lacian	222,37	0,707720	0,000011	0,707703	0,214
NA68	Pizzo Mondello	Norian - Lacian	220,88				
PIG0	Pignola-Abriola	Norian - Sevatian	216,3				
K202	Pignola-Abriola	Norian - Sevatian	215,4	0,708252	0,000006	0,708234	
K201	Pignola-Abriola	Norian - Sevatian	214,5	0,708257	0,00001	0,708239	
KE3	Pignola-Abriola	Norian - Sevatian	213,6				
KE1	Pignola-Abriola	Norian - Sevatian	212,6				
GNC100	Pignola-Abriola	Norian - Sevatian	211,7				
PR16	Pignola-Abriola	Norian - Sevatian	210,8	0,708320	0,000002	0,708302	
PR12	Pignola-Abriola	Norian - Sevatian	208,3	0,708204	0,000017	0,708186	
PR10	Pignola-Abriola	Norian - Sevatian	207,6				
PA142	Pignola-Abriola	Norian - Sevatian	205,6				
PG37	Pizzo Mondello	Rhaetian	207,1				
PG39	Pizzo Mondello	Rhaetian	206,3				
PG40	Pizzo Mondello	Rhaetian	205,59	0,707810	0,000002	0,707792	0,300
PG42	Pizzo Mondello	Rhaetian	204,88	0,707915	0,000016	0,707897	
PG45	Pizzo Mondello	Rhaetian	202,75	0,707792	0,000008	0,707774	

Table 4.2 Sample list and obtained data.

Our 87/86Sr profile reaches the lowest values around the Permian/Triassic boundary (87/86Sr minimum=0.707113±0.00001‰). During the Carnian, 87/86Sr values stabilize around 0.707710, reaching a maximum during the middle Carnian (87/86Sr=0.707822±0.000002) and at the Carnian-Norian transition (87/86Sr=0.707923±0.00001). The Norian-Rhaetian transition is characterized by a decreasing trend, dropping from 0.708302±0.000002 to 0.707774±0.000008 (Fig. 4.1).

The $\delta^{88/86}$Sr profile shows significant variations (Fig. 4.1). Seemingly to the 87/86Sr trend, the Permian-Triassic transition is marked by a minimum, decreasing from the latemost Permian value of +0.239‰ to +0.111‰ at the Permian/Triassic boundary. The Lower and Middle Triassic seem to be characterized by increasing $\delta^{88/86}$Sr, reaching a maximum of +0.350‰ at the base of the Late Triassic, in the middle Carnian, immediately followed by a drop to +0.131‰ (Fig. 4.1). From the late Carnian to the early Norian, $\delta^{88/86}$Sr values stabilize around ca. +0.270‰, to decrease to +0.214‰ around the middle Norian. The only available Rhaetian sample records a value of +0.300‰.

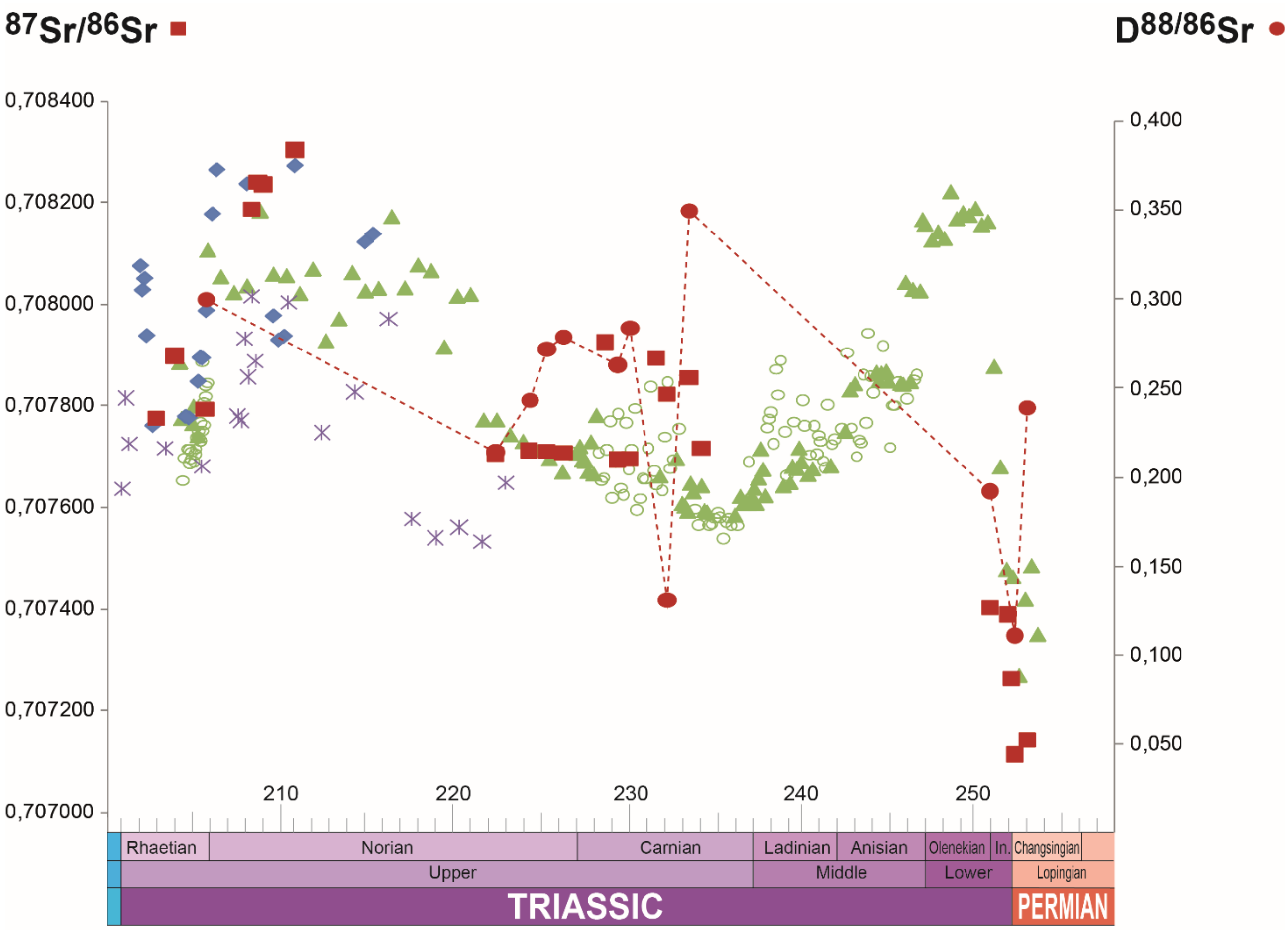

Fig. 4.1 $\Delta^{88/86}$Sr and 87/86Sr profiles. Red bold dots = our $\Delta^{88/86}$Sr; red bold squares = our 87/86Sr data; green bold triangles = 87/86Sr data obtained on conodont samples from Korte et al. (2003); green circles = 87/86Sr data obtained on brachiopod samples from Korte et al. (2003); blue bold diamonds = 87/86Sr data obtained on conodont samples from Callegaro et al. (2010); lilac stars = 87/86Sr data obtained on shell samples from Tackett et al. (2014).

DISCUSSION ON THE PRELIMINARY RESULTS

87/86 Sr record

The obtained 87/86Sr profile seemingly follow the trend proposed by Korte et al. (2003), Callegaro et al. (2012) and Tackett et al. (2014) for the Triassic (Fig. 4.1), confirming the trend highlighted from previous studies and thus supporting the validity of our developed protocol for sample preparation. In particular, the similarity between our 87/86Sr record and other Triassic 87/86Sr profiles confirms that even 30ng of strontium from conodont-samples are sufficient in order to obtain a trustable result.

The 87/86Sr decreasing trends around the Permian/Triassic boundary and the Triassic/Jurassic boundary can be interpreted as inputs of mantle-derived ^{86}Sr, likely introduced into the seawater from hydrothermal circulation at mid-ocean ridges – linked to the rate of sea floor spreading – and/or volcanic activity and/or riverine input – in case of the weathering of less-radiogenic young basalts (e.g., Berner and Rye, 1992; Veizer et al., 1999; Jones and Jenkyns, 2001). The Permian/Triassic 87/86Sr decreasing trend could be ascribed to the weathering of the continental deposits of the Siberian Traps, a Large Igneous Province that took place in Siberia, Russia (251-249 Ma) (Renne and Basu, 1991; Nikishin et al., 1996; Sharma, 1997; Tomshin et al., 1997; Ernst and Buchan, 1997, 1998). The Siberian Traps are thought to be linked to the anoxic event that likely triggered the Permian/Triassic extinction event (e.g., Campbell et al., 1992; Wignall et al., 1992; Jin et al., 2000; Benton et al., 2003; Grice et al., 2005). The minimum reached at the early-middle Carnian transition may be related to the Wrangellia LIP: the emplacement and the weathering of its oceanic flood basalts might had introduced mantle-derived ^{86}Sr in the ocean. The decreasing trend close to the Triassic/Jurassic boundary has been justified by Callegaro et al. (2010) as related to the oceanic spreading phase preceeding the CAMP and to the weathering of its young basalt flows.

$\delta^{88/86}$Sr record

According to the observations of Vollstaed et al. (2014), the $\delta^{88/86}Sr_{sw}$ and $87/86Sr_{sw}$ profiles appear to be not correlated (R^2=-0.2). Vollstaed et al. (2014) reconstructed the Phanerozoic $\delta^{88/86}$Sr record of past seawater through the analyses of brachiopods (integrated with belemnites and carbonates matrices), whose $\delta^{88/86}$Sr values had been demonstrated to be independent of species, habitat and temperature and therefore should represent a trustable achieve for $\delta^{88/86}Sr_{sw}$ reconstructions. From their study, $\delta^{88/86}$Sr appears to reach a minimum within the Permian (0.04‰), immediately followed by a sharp increase at the Permian/Triassic boundary, reaching one of the maximum value of the entire Phanerozoic (0.36‰). The Middle Triassic seems to be characterized by lower values (0.07‰), which appear to increase during the Late Triassic, around 0.120‰. The late Permian and the Early Triassic show the highest $\delta^{88/86}$Sr variation rate of the Phanerozoic (0.024‰/My).

These trends seem to conflict with our results. In fact, our $\delta^{88/86}$Sr profile seems to reach a minimum of 0.111‰ at the Permian/Triassic boundary, followed by higher values during the Late Triassic (around 0.265‰). On the other hand, these higher values are in agreement with the observation that during “aragonite sea” intervals – such as the Triassic, low spreading rates should lead to high Mg/Ca_{sw} ratios and low sea levels (Hardie, 1996), inhibiting the precipitation of inorganic calcite. This may lead to relatively low Sr/Ca_{sw}, high carbonate output fluxes and thus high $\delta^{88/86}$Sr, as a consequence of a large Sr output flux of isotopically light Sr. This scenario is similar to that advocated for Ca isotopes (Farkas et al., 2007), except that the $\delta^{44/40}$Ca were interpreted to reflect changes in Ca isotope fractionation factors between calcite and aragonite (Farkas et al., 2007; Blattler et al., 2012; Vollstaed et al., 2014).

Despite the agreement with the "aragonite sea" expectations, a disparity between our results and Vollstaed data remains. The main differences between Vollstaed et al. (2014) and this work are the type of sample matrix and the sample preparation procedure (Table 4.3).

Discrepancies	**Vollstaed et al. (2014)**	**This work**
Sample matrix	Brachiopods (integrated with belemnites and carbonates matrices)	Conodonts
Sample preparation method	According to Krabbenhoft et al. (2008)	Modified from Krabbenhoft et al. (2008)

Table 4.3 Main discrepancies between this work and Vollstaed et al. (2014).

We can exclude that the discrepancies depend on the sample preparation method, since we demonstrated to obtain expected values of 0‰ for SRM 987 standards treated with our sample preparation procedure. As a consequence, we should consider the choice of the sample matrix.

Strontium precipitates in the carbonate matrix of organism shells as a substitute for Ca. This substitution may be affected by vital effects, depending on the *taxa* and sometimes even on the genus or species of the organism. Sr analyses on brachiopod and conodont matrices seem to show no discernible vital effects (Reinhardt et al., 1998), although a small (ca. 10^{-5}) positive effect has been reported for conodonts (Diener et al., 1996). Nevertheless, the best matrices for Sr analyses are thought to be the low-magnesium calcite secondary layer in brachiopod shells – with strontium concentrations higher than 400 ppm, and conodonts – which typically preserve several thousand ppm of Sr in their phosphatic matrices (e.g., Korte et al., 2003). The major difference between brachiopods and conodonts is that the latter are extinct. Therefore, while data obtained from brachiopod samples are comparable with nowadays living brachiopods, data obtained from conodonts cannot be compared with those of living organisms. Moreover, there are pieces of evidence that conodonts might preserve a *post-mortem* isotopic signal (e.g., Trotter et al., 2015). Furthermore, Tackett et al. (2014) noticed that conodont samples tend to record higher radiogenic values of 87/86Sr compared to coheval brachiopod samples, suggesting that some kind of vital effect might affect the Sr isotopic composition of these extinct organisms. We cannot exclude that these vital effects may play a role also for the $\delta^{88/86}$Sr. More research is required in order to understand (and eventually attempt to quantify) the likely vital effect of conodonts.

References

Benton, M. J., & Twitchett, R. J., 2003. How to kill (almost) all life: the end-Permian extinction event. Trends in Ecology & Evolution, 18(7), 358-365.

Berner, R.A., and Rye, D.M., 1992. Calculation of the Phanerozoic strontium isortope record of the oceans from a carbon cycle model: American Journal of Science, 292, 136–148.

Blattler C. L., Henderson G. M. and Jenkyns H. C., 2012. Explaining the Phanerozoic Ca isotope history of seawater. Geology 40, 843–846.

Broecker, W.S., Li, Y.H., 1970, Interchange of water between the major oceans: Journal of Geophysical Research, v. 75, p. 3545-3552.

Campbell, I.H., Czamanske, G.K., Fedorenko, V.A., Hill, R.I., Stepanov, V., 1992. Synchronism of the Siberian Traps and the Permian-Triassic Boundary. Science, 258, 1760-1763.

Charlier B. L. A., Nowell G. M., Parkinson I. J., Kelley S. P., Pearson D. G. and Burton K. W., 2012. High temperature strontium stable isotope behaviour in the early solar system and planetary bodies. Earth Planet. Sci. Lett. 329–330, 31–40.

Diener, A., Ebneth, S., Veizer, J. & Buhl, D., 1996. Strontium isotope stratigraphy of the Middle Devonian: brachiopods and conodonts. Geochimica et Cosmochimica Acta, 60, 639–652.

Ernst, R.E., and Buchan, K.L., 1997. Giant radiating dyke swarms: Their use in identifying pre-Mesozoic large igneous provinces and mantle plumes, in Mahoney, J.J., and Coffin, M.F., eds., Large igneous provinces: Continental, oceanic, and planetary flood volcanism: American Geophysical Union Geophysical Monograph, 100, 297-333.

Ernst, R.E., and Buchan, K.L., 1998. Arcuate dyke swarms associated with mantle plumes on Earth: Implications for Venusian coronae [extended abstract]: Houston, Texas, Lunar and Planetary Institute, v. 29, p. CD-ROM 1021.dpf.

Farkas J., Bohm F., Wallmann K., Blenkinsop J., Eisenhauer A., van Geldern R., Munnecke A., Voigt S. and Veizer J., 2007. Calcium isotope record of Phanerozoic oceans: Implications for chemical evolution of seawater and its causative mechanisms. Geochim. Cosmochim. Acta 71, 5117–5134.

Garrett, C., St. Laurent, L., 2002, Aspects of deep ocean mixing: Journal of Oceanography, v. 58, p. 11-24.

Gordon, A. L., 1973, Physical Oceanography Antarctic: Journal of the United States, v. 8, p. 61-69.

Grice, K., Cao, C., Love, G. D., Böttcher, M. E., Twitchett, R. J., Grosjean, E., & Jin, Y., 2005. Photic zone euxinia during the Permian-Triassic superanoxic event. Science, 307(5710), 706-709.

Hardie L. A., 1996. Secular variation in seawater chemistry: An explanation for the coupled secular variation in the mineralogies of marine limestones and potash evaporites over the past 600 m.y. Geology, 24, 279–283.

Hodell, D.A; Mueller, P.A; McKenzie, J.A; Mead, G., 1989, Strontium isotope stratigraphy and geochemistry of the late Neogene ocean: Earth and Planetary Science Letters, v. 92, no. 2, p. 165-178, doi:10.1016/0012-821X(89)90044-7.

Huang S., Farkas J. and Jacobsen S. B., 2010. Calcium isotopic fractionation between clinopyroxene and orthopyroxene from mantle peridotites. Earth Planet. Sci. Lett. 292, 337–344.

Heuser, A., Eisenhauer, A., Gussone, N., Bock, B., Hansen, B.T., Nägler, Th.F., 2002. Measurement of calcium isotopes (δ44Ca) using a multicollector TIMS technique. International Journal of Mass Spectrometry 220, 385–397.

Jin, Y. G., Wang, Y., Wang, W., Shang, Q. H., Cao, C. Q., & Erwin, D. H., 2000. Pattern of marine mass extinction near the Permian-Triassic boundary in South China. Science, 289(5478), 432-436.

Jones, C.E. and Jenkyns, H.C., 2001, Seawater strontium isotopes, oceanic anoxic events, and seafloor hydrothermal activity in the Jurassic and Cretaceous: Am. J. Sci., v. 301, p. 112–149.

Korte, C., Kozur, H.W., Bruckschen, P. & Veizer, J., 2003, Strontium isotope evolution of Late Permian and Triassic seawater: Geochemica et Cosmochimica Acta, v. 67, p. 47–62.

Krabbenhoft A., Fietzke J., Eisenhauer A., Liebetrau V., Bohm F. and Vollstaedt H., 2009. Determination of radiogenic and stable strontium isotope ratios (87Sr/86Sr; d88/86Sr) by thermal ionization mass spectrometry applying an 87Sr/84Sr double spike. J. Anal. At. Spectrom. 24, 1267–1271.

Krabbenhoft A., Eisenhauer A., Bohm F., Vollstaedt H., Fietzke J., Liebetrau V., Augustin N., Peucker-Ehrenbrink B., Hansen B. T., Nolte N. and Wallmann K., 2010. Constraining the marine strontium budget with natural strontium isotope fractionations (87Sr/86Sr*–d88/86Sr) of carbonates, hydrothermal solutions and river waters. Geochim. Cosmochim. Acta 74, 4097–4109.

Lehnm G.O., Jacobson, A.D., Holmden, C., 2013. Precise analysis of Ca isotope ratios (d44/40Ca) using an optimized 43-42Ca double spike MC-TIMS method. Int. j. Mass Spectrom. 351, 69-75.

Lehn, G.O., Jacobson, A.D., 2015. Optimization of a 48Ca-43Ca double spike MC-TIMS method for measuring Ca isotope ratios (d44/40Ca and d44/42Ca): limitations from filament reservoir mixing. J. Anal. At. Spectrom. http://dx.doi.org/10.1039/C4JA00412D

McArthur, J.M., Howarth, R.J. and Shields, G.A., 2012. Strontium Isotope Stratigraphy, in The Geologic Time Scale 2012, Gradstein, F.M., Ogg, J.G., Schmitz, M., and Ogg, G. (eds.), published by Elsevier B.V. DOI: 10.1016/B978-0-444-59425-9.00007-X.

Nier A. O., 1938. The isotopic constitution of strontium, barium, bismuth, thallium and mercury. Phys. Rev. 54, 275.

Nikishin, A.M., Ziegler, P.A., Stephenson, R.A., Cloetingh, S.A.P.L., Furne, A.V., Fokin, P.A., Ershov, A.V., Bolotov, S.N., Korotaev, M.V., Alekseev, A.S., Gorbachev, V.I., Shipilov, E.V., Lankreijer, A., Bembinova, E.Y., and Shalimov, I.V., 1996. Late Precambrian to Triassic history of the East European Craton: Dynamics of sedimentary basin evolution. Tectonophysics, 268, 23-63.

Reinhardt, E.G., Blenkinsop, J. & Patterson, R.T., 1998. Assessment of a Sr isotope vital effect (87 Sr/86 Sr) in marine taxa from Lee Stocking Island, Bahamas. Geo-Marine Letters 18, 241–246.

Renne, P. R., & Basu, A. R., 1991. Rapid eruption of the Siberian Traps flood basalts at the Permo-Triassic boundary. Science, 253(5016), 176-179.

Sharma, M., 1997. Siberian traps. Large igneous provinces: Continental, oceanic, and planetary flood volcanism, 273-295.

Tackett, L.S., Kaufman, A.J., Corsetti, F.A., Bottjer, D.J., 2014. Strontium isotope stratigraphy of the Gabbs Formation (Nevada): implications for global Norian–Rhaetian correlations and faunal turnover. Lethaia, 47, 500-511, DOI 10.1111/let.12075.

Tomshin, M.D., Okrugin, A.V., Savvinov, V.T., and Shakhot'ko, L.I., 1997. The Ebe-Khaya dike belt of trachydolerites in the north of the Siberian platform. Russian Geology and Geophysics, 38, 1511-1520.

Trotter, A.J., Williams, S.I., Nicora, A., Mazza, M. and Rigo, M., 2015. Long-term cycles of Triassic climate change: a new $d^{18}O$ record from conodont apatite: Earth and Planetary Science Letters, v. 415, p. 165–174.

Veizer, J., Buhl, D., Diener, A., Ebneth, S., Podlaha, O.G., Bruckschen, P., Jasper, T., Korte, C., Schaaf, M., Ala, D., Azmy, K., 1997, Strontium isotope stratigraphy: potential resolution and event correlation: Paleogeogr., Paleoclimatol., Paleoecol., v. 132, p. 65–77.

Veizer, J., Ala, K., Azmy, K., Bruckschen, P., Buhl, D., Bruhn, F., Carden, G.A.F., Diener, A., Ebneth, S., Godderis, Y., Jasper, T., Korte, C., Pawellek, F., Podlaha, O.G., Strauss, H., 1999, 87Sr/86Sr, δ13C and δ18O evolution of Phanerozoic seawater: Chem. Geol., v. 161, p. 59–88.

Wignall, P. B., & Hallam, A., 1992. Anoxia as a cause of the Permian/Triassic mass extinction: facies evidence from northern Italy and the western United States. Palaeogeography, Palaeoclimatology, Palaeoecology, 93(1), 21-46.

CONCLUDING REMARKS

The late Norian-early Hettangian time interval appears to be marked by a series of $\delta^{13}C_{org}$ decreases that provide new clues on the relationship between carbon cycle disruption, LIP volcanism and the end-Triassic mass extinction. In fact, the late Norian $\delta^{13}C_{org}$ record from the Lagonegro Basin (western Tethys) shows the occurrence of a ca. 5‰ negative shift close to the Norian-Rhaetian transition, preceded by two other $\delta^{13}C_{org}$ decreases of similar magnitude (3-5‰). The Notian-Rhaetian $\delta^{13}C_{org}$ decrease is correlatable (using biostratigraphy) with a negative excursion recognized in the North America realm, supporting the idea that the late Norian carbon cycle was affected at a global scale. The most likely trigger mechanism for the input of isotopically light carbon in the ocean-atmosphere system is the emplacement of a LIP, as supported also by the $\delta^{18}O_{phos}$ profile (Trotter et al., 2015), the $^{87}Sr/^{86}Sr$ curve (Callegaro et al., 2010), and increase in the pCO_2 values (McElwain et al., 1999; Huynh and Poulsen, 2005; Cleveland et al., 2008). This late Norian volcanic activity was thought to be active between 206 Ma, and has been tentatively attributed to the Angayucham province, a complex ocean plateau originally located on the western margin of North America and today outcropping in Alaska.

The Rhaetian organic carbon isotope record from the Lombardy Basin reveals a series of $\delta^{13}C_{org}$ decreases that provide two possible interpretations. Previous works placed the “initial” CIE at the base of the Malanotte Formation and the “precursor” at the top of the Zu3c submember, while the “main” has never been clearly identified. The complete Rhaetian $\delta^{13}C_{org}$ profile shows a great similarity with the St Audrie’s Bay $\delta^{13}C_{org}$ record, where the “main” and “initial” negative carbon isotope excursions were defined for the first time. Therefore, through these chemostratigraphic correlations it is possible to place the “initial” CIE within the Zu3b submember, ca. 90 m below the base of the Malanotte Formation, and the onset of the “main” CIE at the top of the Zu3b. The “main” CIE thus appears to encompass the Zu3c submember and the Malanotte Fm. The “precursor” has been identified in the Zu3a submember. These negative carbon isotope excursions have been linked by several Authors to the CAMP volcanism: as a consequence, all the biotic crises recorded at the top of the Calcari di Zu Formation could be ascribed to this large igneous province activity. This new interpretation of the Lombardy Basin organic carbon isotope record seems to be in agreement with the relative timing of the major end-Triassic events, that are the carbonate productivity crises, at least two bio-calcification crises, the first appearance of calcareous nannofossil *Schizosphaerella* sp. and age of the “main” negative carbon isotope excursion.

The $\delta^{13}C_{org}$ records presented in this work improve the Late Triassic organic carbon isotope record, which we show to be characterized by a series of decreases linked to the emplacement of different LIPs: the late Ladinian-early Norian Wrangellia, the late Norian Angayucham and the late Rhaetian-early Hettangian CAMP. These events may have had extreme environmental consequences, potentially with associated decrease in primary productivity and/or warming, which could have induced humid conditions and episodes of seawater oxygen depletion, biotic crises and extinctions, writing the complex history of this particular period of time.

ACKNOWLEDGMENTS

I would like to thank all the people that guide me through the experience of this PhD project, starting from my tutor Dr. Manuel Rigo, whose enthusiasm, dedication and curiosity represent constant inspirations for my work.

A special thank to my co-tutor Prof. Claudia Agnini, for all the interest and the help.

Thanks to Prof. Giuseppe Concheri and all the staff of the Biotechnology Lab at DAFNAE, who helped me with the TOC analyses.

I would like to thank Prof. Malcolm McCulloch, Dr. Julie Trotter, Dr. Kai Rankenburg, Dr. Breege McKiernan, Dr. Verena Schoepf, Dr. Juan Pablo D'Olivo, Dr. Chris Cornwall, Dr. Claire Ross and all the other capable people of the University of Western Australia.

All the other PhD students of the Department of Geosciences, because “we’re all in the same boat”.

I would like to thank Dr. Anna Breda and Prof. Cristina Stefani for giving me the opportunity to be a teaching assistant. A special thank also to the other girls that worked with me as teaching assistants.

A giant thank to my special travel buddies, Matteo Maron and Stefania Sorgato, who supported (and tolerate) me for the entire time (and more). Matteo, man of few but thoughtful words, I’d like to thank you for all the help and the funny moments. Stefania, thank you for all the encouragement and for sharing the hardest time. Thank you guys for teaching me that can be safe to open myself to others. What can I say…Banana!

Un grazie particolare alla mia famiglia, a mia mamma, le mie zie, i miei zii, cugine e cugini, a mia nonna. Un pensiero va anche alle persone che non ci sono più, e con le quali avrei voluto condividere questa esperienza e le avventure di questi ultimi tre anni.

At the end, the biggest “thank you” to the person who always sustain and tolerate me through everything. Thanks Matteo for all the amazing things you gave me (and give me) everyday. “Se non ti conoscessi e a un certo punto, mentre distrattamente guardo avanti, così come si fa...sovrappensiero…e tu passassi ora, come sei, io per la prima volta – nuovamente – mi sentirei così, come mi sento, ancora un'altra volta – nuovamente – starei proprio così, come sto adesso: Innamorata!”

What can I say now…it’s the end of an era. I’m not a student anymore, even if we never stop learning. If I look back, I realized that it’s true: the sleep of reason produces monster…but so does the PhD! ;)

APPENDIX A

The Pignola-Abriola section (southern Apennines, Italy): a new GSSP candidate for the base of the Rhaetian Stage[1]

Manuel Rigo[1], Angela Bertinelli[2], Giuseppe Concheri[3], Giovanni Gattolin[1,4], Linda Godfrey[5], Miriam E. Katz[6], Matteo Maron[1], Paolo Mietto[1], Giovanni Muttoni[7], Mario Sprovieri[8], Fabio Stellin[3] and Mariachiara Zaffani[1]

[1] Department of Geosciences, University of Padova, via Gradenigo 6, 35131 Padova, Italy
[2] Department of Physics and Geology, University of Perugia, via Pascoli, 06123 Perugia, Italy
[3] Department of Agronomy Food Natural Resources Animals and Environment, University of Padova, Viale dell'Università 16, 35020 Legnaro, Padova, Italy
[4] ENI E&P division, via Emilia 1 20097, San Donato Milanese, Italy
[5] Department Earth and Planetary Sciences, Rutgers University, Piscataway, NJ 08854, USA
[6] Department of Earth and Environmental Sciences, Rensselaer Polytechnic Institute, 1108th St., Troy, NY 12180, USA
[7] Department of Earth Sciences 'Ardito Desio', University of Milano, via Mangiagalli 34, 20133 Milan, Italy
[8] IAMC-CNR, Via del Mare 3, 91021 Torretta Granitola, Trapani, Italy

ABSTRACT

The base of the Rhaetian stage (Norian/Rhaetian boundary, NRB) is still awaiting formal designation by the International Commission on Stratigraphy. At present, only the 4.30-m-thick Steinbergkogel section (Austria) has been proposed as GSSP (Global Stratotype Section and Point) candidate for the base of the Rhaetian. Here we present data from the 63-m-thick Pignola-Abriola section (Southern Apennines, Italy) that we consider an alternative candidate for the Rhaetian GSSP. The Pignola-Abriola basinal section, represented by hemipelagic–pelagic carbonate successions belonging to the Lagonegro Basin, matches all the requirements for a GSSP: 1, it is well exposed with minimal structural deformation; 2, it is rich in age diagnostic fossils (e.g. conodonts and radiolarians); 3, it yields a geochemical record suitable for correlation (e.g. $\delta^{13}C$); and 4, it has a robust magnetostratigraphy and is correlated with the Newark APTS for age approximation of the NRB and additional Rhaetian bioevents. In the Pignola-Abriola section, we opt to place the NRB at the 44.4 metre level, coincident with a prominent negative shift of ca. 6‰ of the $\delta^{13}C_{org/carb}$. This level is located 50 cm below the FAD of conodont Misikella posthernsteini s.s within the radiolarian Proparvicingula moniliformis Zone. Both the negative $\delta^{13}C_{org}$ shift and the FAD of Misikella

[1] This manuscript has been published in Lethaia as RIgo et al. (2015).

posthernsteini occur within Pignola-Abriola magnetozone MPA-5r, at ~205.7 Ma, according to magnetostratigraphical correlation to the Newark APTS. We also illustrate the coeval Mt. Volturino stratigraphical section deposited below the calcite compensation depth (CCD) within the same Lagonegro Basin and characterized by a detailed radiolarian biostratigraphy and strong $\delta^{13}C_{org}$ negative shift around the NRB.

INTRODUCTION

The Rhaetian was first proposed as a stage in 1891 by Carl Wilhelm Ritter von Guembel, named after the Raetia Province of the Roman Empire and applied to all those strata containing the bivalve Avicula contorta, which was a peculiar bivalve of the shallowmarine facies of the western Tethys (such as the Koessen Beds of Austria). The Rhaetian was included as Stufe (=Stage) in the first chronostratigraphical scale of the Triassic System by Von Mojsisovics et al. (1895), as 'Zone der Avicula contorta', and accepted as the last Stage of the Triassic by von Arthaber (1905). Since then, the Rhaetian has been subject to intense debates focusing on whether it should be recognized as an independent Stage (e.g. Pearson 1970; Ager 1987) or assigned to the Jurassic System, as suggested by Slavin (1961, 1963) for ammonoid-barren strata of northwestern Europe (a suggestion that was not met with acceptance), or included in the Norian Stage, as recommended by Tozer (1967) and Silberling & Tozer (1968) and adopted for instance by Zapfe (1974) and Palmer (1983), or even completely eradicated from geological time-scales (e.g. Tozer 1984, 1990). However, most specialists, especially those working in the Tethyan Realm, accepted the Rhaetian as a Stage of the Upper Triassic Series (e.g. Kozur & Mock 1974; Gazdzicki 1978; Gazdzicki et al. 1979; Krystyn 1980, 1990; Fahræus & Ryley 1989). Notably, in the Carta Geologica Italiana published in the 1970s and 1980s, the Rhaetian was always considered as a Stage of the Upper Triassic. In the final report of the IGCP 4 (Zapfe 1983), the Rhaetian Stage was included in the Tethyan timescale, but not in the Canadian or Soviet Union time-scales. In 1991, the Subcommission on Triassic Stratigraphy (STS) confirmed the Rhaetian as an independent Stage, yet a formal marker to define its base is still lacking. Possible markers, mostly in the form of bioevents, to assign the base of the Rhaetian have been listed by Krystyn (2010) in an activity report of the Norian/Rhaetian Working Group and also reported by Ogg in Gradstein et al. (2012); these are:

- FAD (First Appearance Datum) of conodont Misikella posthernsteini;
- Base of the Propavicingula moniliformis radiolarian Zone;
- FAD of conodont Mockina mosheri morphotype A;
- LO (Last Occurrence) of ammonoid genus Metasibirites;

- FAD of the ammonoid Paracochloceras suessi;
- Disappearance of the standard-size bivalve genus Monotis;
- And Prominent change from an extended normal-polarity magnetozone upward into a reversed polarity magnetozone (UT23n to UT23r), from the composite scale illustrated by Hounslow & Muttoni (2010).

At present, the only suggested GSSP candidate for the Rhaetian is represented by the Steinbergkogel section in Salzkammergut (Austria) (Krystyn et al. 2007a,b). The Steinbergkogel section, exposed in an abandoned quarry surrounded by a forested area, is comprised of red and grey, marine pelagic, condensed Hallstatt Limestone beds with ammonoids, bivalves, conodonts and other micro-fossils such as calcareous coccoliths, dinoflagellate cysts and sporomorphs (e.g. Gardin et al. 2012). This section is composed of three sub-sections named STK-A, STK-B and STK-C, with STK-A correlative to STK-C and STK-B stratigraphically coeval. In this composite section, three events have been suggested as possible markers for the base of the Rhaetian: (1) first occurrence (FO) of Misikella hernsteini, corresponding to the FO Mockina mosheri morphotype A, and close to the FO of the ammonoid Tragorhacoceras, as well as the appearance of the genus Rhaetites (Krystyn et al. 2007a); (2) FAD of Misikella posthernsteini (Krystyn 2008), correlated to the base of the radiolarian Propavicingula moniliformis Zone (e.g. Kozur 2003; Giordano et al. 2010) and the FO of Paracochloceras suessi (Krystyn et al. 2007a); and (3) FO of the ammonoid Cycloceltites and Choristoceras and disappearance of Sagenites, Dionites and Pinacoceras (Krystyn et al. 2007a). Ammonoid biostratigraphy is considered one of the main tools for high-resolution dating and correlation of Triassic sedimentary sequences (Balini et al. 2010). Unfortunately, for the upper Norian and Rhaetian, ammonoids are documented only locally. For instance, the only sedimentary formation in Italy with documented (but poorly preserved) ammonoids attributed to Choristoceras cf. rhaeticum (Gumbel) is the Calcare di Chiampomano outcropping in the Preone Valley near Udine (northeastern Southern Alps) (Guembel 1861). Conodonts and radiolarians are instead more frequent and are thus used as primary biostratigraphic tools for the definition of upper Norian and Rhaetian strata and correlations (e.g. Carter & Orchard 2007; Rigo et al. 2007, 2012a; Giordano et al. 2010). Here, we present data from the 63-m-thick Pignola-Abriola section (Lagonegro Basin, Southern Apennines, Italy). We show that this section presents all the desirable attributes of a new, valid GSSP candidate for the base of the Rhaetian Stage. We also illustrate data from the ancillary and coeval Mt. Volturino stratigraphical section deposited in the same basin but presumably below the CCD.

GEOLOGICAL SETTING

The Pignola-Abriola and Mt. Volturino sections belong to the Lagonegro Basin succession (Southern Apennines) and are made up of hemipelagic to pelagic marine deposits. The Lagonegro Basin is considered part of the southwestern branch of the Tethys Ocean and is bordered to the north by the Apenninic and Apulian carbonate platforms (e.g. Sengor et al. 1984; Stampfli et al. 1991; Stampfli & Marchant 1995; Catalano et al. 2001; Ciarapica & Passeri 2002, 2005). The deepening-upward Lagonegro Basin succession is characterized by Permian to Miocene formations deposited in shallow to deep basinal environments. The lower part of the succession is represented by the 'Lagonegro lower sequence' (e.g. Mostardini & Merlini 1986; Ciarapica et al. 1990; Ciarapica & Passeri 2005; Rigo et al. 2005) and includes the following formations (from oldest to youngest): Monte Facito Formation (Permian to upper Ladinian); Calcari con Selce (upper Ladinian to Rhaetian); Scisti Silicei (Rhaetian to Tithonian); and Flysch Galestrino (Tithonian to Lower Cretaceous). This lower sequence, always detached from its basement, is dissected into several tectonic units piled up between the Apenninic and Apulian carbonate platforms (e.g. Mostardini & Merlini 1986) during Apenninic orogenesis. The Upper Triassic–Middle Jurassic Calcari con Selce and Scisti Silicei formations consist of pelagic carbonates and siliceous deposits (i.e. cherts and radiolarites) bearing conodonts, pelagic bivalves (e.g. genus Halobia), radiolarians and sparse ammonoids. In proximal palaeogeographical settings, the Calcari con Selce persisted from the Late Triassic to the Early-Middle Jurassic (e.g. Scandone 1967; Bertinelli et al. 2005a; Passeri et al. 2005), whereas in more distal settings, a transition from carbonate sedimentation of the Calcari con Selce to siliceous deposition of Scisti Silicei occurred between the latest Triassic and the earliest Jurassic and is interpreted as due to the subsidence of the ocean floor below the CCD (e.g. Amodeo 1999; Giordano et al. 2010). A precursory switch from carbonate to siliceous deposition is documented during the Carnian (Rigo et al. 2007) and is interpreted as due to a transitory shift towards more humid climate conditions (Rigo & Joachimski 2010; Rigo et al. 2012a; Trotter et al. 2015). Because of the difficulties in placing a boundary between the Calcari con Selce and the Scisti Silicei, Miconnet (1982) first introduced the term 'Transitional Interval' to designate the stratigraphical portion of the Lagonegro succession that was included in the upper part of the Calcari con Selce and characterized by an increase of red radiolaritic intercalation, typical of the overlying Scisti Silicei (Amodeo 1999; Bertinelli et al. 2005a; Passeri et al. 2005; Reggiani et al. 2005; Rigo et al. 2012b). In particular, the base of the Transitional Interval is conventionally marked by a 2.5- to 4-m-thick interval of red shales (Amodeo 1999; Bertinelli et al. 2005b; Reggiani et al. 2005; Rigo et al. 2012b) of Sevatian 1 age (Mockina bidentata Zone – late Norian) (Rigo et al. 2005, 2012b). However, in-depth investigations, mostly for biostratigraphy (e.g. De Wever & Miconnet 1985; Bertinelli et al. 2005a; Passeri et al. 2005; Reggiani et al. 2005; Rigo et al. 2005, 2012b), revealed that this red shale interval shows atypical features in the Pignola-Abriola section, while it is easily recognized in the Mt. Volturino section.

PIGNOLA-ABRIOLA SECTION: CANDIDATE FOR THE RHAETIAN GSSP

Lithostratigraphy

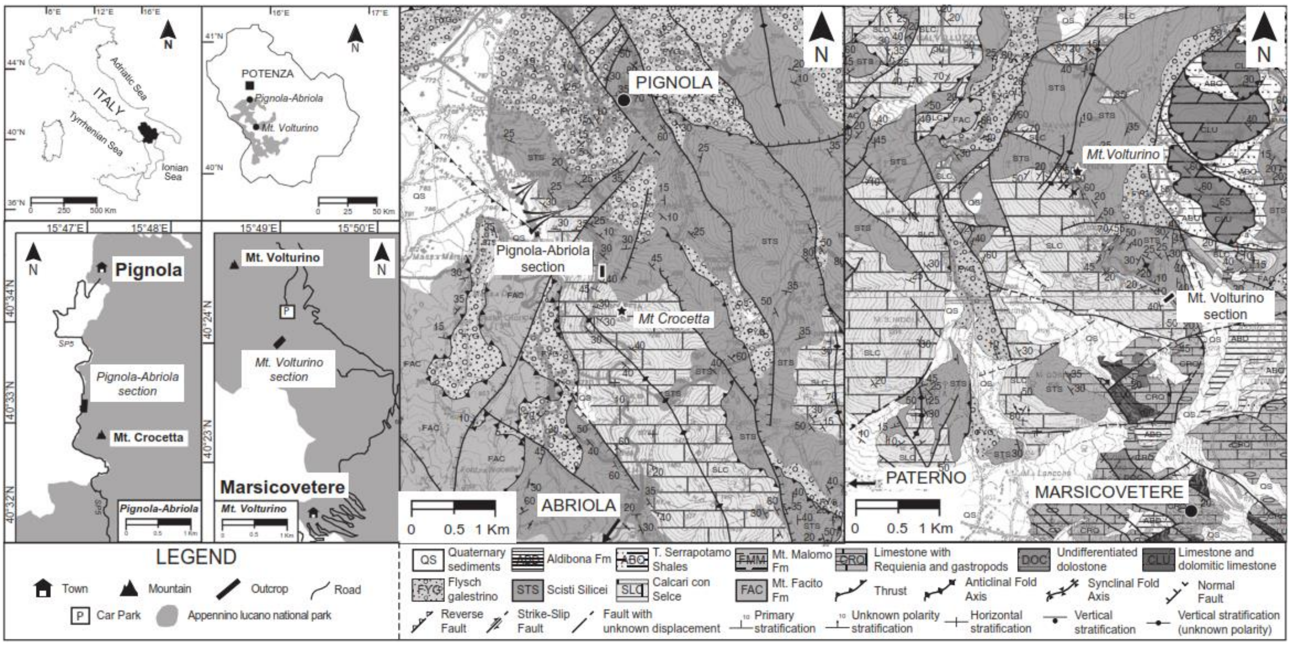

Fig. A1 Geological map (modified from Foglio Geologico 489-Marsico Nuovo and Foglio Geologico 505-Moliterno; http://www.isprambiente.gov.it/Media/carg/) and location map of the Pignola-Abriola and Mt. Volturino sections. Both sections crop out in Southern Apennines, near Potenza (Southern Italy), in the protected area of the Parco Appennino Lucano Val d'Agri Lagonegrese. The PignolaAbriola section crops out along the main road SP 5 'della Sellata', on the western flank of Mt. Crocetta (Lat: 40°33 23,50″N; Long: 15°47 0 1,71″E). The Mt. Volturino section is exposed close to the homonymous mountain peak, to the north of Marsicovetere village (Lat: 40°24 0 13,46″N; Long: 15°49 0 2,25″E).

The Pignola-Abriola section was measured on the western side of Mt. Crocetta along road SP5 'della Sellata' connecting the villages of Pignola and Abriola (Geographic coordinate system, datum WGS 84: 40° 33 0 23.50″N, 15° 47 0 1.71″E) (Fig. A1). The Pignola-Abriola section is located in an area of minimal structural deformation and within the protected area of the Parco Appennino Lucano Val d'Agri Lagonegrese (Fig. A1). The section is a ca. 63-m-thick basinal succession dominated by the Calcari con Selce and encompassing the Norian/Rhaetian boundary (Amodeo et al. 1993; Amodeo 1999; Bazzucchi et al. 2005; Rigo et al. 2005, 2012b; Giordano et al. 2010) (Fig. A2). Thinly bedded cherty limestones (partially dolomitized in the lowermost part of the section) constitute the dominant lithology, sometimes intercalated with centimetre-thick calcarenites due to sporadic gravity flows/turbiditic events (e.g. Amodeo 1999; Bertinelli et al. 2005a; Giordano et al. 2011). The siliciclastic input increases in the upper part of the Calcari con Selce at the transition with the overlying Scisti Silicei, where shales, radiolarites and subordinate marls dominate. The lower portion of the section (ca. 0– 6.5 m) (Fig. A2) consists mainly of well-stratified, thinly bedded cherty dolostones; chert nodules become frequent above ca. 3.5 m. Calcarenites linked to gravity flow events and containing frag- ments of benthic organisms are subordinate. From ca. 6.5 up to metre 13, repeated intercalations of shales, several centimetres thick, are present. Cherty layers become abundant at ca. 13 m from the base. Between ca. 13 and 22.5 m, limestones gradually replace dolostones and consist mainly of mudstones–wackestones, and less commonly packstones, with abundant radiolarians and rare bivalves. From 22.5 m up to ca. 39 m, shale frequency decreases and centimetre-thick chert bands in limestone beds are common. In addition, three diameter-thick, often amalgamated and partially dolomitized, fining-upward beds of calcarenite occur between ca. 34 and 35.5 m and provide useful lithomarkers (Maron et al. 2015). Between 39 and 43.5 m, nodules and especially layers and bands of black radiolarian cherts become abundant, with an increase in terrigenous input up to 56 m. The shales are typically dark and rich in organic matter, often interbedded with silicified limestones and thin calcarenites, deposited in low oxygen (dysoxic to anoxic) conditions. This frequent alternation of shales, limestones, finegrained calcarenites, marls and chert beds constitute the so-called Transition Interval (Miconnet 1982; Amodeo 1999) separating the Calcari con Selce from the Scisti Silicei, although at Mt. Crocetta the lower part of Scisti Silicei does not crop out extensively. The uppermost part of the Pignola-Abriola section (ca. m 56–58) is characterized by diameter-thick micritic limestone beds with few clayey intercalations, overlain by red radiolarites and chert layers typical of the Scisti Silicei, extending up to the top of the measured section (at ca. m 63).

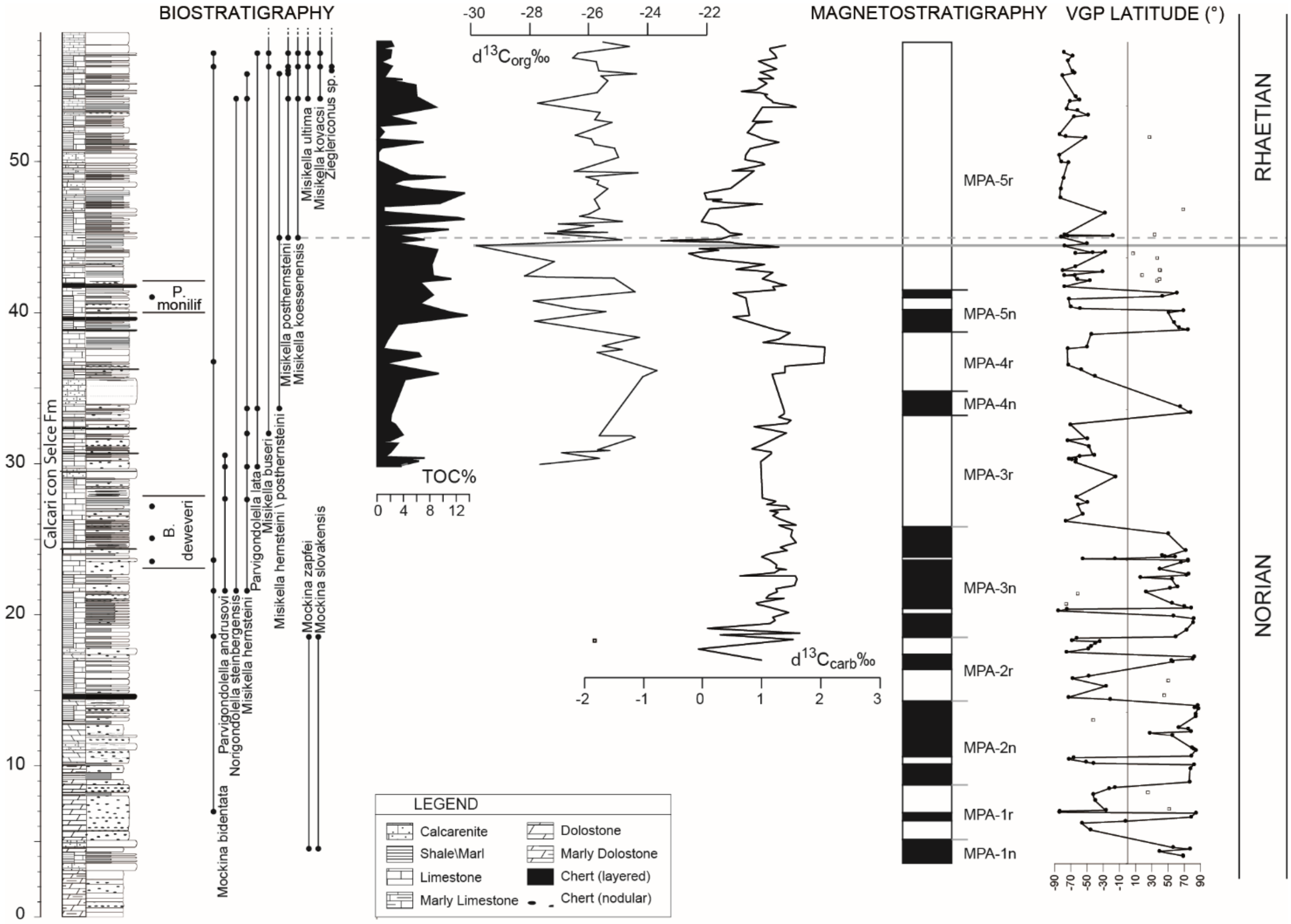

Fig. A2 The Pignola-Abriola section with, from left to right, stratigraphical log, radiolarian and conodont biostratigraphy, total organic matter percentage (TOC), and δ13Corg and δ13Ccarb curves. Magnetostratigraphy and the virtual geomagnetic poles (VGP) are from Maron et al. (2015). The prominent δ13Corg negative shift located close to the FAD of conodont Misikella posthernsteini s.s. is here reported as primary proxy for the base of the Rhaetian. Notably, the δ13Corg negative peak occurs within the base of the radiolarian Proparvicingula moniliformis Zone.

Biostratigraphy

The Pignola-Abriola section has been studied in detail for conodonts and radiolaria (Amodeo 1999; Bazzucchi et al. 2005; Rigo et al. 2005, 2012b; Giordano et al. 2010) (Figs A2, A3). Conodonts are common throughout the entire section, even though they are rare around the NRB, as first noted by Krystyn et al. (2007a,b). The Conodont Alteration Index (CAI) is 1.5, suggesting that burial temperatures never exceeded 100 °C (sensu Epstein et al. 1977; Bazzucchi et al. 2005; Giordano et al. 2010; Maron et al. 2015). In stratigraphical order, the following updated and main bioevents have been recognized:

- at metre 7, sample PI5, the first occurrence (FO)
- of Mockina bidentata;
- at metre 21.4, sample PR16, FO of Misikella hernsteini,

- co-occurring with Parvigondolella andrusovi;
- at metre 32, sample GNC3, the FO of Misikella buseri;
- at metre 33.4, sample PR10, the FO of Misikella hernsteini/posthernsteini morphocline;
- at metre 44.9, in sample PIG24, the first appearance datum (FAD) of Misikella posthernsteini s.s.;
- and at metre 55.5, sample GNC100, the FO of Misikella ultima in association with Misikella koessenensis.

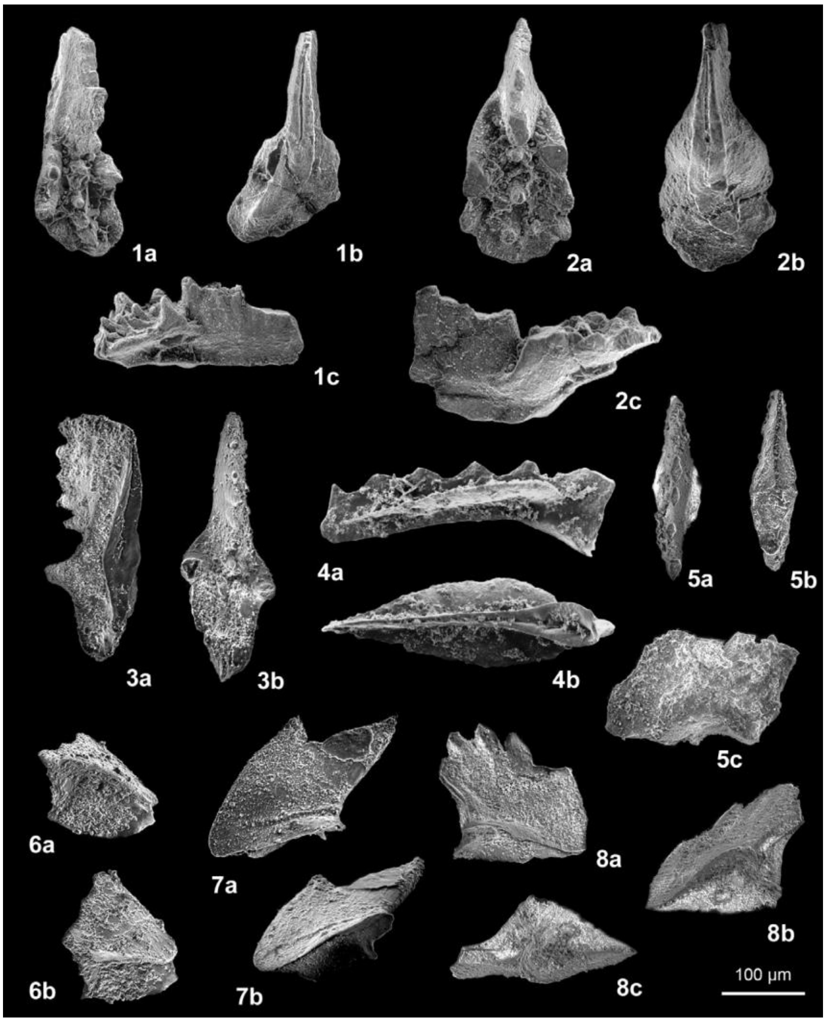

Fig. A3 SEM micrographs of upper Norian to Rhaetian conodonts from the Pignola-Abriola section Calcari con Selce Fm (after Bazzucchi et al. 2005 and Giordano et al. 2010, modified). Scale bar = 100 lm. 1, a, b, c, Mockina zapfei Kozur); sample PIG 0. 2, a, b, c, Mockina slovakensis (Kozur); sample PIG 0. 3, a, b: Mockina bidentata (Mosher); PIG 7. 4, a, b: Norigondolella steinbergensis (Mosher); PR 16. 5, a, b, c, Misikella hernsteini (Mostler); sample PIG 16. 6, a, b, Misikella posthernsteini Kozur & Mock; sample PIG 24. 7, a, b, Misikella kovacsi Orchard; sample PIG 40. 8, a, b, c, Misikella ultima Kozur & Mock; sample PIG 40.

The radiolarian associations (Figs A2, A4) are well preserved and conform to the biozonation proposed by Carter (1993), which consists of radiolarian assemblage zones biochronologically correlated to the North America ammonoid zonation proposed by Tozer (1979):

- Sample PR14 at metre 25 yielded a radiolarian assemblage referable to the Betraccium deweveri Zone (U.A. 1 Carter 1993) based on the presence of Betraccium deweveri Pessagno & Blome, Praemesotaturnalis gracilis Kozur & Mostler, Tetraporobrachia sp. aff. T. composita Carter, Ayrtonius elizabethae Sugiyama, Citriduma sp. A sensu Carter (1993), Globolaxtorum sp. cf. G. hullae (Yeh & Cheng), Lysemela sp. cf. L. Olbia Sugiyama, Livarella valida Yoshida and Livarella sp. sensu Carter (1993) (Giordano et al. 2010); a similar assemblage was found also in sample PR15 at metre 23.5 and sample PR13 at metre 27.5. The presence of Globolaxtorum sp. cf. G. hullae Yeh & Cheng in this assemblage is atypical, because the genus Globolaxtorum is usually referred only to the Proparvicingula moniliformis and Globolaxtorum tozeri zones (O'Dogherty et al. 2009).
- Sample PA25 at metre 41 yielded a radiolarian assemblage referable to the Proparvicingula moniliformis Zone, Assemblage 1 and 2, Subassemblage 2a (U.A. 2–8 Carter 1993), for the presence of Fontinella primitiva Carter, Praemesosaturnalis sp. cf. P. sandspitensis Blome, Globolaxtorum sp. cf. G. hullae Yeh & Cheng and Livarella densiporata Kozur & Mostler (Bazzucchi et al. 2005; Giordano et al. 2010).

Misikella posthernsteini is a phylogenetic descendent of M. hernsteini (e.g. Mostler et al. 1978; Kozur & Mock 1991; Giordano et al. 2010). Both species display a similar cusp as posterior denticle, but they differ in (1) number of blade denticles, which are 3 (rarely 4) in M. posthernsteini and 4–6 in M. hernsteini; and (2) shape of the basal cavity, which is shaped like a heart or drop in M. posthernsteini and M. hernsteini, respectively. All specimens with intermediate features are grouped in the Misikella hernsteini/posthernsteini morphoclines and are here referred to as Misikella hernsteini/posthernsteini transitional forms; they are characterized by the reduction of the number of blade denticles and the evolution of the drop-shaped basal cavity into a heart shape. These transitional forms are also well documented in other sections of the Lagonegro Basin (e.g. Giordano et al. 2010), as well as the Lombardian Basin of northern Italy (Muttoni et al. 2010). The occurrence of the Misikella hernsteini/posthernsteini morphoclines is followed by the occurrence of Misikella posthernsteini sensu stricto (m 44.9, sample PIG24), providing a continuous and reliable biostratigraphical signal (Remane 2003). Calibration with radiolarian biostratigraphy (Giordano et al. 2010) reveals that only those specimens of Misikella posthernsteini characterized by a heart-shaped basal cavity due to a real groove on the posterior margin of the basal cavity developed by the extension of a distinct furrow

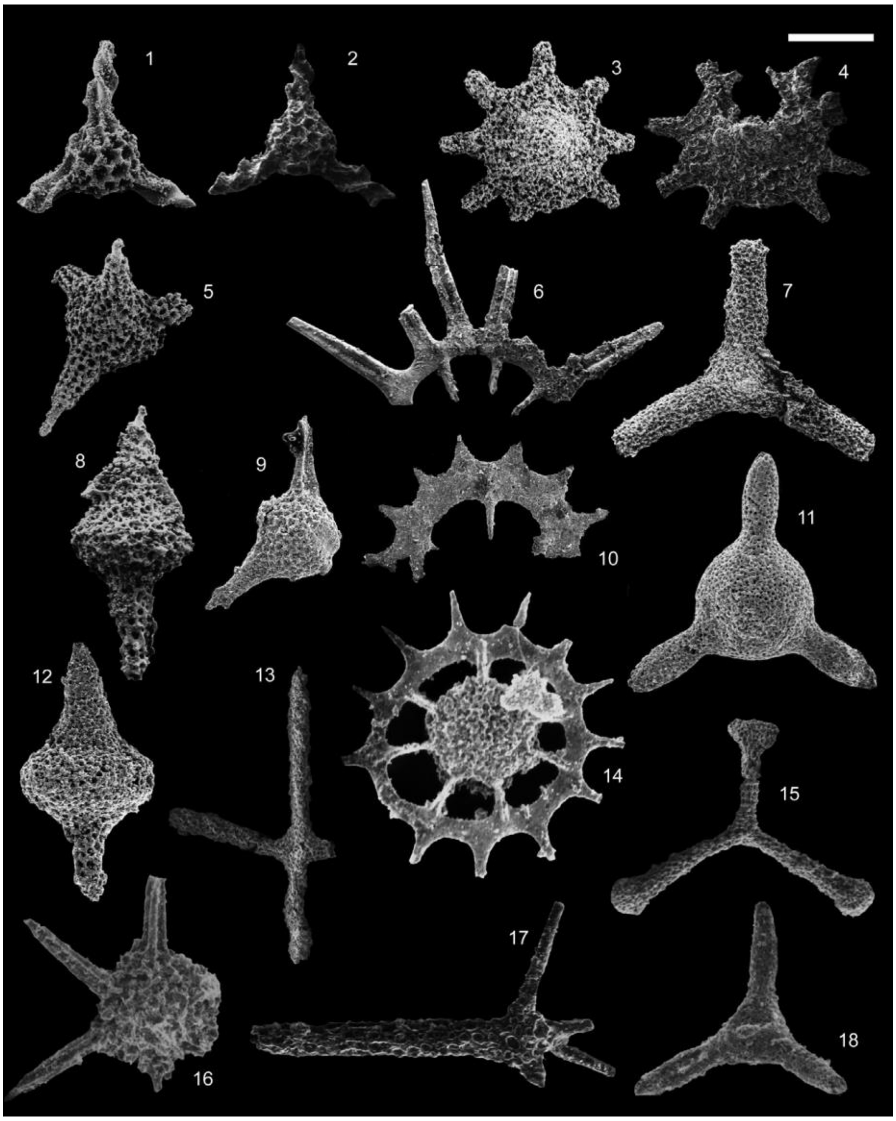

Fig. A3 Upper Norian–Rhaetian radiolarians from the Calcari con Selce (Pignola-Abriola section) and from the Scisti Silicei (Mt. Volturino section). Samples PR13, PR14 and PR15 from Pignola-Abriola, and sample MVV5 from Mt. Volturino, are referred to the Betraccium deweveri Zone; sample PA25 (Pignola-Abriola) is referred to the Proparvicingula moniliformis Zone, Assemblage 1; sample MV23 (Mt. Volturino) is referred to the Proparvicingula moniliformis Zone, Assemblage 1–2 and MV 31 (Mt. Volturino) to the Globolaxtorum tozeri Zone Assemblage 3. Scale bar = 100 lm for 1–2, 8–12, 14–15; 150 lm for 6; 200 lm for 3–5, 7, 16–18 (after Bazzucchi et al. 2005 and Giordano et al. 2010, 2011, modified). 1. Betraccium deweveri Pessagno & Blome, sample PR14. 2. Betraccium deweveri Pessagno & Blome, sample MVV53. Citriduma sp. A, sensu Carter (1993), sample PR13. 4. Citriduma sp. A, sensu Carter (1993), sample MVV5. 5. Tetraporobrachia sp. aff. T. composita Carter, sample PR14. 6. Praemesotaturnalis gracilis (Kozur & Mostler), sample PR14. 7, Livarella sp., sensu Carter (1993), sample PR14. 8. Globolaxtorum sp. cf. G. hullae (Yeh & Cheng), sample PR14. 9. Fontinella primitiva Carter, sample PA 25. 10. Praemesosaturnalis sp. cf. P. sandspitensis (Blome), sample PA25. 11, Livarella densiporata Kozur & Mostler, sample PA25. 12, Globolaxtorum hullae (Yeh & Cheng), sample PA25. 13. Pseudohagiastrum sp. A sensu Carter 1993, sample MV23 14. Praemesosaturnalis sp. aff. P. sandspitensis (Blome), sample MV31. 15. Paronaella pacofiensis Carter, sample MV23. 16. Octostella dihexacanthus (Carter), sample MV31. 17. Pseudohagiastrum giganteum Carter & Hori, sample MV 31. 18. Livarella valida Yoshida, sample MV31.

along the backside of the cusp occurred within the radiolarian Proparvicingula moniliformis Zone (sensu Carter 1993). These specimens were interpreted as Misikella posthernsteini sensu stricto (Giordano et al. 2010). Recently, calcareous nannofossils (e.g. Prinsiosphaera sp.) also were recorded and estimated to contribute between 2.5 and 15% to the amount of carbonate production at the Pignola-Abriola section (Preto et al. 2013). Notably, thin cross-section bivalve shells have been observed in the limestone beds of the PignolaAbriola section, but no good specimens have been collected from these strata. However, a single specimen of Monotis limaeformis Gemmellaro was documented in the Mt. Sirino area (De Lorenzo 1894), ca. 50 km to the south of the Pignola-Abriola section. This species is strictly related to the Monotis salinaria group (De Lorenzo 1894; Grant-Mackie 1978), which is Sevatian in age (late Norian) (e.g. McRoberts 2010).

Chemostratigraphy

The Pignola-Abriola section has been investigated for organic carbon isotope (d13Corg) and total organic carbon (TOC) variations. Rock samples were collected from the section (76 samples) (Table A1), washed in millipore water and selected to avoid the sampling of not representative portions of the sample (e.g. fracture-filling mineralization, bioturbation, diagenetic alterations). Several grams of each sample (<5 g) were reduced to a fine powder using a Retsch RM0 grinder and dried overnight at 40 °C. The TOC investigations were conducted following the standard acid attack method (Schlanger & Jenkyns 1976), which requires the reaction of the powders with a 10% HCl solution in silver capsules. Once the reaction was finished, the samples were dried on a hot plate at 50 °C. All samples were analysed using a Vario Macro CNS Elementar Analyser at the University of Padova. Results were calibrated against Sulphanilamide standard (N = 16.25%; C = 41.81%; S = 18.62%; H = 4.65%). The analytical uncertainty of the instrument is r = 0.5% (% RSD, relative standard deviation). For the d13C measurements, pulverized rock samples were acid-washed with 10% HCl for at least three hours (usually overnight). Successively, the samples were neutralized in millipore water, dried at 40 °C overnight and wrapped in tin capsules. Fortyone samples were analysed using a GVI Isoprime CF-IRMS mass spectrometer at Rutgers University: multiple blank capsules and isotope standards (NBS 22 = _30.03&; Coplen et al. 2006; and an in-house standard) were added for every batch of isotopic analysis. The standard deviation of the in-house standards during the period of analyses was better than 0.2‰. Fifteen samples were analysed using a Delta V Advantage mass spectrometer connected to a Flash HT Elementar Analyser at the University of Padova. For every set of analysis, multiple blank capsules and isotope standards (IAEA CH6 = -10.45‰, IAEA CH-7 = -32.15‰, Coplen et al. 2006) were included. The standard deviation of the in-house standard during the period of analyses was better than σ = 0.3‰.

Table A1 Stable isotope composition of carbon (δ13Corg) and percentage of organic matter (TOC) versus sample height position of the Pignola-Abriola and Mt. Volturino sections.

PIGNOLA-ABRIOLA

m	Sample	TOC%	d13Corg
58.10	Pa i 191	1.984	
57.80	Pai 189	2.321	−25.56
57.65	GNM 119	0.149	
57.50	Pai 187	2.014	−24.66
57.05	Pai 185	1.863	−26.43
56.76	GNM 117	0.452	−26.61
56.50	Pai 184	2.103	−25.80
55.70	GNI 29	0.960	−24.41
55.63	Pai 180	3.654	−25.71
55.55	GNI 28	1.259	−25.63
55.25	GNI 27	5.548	−25.40
54.45	Pai 173	5.663	−25.77
53.75	GNM 102	8.410	−27.83
53.15	Pai 168	1.359	−25.67
52.65	GNI 26	5.684	−25.85
52.50	Pai 166	0.136	−25.26
52.13	Pa i 164	0.963	
51.65	Pai 162	0.079	−26.52
51.40	GNI 25	6.664	−25.97
51.05	GNM 85	0.618	−25.86
50.80	Pai 160	0.096	−25.17
50.20	Pai 157	0.107	−25.03
49.25	GNI 24	4.780	−26.56
49.15	GNI 23	9.895	−24.36
48.90	GNI 22	3.667	−26.15
48.65	Pai 155	2.113	−25.72
48.40	GNI 21	5.074	−25.77
48.10	GNI 20	12.653	−25.40
47.40	GNI 19B	9.024	−25.86
47.20	Pa i 146 Dark	1.895	
47.20	Pa i 146 Bright	0.945	
46.80	GNI 19	0.943	−25.68
46.45	GNI 18	11.623	−26.05
46.30	GNI 17	12.589	−26.37
45.95	Pai 143	0.106	−24.90
45.80	GNI 16	0.728	−27.10
45.65	Pai 142	10.337	−25.89
45.30	GNI 15	2.032	−27.13
45.23	GNI 14	2.566	−25.42
45.18	Pai 139		−27.58
44.95	Pai 136	6.856	−25.80
44.75	Pai 134	2.321	−24.91
44.35	GNM 52	8.663	−29.95
43.30	GNP 3	7.845	−27.26
42.60	Pa i 119	8.045	
42.35	GNP 2	10.681	−28.28
42.28	GNM 41A	8.327	−27.55
42.20	Pai 116	6.125	−25.18
41.30	Pai 111	8.014	−24.46
40.70	GNM 37	6.074	−27.97
40.19	GNM 35B	10.557	−26.55
40.00	Pai 108	13.025	−25.47
39.35	GNP 1	2.967	−27.93
38.30	Pai 104	1.451	−24.31
37.73	GNI 13	0.818	−25.58
37.50	GNI 12	5.960	−24.90
37.30	GNI 11	6.261	−25.76
36.80	Pai 101	0.941	
36.10	GNI 10	8.876	−23.70
35.70	GNI 9	3.992	−24.19
33.80	Parc 1	2.354	
33.40	Parc 3	1.979	−25.97
32.95	Parc 6	1.853	

MT. VOLTURINO

m	Sample	TOC%	d13Corg
71.00	MV49	0.611	−19.88
68.00	MV45.60	0.115	
66.00	MV44	0.161	−21.89
65.00	MV 43	0.174	−25.15
64.00	MV42	0.294	
57.50	MMV 9	0.095	
56.00	MVV8	0.371	
52.00	MMV 1	0.693	−28.05
51.50	MV 35	0.380	
51.00	MMV 2	1.111	−27.78
50.66	MMV 3		−27.36
50.50	MMV 4	0.941	−26.33
49.50	MMV 6	0.925	−26.56
49.00	MMV 7	1.192	−27.52
48.20	MMV 8		−25.23
47.10	MMV 9		−27.46
46.60	MMV 10		−26.50
46.50	MV 31	0.124	
46.20	MMV 11		−25.42
45.00	MVV 6	0.706	
42.50	MV 27B	0.288	−23.47
42.45	MMV 13		−27.35
41.50	MV 24	0.195	−24.29
41.43	MMV 16		−24.25
41.00	MV 23	0.295	−26.13
40.20	MV 22		−26.12
39.50	MV 21	0.198	
39.00	MV 20B	0.384	
38.45	MMV 22		−24.73
38.00	MMV 23		−24.67
38.00	MV 17	0.293	−26.07
37.50	MV 16	0.500	−23.15
36.30	MMV 27		−24.30
37.00	MV15	0.479	
36.00	MVV 5	0.329	−24.52
35.60	MMV 29		−24.35
35.00	MV11	1.092	−24.86
34.00	MVC7	0.310	−23.65
34.00	MMV 32	0.389	
33.50	MMV 33	0.891	
32.00	MVV4	0.367	
31.00	MVC6	0.215	−25.60
30.50	MV7	0.323	−24.83
29.00	MVC 5	0.218	−26.29

PIGNOLA-ABRIOLA				MT. VOLTURINO			
m	Sample	TOC%	d13Corg	m	Sample	TOC%	d13Corg
32.70	Parc 7	2.580					
32.05	Parc 10	3.668					
31.70	GNI 8	1.855					
31.65	GNI 7	0.309	−24.58				
31.60	GNI 6	0.164					
31.50	Parc 12	2.923	−25.96				
30.89	Parc 15	1.880					
30.70	GNI 5	1.348					
30.65	GNI 4	0.152	−25.30				
30.55	GNI 3	6.841	−26.95				
30.40	Parc 16	2.036					
30.30	GNI 2	5.996	−25.66				
29.90	GNI 1	2.589	−27.68				

δ13Corg and δ13Ccarb profiles. The recorded δ13Corg shows a minimum of -29.95‰ and a maximum of –23.70‰, with an average value of ca. -25.95‰. Between metre 36 and 44.4, the curve depicts an important negative shift, with amplitude of ca. 6‰, over a span where the TOC content roughly doubled (Fig. A2). This shift exhibits a marked negative peak at metre 44.4 m (δ13Corg= -29.95‰, highlighted by the grey line in Fig. A2), ca. 50 cm below and thus almost coincident with the FAD of the conodont Misikella posthernsteini s.s. (dashed line in Fig. A2; Maron et al. 2015) and 4 m above the beginning of the radiolarian Proparvicingula moniliformis Zone, Assemblage 1 (sensu Carter 1993; Giordano et al. 2010) (Fig. A2). Because it is relatively easy to recognize and has good potential for global correlation, we propose the lowest δ13Corg value close to the FAD of M. posthernsteini s.s., within the P. moniliformis Zone (sensu Carter 1993; Giordano et al. 2010), as a geochemical marker for the GSSP of the Rhaetian (Fig. A2). This negative peak occurs during a δ13Corg short-term excursion, which falls within alonger term decrease of the δ13Corg. The stable isotope composition of carbonate ranges from -1.80 ± 1.00‰ to 2.07 ± 1.00‰, with a mean of ca. 0.99 ‰ 1.00‰ (Preto et al. 2013). Around the NRB, the δ13Ccarb curve follows almost perfectly the trend of the δ13Corg curve, showing a significant negative shift at ca. 45 m (δ13Ccarb = -0.69 ± 1.00‰), almost coincident with the FAD of the M. posthernsteini (Fig. A2). The close parallelism between the δ13Corg and δ13Ccarb confirms that the Pignola-Abriola isotopic signal is primary. Decreasing trends in both curves are regarded as due to an input of isotopically light carbon in the ocean system, which may be linked to decrease in primary productivity, decrease in organic carbon burial, clathrates dissociation, wildfires, isolation of epicontinental seas and/or emplacement of large igneous provinces (LIPs) (e.g. Hesselbo et al. 2002; Higgins & Schrag 2006; Jenkyns 2010; Tanner 2010; Meyer 2014).

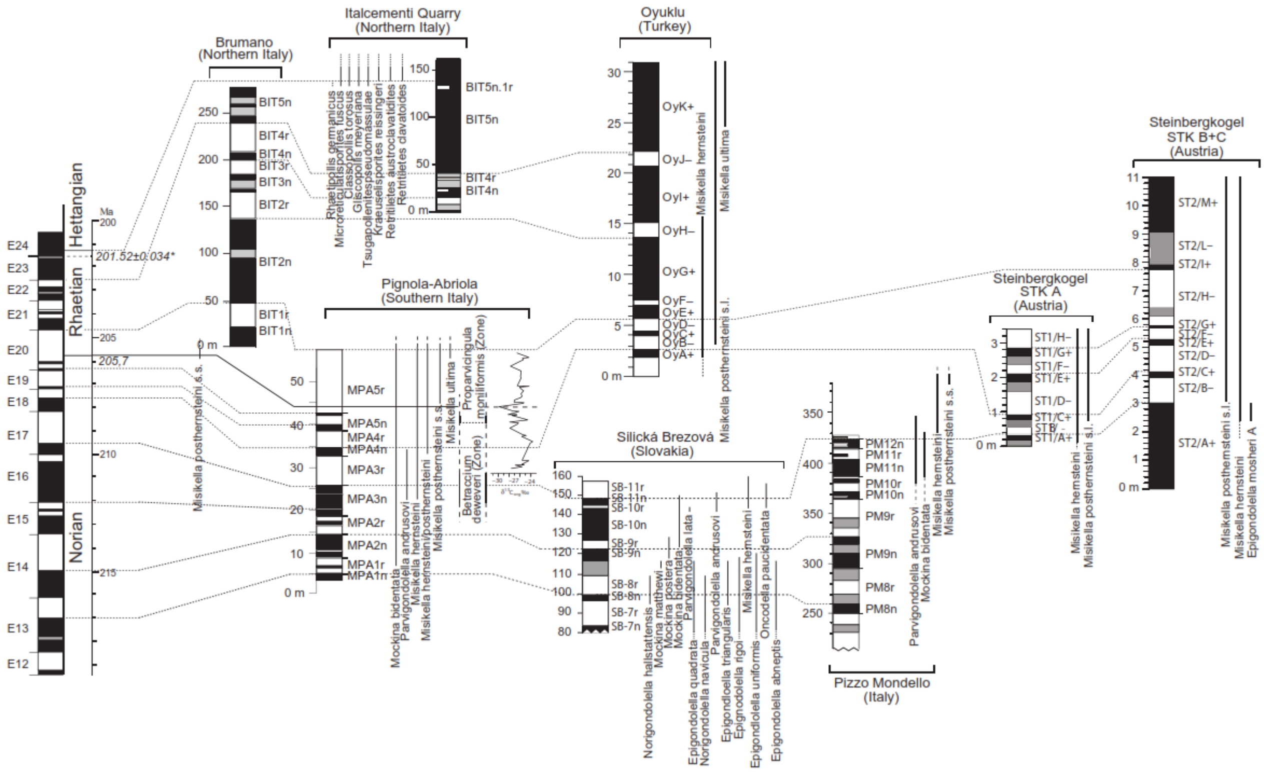

Fig. A5 Correlation of the magnetostratigraphy and biostratigraphy of the Pignola-Abriola section with data from Tethyan marine sections in literature, as Steinbergkogel (STK-A and B+C; Husing et al. 2011), current GSSP candidate for the Rhaetian Stage (Krystyn et al. 2007a,b), Brumano/Italcementi Quarry (Muttoni et al. 2010, 2014), Oyuklu (Gallet et al. 2007), Pizzo Mondello (Muttoni et al. 2004, 2014) and Silicka Brezova (Channell et al. 2003). Conodont biostratigraphy of Silicka Brezova reclassified after Mazza et al. (2012); the specimens of conodont Misikella posthernsteini in Steinbergkogel (as considered in Krystyn et al. 2007a,b) are here atTributed to the Misikella hernsteini/posthernsteini transitional form (after Giordano et al. 2010). The Pignola-Abriola section is correlated to the Newark Astrochronological Polarity Time Scale (APTS; Olsen et al. 2011) following the correlation of Maron et al. (2015). The level containing the Norian/Rhaetian boundary in Pignola-Abriola, placed with a negative δ13Corg spike of ca. -30‰ and virtually coincident with the first appearance datum (FAD) of conodont M. posthernsteini s.s., is dated at 205.7 Ma (Maron et al. 2015), within magnetozone E20r of the Newark APTS.

Magnetostratigraphy

A total of 220 samples have been collected for palaeomagnetic analyses and 9 for rock magnetism experiments (IRM). The analyses were performed at the Alpine Laboratory of Paleomagnetism (ALP) of Peveragno, Italy. The samples were thermally demagnetized up to 675 °C and then analysed with a 2G three-axial DC-SQUID cryogenic magnetometer. For details, see Maron et al. (2015). The analysis of the NRM indicates a mean magnetization of the samples of 0.08 mA/m. Rock magnetic experiments indicate haematite and magnetite as the main carriers of the magnetization, with subsidiary iron sulphide (Maron et al. 2015). The characteristic component of magnetization (ChRM) wasisolated in 121 samples (ca. 55%) mainly up to 450–550° (maximum of 625 °C), showing north-down and south-up directions. The reversal test of McFadden & McElhinny (1990) was applied to the ChRM component directions and resulted positive (Maron et al. 2015). A sequence of virtual geomagnetic poles (VGPs) was obtained from the ChRM directions. the VGP latitudes have been arranged in stratigraphical order to obtain a sequence of geomagnetic polarity reversals along the Pignola-Abriola section. A total of 22 polarity reversals have been recognized and grouped in 10 magnetozones labelled from MPA1n to MPA5r (Fig. A2). The Pignola-Abriola section was then correlated to Tethyan sections from the literature provided with magnetostratigraphy and conodont biostratigraphy (Fig. A5). The magnetostratigraphy of the Steinbergkogel section (Husing et al. 2011), GSSP candidate for the Rhaetian stage (Krystyn et al. 2007a,b; Krystyn 2008), is comparable with the data from Pignola-Abriola, only introducing a revision in the biostratigraphy of Steinbergkogel. We think that the first occurrence (FO) of conodont Misikella posthernsteini at Steinbergkogel (see specimens in plate 1 in Krystyn et al. 2007a) should be considered equivalent to the FO of Misikella hernsteini/posthernsteini transitional forms (sensu Giordano et al. 2010) in the Pignola-Abriola section (Maron et al. 2015). In particular, the main reversal interval in Steinbergkogel (ST1/B- to ST1/H- in STK-A subsection; ST2/B- to ST2/H- in STK-B+C subsection) is considered equivalent to magnetozones from MPA3r to MPA5r at Pignola-Abriola (Fig. A5). In addition, we find that the Norian/Rhaetian Oyuklu section (Gallet et al. 2007) is comparable with Pignola-Abriola whereby interval from Oyuklu magnetozone OyBto OyD- should correspond to magnetozones MPA4r to MPA5r at Pignola-Abriola (Fig. A5). Moreover, the upper part of the Carnian–Norian Pizzo Mondello section (Muttoni et al. 2004), from magnetozone PM-8n to PM-12n, should correspond to the lower part of the Pignola-Abriola section from MPA1n to MPA3n, equivalent to the magnetozones SB-8n to SB-11n in the Silicka Brezova section (Channell et al. 2003) (Fig. A5). Notably, conodont biostratigraphy of Silicka Brezova section has been reclassified after Mazza et al. (2012). The Pignola Abriola section also has been correlated with the Brumano/Italcementi Quarry composite section, upper Rhaetian to Hettangian in age (Muttoni et al. 2010, 2014), using as tie point the FO of M. posthernsteini s.s. We conclude that the magnetostratigraphy of the Brumano/Italcementi Quarry section is substantially younger than the magnetostratigraphy of Pignola-Abriola.

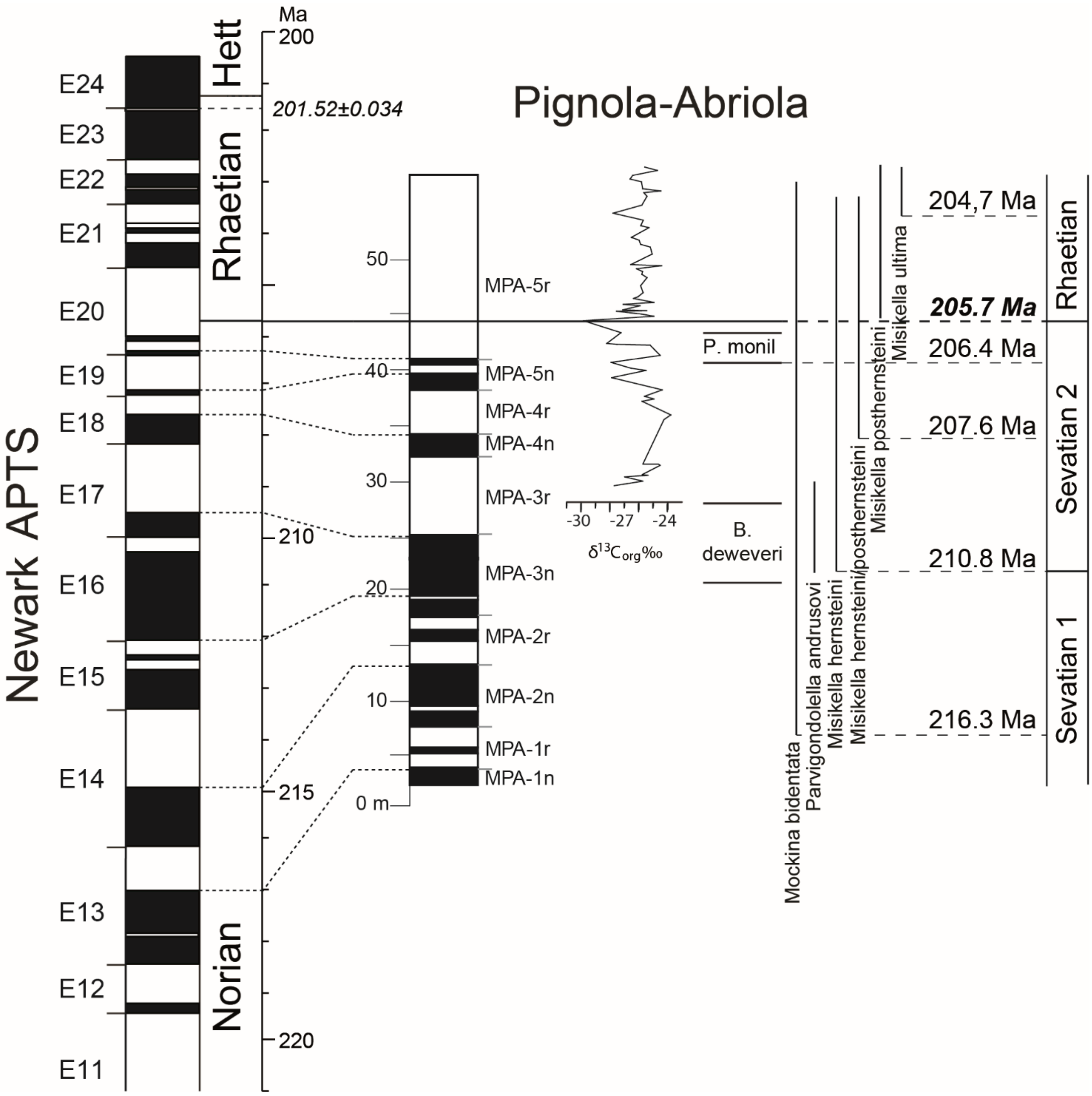

Fig. A6 Litho- and magnetostratigraphical correlations between the Pignola-Abriola section and the Newark APTS based on Maron et al. (2015). Chemostratigraphy and biostratigraphy are reported on the right. Calibrated ages of the main bioevents are referred to the age model after Maron et al. (2015).

Prospects for high-precision geochronology. Sedimentation rates were estimated by comparing the thickness of the Pignola-Abriola magnetozones with the duration of their equivalent magnetozones in the Newark APTS (Olsen et al. 2011) (Fig. A6). The resulting preferred correlation option implies depositional rates that are very low (ca. 2.6 m/My) in the lower portion of the section (from the base to ca. 26 m), increasing to ca. 5.6 m/My from metre 26, and reaching ca. 9.8 m/ My from metre 43.5 upwards (Maron et al. 2015). the presence of more marls, shales and marly limestones in the upper part of the section suggests a major input of siliciclastic fraction, consistent with the observed increase of sedimentation rates and the higher concentration of magnetic minerals. The age model derived from this preferred correlation option was used to date the level containing the Norian/Rhaetian boundary (approximated by the carbon isotope shift and associated bioevents; see above) to ca. 205.7 Ma (see Maron et al. 2015 for details), in substantial agreement with the high-precision U-Pb geochronology constraints by Wotzlaw et al. (2014). Considering a Triassic/Jurassic boundary at 201.3 Ma (Schoene et al. 2010; Guex et al. 2012), the Rhaetian is ca. 4.4 Myr long; considering the Carnian/Norian boundary at ca. 227 Ma (Muttoni et al. 2004; Maron et al. 2015), the Norian Stage is ca. 21.3 Myr long.

Age of the main events around the Norian/Rhaetian boundary. The calibration of the Pignola-Abriola magnetostratigraphy with the Newark APTS (Olsen et al. 2011) allows dating the main events recorded around the Norian/Rhaetian boundary. For instance, the Sevatian1/Sevatian2 boundary, defined by the FO of conodont Misikella hernsteini, is placed at ca. 210.8 Ma, while the FO of Mockina bidentata (Alaunian/Sevatian boundary) is at ca. 216.2 Ma (Fig. A6). The FO of the M. hernsteini/posthernsteini transitional morphotype, corresponding to the older Misikella posthernsteini specimens sensu Krystyn et al. (2007a), is placed at ca. 207.6 Ma (Fig. A6). The FO of Misikella ultima is at ca. 204.7 Ma, while the base of the Proparvicingula moniliformis Zone (proxy for the NRB) is placed at ca. 206.2 Ma. Finally, the age of the prominent negative δ13Corg spike located only 50 cm below the FAD of M. posthernsteini s.s. is of ca. 205.7 Ma (Fig. A6).

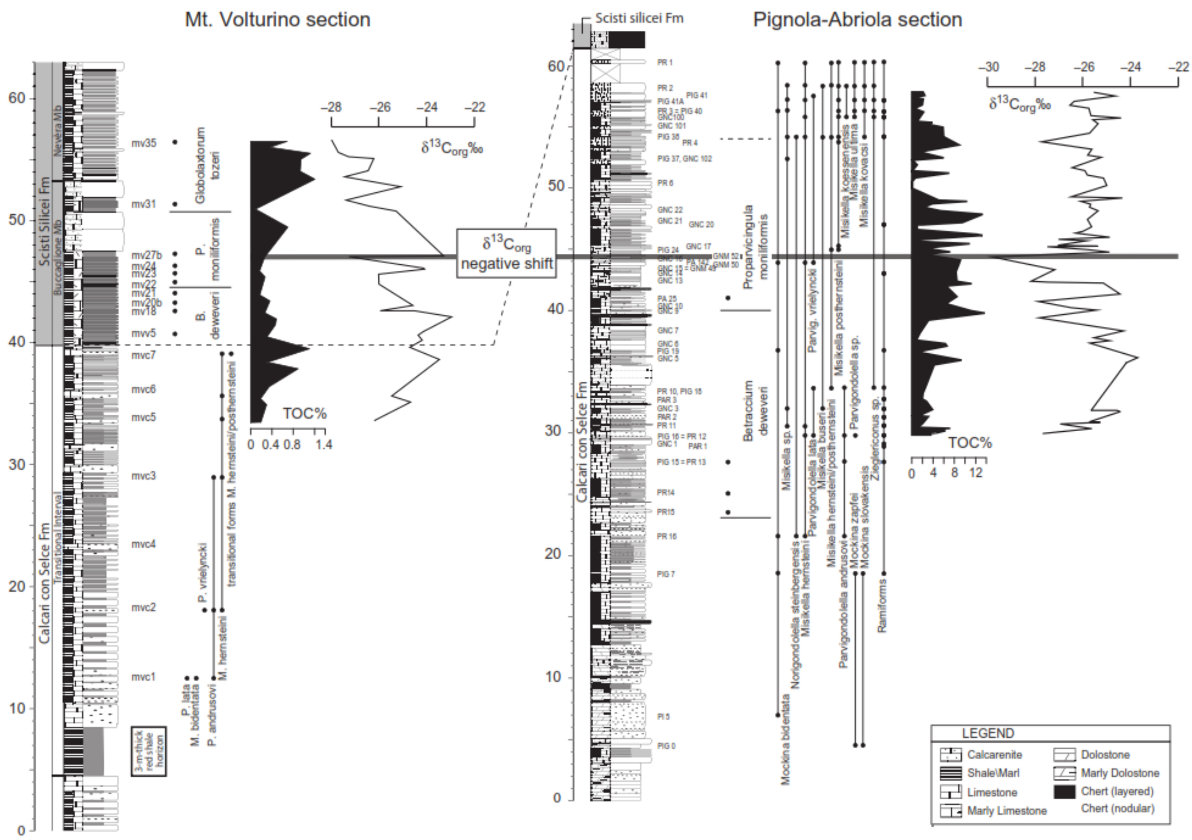

Fig. A7 Stratigraphical log, radiolarian and conodont biostratigraphy of the Mt. Volturino section. Total organic matter percentage (TOC) and δ13Corg are compared to the δ13Corg curve of the Pignola-Abriola section, emphasizing the prominent negate shift that is present in both sections and used to define the NRB.

DEMONSTRATION OF REGIONAL AND GLOBAL CORRELATIONS

Regional correlations

The litho- and biostratigraphical correlations of the NRB interval in the Lagonegro Basin were well illustrated and discussed by several authors since the end of the 19th century, such as De Lorenzo (1894), Scandone (1967), De Capoa (1970, 1984), Miconnet (1982), Amodeo (1999), Bertinelli et al. (2005), Bazzucchi et al. (2005), Reggiani et al. (2005), Rigo et al. (2005, 2012b) and Giordano et al. (2010, 2011). From a biostratigraphical perspective in different localities and sections from the Lagonegro Basin, a well-defined NRB has been documented with the occurrence of the Misikella posthernsteini s.s., such as in the Mt. S. Enoc, Pignola-Abriola and Sasso di Castalda sections (e.g. Giordano et al. 2010). We thus studied a second key stratigraphical section, known as Mt. Volturino, which is coeval to the GSSP candidate Pignola-Abriola section but deposited in a deeper depositional setting of the Lagonegro Basin, below the CCD (Giordano et al. 2010, 2011). The Mt. Volturino section exposed ca. 17 km to the south of Pignola-Abriola and yielded conodont and radiolarian biostratigraphy as well as a strong δ13Corg peak around the NRB (Fig. A7). The litho-, bio- and chemostratigraphy of the Mt. Volturino section is described hereafter.

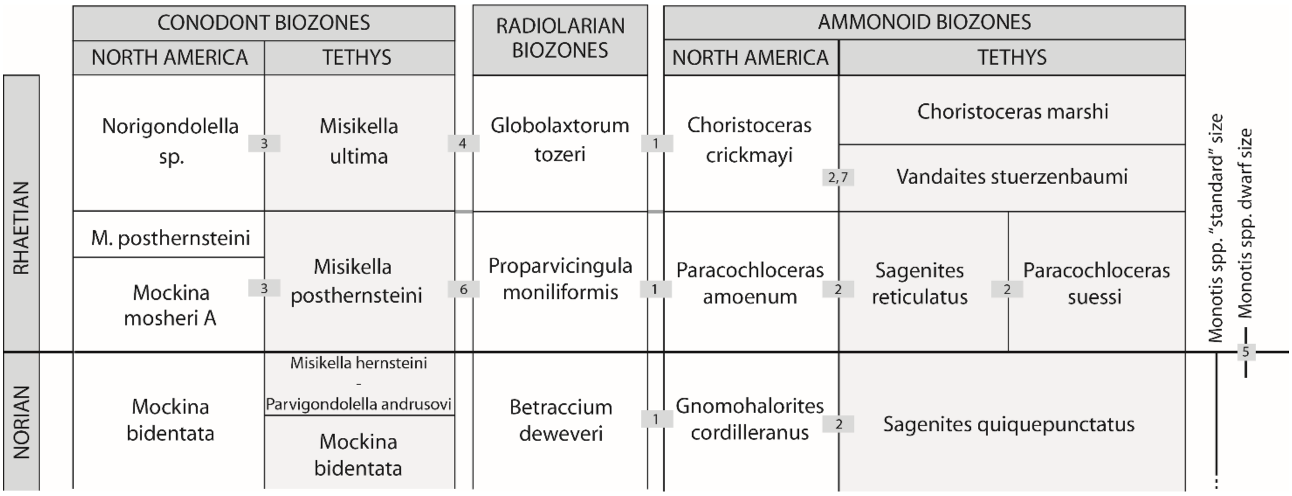

Fig. A8 Biochronostratigraphical correlation scheme around the NRB. References are 1. Dagys & Dagys (1994); 2. Orchard (1991); 3. Palfy et al. (2007); 4. McRoberts et al. (2008); 5. Giordano et al. (2010); 6. Whiteside & Ward (2011); 7. Carter (1993); 8. Orchard et al. (2007).

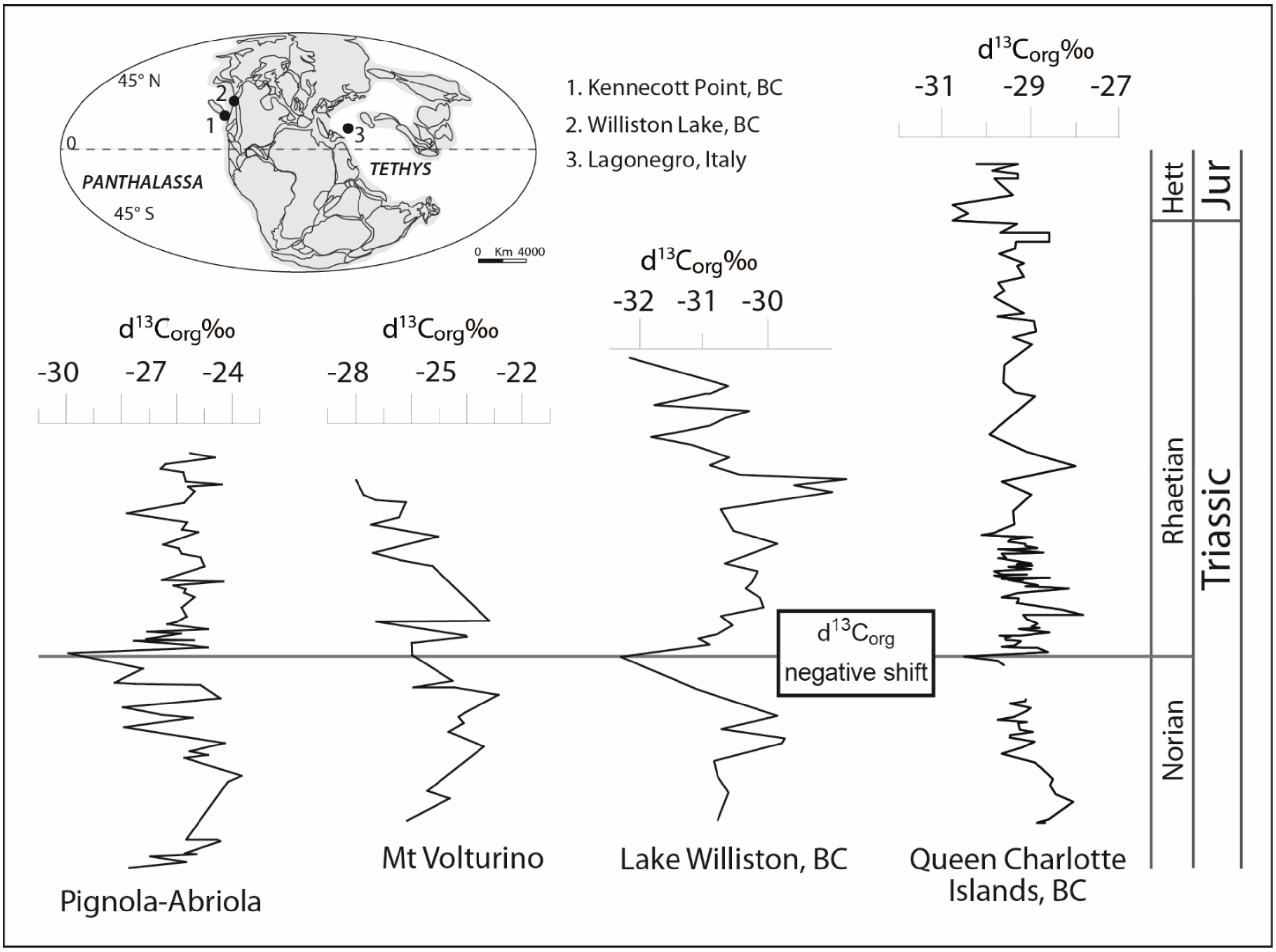

Fig. A9 Correlations of the prominent δ13Corg negative shift considered as possible marker for the base of the Rhaetian Stage from different localities around the world: Pignola-Abriola and Mt. Volturino sections (this work, Lagonegro Basin, Italy), Lake Williston and Kennecott Point (British Columbia, Canada) (Ward et al. 2001, 2004; Wignall et al. 2007; Whiteside & Ward 2011). Paleomap is modified after scotese.com.

Monte Volturino section

Lithostratigraphy. The section is located along the southern slope of Mt. Volturino (between La Torre and Coste Roberto) (Geographical coordinate system, datum WGS 84: 40°24 0 13.46″N; 15°49 2.25″ E) within the area of the Parco Appennino Lucano Val d'Agri Lagonegrese, the same protected area of the Pignola-Abriola section (Fig. A1). The Mt. Volturino section shows a very good exposure of the Calcari con Selce in transition with the overlying Scisti Silicei. The lower 4 metres of the section is represented by cherty limestones (mostly mudstone and wackestones) ascribed to the Calcari con Selce. At 4 m above the base of the section, a 4-m-thick unit of red shales marks the base of the 'Transitional Interval' (i.e. upper part of Calcari con Selce) (Fig. A7). Above this horizon, a portion of ca. 9.70 m is characterized by thin red shale layers intercalated to thick cherty limestones beds. The overlying 8.30 m consists instead of thicker red shale layers with thinner cherty limestones intercalations. At 26 m above the base of the section, a 1-m-thick layer of red shales occurs, overlain by an interval rich in shales and silicified limestones characterized by 7 m of very thin cherty limestones (often silicified) alternating with red shales, red cherts and radiolarites (Fig. A7). Within the upper part of the 'Transitional Interval', between 28.70 and 38.0 m, thin dark shales and cherty layers, radiolarites and partially silicified laminated limestones become dominant and are capped by 1 m of dark shales. Above this organicrich interval, only siliceous sedimentation occurs, dominated by radiolarites, representing the base of the Buccaglione member of the Scisti Silicei. The basal 12 m of the Buccaglione member consists of red radiolarites, radiolarian cherts and siliceous shales, overlain by a 3-m-thick graded calciruditic bed at 47 m. A 1-m-thick transitional bed character- ized by thin calcarenites intercalated with green to red shales is overlain by the Nevera member of the Scisti Silicei, which consists in black siliceous shales interbedded with silicified calcarenites rich in organic matter (Fig. A7).

Biostratigraphy. The Mt. Volturino section yielded pyritized radiolarians, in particular in the Transitional interval, and conodont associations in the calcareous portion of the section (e.g. Giordano et al. 2010, 2011). The biozonations are those proposed by Kozur (2003) and Carter (1993) for conodont and radiolarian biostratigraphy, respectively. Conodont CAI is 2.5–3 (sensu Epstein et al. 1977). Mockina bidentata, Parvigondolella lata and Parvigondolella andrusovi first occur at ca. 12 m (Giordano et al. 2010, 2011), defining the base of the Mockina bidentata Zone (Kozur & Mock 1991) (Figs A3, A7). Misikella hernsteini first occurs at 18 m, along with Parvigondolella vrielyncki, followed by the first occurrence of the Misikella hernsteini/M. posthernsteini transitional form at 39 m (Giordano et al. 2010, 2011) (Figs A3, A7). From the base of the Scisti Silicei at ca. 39.7 m up to metre 44.5, well-preserved radiolarian assemblages documented the upper Norian Betraccium deweveri Zone (U.A. 1 Carter 1993), in particular by the presence of Citriduma sp. A, sensu Carter (1993) and Betraccium deweveri Pessagno & Blome in sample MVV5 (Giordano et al. 2010, 2011) (Figs A4, A7). Between metres 44.5 and 51.5, the conjunct occurrence of Paraonella pacofiensis Carter and Pseudohagiastrum sp. A (sensu Carter 1993) can be referred to the Proparvicingula moniliformis Zone, in particular to the Unitary Association 5–18 (sensu Carter 1993), which corresponds to the upper part of the Assemblage 1 and the lower-mid part of Assemblage 2 (=2a, 2b, 2c) of the Proparvicingula moniliformis Zone (Carter 1993). Sample MV 31 at 51.5 m, with Pseudohagiastrum giganteum Carter & Hori, Praemesosaturnalis sp. aff. P. sandspitensis (Blome), Livarella valida Yoshida, Octostella dihexacanthus (Carter), is referable to the Globolaxtorum tozeri Zone, Assemblage 3 (U.A. 24–27) (Giordano et al. 2010, 2011) (Figs A4, A7). Notably, in sample MV27b, Serilla sp. aff. S. tledoensis is referable to the Unitary Association 16–27 (Carter 1993), which corresponds to the middle-Proparvicingula moniliformis Zone (Subassemblage 2c, 2d) and Globolaxtorum tozeri Zone (Assemblage 3) (Fig. A7).

Chemostratigraphy. The Mt. Volturino section has been studied for its δ13Corg and TOC composition. Forty-four samples were analysed following the methods described above. The δ13Corg values range between a minimum of -28.05‰ and a maximum of -23.15‰, with an average value of ca. -25.60‰ (Fig. A7; Table 1). The curve displays a main negative shift at m 47 with amplitude in the order of ca. 3‰. This negative shift likely corresponds to the Pignola Abriola negative peak that occurs at 44.4 m (δ13Corg = -29.95‰), almost coincident with the FAD of the conodont M. posthernsteini s.s. in the Pignola-Abriola section. Unfortunately, the conodont M. posthernsteini was not recovered in the Mt. Volturino section. Nevertheless, the Mt. Volturino and the Pignola-Abriola negative fluctuations both occur in the Proparvicingula moniliformis Zone (sensu Carter 1993; Giordano et al. 2010) (Fig. A7).

Long distance and global correlation. The succession of conodont and radiolarian faunas in the both Pignola-Abriola and Mt. Volturino sections record specific bioevents that occurred homotaxially within other Tethyan (e.g. Austria, Turkey, Slovakia, Sicily, Lombardian Basin) as well as extra-Tethyan stratigraphical successions (e.g. British Columbia, Nevada) (Fig. A8). In particular, the FAD of the Tethyan conodont Misikella posthernsteini was voted by the Task Force for the NRB in 2010 and conventionally adopted to establish the NRB (Krystyn 2010). The appearance of the Tethyan Misikella posthernsteini s.s. has been correlated with the appearance of the North American Mockina mosheri morphotype A (e.g. Giordano et al. 2010; Tackett et al. 2014), through the appearance of both the conodont species just above the base of the radiolarian Proparvicingula Moniliformis Zone, in particular within Assemblage 1 sensu Carter (1993) as stated by Carter & Orchard (2007) and Giordano et al. (2010) and Tackett et al. (2014) (Fig. A8). Moreover, the base of the Mockina mosheri Zone seems to coincide with the base of the North American ammonoid Paracochloceras amoenum Zone (e.g. Orchard & Tozer 1997). In the upper part of the radiolarian Betraccium deweveri Zone, the bivalve Monotis fauna disappeared globally: this event has been largely used to define the base of the Rhaetian, especially in the North America (Fig. A8). Instead, the rare dwarf Monotis specimens and thinshelled pectinids that replaced the standard-size Monotis are considered Rhaetian (Wignall et al. 2007; McRoberts et al. 2008; McRoberts 2010). In fact, the dwarf Monotis species were found in association with ammonoids belonging to the Paracochloceras Genus and with the conodont M. posthernsteini (McRoberts et al. 2008). The extinction of the standard-size Monotis species occurs at the lower boundary of the Sagenites reticulatus Zone (Dagys & Dagys 1994). In the Tethyan realm, the base of the Sagenites reticulatus Zone is considered coeval to the base of the Paracochloceras suessi Zone (Dagys & Dagys 1994; Krystyn et al. 2007a) and ex-Cochloceras suessi Zone sensu Kozur (2003) (Fig. A8). Moreover, the base of the P. suessi Zone seems to coincide to the FAD of the conodont M. posthernsteini (Kozur 2003; Krystyn & Kuerschner 2005; Krystyn et al. 2007a, 2007b; Moix et al. 2007). In the North America, the base of the Sagenites reticulatus Zone correlates to the base of the ammonoid Paracochloceras amoenum Zone (Krystyn 1990; Dagys & Dagys 1994). Carter (1993) correlates the base of the radiolarian Proparvicingula moniliformis Zone with the base of the Paracochloceras amoenum Zone, later confirmed by Orchard et al. (2007) and the base of the radiolarian Globolaxtorum tozeri Zone with the base of the ammonoid Choristoceras crickmayi Zone (Carter 1993). Notably, in North America Misikella posthernsteini occurred in the Choristoceras crickmayi Ammonoid Zone (Orchard 1991; Orchard et al. 2007), differing from the Tethyan Misikella posthernsteini that instead occurs at the base of radiolarian Proparvicingula moniliformis Zone (Giordano et al. 2010), as also observed in the candidate Pignola-Abriola section (Fig. A2). The Choristoceras crickmayi Ammonoid Zone is considered coeval to the base of the Tethyan ammonoid Vandaites stuerzenbaumi Zone (Dagys & Dagys 1994; Whiteside & Ward 2011) (Fig. A8). In particular, the Vandaites stuerzenbaumi Zone is represented by two subzones that are the Vandaites saximontanus Subzone (ex-'Choristoceras' haueri Subzone) and the homonymous Vandaites stuerzenbaumi Subzone (Maslo 2008). Moreover, the base of the radiolarian Globolaxtorum tozeri seems to coincide with the base of the conodont Misikella ultima (Palfy et al. 2007) (Fig. A8). Around the NRB, some bioevents described above occurred in a very short time interval and therefore could be interpreted as coeval: (1) occurrence of the conodonts Misikella posthernsteini s.s. and Mockina mosheri morphotype A; (2) the occurrence of ammonoid Paracochloceras amoenum, which corresponds to the base of the Sagenites reticulatus Zone (coeval to the base of the Paracochloceras suessi); and (3) the base of the radiolarian Proparvicingula moniliformis, and the disappearance of standard-size bivalve Monotis spp. (Fig. A8). These bioevents support, and are supported by, the geochemical evidence (δ13Corg) documented at Pignola-Abriola and Mt. Volturino sections around the NRB (Fig. A7).

THE δ13Corg NEGATIVE SHIFT: NEW PROPOSAL AS PRIMARY PROXY FOR THE NRB

Even if Misikella posthernsteini has been voted as primary marker for the base of the Rhaetian stage (Krystyn 2010), and it is commonly used to recognize the NRB in the Tethys (Balini et al. 2010), Misikella posthernsteini appears to be rare in the North American realm, where it seems to occur in a younger stratigraphic interval than in the Tethys (Fig. A8), weakening its potential as primary tool for global correlations. For these reasons, we propose the prominent negative δ13Corg peak occurring in proximity of the FAD of Tethyan Misikella posthernsteini s.s. as the primary event to define the base of the Rhaetian stage. Notably, the organic carbon isotope system appears unaffected by diagenetic alteration, because temperatures approaching those of oil generation are required to alter significantly the δ13Corg primary signal (Hayes et al. 1999; Cramer & Saltzman 2007). The δ13Corg negative shift documented in the candidate Pignola-Abriola section and in the coeval Mt. Volturino section seems to correspond to similar shifts in other sections from the North American realm, such as Williston Lake (Wignall et al. 2007), Kennecott Point (Ward et al. 2001, 2004) and Frederick Island (Whiteside & Ward 2011), that are wellcalibrated biostratigraphically (Fig A9). The occurrence of this negative peak also on the eastern side of the Panthalassa shows that the δ13Corg negative shift recorded at the NRB provides a globally correlatable chronostratigraphical event and thus a useful geochemical/physical proxy in identifying the base of the Rhaetian stage (Fig. A9).

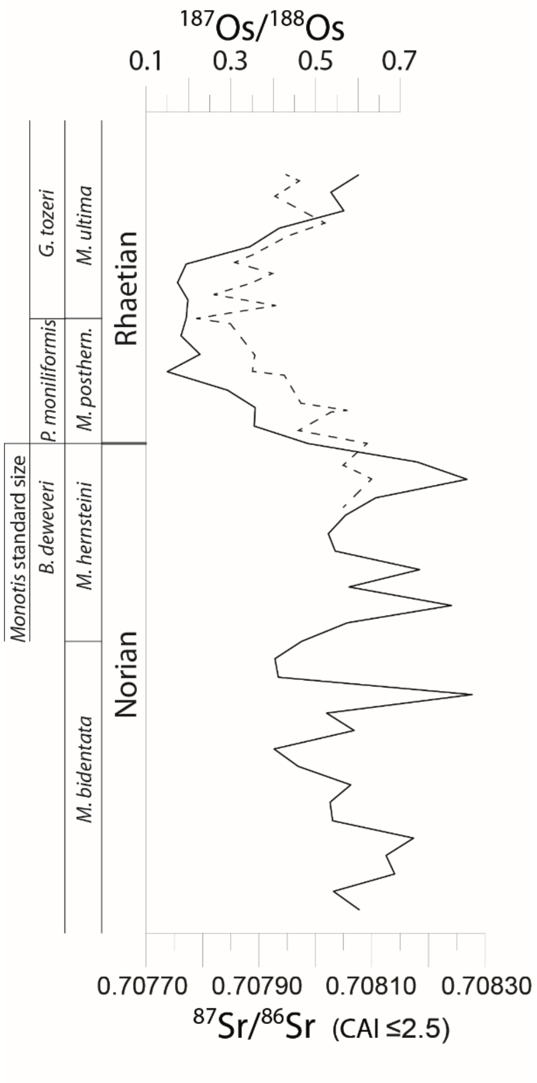

Fig. A10 Strontium and Osmium curves around the NRB (Kuroda et al. 2010; Callegaro et al. 2012) with integrated bivalve, radiolarian and conodont biostratigraphical schemes.

87Sr/86Sr and 187Os/188Os datasets

A recent late Norian to Rhaetian marine Sr curve based on analyses of biogenic apatite and carbonate (e.g. Korte et al. 2003; Cohen & Coe 2007; Callegaro et al. 2012; Tackett et al. 2014) highlights two significant shifts, one in the late Norian and one in the late Rhaetian (Fig. A10). Although Callegaro et al. (2012) used only conodonts with CAI < 2 for their evaluation of the Sr isotopic signal, here we include also results from conodonts with CAI = 2.5 because the threshold CAI value for the maintenance of the pristine Sr isotopic composition is precisely 2.5 (Ebneth et al. 1997; Korte et al. 2003). This curve is well mimicked by the Rhaetian seawater 187Os/188Os curve illustrated by Cohen & Coe (2002) and Kuroda et al. (2010) (Fig. A10). A first decreasing trend is documented in both the 87Sr/86Sr and 187Os/188Os curves, starting in the latest Norian, more precisely in the uppermost conodont Misikella hensteini-Parvigondolella andrusovi Zone (Callegaro et al. 2012) or top of the Betraccium deweveri radiolarian Zone (Kuroda et al. 2010), from 0.70798 to 0.70777 for 87Sr/86Sr and from 0.6 to 0.2 for 187Os/188Os (Fig. A10). These lowest values mostly coincide with the base of the conodont Misikella ultima Zone, which mostly corresponds to the base of the Globolaxtorum tozeri radiolarian Zone (Palfy et al. 2007), marking the change in trend to higher values both of the

87Sr/86Sr and 187Os/188Os curves (Fig. A10). In this context, the δ13Corg negative shift that marks the base of the Rhaetian stage according to our proposition falls within a decreasing trend of both the 87Sr/86Sr and 187Os/188Os curves.

CONCLUSIONS

In this work, we propose the Pignola-Abriola section as candidate GSSP for the Rhaetian Stage. The Pignola-Abriola section fulfils the requirements for the selection of boundary stratotypes of chronostratigraphical units:

1. The Pignola-Abriola section is well exposed in an area of minimal structural deformation with easy access along the SS 5 road 'la Sellata' and is located in the protected area of the Parco Appennino Lucano Val d'Agri Lagonegrese.
2. The Pignola-Abriola section is a continuous 63m-thick basinal succession, consisting of thinly bedded cherty limestones, shales and sparse layers of calcarenites (Calcari con Selce Fm), deposited in the Lagonegro Basin (Southern Apennines).
3. The Pignola-Abriola section is fossiliferous, with distinctive and well-preserved conodont and radiolarian cosmopolitan fauna; the FAD of the conodont Misikella posthernsteini s.s. and the base of the radiolarian Proparvicingula moniliformis Zone, which are two bioevents suggested to mark the base of the Rhaetian, are well-documented and intercalibrated.
4. The Pignola-Abriola section shows a marked negative δ13Corg excursion of ca. 6‰ within an overall decreasing trend, and that is mirrored by a negative shift of δ13C org curve, occurring ca. 0.5 metres below the FAD of M. posthernsteini s.s. and within the radiolarian P. moniliformis Zone. This negative carbon isotope shift is here suggested as the primary physical marker for the Norian/Rhaetian boundary.
5. The Pignola-Abriola section is subdivided into 10 magnetozones, calibrated with conodont and radiolarian biostratigraphy and statistically correlated with the Newark APTS.

ACKNOWLEDGEMENTS

We are indebted to G. Ciarapica, L. Passeri, N. Giordano, N. Preto and G. Roghi for discussion and assistance in field during the last 10 years. Thanks to Ing. Donato Rosa, Ing. Mancusi, Geom. Pietrafesa (Department for Environment, Town Planning and Building of the Pignola district) and to Ignazio Petrone, Mayor of Pignola (Potenza) in the 2011. Thanks also to the Corpo Forestale dello Stato – Stazione di Pignola and to Ing. Domenico Totaro, President of the Appennino Lucano National Park. We thank the editor, the anonymous reviewer and the Chairman of the Subcommission on Triassic Stratigraphy (ICS) Prof. Marco Balini (Milano University) for their constructive comments on the manuscript. This study has benefited from financial support of Progetto d'Ateneo 2009 (CPDA090175/09 to Rigo), and Ex 60% (60A05-2288/09 and 60A05-3279/13 to Rigo) and PRIN Preto (20107ESMX9_002), PRIN 2008 2008BEF5Z7_004 to Bertinelli and 2008BEF5Z7_005 to Rigo. Acknowledgement is made to the donors of the American Chemical Society Petroleum Research Fund for partial support of this research (grant 49637-DN18 to Katz). Stable isotope analyses were funded through NSF grant EAR 0844252 to Godfrey.

References

Ager, D.V. 1987. A defence of the Rhaetian stage. Albertiana, 6 (1987), 4-13.

Amodeo, F. 1999. Il Triassico terminale–Giurassico del Bacino Lagonegrese. Studi stratigrafici sugli Scisti Silicei della Basilicata (Italia meridionale). Mémoires de Géologie (Lausanne), 33, 1-123.

Amodeo, F., Molisso, F., Kozur, H., Marsella, E. & D'Argenio, B. 1993. Age of Transitional Beds between Cherty Limestone (Calcari con selce) and Radiolarites (Scisti Silicei) in the Lagonegro Domain (Southern Italy). First evidence of Rhaethian conodonts in Peninsular Italy. Bollettino del Servizio Geologico d'Italia, 110, 3-22.

Bazzucchi, P., Bertinelli, A., Ciarapica, G., Marcucci, M., Passeri, L., Rigo, M. & Roghi, G. 2005. The Late Triassic-Jurassic stratigraphic succession of Pignola (Lagonegro-Molise Basin, Southern Apennines, Italy). Bollettino della Società Geologica Italiana, 124 (1), 143-153.

Bertinelli, A., Ciarapica, G. & Passeri, L. 2005a. Late Triassic-Jurassic basinal successions in Molise and northern Basilicata; the northernmost witness of the Ionian Ocean. Bollettino della Società Geologica Italiana, 124 (1), 177-188.

Bertinelli, A., Ciarapica, G., De Zanche, V., Marcucci, M., Mietto, P., Passeri, L., Rigo, M. & Roghi, G. 2005b. Stratigraphic evolution of the Triassic-Jurassic Sasso di Castalda succession (Lagonegro Basin, Southern Apennines, Italy). Bollettino della Società Geologica Italiana, 124 (1), 161-175.

Carter, E.S. 1993. Biochronology and paleontology of uppermost Triassic (Rhaetian) radiolarians, Queen Charlotte Islands, British Columbia, Canada. Mémoires de Géologie (Lousanne), 11, 175 pp.

Casacci, M., Bertinelli, A., Algeo, T.J. & Rigo. M. Submitted. Carbonate-to-biosilica transition at the Norian-Rhaetian boundary controlled by rift-related subsidence in the western Tethyan Lagonegro Basin (southern Italy). Palaeogeography, Palaeoecology, Palaeobiology.

Catalano, R., Doglioni, C. & Merlini, S. 2001. On the mesozoic Ionian basin.Geophysical Journal International, 144 (1), 49-64.

Channell, J.E.T., Kozur, H.W., Sievers, T., Mock, R., Aubrecht, R. & Sykora, M. 2003. Carnian–Norian biomagnetostratigraphy at Silická Brezová (Slovakia): correlation to other Tethyan sections and to the Newark Basin. Palaeogeography, Palaeoclimatology, Palaeoecology, 191 (2), 65-109.

Ciarapica, G. & Passeri, L. 2002. The palaeogeographic duplicity of the Apennines. Bollettino della Società Geologica Italiana, 121 (1), 67-75.

Ciarapica, G. & Passeri, L. 2005. Ionian Tethydes in the Southern Apennines. In: Finetti, I.R. (Ed.), CROP Project: Deep Seismic Exploration of the Central Mediterranean and Italy. Elsevier, Amsterdam, 209-224.

Ciarapica, G., Cirilli, S., Fratoni, R.P., Passeri, L. & Zaninetti, L. 1990. The Monte Facito Formation (Southern Apennines). Bollettino della Società Geologica Italiana, 109 (1), 135-142.

Coplen, T.B., Brand, W.A., Gehre, M., Gröning, M., Meijer, H.A., Toman, B. & Verkouteren, R.M. 2006. New guidelines for $\delta^{13}C$ measurements.Analytical Chemistry, 78 (7), 2439-2441.

Epstein, A.G., Epstein, J.B. & Harris, L.D. 1977. Conodont color alteration; an index to organic metamorphism (No. 995). US Govt. Print. Off.

Fåhræus, L.E. & Ryley, C.C. 1989. Multielement species of *Misikella* Kozur and Mock, 1974 and *Axiothea* n. gen. (Conodonta) from the Mamonia Complex (Upper Triassic), Cyprus. Canadian Journal of Earth Sciences, 26 (6), 1255-1263.

Gallet, Y., Krystyn, L., Marcoux, J. & Besse, J. 2007. New constraints on the end-Triassic (Upper Norian–Rhaetian) magnetostratigraphy. Earth and Planetary Science Letters, 255 (3), 458-470.

Gazdzicki, A. 1978. Conodonts of the genus Misikella Kozur and Mock, 1974 from the Rhaetian of the Tatra Mts (West Carpathians). Acta Palaeontologica Polonica, 23 (3), 341-354.

Gazdzicki, A., Kozur, H.W. & Mock, R. 1979. The Norian-Rhaetian boundary in the light of micropaleontological data. Geologija, 22 (1), 71-112.

Giordano, N., Ciarapica, G., Bertinelli, A. & Rigo, M. 2011. The Norian-Rhaetian interval in two sections of the Lagonegro area: the transition from carbonate to siliceous deposition. Italian Journal of Geosciences, 130 (3), 380-393.

Giordano, N., Rigo, M., Ciarapica, G., & Bertinelli, A. 2010. New biostratigraphical constraints for the Norian/Rhaetian boundary: data from Lagonegro Basin, Southern Apennines, Italy. Lethaia, 43, 573-586.

Gradstein, F.M., Ogg, J.G., Schmitz, M.D. & Ogg, G.M., Eds, 2012, The Geological Time Scale 2012, Amsterdam, Elsevier, 2 vols., 1144 pp.

Hounslow, M.W. & Muttoni, G. 2010. The geomagnetic polarity timescale for the Triassic: linkage to stage boundary definitions. Geological Society, London, Special Publications, 334 (1), 61-102.

Hüsing, S. K., Deenen, M. H., Koopmans, J. G. & Krijgsman, W. 2011. Magnetostratigraphic dating of the proposed Rhaetian GSSP at Steinbergkogel (Upper Triassic, Austria): Implications for the Late Triassic time scale. Earth and Planetary Science Letters, 302 (1), 203-216.

Kozur, H.W & Mock, R. 1974. *Misikella posthernsteini* n. sp., die jündste Conodontenart der tethyalen Trias. *Ćasopis* Mineral. Geology, 19, 245-250.

Kozur, H.W. & Mock, R. 1991. New Middle Carnian and Rhaetian conodonts from Hungary and the Alps. Stratigraphic importance and tectonic implications for the Buda Mountains and adjacent areas. Jahrbuch der Geologischen Bundesanstalt, 134 (2), 271-297.

Krystyn, L. 1980. Triassic conodont localities of the Salzkammergut region. Abh. Geol. B.-A, 35, 61-98.

Krystyn, L. 1990. A Rhaetian stage-chronostratigraphy, subdivisions and their intercontinental correlation. Albertiana, 8, 15-24.

Krystyn, L. 2008. An ammonoid-calibrated Tethyan conodont time scale of the late Upper Triassic. Berichte der Geologischen Bundesanstalt, 76, 9-11.

Krystyn, L. 2010. Decision report on the defining event for the base of the Rhaetian stage. Albertiana, 38, 11-12.

Krystyn, L., Bouquerel, H., Kuerschner, W., Richoz, S. & Gallet, Y. 2007a. Proposal for a candidate GSSP for the base of the Rhaetian Stage. The Global Triassic. New Mexico Museum of Natural History and Science Bulletin, 41, 189-199.

Krystyn, L., Richoz, S., Gallet, Y., Bouquerel, H., Kürschner, W. M. & Spötl, C. 2007b. Updated bio-and magnetostratigraphy from Steinbergkogel (Austria), candidate GSSP for the base of the Rhaetian stage. Albertiana, 36, 164-172.

Longridge, L.M., Carter, E S., Smith, P.L. & Tipper, H.W. 2007. Early Hettangian ammonites and radiolarians from the Queen Charlotte Islands, British Columbia and their bearing on the definition of the Triassic–Jurassic boundary. Palaeogeography, Palaeoclimatology, Palaeoecology, 244(1), 142-169.

Maron, M., Rigo, M., Bertinelli, A., Katz, M.E., Godfrey, L., Zaffani, M. & Muttoni, G. 2015. Magnetostratigraphy, biostratigraphy, and chemostratigraphy of the Pignola-Abriola section: New constraints for the Norian-Rhaetian boundary. Geological Society of America Bulletin, 127 (7/8), 962–974.

Mazza, M., Rigo, M. & Gullo, M. 2012. Taxonomy and biostratigraphic record of the Upper Triassic conodonts of the Pizzo Mondello section (western Sicily, Italy), GSSP candidate for the base of the Norian. Rivista Italiana di Paleontologia e Stratigrafia, 118 (1), 85-130.

McFadden, P.L. & McElhinny, M.W. 1990. Classification of the reversal test in palaeomagnetism. Geophysical Journal International, 103 (3), 725-729.

Mock, R. 1980. Field Trip D 'Triassic of the West Carpathians, in Second European conodont symposium' ECOS II. Abhandl. Geol. Bundesanst. 35, 129-144.

Miconnet, P. 1983. La région de Lagonegro (Italie méridionale): évolution géologique d'un bassin dans son cadre alpin. Doctoral dissertation III cicle, Université des Sciences et Techniques de Lille, Lille, France, 185 pp.

Mostardini, F. & Merlini, S. 1986. Appennino Centro Meridionale - Sezioni Geologiche e Proposta di Modello Strutturale. Memorie della Società Geologica Italiana, 35, 177-202.

Mostler, H., Scheuring, R. & Ulrichs, M. 1978. Zur Mega-, Mikrofauna und Mikroflora der Kossenen Schichten (alpine Obertrias) von Weissloferbach in Tirol unter besonderer Berucksichtigung der in der suessi-und marshi-Zone auftreitenden Conodonten. Osterreichische Akademie der Wissenschaften Erdwissenschaftliche Kommission Schriftenreihe, 4, 141-174.

Muttoni, G., Mazza, M., Mosher, D., Katz, M. E., Kent, D. V. & Balini, M. 2014. A Middle–Late Triassic (Ladinian–Rhaetian) carbon and oxygen isotope record from the Tethyan Ocean. Palaeogeography, Palaeoclimatology, Palaeoecology, 399, 246-259.

Muttoni, G., Kent, D.V., Jadoul, F., Olsen, P.E., Rigo, M., Galli, M.T. & Nicora, A. 2010. Rhaetian magneto-biostratigraphy from the Southern Alps (Italy): constraints on Triassic chronology. Palaeogeography, Palaeoclimatology, Palaeoecology, 285 (1), 1-16.

Muttoni, G., Kent, D.V., Olsen, P.E., Di Stefano, P., Lowrie, W., Bernasconi, S.M. & Hernández, F.M. 2004. Tethyan magnetostratigraphy from Pizzo Mondello (Sicily) and correlation to the Late Triassic Newark astrochronological polarity time scale. Geological Society of America Bulletin, 116 (9-10), 1043-1058.

O'Dogherty, L., Carter, E.S., Dumitrica, P., Goričan, Š., Wever, P.D., Hungerbühler, A., Bandini, A.N. & Takemura, A. 2009. Catalogue of Mesozoic radiolarian genera. Part 1: Triassic. Geodiversitas, 31 (2), 213-270.

Orchard, M.J. & Tozer, E.T. 1997. Triassic conodont biochronology, its calibration with the ammonoid standard, and a biostratigraphic summary for the Western Sedimentary Basin. Bullettin Of Canadian Petroleum Geology, 45 (4), 675-692.

Orchard, M.J., Whalen P.A., Carter E.S. & Taylor H.J. 2007. Latest Triassic conodonts and radiolarian-bearing successions in Baja California Sur. Lucas, S.G. and Spielmann, J.A., eds., 2007, The Global Triassic. New Mexico Museum of Natural History and Science Bulletin 41, 355-365.

Pálfy, J., Demény, A., Haas, J., Carter, E. S., Görög, Á., Halász, D., Oravecz-Scheffer, A., Hetényi, M., Márton, E., Orchard M. J., Ozsvárt, P., Veto, I. and Zajzon, N., 2007, Triassic–Jurassic boundary events inferred from integrated stratigraphy of the Csovár section, Hungary: Palaeogeography, Palaeoclimatology, Palaeoecology, 244, 11-33.

Palmer, A.R. 1983. The decade of North American geology 1983 Geologic time scale. Geology, 11 (9), 503-504.

Passeri, L., Bertinelli, A. & Ciarapica, G. 2005. Paleogeographic meaning of the Late Triassic-Early Jurassic Lagonegro units. Bollettino della Società Geologica Italiana, 124 (1), 231-245.

Pearson, D.A.B. 1970. Problems of Rhaetian stratigraphy with special reference to the lower boundary of the stage. Quarterly Journal of the Geological Society, 126 (1-4), 125-150.

Preto, N., Agnini, C., Rigo, M., Sprovieri, M. & Westphal, H. 2013. The calcareous nannofossil Prinsiosphaera achieved rock-forming abundances in the latest Triassic of western Tethys: consequences for the δ 13 C of bulk carbonate. Biogeosciences, 10 (9), 6053-6068.

Reggiani, L., Bertinelli, A., Ciarapica, G., Marcucci, M., Passeri, L., Ricci, C. & Rigo, M. 2005. Triassic-Jurassic stratigraphy of the Madonna del Sirino succession (Lagonegro Basin, Southern Apennines, Italy). Bollettino della Società Geologica Italiana, 124, 281-291.

Remane, J. 2003. Chronostratigraphic correlations: their importance for the definition of geochronologic units. Palaeogeography, Palaeoclimatology, Palaeoecology, 196 (1), 7-18.

Rigo, M., Preto, N., Franceschi, M. & Guaiumi, C. 2012a. Stratigraphy of the Carnian-Norian Calcari con Selce Formation in the Lagonegro Basin, Southern Apennines. Rivista Italiana di Paleontologia e Stratigrafia, 118, 143-154.

Rigo, M., Trotter, J.A., Preto, N. & Williams, I.S. 2012b. Oxygen isotopic evidence for Late Triassic monsoonal upwelling in the northwestern Tethys. Geology, 40 (6), 515-518.

Rigo, M., De Zanche, V., Mietto, P., Preto, N. & Roghi, G. 2005. Biostratigraphy of the Calcari con Selce formation. Bollettino della Società Geologica Italiana, 124, 293-300.

Rigo, M., Preto, N., Roghi, G., Tateo, F. & Mietto, P. 2007. A rise in the Carbonate Compensation Depth of western Tethys in the Carnian (Late Triassic): Deep-water evidence for the Carnian Pluvial Event. Palaeogeography, Palaeoclimatology, Palaeoecology, 246, 188-205.

Rigo, M., Bertinelli, A., Concheri, G., Gattolin, G., Godfrey, L., Katz, M., Maron, M., Muttoni, G., Sprovieri, M., Stellin, F. & Zaffani, M. 2015. The Pignola-Abriola section (southern Apennines, Italy): a new GSSP candidate for the base of the Rhaetian Stage. Lethaia. DOI: 10.1111/let.12145

Scandone, P. 1967. Studi di geologia lucana: la serie calcareo-silico-marnosa ed i suoi rapporti con l’Appennino calcareo. Bollettino della Società dei Naturalisti in Napoli, 76 (2), 301-469.

Schlanger, S.O. & Jenkyns, H.C. 1976. Cretaceous oceanic anoxic events: causes and consequences. Netherlands Journal of Geosciences/Geologie en Mijnbouw, 55, 179–184.

Şengör, A.M.C., Yılmaz, Y. & Sungurlu, O. 1984. Tectonics of the Mediterranean Cimmerides: nature and evolution of the western termination of Palaeo-Tethys. Geological Society, London, Special Publications, 17 (1), 77-112.

Silberling, N.J. & Tozer, E.T. 1968. Biostratigraphic classification of the marine Triassic in North America. Geological Society of America Special Papers, 110, 1-56.

Slavin, V.I. 1961. Stratigraphic position of the Rhaetian Stage. Sovyetskaya Geologiya, 3, 68-78.

Slavin, V.I. 1963. Au sujet du Rhétian. Bureau Recherches Geoloie et Minieres Memoir, 15, 29-32.

Stampfli, G.M. & Marchant, R.H. 1995. Plate configuration and kinematics in the Alpine region. Accademia Nazionale delle Scienze, Scritti e Documenti, 14, 147-166.

Stampfli, G., Marcoux, J. & Baud, A. 1991. Tethyan margins in space and time. Palaeogeography, Palaeoclimatology, Palaeoecology, 87 (1), 373-409.

Tozer, E.T., 1967, A standard for Triassic time. Geological Survey of Canada, Bulletin, 156, 103 pp.

Tozer, E.T. 1980. Latest Triassic (Upper Norian) ammonoid and Monotis faunas and correlations. Rivista Italiana di Paleontologia e Stratigrafia, 85 (3-4), 843-876.

Tozer, E.T. 1984. The Trias and its ammonoids: The evolution of a time scale. Geological Survey of Canada, Miscellaneous Rep. 35, 171 pp.

Tozer, E.T. & Calon, T.J. 1990. Triassic ammonoids from Jabal Safra and Wadi Alwa, Oman, and their significance. Geological Society, London, Special Publications, 49 (1), 203-211.

Trotter, A.J., Williams, S.I., Nicora, A., Mazza, M. & Rigo, M 2015. Long-term cycles of Triassic climate change: a new $\delta^{18}O$ record from conodont apatite. Earth and Planetary Science Letters, 415, 165-174.

Yeh, K.Y. & Cheng, Y.N. 1996. An Upper Triassic (Rhaetian) radiolarian assemblage from Busuanga Island, Philippines. Bulletin of the National Museum of Natural Science, Taiwan, 7, 1-43.

Ward, P.D., Garrison, G.H., Haggart, J.W., Kring, D.A. & Beattie, M.J. 2004. Isotopic evidence bearing on Late Triassic extinction events, Queen Charlotte Islands, British Columbia, and implications for the duration and cause of the Triassic-Jurassic mass extinction. Earth Planetary Science Letters, 224, 589-600.

Ward, P. D., Haggart, J. W., Carter, E. S., Wilbur, D., Tipper, H. W. & Evans, T. 2001. Sudden productivity collapse associated with the Triassic-Jurassic boundary mass extinction. Science, 292 (5519), 1148-1151.

Whiteside, J. & Ward, P.D. 2011. Ammonoid diversity and disparity track episodes of chaotic carbon cycling during the early Mesozoic. Geology, 39, 99–102.

Wignall, P.B., Zonneveld, J.-P., Newton, R.J., Amor, K., Sephton, M.A. & Hartley, S. 2007: The end Triassic mass extinction record of Williston Lake, British Columbia. Palaeogeography, Palaeoclimatology, Paleoecology, 253, 385-406.

Wotzlaw, J.F., Guex, J., Bartolini, A., Gallet, Y., Krystyn, L., McRoberts, C.A., Taylor, D., Schoene, B. & Schaltegger, U. 2014. Towards accurate numerical calibration of the Late Triassic: high precision U-Pb geochronology constraints on the duration of the Rhaetian. Geology, 42, 571–574.

Zapfe, H. 1974. Trias in Osterreich. In: Zapfe (Ed.): The stratigraphy of the Alpine Mediterranean Triassic. Schriftenreihe der Erdwissenschaftlichen Kommission, Osterreichische Akademie der Wissenschaften, 2, 245-51.

APPENDIX B

The Norian "chaotic carbon interval": new clues from the $\delta^{13}C_{org}$ record of the Lagonegro Basin (southern Italy)

Supplementary Material

TOC and d13Corg analyses: sample list and results

Pignola-Abriola

m	Sample	TOC%	d13Corg
58.10	Pa i 191	1.984	
57.80	Pai 189	2.321	-25.56
57.65	GNM 119	0.149	
57.50	Pai 187	2.014	-24.66
57.05	Pai 185	1.863	-26.43
56.76	GNM 117	0.452	-26.61
56.50	Pai 184	2.103	-25.80
55.70	GNI 29	0.960	-24.41
55.63	Pai 180	3.654	-25.71
55.55	GNI 28	1.259	-25.63
55.25	GNI 27	5.548	-25.40
54.45	Pai 173	5.663	-25.77
53.75	GNM 102	8.410	-27.83
53.15	Pai 168	1.359	-25.67
52.65	GNI 26	5.684	-25.85
52.50	Pai 166	0.136	-25.26
52.13	Pa i 164	0.963	
51.65	Pai 162	0.079	-26.52
51.40	GNI 25	6.664	-25.97
51.05	GNM 85	0.618	-25.86
50.80	Pai 160	0.096	-25.17
50.20	Pai 157	0.107	-25.03
49.25	GNI 24	4.780	-26.56
49.15	GNI 23	9.895	-24.36
48.90	GNI 22	3.667	-26.15
48.65	Pai 155	2.113	-25.72
48.40	GNI 21	5.074	-25.77
48.10	GNI 20	12.653	-25.40
47.40	GNI 19B	9.024	-25.86

47.20	Pa i 146	1.895	
46.80	GNI 19	0.943	-25.68
46.45	GNI 18	11.623	-26.05
46.30	GNI 17	12.589	-26.37
45.95	Pai 143	0.106	-24.90
45.80	GNI 16	0.728	-27.10
45.65	Pai 142	10.337	-25.89
45.30	GNI 15	2.032	-27.13
45.23	GNI 14	2.566	-25.42
45.18	Pai 139		-27.58
44.95	Pai 136	6.856	-25.80
44.75	Pai 134	2.321	-24.91
44.35	GNM 52	8.663	-29.95
43.30	GNP 3	7.845	-27.26
42.60	Pa i 119	8.045	
42.35	GNP 2	10.681	-28.28
42.28	GNM 41A	8.327	-27.55
42.20	Pai 116	6.125	-25.18
41.30	Pai 111	8.014	-24.46
40.70	GNM 37	6.074	-27.97
40.19	GNM 35B	10.557	-26.55
40.00	Pai 108	13.025	-25.47
39.35	GNP 1	2.967	-27.93
38.30	Pai 104	1.451	-24.31
37.73	GNI 13	0.818	-25.58
37.50	GNI 12	5.960	-24.90
37.30	GNI 11	6.261	-25.76
36.80	Pai 101	0.941	
36.10	GNI 10	8.876	-23.70
35.70	GNI 9	3.992	-24.19
33.80	Parc 1	2.354	-27.78
33.40	Parc 3	1.979	-25.97
32.95	Parc 6	1.853	-27.50
32.70	Parc 7	2.580	
32.05	Parc 10	3.668	-27.87
31.70	GNI 8	1.855	-25.67
31.65	GNI 7	0.309	-24.58
31.60	GNI 6	0.164	-24.45
31.50	Parc 12	2.923	-25.96
30.89	Parc 15	1.880	-27.18
30.70	GNI 5	1.348	-25.72
30.65	GNI 4	0.152	-25.30
30.55	GNI 3	6.841	-26.95
30.40	Parc 16	2.036	
30.30	GNI 2	5.996	-25.66
29.90	GNI 1	2.589	-27.68
28.00	Pai 76	2.654	-24.91

27.60	Pai 74	0.092	-23.73
27.40	Pai 72	3.854	-20.78
27.10	Pai 70	0.221	-23.89
26.80	Pai 68	0.191	-23.50
26.60	Pai 65	2.966	-25.38
25.80	Pai 63	0.412	-26.52
25.00	Pa i 61	0.323	
24.82	Pa i 60	3.771	
23.80	Pai 56	0.320	-23.51
23.55	Pai 55	3.657	-23.80
23.30	Pai 54	0.226	-23.31
23.00	Pai 52	0.358	-26.73
22.60	Pai 50	2.851	-26.61
22.10	Pai 49	0.126	-26.64
21.70	Pai 47	0.160	-27.71
21.50	Pa i 46	1.674	
21.00	Pai 43	0.891	-24.84
20.80	Pai 41	3.221	-27.57
19.80	Pai 39	0.153	-28.61
19.65	Pa i 38	7.345	
19.30	Pai 37	0.152	-25.73
18.88	Pai 35	1.861	-25.07
18.60	Pa i 34	0.301	
18.10	pa 9	0.301	-26.36
17.94	Pa i 32	4.233	-24.91
17.50	Pa i 31	1.981	-25.23
17.20	pa 8	0.419	-26.08
16.90	Pa i 29	6.425	-25.60
16.49	Pai 19	3.364	-26.19
16.40	pa 7	0.399	
16.22	Pai 16	3.526	-25.95
11.80	pa 2	0.336	-24.76
11.13	Pa i 11	3.668	
9.74	Pa i 9	3.045	
7.75	pa 1	0.367	-25.11
0.00	Pai 0	2.341	-24.67

Mt. Volturino

m	Sample	TOC%	d13Corg
71.00	MV49	0.611	-19.88
68.00	MV45.60	0.115	
66.00	MV44	0.161	-21.89
65.00	MV 43	0.174	-25.15
64.00	MV42	0.294	
57.50	MMV 9	0.095	

56.00	MVV8	0.371	
52.00	MMV 1	0.693	-28.05
51.50	MV 35	0.380	
51.00	MMV 2	1.111	-27.78
50.66	MMV 3		-27.36
50.50	MMV 4	0.941	-26.33
49.50	MMV 6	0.925	-26.56
49.00	MMV 7	1.192	-27.52
48.20	MMV 8		-25.23
47.10	MMV 9		-27.46
46.60	MMV 10		-26.50
46.50	MV 31	0.124	
46.20	MMV 11		-25.42
45.00	MVV 6	0.706	
42.50	MV 27B	0.288	-23.47
42.45	MMV 13		-27.35
42.00	MV 25		-20.67
41.50	MV 24	0.195	-24.29
41.43	MMV 16		-24.25
41.00	MV 23	0.295	-26.13
40.20	MV 22		-26.12
39.50	MV 21	0.198	
39.00	MV 20B	0.384	
38.45	MMV 22		-24.73
38.00	MMV 23		-24.67
38.00	MV 17	0.293	-26.07
37.50	MV 16	0.500	-23.15
36.30	MMV 27		-24.30
37.00	MV15	0.479	
36.00	MVV 5	0.329	-24.52
35.60	MMV 29		-24.35
35.00	MV11	1.092	-24.86
34.00	MVC7	0.310	-23.65
34.00	MMV 32	0.389	
33.50	MMV 33	0.891	
32.00	MVV4	0.367	
31.00	MVC6	0.215	-25.60
30.50	MV7	0.323	-24.83
29.00	MVC 5	0.218	-26.29
28.00	MV 6	0.564	-28.10
27.00	MV 5		-25.48
24.50	MVC4	0.205	-24.83
23.00	MVV 2	0.318	-23.13
22.00	MV 1	0.388	-24.87
21.00	V7	0.246	-22.47
19.00	V8	0.230	
18.50	MVC 3	0.231	-26.77

18.00	V9	0.294	-24.77
17.50	V10	0.145	
16.50	MVVR	0.321	-25.17
15.00	V11	0.161	
14.00	V12	0.298	-26.14
13.50	MVC 2	0.205	-26.01
11.00	V13	0.313	-27.40
9.00	V14	0.313	-26.61
8.00	MVC1	0.198	-24.60
7.00	V6	0.289	-25.35
6.00	V5	0.211	-26.11
4.00	V4	0.226	-25.25
3.00	V3	0.298	
1.50	V2	0.260	
1.00	V1	0.205	-26.31

Madonna del Sirino

m	Sample	TOC%	d13Corg
77.50	MS 61	0.531	-20.26
76.00	MS 56	0.295	-24.95
73.50	MS 53	0.694	
72.25	MS 52	0.103	-26.37
67.50	MS 49	0.207	-27.01
67.00	MS 48		-22.36
66.20	MSSS 24		-25.66
66.00	MS 46	0.178	
65.00	MSSS 23		-24.72
64.70	MS 45	0.309	-25.30
64.50	MS 42		-24.46
63.80	MS 40	0.097	-25.76
63.00	ms 39		-24.75
62.50	ms 37		-23.14
62.00	ms 35		-21.83
61.50	MS 33b	0.147	-25.10
60.50	MS 30	0.082	
59.75	MS 29	0.098	
59.00	MS SS 17.1	0.282	
58.00	MS 28	0.856	-25.03
57.00	MS 26	0.076	
55.75	MS 24	0.173	-25.42
54.50	MS 22	0.364	-26.20
53.75	MS 21	0.301	-24.03
52.00	MS 20	0.179	-30.35
50.00	MS 19	0.304	-25.66
49.00	ms 17		-22.62

49.00	MS SS 49		
47.50	ms 16		-22.42
47.00	MS SS 47	0.147	-25.99
46.00	MS SS 46	0.188	-26.26
42.00	MS CS 42	0.051	-26.72
39.00	MS CS 39	0.068	-26.97
33.00	MS SS 33	0.395	-24.77
31.0	msss 31		-27.05
29.00	MS SS 29	0.109	-24.62
28.50	ms 7		-24.90
27.50	ms 8		-24.55

Duration of isotopic excursions in Pignola-Abriola section (age model by Maron et al. 2015)

Duration of isotopic excursions has been calculated by applying the age model proposed by Maron et al. (2015) on the Pignola-Abriola section. This model calculates the average accumulation rates of the Pignola-Abriola section, based on the magnetostratigraphic correlation with the Newark APTS. The sedimentation rate raises from 2.6 m/My (from 0 to 25.6 m) to 5.6 m/My (from 25.6 to 41.2 m), leading to a dramatic increase to 9.8 m/My up to the end of the section. The values of the sedimentation rate are very low, but acceptable for a pelagic basin. The increase in sediment supply coincides with an increase in siliciclastic fraction and the deposition of more shale, marl and marly limestone levels (Maron et al., 2015). The formulae applied for the age estimation are:

1) from 0 to 25.6 m: Age = -0.371*meter + 217.89
2) from 25.6 to 41.6 m: Age = -0.1702*meter + 212.89
3) over 41.6 m: Age = -0.1017*meter + 210.09

For more detailed on the model construction and applications, please refer to Maron et al. (2015).

APPENDIX C

Through a complete Rhaetian δ13Corg record: carbon cycle disturbances, volcanism, end-Triassic mass extinction. A composite succession from the Lombardy Basin (N Italy)

Supplementary material

d13Corg analyses: sample list and results

Section	sample	m	d13Corg
Malanotte	j 27	78,0	-27,03
Malanotte	j 26	76,5	-27,65
Malanotte	j 25	75,0	-27,09
Malanotte	j 24	73,0	-27,79
Malanotte	j 23	72,0	-26,81
Malanotte	j 22	70,0	-27,51
Malanotte	j 21	69,0	-28,63
Malanotte	j 20	68,2	-28,21
Malanotte	j 19	68,0	-27,99
Malanotte	j 18	65,0	-27,41
Malanotte	j 16	64,0	-27,57
Malanotte	j 15	62,0	-26,76
Malanotte	j 13	60,5	-26,50
Malanotte	j 11	60,2	-26,82
Malanotte	j 9	59,5	-26,71
Malanotte	j 7	59,2	-28,73
Malanotte	j 6	59,0	-29,62
Malanotte	z 124	9,12	-28,22
Malanotte	z 123	8,27	-27,82
Malanotte	z 122	7,92	-27,69
Malanotte	z 121	7,57	-28,00
Malanotte	z 120	7,47	-27,05
Malanotte	Z 119	7,32	-28,46
Malanotte	Z 118	6,92	-27,53
Malanotte	Z 117	4,77	-27,45
Malanotte	Z 116	4,22	-27,48
Malanotte	Z 115	3,92	-27,54
Malanotte	Z 114	3,27	-27,26
Malanotte	Z 110	2,27	-27,84
Malanotte	Z 109	1,87	-27,93

Malanotte	Z 108	1,82	-28,19
Malanotte	z 107	1,45	-27,18
Malanotte	Z 106	1,25	-28,00
Malanotte	Z 104	0,4	-27,70
Malanotte	z 103	0,15	-26,98
Malanotte	z 102	0,14	-27,41
Malanotte	Z 101 bis	0,07	-28,65
Malanotte	Z 101	0	-28,75
Italcementi freshly caved	j 5	58,8	-27,45
Italcementi freshly caved	j 4	58,5	-27,80
Italcementi freshly caved	j 7-12	58,0	-26,52
Italcementi freshly caved	j 3	58,0	-27,90
Italcementi freshly caved	j 2	54,0	-27,78
Italcementi freshly caved	zu 1	47,0	-26,24
Italcementi freshly caved	zu 2	46,0	-27,07
Italcementi freshly caved	zu 4-13	45,8	-26,29
Italcementi freshly caved	zu 5-13	45,5	-26,08
Italcementi freshly caved	zu 9-13	44,5	-24,96
Italcementi freshly caved	zu 11-13	44,0	-25,02
Italcementi freshly caved	zu 12-13	43,5	-25,74
Italcementi freshly caved	zu 3	43,5	-29,45
Italcementi freshly caved	zu 4	43,2	-25,99
Italcementi freshly caved	zu 13-13	43,0	-26,75
Italcementi freshly caved	zu 5	42,8	-26,30
Italcementi freshly caved	zu 14-13	42,5	-26,40
Italcementi freshly caved	zu 6	40,2	-24,92
Italcementi freshly caved	zu 15b-13	40,0	-25,96
Italcementi freshly caved	zu 8	39,9	-25,17
Italcementi freshly caved	zu 10	39,3	-25,67
Italcementi freshly caved	zu 11	39,0	-25,84
Italcementi freshly caved	zu 12	38,3	-26,38
Italcementi freshly caved	zu 13	36,5	-27,08
Italcementi freshly caved	zu 16-13	36,0	-25,74
Italcementi freshly caved	zu 14	36,0	-26,66
Italcementi freshly caved	zu 15	34,5	-26,88
Italcementi freshly caved	zu 21-13	29,0	-26,00
Italcementi freshly caved	zu 16	26,0	-26,40
Italcementi freshly caved	zu 25-13	25,0	-24,36
Italcementi freshly caved	zu 17	22,7	-26,77
Italcementi freshly caved	j01-12	21,5	-25,53
Italcementi freshly caved	zu 18	21,0	-25,17
Italcementi freshly caved	zu 19	19,0	-25,95
Italcementi freshly caved	zu 20	17,5	-28,37
Italcementi freshly caved	zu 21	15,0	-26,64
Italcementi freshly caved	zu 22	13,0	-27,39
Italcementi freshly caved	zu 24	5,5	-26,25

Italcementi freshly caved	zu 25	4,5	-25,42
Italcementi freshly caved	zu 26	3,2	-25,64
Italcementi freshly caved	zu 27	2,8	-26,36
Italcementi freshly caved	zu 28	0,5	-25,16
Brumano	Z 245	188	-25,14
Brumano	Z 244	185,4	-25,35
Brumano	Z 243	184,6	-24,74
Brumano	z 241	181	-25,06
Brumano	z 240	178	-25,07
Brumano	z 239	176,8	-24,90
Brumano	z 238	175,7	-25,76
Brumano	Z 237	174,7	-24,91
Brumano	Z 236	174,3	-25,88
Brumano	Z 235	173,7	-25,10
Brumano	z 234	172,3	-27,81
Brumano	Z 233	171,5	-26,42
Brumano	Z 231	166	-28,13
Brumano	Z 230	165,8	-26,24
Brumano	Z 229	165,7	-25,27
Brumano	z 228	165,3	-27,43
Brumano	z 227	164	-25,94
Brumano	z 226	163,5	-26,00
Brumano	z 225	162	-25,22
Brumano	Z 224	161,8	-25,56
Brumano	z 223	161	-25,02
Brumano	z 222	160	-25,11
Brumano	z 220	155,4	-24,00
Brumano	z 219	154	-24,63
Brumano	z 218	151,7	-25,89
Brumano	z 217	151,3	-25,47
Brumano	z 216	150,3	-25,70
Brumano	z 215	149,3	-24,82
Brumano	z 214	146,3	-25,26
Brumano	z 213	145,5	-25,31
Brumano	z 212	145,3	-27,55
Brumano	z 211	144,3	-25,30
Brumano	z 210	141,7	-25,18
Brumano	z 208	141	-26,52
Brumano	z 206 bis	140,3	-25,43
Brumano	z 206	139,7	-26,18
Brumano	z 205	138	-25,57
Brumano	z 204	131,9	-25,43
Brumano	z 203	131,6	-24,50
Brumano	z 202	131	-24,47
Brumano	z 201	130	-25,41
Brumano	z 197	121	-25,50

Brumano	z 196	118	-25,67
Brumano	z 195	116,7	-26,15
Brumano	z 194	114	-25,69
Brumano	z 193	113,7	-25,36
Brumano	z 192	107,5	-25,23
Brumano	z 190	94,7	-25,83
Brumano	z 189	88	-25,43
Brumano	z 188	81,7	-25,42
Brumano	z 187	80	-25,44
Brumano	z 186	77,5	-26,39
Brumano	z 185	75	-26,41
Brumano	z 184	69,3	-25,51
Brumano	z 183	65,5	-25,48
Brumano	z 182	62	-25,53
Brumano	z 181	61	-27,86
Brumano	z 180	52	-25,62
Brumano	z 179	49,7	-26,26
Brumano	z 178	48	-24,89
Brumano	z 177	47	-25,24
Brumano	z 175	46,3	-24,83
Brumano	z 174	41	-25,45
Brumano	z 173	40	-26,44
Brumano	z 172	39	-26,37
Brumano	z 171	37,3	-26,13
Brumano	z 169	36	-25,63
Brumano	z 168	34,8	-25,84
Brumano	z 167	34	-25,48
Brumano	z 166	32,5	-24,70
Brumano	z 165	30,17	-26,39
Brumano	z 164	28,17	-25,61
Brumano	z 163	25,6	-25,22
Brumano	z 162	25,3	-26,90
Brumano	z 161	25	-26,48
Brumano	z 160	24,71	-26,45
Brumano	z 159	24,37	-26,64
Brumano	z 158	24	-26,26
Italcementi active quarry	z 54	55,4	-25,26
Italcementi active quarry	Z 53	55	-24,39
Italcementi active quarry	z 52	53,3	-23,68
Italcementi active quarry	Z 51	53	-26,41
Italcementi active quarry	Z 50	52,6	-26,98
Italcementi active quarry	z 49	52	-24,89
Italcementi active quarry	z 48	51,4	-23,86
Italcementi active quarry	Z 47A	48,1	-24,86
Italcementi active quarry	z 47	48	-24,44
Italcementi active quarry	Z 46	46	-25,05

Italcementi active quarry	Z 44	42,3	-25,54
Italcementi active quarry	Z 43	39	-25,40
Italcementi active quarry	Z 42	38,6	-26,07
Italcementi active quarry	Z 41	38	-25,52
Italcementi active quarry	Z 40	37,5	-24,75
Italcementi active quarry	Z 39	37	-24,88
Italcementi active quarry	Z 38	36,3	-25,02
Italcementi active quarry	Z 37	33,9	-25,19
Italcementi active quarry	Z 36	33,8	-25,00
Italcementi active quarry	Z 35	33,2	-25,06
Italcementi active quarry	Z 34 bis	33	-25,48
Italcementi active quarry	Z 34	33	-24,48
Italcementi active quarry	Z 33	32,6	-24,97
Italcementi active quarry	Z 32	32,2	-24,55
Italcementi active quarry	Z 31	31,4	-27,18
Italcementi active quarry	Z 30	31	-27,27
Italcementi active quarry	Z 29	27,6	-27,00
Italcementi active quarry	Z 28	27	-25,31
Italcementi active quarry	Z 27	26	-25,58
Italcementi active quarry	Z 26	25,2	-25,41
Italcementi active quarry	Z 25	24	-25,53
Italcementi active quarry	Z 23	16	-25,61
Italcementi active quarry	Z 22	15,4	-25,39
Italcementi active quarry	Z 21	14,8	-26,38
Italcementi active quarry	Z 20	14,4	-25,39
Italcementi active quarry	Z 19	14	-25,88
Italcementi active quarry	Z 18	13,2	-25,79
Italcementi active quarry	z 17	12	-25,39
Italcementi active quarry	Z 16	10	-25,85
Italcementi active quarry	Z 15	9	-25,38
Italcementi active quarry	Z 14	8,4	-25,79
Italcementi active quarry	z 13	3,4	-25,73
Italcementi active quarry	z 13	3,4	-25,87
Italcementi active quarry	Z 12	0,8	-24,64
Italcementi active quarry	Z 11	-0,2	-25,00
Italcementi active quarry	Z 10	-1,1	-24,41
Italcementi active quarry	Z 9	-1,7	-25,42
Italcementi active quarry	Z 8	-2,3	-24,00
Italcementi active quarry	Z 7	-2,8	-24,26
Italcementi active quarry	Z 6	-3,3	-24,54
Italcementi active quarry	Z 5	-9,8	-25,55
Italcementi active quarry	Z 4	-10,1	-25,38
Italcementi active quarry	Z 3	-10,4	-25,39
Italcementi active quarry	Z 2	-10,7	-25,19
Italcementi active quarry	Z 1	-18,2	-25,86

TOC analyses: sample list and results

Section	Sample	m	TOC(%)
Malanotte	7/12	58	0,50
Malanotte	4/13	45,8	0,24
Malanotte	5/13	45,5	0,90
Malanotte	9/13	44,5	1,02
Malanotte	11/13	44	0,95
Malanotte	12/13	43,5	0,67
Malanotte	13/13	43	1,52
Malanotte	14/13	42,5	0,63
Malanotte	15B/13	40	0,43
Malanotte	16/13	36	0,11
Malanotte	1/12	21,5	0,12
Malanotte	21/13	15	0,24
Malanotte	25/13	4,5	0,34
Malanotte	124	9,12	0,21
Malanotte	123	8,27	0,24
Malanotte	122	7,92	0,22
Malanotte	121	7,57	0,26
Malanotte	120	7,47	0,36
Malanotte	119	7,32	0,30
Malanotte	118	6,92	0,13
Malanotte	117	4,77	0,11
Malanotte	116	4,22	0,16
Malanotte	115	3,92	0,15
Malanotte	114	3,27	0,45
Malanotte	113	2,77	0,07
Malanotte	110	2,27	0,25
Malanotte	109	1,87	0,07
Malanotte	108	1,82	0,18
Malanotte	107	1,45	0,21
Malanotte	106	1,25	0,15
Malanotte	105	0,82	0,09
Malanotte	104	0,4	0,14
Malanotte	103	0,15	0,23
Malanotte	102	0,14	0,12
Malanotte	101 bis	0,07	0,88
Malanotte	101	0	0,93
Italcementi	54	55,4	0,20
Italcementi	53	55	0,09
Italcementi	52	53,3	0,26
Italcementi	51	53	0,45
Italcementi	50	52,6	0,87

Italcementi	49	52	0,16
Italcementi	48	51,4	0,17
Italcementi	47A	48,1	0,14
Italcementi	47	48	0,15
Italcementi	46	46	0,16
Italcementi	44	42,3	0,45
Italcementi	43	39	0,22
Italcementi	42	38,6	0,15
Italcementi	41	38	0,24
Italcementi	40	37,5	0,24
Italcementi	39	37	0,43
Italcementi	38	36,3	0,32
Italcementi	37	33,9	0,26
Italcementi	36	33,8	0,29
Italcementi	35	33,2	0,24
Italcementi	34	33	0,16
Italcementi	33	32,6	0,17
Italcementi	32	32,2	0,25
Italcementi	31	31,4	0,92
Italcementi	30	31	0,36
Italcementi	29	27,6	0,42
Italcementi	28	27	0,20
Italcementi	27	26	0,18
Italcementi	26	25,2	0,90
Italcementi	25	24	0,26
Italcementi	24	20	0,28
Italcementi	23	16	0,26
Italcementi	22	15,4	0,27
Italcementi	21	14,8	0,21
Italcementi	20	14,4	0,13
Italcementi	19	14	0,12
Italcementi	18	13,2	0,20
Italcementi	17	12	0,15
Italcementi	16	10	0,26
Italcementi	15	9	0,14
Italcementi	14	8,4	0,16
Italcementi	13	3,4	0,01
Italcementi	12	0,8	0,20
Italcementi	11	-0,2	0,38
Italcementi	10	-1,1	0,35
Italcementi	9	-1,7	0,35
Italcementi	8	-2,3	0,33
Italcementi	7	-2,8	0,32
Italcementi	6	-3,3	0,12
Italcementi	5	-9,8	
Italcementi	3	-10,4	0,18
Italcementi	1	-18,2	0,05

Brumano	245	188	0,44
Brumano	244	185,4	0,22
Brumano	243	184,6	0,45
Brumano	241	181	0,32
Brumano	240	178	0,32
Brumano	239	176,8	0,81
Brumano	238	175,7	0,71
Brumano	237	174,7	0,87
Brumano	236	174,3	0,44
Brumano	235	173,7	0,75
Brumano	234	172,3	0,58
Brumano	233	171,5	0,48
Brumano	232	166	0,67
Brumano	231	165,8	0,80
Brumano	230	165,7	0,85
Brumano	229	165,3	0,46
Brumano	228	164	0,77
Brumano	227	163,5	0,56
Brumano	226	162	0,43
Brumano	225	161,8	0,37
Brumano	224	161	0,50
Brumano	223	160	0,46
Brumano	222	155,4	0,45
Brumano	221	154	0,35
Brumano	220	151,7	0,40
Brumano	219	151,3	0,61
Brumano	218	150,3	0,48
Brumano	217	149,3	0,66
Brumano	216	146,3	0,42
Brumano	215	145,5	0,43
Brumano	214	145,3	0,61
Brumano	213	144,3	0,27
Brumano	212	141,7	0,26
Brumano	211	141	0,45
Brumano	210	140,3	0,43
Brumano	209	139,7	0,60
Brumano	208	138	0,71
Brumano	206	131,9	0,55
Brumano	205	131,6	0,94
Brumano	204	131	1,11
Brumano	203	130	1,02
Brumano	202	121	0,99
Brumano	200	118	0,31
Brumano	197	116,7	0,19
Brumano	196	114	0,35
Brumano	195	113,7	0,28

Brumano	194	107,5	0,53
Brumano	193	94,7	0,85
Brumano	190	88	0,69
Brumano	189	81,7	0,33
Brumano	188	80	0,44
Brumano	187	77,5	0,30
Brumano	185	75	0,35
Brumano	184	69,3	0,17
Brumano	183	65,5	0,38
Brumano	182	62	0,22
Brumano	181	61	0,10
Brumano	180	52	0,45
Brumano	179	49,7	0,21
Brumano	178	48	0,73
Brumano	176	47	0,52
Brumano	175	46,3	0,75
Brumano	174	41	0,43
Brumano	173	40	0,76
Brumano	172	39	0,34
Brumano	171	37,3	0,62
Brumano	169	36	0,40
Brumano	168	34,8	0,71
Brumano	167	34	0,74
Brumano	166	32,5	0,42
Brumano	165	30,17	0,97
Brumano	164	28,17	0,53
Brumano	163	25,6	0,67
Brumano	162	25,3	0,51
Brumano	161	25	0,30
Brumano	160	24,71	0,35
Brumano	159	24,37	0,77
Brumano	158	24	0,72

References

Ager, D.V. 1987. A defence of the Rhaetian stage. Albertiana, 6 (1987), 4-13.

Allen, M.R., Frame, D.J., Huntingford, C., Jones, C.D., Lowe, J.A., Meinshausen, M., Meinshausen, N., 2009. Warming caused by cumulative carbon emissions towards the trillionth tonne. Nature, 458, 1163-1166.

Amodeo, F., 1999, Il Triassico terminale–Giurassico del Bacino Lagonegrese. Studi stratigrafici sugli Scisti Silicei della Basilicata (Italia meridionale): Memoires de Geologie (Lausanne), v. 33, p. 1–123.

Amodeo, F., Baumgartner, P.O., 1994, Stratigraphic revision of the Scisti Silicei Formation (Upper Triassic-Upper Jurassic), Lagonegro Basin, southern Italy. Preliminary report: Paleopelagos, v. 4, p. 35-46.

Amodeo, F., Molisso, F., Kozur, H., Marsella, E. & D'Argenio, B. 1993. Age of Transitional Beds between Cherty Limestone (Calcari con selce) and Radiolarites (Scisti Silicei) in the Lagonegro Domain (Southern Italy). First evidence of Rhaethian conodonts in Peninsular Italy. Bollettino del Servizio Geologico d'Italia, 110, 3-22.

Argnani, A., 2005, Possible record of a Triassic ocean in the Southern Apennines: Boll. Soc. Geol. Ital., v. 124, p. 109–121.

Atudorei, N.V., 1999, Constraints on the Upper Permian to Upper Triassic marine carbon isotope curve. Case studies from the Tethys. PhD Thesis: Lausanne University, p. 155.

Bachan, A., van de Schootbrugge, B., Fiebig, J., McRoberts, C.A., Ciarapica, G. and Payne, J.L., 2012. Carbon cycle dynamics following the end-Triassic mass extinction: Constraints from paired d13Ccarb and d13Corg records. Geochem. Geophys. Geosyst., 13, Q09008, doi:10.1029/2012GC004150.

Bartolini, A., J. Guex, J. E. Spangenberg, B. Schoene, D. G. Taylor, U. Schaltegger, and V. Atudorei, 2012. Disentangling the Hettangian carbon isotope record: Implications for the aftermath of the end- Triassic mass extinction. Geochem. Geophys. Geosyst., 13, Q01007, doi:10.1029/2011GC003807.

Bazzucchi, P., Bertinelli, A., Ciarapica, G., Marcucci, M., Passeri, L., Rigo, M. and Roghi, G., 2005, The Late Triassic–Jurassic stratigraphic succession of Pignola (Lagonegro-Molise Basin, Southern Apennines, Italy): Bollettino Società Geologica Italiana, v. 124, p. 143–153.

Beerling, D.J., Berner, R.A., 2002. Biogeochemical constraints on the Triassic–Jurassic boundary carbon cycle event. Glob. Biogeochem. Cycles, 16, 1 –13.

Benton, M. J. and Twitchett, R. J., 2003, How to kill (almost) all life: the end-Permian extinction event: Trends in Ecology and Evolution, v. 18, p. 358–365.

Berner, R.A., 1982, Burial of organic carbon and pyrite sulfur in the modern ocean: its geochemical and environmental significance: Am. J. Sci., v. 282, p. 451–473.

Berner, R.A., 1994, GEOCARB II: a revised model of atmospheric CO2 over Phanerozoic time: Am. J. Sci., v. 294, p. 56–91.

Berner, R.A., and Rye, D.M., 1992. Calculation of the Phanerozoic strontium isortope record of the oceans from a carbon cycle model: American Journal of Science, 292, 136–148.

Berner, R.A., Lasaga, A.C., Garrels, R.M., 1983, The carbonate–silicate geochemical cycle and its effect on atmospheric carbon dioxide over the last 100 million years: Am. J. Sci., v. 283, p. 641–683.

Bertinelli, A., 2003, Il Bacino Lagonegrese-Molisano nel contesto della Tetide occidentale durante il Triassico superiore-Giurassico. PhD thesis: Università degli Studi di Perugia, p. 215.

Bertinelli, A., Casacci, M., Concheri, G., Gattolin, G., Godfrey, L., Katz, M.E., Maron, M., Mazza, M., Mietto, P., Muttoni, G., Rigo, M., Sprovieri, M., Stellin, F., Zaffani, M., 2016, The Norian/Rhaetian boundary interval at Pignola-Abriola section (southern Apennines, Italy) as a GSSP candidate for the Rhaetian stage: an update: Albertiana, v. 43, p. 6-19.

Bertinelli, A., Ciarapica, G. and Passeri, L., 2005a, Late Triassic-Jurassic basinal successions in Molise and northern Basilicata: the northernmost witness of the Lagonegro domain: Bollettino Società Geologica Italiana, v. 124, p. 177–188.

Bertinelli, A., Ciarapica, G., De Zanche, V., Marcucci, M., Mietto, P., Passeri, L., Rigo, M. and Roghi, G., 2005b, Stratigraphic evolution of the Triassic–Jurassic Sasso di Castalda succession (Lagonegro basin, Southern Apennines, Italy): Bollettino Società Geologica Italiana, v. 124, p. 161–175.

Blackburn, T.J., Olsen, P.E., Bowring, S.A., McLean, N.M., Kent, D.V., Puffer, J., McHone, G., Rasbury, E.T., Et-Touhami, M., 2013, Zircon U-Pb Geochronology Links the End-Triassic Extinction with the Central Atlantic Magmatic Province: Science, v. 340, p. 941.

Blattler C. L., Henderson G. M. and Jenkyns H. C., 2012. Explaining the Phanerozoic Ca isotope history of seawater. Geology 40, 843–846.

Bomfleur, B., Schöner, R., Schneider, J.W., Viereck, L., Kerp, H., McKellar, J.L., 2014, From the Transantarctic Basin to the Ferrar Large Igneous Province-New palynostratigraphic age constraints for Triassic–Jurassic sedimentation and magmatism in East Antarctica: Review of Palaeobotany and Palynology, v. 207, p. 18–37.

Bonis, N.R., Kürschner, W.M. and Krystyn, L., 2009. A detailed palynological study of the Triassic-Jurassic transition in key sections of the Eiberg Basin (Northern Calcareous Alps, Austria). Review of Palaeobotany and Palynology, 156(3-4): 376-400.

Brodie, C. R., J. S. L. Casford, J. M. Lloyd, M. J. Leng, T. H. E. Heaton, C. P. Kendrick, and Z. Yongqiang, 2011b. Evidence for bias in C/N, d13C and d15N values of bulk organic matter, and on environmental interpretation, from a lake sedimentary sequence by pre-analysis acid treatment methods. Quat. Sci. Rev., 30, 3076–3087, doi:10.1016/j.quascirev.2011.07.003.

Broecker, W.S., Li, Y.H., 1970, Interchange of water between the major oceans: Journal of Geophysical Research, v. 75, p. 3545-3552.

Byers, B.A., Ash, S.R., Chaney, D., DeSoto, L., 2014, First known fire scar on a fossil tree trunk provides evidence of Late Triassic wildfire: Palaeogeography, Palaeoclimatology, Palaeoecology, v. 411, p. 180-187.

Caldeira, K. and Wickett, M.E., 2003. Anthropogenic carbon and ocean pH. Nature, 425,365.

Callegaro, S., Rigo, M., Chiaradia, M. & Marzoli, A., 2012, Latest Triassic marine Sr isotopic variations, possible causes and implications: Terra Nova, v. 24, p. 130–135.

Campbell, I.H., Czamanske, G.K., Fedorenko, V.A., Hill, R.I., Stepanov, V., 1992. Synchronism of the Siberian Traps and the Permian-Triassic Boundary. Science, 258, 1760-1763.

Carter, E.S. 1993. Biochronology and paleontology of uppermost Triassic (Rhaetian) radiolarians, Queen Charlotte Islands, British Columbia, Canada. Mémoires de Géologie (Lousanne), 11, 175 pp.

Casacci, M., Bertinelli, A., Algeo, T.J., Rigo, M., 2016, Carbonate to biosilica transition at the Norian-Rhaetian boundary controlled by rift-related subsidence in the western Tethyan Lagonegro Basin (southern Italy): Palaeogeography, Palaeoclimatology, Palaeoecology, http://dx.doi.org/10.1016/j.palaeo.2016.05.007.

Catalano, R., Doglioni, C. and Merlini, S., 1991, On the Mesozoic Ionian basin: Geophysical Journal International, v. 144, p. 49–64.

Channell, J.E.T., Kozur, H.W., Sievers, T., Mock, R., Aubrecht, R. & Sykora, M. 2003. Carnian–Norian biomagnetostratigraphy at Silická Brezová (Slovakia): correlation to other Tethyan sections and to the Newark Basin. Palaeogeography, Palaeoclimatology, Palaeoecology, 191 (2), 65-109.

Charlier B. L. A., Nowell G. M., Parkinson I. J., Kelley S. P., Pearson D. G. and Burton K. W., 2012. High temperature strontium stable isotope behaviour in the early solar system and planetary bodies. Earth Planet. Sci. Lett. 329–330, 31–40.

Ciarapica, G. & Passeri, L. 2002. The palaeogeographic duplicity of the Apennines. Bollettino della Società Geologica Italiana, 121 (1), 67-75.

Ciarapica, G. & Passeri, L. 2005. Ionian Tethydes in the Southern Apennines. In: Finetti, I.R. (Ed.), CROP Project: Deep Seismic Exploration of the Central Mediterranean and Italy. Elsevier, Amsterdam, 209-224.

Ciarapica, G. and Passeri, L., 1998, Evoluzione paleogeografica degli Appennini: Atti Tic. Sc. Terra, v. 40; p. 233-29.

Ciarapica, G., Cirilli, S., Fratoni, R.P., Passeri, L. & Zaninetti, L. 1990. The Monte Facito Formation (Southern Apennines). Bollettino della Società Geologica Italiana, 109 (1), 135-142.

Cirilli, S., Galli, M.T., Jadoul, F., Rettori, R., Spina, A., 2000. Implicazioni stratigrafico-paleoclimatiche ed evoluzione paleogeografica della successione Retico-Hettangiana del Monte Albenza (Prealpi Bergamasche). In: A. Cherchi and C. Corradini (eds), Crisi biologiche, radiazioni adattative e dinamica delle piattaforme carbonatiche.

Cirilli, S., Marzoli, A., Tanner, L., Bertrand, H., Buratti, N., Jourdan, F., Bellieni, G., Kontak, D., Renne, P.R., 2009. Latest Triassic onset of the Central Atlantic Magmatic Province (CAMP) volcanism in the Fundy Basin (Nova Scotia): New stratigraphic constraints. Earth and Planetary Science Letters 286 (3–4), 514–525.

Cleveland, D.M., Nordt, L.C., Dworkin, S.I., Atchley, S.C., 2008, Pedogenic carbonate isotopes as evidence for extreme climatic events preceding the Triassic-Jurassic boundary: implications for the biotic crisis?: Geological Society of America Bullettin, v. 120, p. 1408-1415.

Cohen, A. S., Coe, A. L., 2007, The impact of the Central Atlantic Magmatic Province on climate and on the Sr- and Os-isotope evolution of seawater: Palaeogeogr. Palaeoclimatol. Paleoecol., v. 244, p. 374–390.

Coplen, T.B., Brand, W.A., Gehre, M., Gröning, M., Meijer, H.A., Toman, B. & Verkouteren, R.M. 2006. New guidelines for $\delta^{13}C$ measurements.Analytical Chemistry, 78 (7), 2439-2441.

Courtillot, V.E., Renne, P.R., 2003, On the ages of flood basalt events: Geoscience, v. 335, p. 113–140.

Cramer, B.D., Saltzman, M.R., 2007, Early Silurian paired $d^{13}C_{carb}$ and $d^{13}C_{org}$ analyses from the Midcontinent of North America: Implications for paleoceanography and paleoclimate: Palaeogeography, Palaeoclimatology, Palaeoecology, v. 256, p. 195-203.

Dagys, A.S. and Dagys, A.A., 1994, Global correlation of the terminal Triassic. In: Guex, J., Baud, A. (eds): Recent Developments on Triassic Stratigraphy. Memoires de Geologie, Lausanne, v. 22, p. 25–34.

Dal Corso, J., Gianolla, P., Newton, R.J., Franceschi, M., Roghi, G., Caggiati, M., Raucsik, B., Budai, T., Haas, J., Preto, N., 2015, Carbon isotope records reveal synchronicity between carbon cycle perturbation and the “Carnian Pluvial Event” in the Tethys realm (Late Triassic): Global and Planetary Change, v. 127 , p. 79-90.

Dal Corso, J., Marzoli, A., Tateo, F., Jenkyns, H.C., Bertrand, H., Youbi, N., Mahmoudi, A., Font, E., Buratti, N., Cirilli, S., 2013, The dawn of CAMP volcanism and its bearing on the end-Triassic carbon cycle disruption: The Geological Society of London, v. 171, p. 153-164.

Dal Corso, J., Mietto, P., Newton, R.J., Pancost, R.D., Preto, N., Roghi, G., Wignall, P.B., 2014, Discovery of a major negative δ13C spike in the Carnian (Late Triassic) linked to the eruption of Wrangellia flood basalts: Geology, v. 40, p. 79–82, doi:10.1130/G32473.1.

Deenen, M.H.L., Ruhl, M., Bonis, N.R., Krijgsman, W., Kuerschner, W.M., Reitsma. M., van Bergen, M.J., 2010. A new chronology for the end-Triassic mass extinction. Earth and Planetary Science Letters, 291, 113–125.

Diakow, L., Orchard, M.J., and Friedman, R., 2011, Absolute ages for the Norian Stage: a contribution from southern British Columbia, Canada: Canadian Paleontology Conference, Proceedings no. 9, p. 27-28.

Diener, A., Ebneth, S., Veizer, J. & Buhl, D., 1996. Strontium isotope stratigraphy of the Middle Devonian: brachiopods and conodonts. Geochimica et Cosmochimica Acta, 60, 639–652.

Epstein, A.G., Epstein, J.B. & Harris, L.D. 1977. Conodont color alteration; an index to organic metamorphism (No. 995). US Govt. Print. Off.

Ernst, R.E., and Buchan, K.L., 1997. Giant radiating dyke swarms: Their use in identifying pre-Mesozoic large igneous provinces and mantle plumes, in Mahoney, J.J., and Coffin, M.F., eds., Large igneous provinces: Continental, oceanic, and planetary flood volcanism: American Geophysical Union Geophysical Monograph, 100, 297-333.

Ernst, R.E., and Buchan, K.L., 1998. Arcuate dyke swarms associated with mantle plumes on Earth: Implications for Venusian coronae [extended abstract]: Houston, Texas, Lunar and Planetary Institute, v. 29, p. CD-ROM 1021.dpf.

Ernst, R.E., Buchan, K.L., 2001, Large mafic magmatic events through time and links to mantle-plume heads: Geological Society of America Special Paper, v. 352, p. 483-575.

Ernst, R.E., Wingate, M.T.D., Buchan, K.L., Li, Z.X.., 2008, Global record of 1600–700 Ma Large Igneous Provinces (LIPs): Implications for the reconstruction of the proposed Nuna (Columbia) and Rodinia supercontinents: Precambrian Research, v. 160, p. 159–178, doi: 10.1016/j.precamres.2007.04.019.

Erwin, D. H., 2006, Extinction: How Life on Earth Nearly Ended 250 Million Years Ago: Princeton University Press, Princeton.

Fåhræus, L.E. & Ryley, C.C. 1989. Multielement species of *Misikella* Kozur and Mock, 1974 and *Axiothea* n. gen. (Conodonta) from the Mamonia Complex (Upper Triassic), Cyprus. Canadian Journal of Earth Sciences, 26 (6), 1255-1263.

Farkas J., Bohm F., Wallmann K., Blenkinsop J., Eisenhauer A., van Geldern R., Munnecke A., Voigt S. and Veizer J., 2007. Calcium isotope record of Phanerozoic oceans: Implications for chemical evolution of seawater and its causative mechanisms. Geochim. Cosmochim. Acta 71, 5117–5134.

Faure, G., 1986, Principles of Isotope Geology: second edition, John Wiley and Sons, New York, p. 589.

Fernandes, M., and Krull E., 2008. How does acid treatment to remove carbonates affect the isotopic and elemental composition of soils and sediments?. Environ. Chem., 5, 33–39, doi:10.1071/EN07070.

Finetti, I., 1982, Structure, stratigraphy and evolution of central Mediterranean: Boll. Geofis. Teor. Appl., v. 24, p. 247–315.

Finetti, I., Lentini, F., Carbone, S., Catalano, S., Del Ben, A., 1996, Il sistema Appennino Meridionale-Arco Calabro-Sicilia nel Mediterraneo Centrale: studio geologico-geofisico: Boll. Soc. Geol. Ital., v. 115, p. 529–559.

Fio, K., J. E. Spangenberg, I. Vlahović, J. Sremac, I. Velić, and E. Mrinjek, 2010. Stable isotope and trace element stratigraphy across the Permian–Triassic transition: A redefinition of the boundary in the Velebit Mountain, Croatia. Chem. Geol., 278, 38–57, doi:10.1016/j.chemgeo.2010.09.001.

Froelich, P. N., 1980. Analysis of organic carbon in marine sediments. Limnol. Oceanogr., 25, 564–572, doi:10.4319/lo.1980.25.3.0564.

Furin, S., Preto, N., Rigo. M., Roghi, G., Gianolla, P., Crowley, J.L. & Bowring, S.A., 2006, High precision U–Pb zircon age from the Triassic of Italy: implications for the Triassic time scale and the Carnian origin of calcareous nannoplankton and dinosaurs: Geology, v. 35, p. 146.

Gallet, Y., Krystyn, L., Marcoux, J. & Besse, J. 2007. New constraints on the end-Triassic (Upper Norian–Rhaetian) magnetostratigraphy. Earth and Planetary Science Letters, 255 (3), 458-470.

Galli, M. T., Jadoul, F., Bernasconi, S. M., Cirilli, S., and Weissert H., 2007. Stratigraphy and palaeoenvironmental analysis of the Triassic-Jurassic transition in the western southern Alps (northern Italy). Palaeogeogr. Palaeoclimatol. Palaeoecol., 244, 52–70.

Galli, M.T., 2002. Il limite Triassico-Giurassico neele Prealpi Bergamasche: un approccio stratigrafico integrato. PhD tesi, University of Milan.

Galli, M.T., Jadoul, F., Bernasconi, S.M., Weissert, H., 2005, Anomalies in global carbon cycling at the Triassic/Jurassic boundary: evidence from a marine C-isotope record: Palaeogeogr. Palaeoclimatol. Palaeoecol., v. 216, p. 203–214.

Galy, V., J. Bouchez, and C. France-Lanord, 2007. Determination of total organic carbon content and d13C in carbonaterich detrital sediments. Geostand. Geoanal. Res., 31, 199–207, doi:10.1111/j.1751-908X.2007.00864.x.

Garrett, C., St. Laurent, L., 2002, Aspects of deep ocean mixing: Journal of Oceanography, v. 58, p. 11-24.

Gawlick, H.J., Bohm, F., 2000, Sequence and isotope stratigraphy of Late Triasic distal periplatform limestones from the Nothern Calcareous Alps (Kälberstein Quarry, Berchtesgaden Hallstatt Zone): Int. J. Earth Sciences, v. 89, p. 108-129.

Gazdzicki, A. 1978. Conodonts of the genus Misikella Kozur and Mock, 1974 from the Rhaetian of the Tatra Mts (West Carpathians). Acta Palaeontologica Polonica, 23 (3), 341-354.

Gazdzicki, A., Kozur, H.W. & Mock, R. 1979. The Norian-Rhaetian boundary in the light of micropaleontological data. Geologija, 22 (1), 71-112.

Giordano, N., Ciarapica, G., Bertinelli, A. & Rigo, M., 2011, The Norian-Rhaetian interval in two sections of the Lagonegro area: the transition from carbonate to siliceous deposition: Italian Journal of Geoscience, v. 130, p. 380–393.

Giordano, N., Rigo, M., Ciarapica, G. & Bertinelli, A., 2010, New biostratigraphical constraints for the Norian/Rhaetian boundary: data from Lagonegro Basin, Southern Apennines, Italy: Lethaia, v. 43, p. 573–586.

Gordon, A. L., 1973, Physical Oceanography Antarctic: Journal of the United States, v. 8, p. 61-69.

Gradstein, F.M., Ogg, J.G., Schmitz, M.D. and Ogg, G.M., eds, 2012, The Geological Time Scale 2012: Amsterdam, Elsevier, 2 vols., 1144 pp.

Greenberg, J.M., 1998, Making a comet nucleus: Astronomy and Astrophysics, v. 330, p. 375–380.

Greene, S.E., Bottjer, D.J., Corsetti, F.A., Berelson, W.M., Zonneveld, J.P., 2010, Might ocean acidification leave a diagenetic record?: Geological Society of America Abstracts with Programs, 42 (5), 437.

Greene, S.E., Martindale, R.C., Ritterbush, K.A., Bottjer, D.J., Corsetti, F.A., Berelson, W.M., 2012, Recognizing ocean acidification in deep time: An evaluation of the evidence for acidification across the Triassic-Jurassic boundary: Earth-Science Reviews, v. 113, p. 72-93.

Grice, K., Cao, C., Love, G. D., Böttcher, M. E., Twitchett, R. J., Grosjean, E., & Jin, Y., 2005. Photic zone euxinia during the Permian-Triassic superanoxic event. Science, 307(5710), 706-709.

Guex, J., Bartolini, A., Atudorei, V. & Taylor, D., 2004, High-resolution ammonite and carbon isotope stratigraphy across the Triassic–Jurassic boundary at New York Canyon (Nevada): Earth and Planetary Science Letters, v. 225, p. 29–41.

Hallam, A., 2002, How catastrophic was the end-Triassic mass extinction?: Lethaia, v. 35, p. 147-157.

Hallam, A., Wignall, P.B., 1999. Mass extinction and sea level change. Earth-Science Review, 48, 217– 258.

Hames, W.E., Renne, P.R., Ruppel, C., 2000. New evidence for geologically instantaneous emplacement of earliest Jurassic Central Atlantic magmatic province basalts on the North American margin. Geology 28, 859–862.

Hardie L. A., 1996. Secular variation in seawater chemistry: An explanation for the coupled secular variation in the mineralogies of marine limestones and potash evaporites over the past 600 m.y. Geology, 24, 279–283.

Hastie, W.W., Watkeys, M.K., Aubourg, C., 2014, Magma flow in dyke swarms of the Karoo LIP: Implications for the mantle plume hypothesis: Gondwana Research, v. 25, p. 736–755.

Hauser, M., Martini, R., Burns, S., Dumitrica, P., Krystyn, L., Matter, A., Peters, T. and Zaninetti, L., 2001, Triassic stratigraphic evolution of the Arabian-Greater India embayment of the southern Tethys margin: Eclogae Geologicae Helvetiae, v. 94, p. 29-62.

Hayes, J.M., Strauss, H., Kaufman, A.J., 1999, The abundance of 13C in marine organic matter and isotopic fractionation in the global biogeochemical cycle of carbon during the past 800 Ma: Chem. Geol., v. 161, p. 103–125.

Hesselbo, S. P., McRoberts, C. A., and Pálfy, J., eds., 2007. Special Issue: Triassic-Jurassic Boundary Events: Palaeogeography, Palaeoclimatology, Palaeoecology, v. 244. 423 p.

Hesselbo, S.P., Robinson, S.A., Surlyk, F. & Piasecki, S., 2002, Terrestrial and marine extinction at the Triassic-Jurassic boundary synchronized with major carbon- cycle perturbation: a link to initiation of massive volcanism?: Geology, v. 30, p. 251–254.

Heuser, A., Eisenhauer, A., Gussone, N., Bock, B., Hansen, B.T., Nägler, Th.F., 2002. Measurement of calcium isotopes (δ44Ca) using a multicollector TIMS technique. International Journal of Mass Spectrometry 220, 385–397.

Higgins, J.A. & Schrag, D.P., 2006, Beyond methane: towards a theory for the Paleocene–Eocene thermal maximum: Earth Planetary Science Letters, v. 245, p. 523–537.

Hillebrandt, A.V., Krystyn, L. and Kürschner, W.M., 2007. A candidate GSSP for the base of the Jurassic in the Northern Calcareous Alps (Kuhjoch section, Karwendel Mountains, Tyrol, Austria). International Subcommission on Jurassic Stratigraphy Newsletter, 34(1): 2-20.

Hodell, D.A, Mead, G., Mueller, P.A., 1990, Variation in the strontium isotopic composition of seawater (8 Ma to present); implications for chemical weathering rates and dissolved fluxes to the oceans: Chemical Geology, v. 80, no. 4, p. 291-307, doi:10.1016/0168-9622(90)90011-Z.

Hodell, D.A; Mueller, P.A; McKenzie, J.A; Mead, G., 1989, Strontium isotope stratigraphy and geochemistry of the late Neogene ocean: Earth and Planetary Science Letters, v. 92, no. 2, p. 165-178, doi:10.1016/0012-821X(89)90044-7.

Holmden, C., Creaser, R.A., Muehlenbachs, K., Leslie, S.A., Bergstrom, S.M., 1998, Isotopic evidence for geochemical decoupling between ancient epeiric seas and bordering oceans: Implications for secular curves: Geology, v. 26, p. 567–570.

Hönisch et al., 2012. The Geological Record of Ocean Acidification. Science, 335, 1058-1063.

Hornung, T., Brandner, R., 2005, Biochronostratigraphy of the Reingraben Turnover (Hallstatt Facies Belt): Local black shale events controlled by regional tectonics, climatic change and plate tectonics: Facies, v. 51, p. 460-479.

Hounslow, M.W. & Muttoni, G. 2010. The geomagnetic polarity timescale for the Triassic: linkage to stage boundary definitions. Geological Society, London, Special Publications, 334 (1), 61-102.

Hounslow, M.W., Posen, P.E., Warrington, G., 2004. Magnetostratigraphy and biostratigraphy of the Upper Triassic and lowermost Jurassic succession, St. Audrie's Bay, UK. Palaeogeogr. Palaeoclimatol. Palaeoecol., 213, 331–358.

Huang S., Farkas J. and Jacobsen S. B., 2010. Calcium isotopic fractionation between clinopyroxene and orthopyroxene from mantle peridotites. Earth Planet. Sci. Lett. 292, 337–344.

Huon, S., F. E. Grousset, D. Burdloff, G. Bardoux, and A. Mariotti, 2002. Sources of fine-sized organic matter in North Atlantic Heinrich layers: d13C and d15N tracers, Geochim. Cosmochim. Acta, 66, 223–239, doi:10.1016/S0016-7037(01)00776-1.

Hüsing, S. K., Deenen, M. H., Koopmans, J. G. & Krijgsman, W. 2011. Magnetostratigraphic dating of the proposed Rhaetian GSSP at Steinbergkogel (Upper Triassic, Austria): Implications for the Late Triassic time scale. Earth and Planetary Science Letters, 302 (1), 203-216.

Huynh, T.T., Poulsen, C.J., 2005, Rising atmospheric CO2 as a possible trigger for the end-Triassic mass extinction: Palaeogeography, Palaeoclimatology, Palaeoecology, v. 217, p. 223-242.

Immenhauser, A., Della Porta, G., Kenter, J.A.M., Bahamonde, J.R., 2003, An alternative model for positive shifts in shallow-marine carbonate d13C and d18O: Sedimentology, v. 50, p. 953–959.

IPCC, 2014: Climate Change 2014: Synthesis Report. Contribution of Working Groups I, II and III to the Fifth Assessment Report of the Intergovernmental Panel on Climate Change [Core Writing Team, R.K. Pachauri and L.A. Meyer (eds.)]. IPCC, Geneva, Switzerland, 151 pp.

Jadoul, F, Gnaccolini, M., 1992. Sedimentazione ciclica nel Trias Lombardo: osservazioni e prospettive. Rivista Italiana di Paleontologia e Stratigrafia, 97, 307-328.

Jadoul, F., and Galli, M. T., 2008. The Hettangian shallow water carbonates after the Triassic/Jurassic biocalcification crisis: The Albenza formation in the western Southern Alps. Riv. Ital. Paleontol. Stratigr., 114, 453–470.

Jadoul, F., Galli, M.T., Berra, F., Cirilli, S., Ronchi, P., Paganoni, A., 2004. The Late Triassic–Early Jurassic of the Lombardy Basin: stratigraphy, palaeogeography and palaeontology. 32nd International Geological Congress, Field Trip Guide Book, P68, 6, 36 pp.

Jenkyns, H.C., 2010, Geochemistry of oceanic anoxic events: Geochemistry Geophysics Geosystems, v. 11, p. 1-30.

Jerram, D.A., Widdowson, M., 2005, The anatomy of continental flood basalt provinces. Geological constraints on the processes and products of flood volcanism: Lithos, v. 79, p. 385–405, doi: 10.1016/j.lithos.2004.09.009.

Jin, Y. G., Wang, Y., Wang, W., Shang, Q. H., Cao, C. Q., & Erwin, D. H., 2000. Pattern of marine mass extinction near the Permian-Triassic boundary in South China. Science, 289(5478), 432-436.

Jones, C.E. and Jenkyns, H.C., 2001, Seawater strontium isotopes, oceanic anoxic events, and seafloor hydrothermal activity in the Jurassic and Cretaceous: Am. J. Sci., v. 301, p. 112–149.

Jourdan, F., Féraud, G., Bertrand, H., Watkeys, M.K., Renne, P.R., 2007, Distinct brief major events in the Karoo large igneous province clarified by new $^{40}Ar/^{39}Ar$ ages on the Lesotho basalts: Lithos, v. 98, p. 195–209.

Kaiho, K., Chen, Z.Q., Sawada, K., 2009, Possible causes for a negative shift in the stable carbon isotope ratio before, during and after the end-Permian mass extinction in Meishan, South China: Australian Journal of Earth Sciences, v. 56, p. 799–808.

Kemp, D.B., Coe, A.L., Cohen, A.S., Schwark, L., 2005, Astronomical pacing of methane release in the early Jurassic period: Nature, v. 437, p. 396‑399.

Kennedy, P., H. Kennedy, and S. Papadimitriou, 2005. The effect of acidification on the determination of organic carbon, total nitrogen and their stable isotopic composition in algae and marine sediment. Rapid Commun. Mass Spectrom., 19, 1063–1068, doi:10.1002/rcm.1889.

Kent, D.V., and Muttoni, G., 2003. Mobility of Pangea: Implications for Late Paleozoic and early Mesozoic paleoclimate. P.M. Letourneau, P.E. Olsen, Editors, The Great Rift Valleys of Pangea in Eastern North America. Tectonics, Structure, and Volcanism. Volume 1, 12-20, Columbia University Press.

Kent, D.V., Olsen, P.E., 2008. Early Jurassic magnetostratigraphy and paleolatitudes from the Hartford continental rift basin (eastern North America): Testing for polarity bias and abrupt polar wander in association with the central Atlantic magmatic province. Journal of Geophysical Research B: Solid Earth 113 (6), 1–24.

Kleypas. J.A., Feely, R.A., Langdon, C., Sabine, C.L., Robbins, L.L., 2006. Impacts of Ocean Acidification on Coral Reefs and Other Marine Calcifiers: A Guide for Future Research, report of a workshop held 18-20 April 2005, St. Petersburg, FL, sponsored by NSF, NOAA, and the U.S. Geological Survey, 88pp.

Konitzer, S.F., Leng, M.J., Davies, S.J., Stephenson, M.H., 2012. An assessment of geochemical preparation methods prior to organic carbon concentration and carbon isotope ratio analyses of fine-grained sedimentary rocks. Geochem., Geophys., Geosys., 13, 1-12, doi:10.1029/2012GC004094.

Korte, C., Kozur, H.W., Bruckschen, P. & Veizer, J., 2003, Strontium isotope evolution of Late Permian and Triassic seawater: Geochemica et Cosmochimica Acta, v. 67, p. 47–62.

Korte, C., Kozur, H.W., Veizer, J., 2005, 13C and 18O values of Triassic brachiopods and carbonate rocks as proxies for coeval seawater and palaeotemperature: Palaeogeography, Palaeoclimatology, Palaeoecology, v. 226, p. 287–306.

Kozur, H. & Mock, R., 1991, New Middle Carnian and Rhaetian conodonts from Hungary and the Alps, stratigraphic importance and tectonic implications for the Buda Mountains and adjacent areas: Jahrbuch der Geologischen Bundesanstalt, v. 134, p. 271–297.

Kozur, H.W & Mock, R. 1974. *Misikella posthernsteini* n. sp., die jündste Conodontenart der tethyalen Trias. *Ćasopis* Mineral. Geology, 19, 245-250.

Krabbenhoft A., Eisenhauer A., Bohm F., Vollstaedt H., Fietzke J., Liebetrau V., Augustin N., Peucker-Ehrenbrink B., Hansen B. T., Nolte N. and Wallmann K., 2010. Constraining the marine strontium budget with natural strontium isotope fractionations (87Sr/86Sr*–d88/86Sr) of carbonates, hydrothermal solutions and river waters. Geochim. Cosmochim. Acta 74, 4097–4109.

Krabbenhoft A., Fietzke J., Eisenhauer A., Liebetrau V., Bohm F. and Vollstaedt H. (2009) Determination of radiogenic and stable strontium isotope ratios (87Sr/86Sr; d88/86Sr) by thermal ionization mass spectrometry applying an 87Sr/84Sr double spike. J. Anal. At. Spectrom. 24, 1267–1271.

Krystyn, L. 1980. Triassic conodont localities of the Salzkammergut region. Abh. Geol. B.-A, 35, 61-98.

Krystyn, L. 1990. A Rhaetian stage-chronostratigraphy, subdivisions and their intercontinental correlation. Albertiana, 8, 15-24.

Krystyn, L. 2008. An ammonoid-calibrated Tethyan conodont time scale of the late Upper Triassic. Berichte der Geologischen Bundesanstalt, 76, 9-11.

Krystyn, L. 2010. Decision report on the defining event for the base of the Rhaetian stage. Albertiana, 38, 11-12.

Krystyn, L., Boehm, F., Kürschner, W.M. and Delecat, S., 2005. The Triassic-Jurassic boundary in the Northern Calcareous Alps. In: Palfy J. and Oszvart P. (Eds), Program, Abstracts and Field Guide. 5th Field Workshop of IGCP 458 Project (Tata and Hallein, September 2005).

Krystyn, L., Bouquerel, H., Kuerschner, W., Richoz, S. & Gallet, Y. 2007a. Proposal for a candidate GSSP for the base of the Rhaetian Stage. The Global Triassic. New Mexico Museum of Natural History and Science Bulletin, 41, 189-199.

Krystyn, L., Richoz, S., Gallet, Y., Bouquerel, H., Kürschner, W.M., Spotl, C., 2007. Updated bio- and magnetostratigraphy from Steinbergkogel (Austria), candidate GSSP for the base of the Rhaetian stage. Albertiana, 36: 164-173.

Kump, L.R., Arthur, M.A., 1999, Interpreting carbon-isotope excursions: carbonates and organic matter: Chemical Geology, v. 161, p. 181-198.

Kuroda, J., Hori, R.S., Suzuki, K., Grocke, D.R., Ohkouchi, N., 2010, Marine osmium isotope record across the Triassic-Jurassic boundary from a Pacific pelagic site: Geology, v. 38, p. 1095–1098.

Kürschner, W.M., Bonis, N.R. and Krystyn, L., 2007. Carbon-isotope stratigraphy and palynostratigraphy of the Triassic-Jurassic transition in the Tiefengraben section - Northern Calcareous Alps (Austria). Palaeogeography, Palaeoclimatology, Palaeoecology, 244(1-4): 257-280.

Lakew, T., 1990. Microfacies and cyclic sedimentation of the Upper Triassic (Rhaetian) Calcare di Zu (Southern Alps). Facies, 22, 187–232.

Larson, T. E., J. M. Heikoop, G. Perkins, S. J. Chipera, and M. A. Hess, 2008. Pretreatment technique for siderite removal for organic carbon isotope and C:N ratio analysis in geological samples. Rapid Commun. Mass Spectrom., 22, 865–872, doi:10.1002/rcm.3432.

Lehn, G.O., Jacobson, A.D., 2015. Optimization of a 48Ca-43Ca double spike MC-TIMS method for measuring Ca isotope ratios (d44/40Ca and d44/42Ca): limitations from filament reservoir mixing. J. Anal. At. Spectrom. http://dx.doi.org/10.1039/C4JA00412D

Longridge, L.M., Carter, E S., Smith, P.L. & Tipper, H.W. 2007. Early Hettangian ammonites and radiolarians from the Queen Charlotte Islands, British Columbia and their bearing on the definition of the Triassic–Jurassic boundary. Palaeogeography, Palaeoclimatology, Palaeoecology, 244(1), 142-169.

Lucas, S. G. & Orchard, M. J., 2004, Triassic. In: Selley, R. C., Cocks, L. M. R. & Plimer, I. R. (eds) Encyclopedia of Geology. Elsevier, Amsterdam, p. 344–351.

Lucas, S. G., 1999, The epicontinental Triassic, an overview: Zentralblatt fur Geologie und Palaontologie Teil I, 1998, p. 475–496.

Lucas, S.G., 2010, The Triassic Timescale. Geological Society, London, special publication, v. 334, p. 103-118.

Majzon, L., 1954. Contributions to the stratigraphy of the Dachstein-Limestone. Budapest Acta Geol. Acad. Sci. Hongrie, 2, 243–249.

Maron, M., Rigo, M., Bertinelli, A., Katz, M.E., Godfrey, L., Zaffani, M., and Muttoni, G., 2015, Magnetostratigraphy, biostratigraphy and chemostratigraphy of the Pignola-Abriola section: New constraints for the Norian-Rhaetian boundary: Geological Society of America Bulletin, v. 127, p. 962-974, doi:10.1130/B31106.1.

Marzoli A., Bertrand, H., Chiaradia, M., Fontignie, D., Youbi, N., Bellieni, G., 2006°, The genesis of CAMP basalts (Morocco) from enriched lithosphere to late asthenosphere mantle sources: Geochimica et Cosmochimica Acta, v. 70, p. 396, doi: 10.1016/j.gca.2006.06.799.

Marzoli, A., Bertrand, H., Knight, K.B., Cirilli, S., Buratti, N., Vérati, C., Nomade, S., Renne, P.R., Youb,i N., Martini, R., Allenbach, K., Neuwerth, R., Rapaille, C., Zaninetti, L., Bellieni, G., 2004, Synchrony of the Central Atlantic magmatic province and the Triassic-Jurassic boundary climatic and biotic crisis: Geology, v. 32, p. 973–976.

Marzoli, A., Rapaille, C., Reisberg, L., Bertrand, H., 2006b, Trace element and Sr-Nd-Pb-Os evidence for a lithospheric mantle source for the European CAMP basalts: Geochimica et Cosmochimica Acta, v. 70, p. 397.

Marzoli, Andrea, Renne, P.R., Piccirillo, E.M., Ernesto, M., Bellieni, G., and De Min, A., 1999. Extensive 200 Million-Year-Old Continental Flood Basalts of the Central Atlantic Magmatic Province, *Science*, 284, 616-618.

Mazza, M., Furin, S., Spötl, C., Rigo, M., 2010, Generic turnovers of Carnian/Norian conodonts: climatic control or competition?: Palaeogeogr. Palaeoclimatol. Palaeoecol., v. 290, p. 120–137.

Mazza, M., Rigo, M. & Gullo, M. 2012. Taxonomy and biostratigraphic record of the Upper Triassic conodonts of the Pizzo Mondello section (western Sicily, Italy), GSSP candidate for the base of the Norian. Rivista Italiana di Paleontologia e Stratigrafia, 118 (1), 85-130.

McArthur, J.M., Howarth, R.J. and Shields, G.A., 2012. Strontium Isotope Stratigraphy, in The Geologic Time Scale 2012, Gradstein, F.M., Ogg, J.G., Schmitz, M., and Ogg, G. (eds.), published by Elsevier B.V. DOI: 10.1016/B978-0-444-59425-9.00007-X.

McElwain J.C., Beerling D.J., Woodward F.I., 1999, Fossil plants and global warming at the Triassic-Jurassic boundary: Science, v. 285, p. 1386-1390.

McElwain, J.C., Popa, M.E,. Hesselbo, S.P., Haworth, M., Surlyk, F., 2007. Macroecological responses of terrestrial vegetation to climatic and atmospheric change across the Triassic/Jurassic boundary in East Greenland. Paleobiology, 33, 547–573.

McElwain, J.C., Wagner, P.J. and Hesselbo, S.P., 2009. Fossil Plant Relative Abundances Indicate Sudden Loss of Late Triassic Biodiversity in East Greenland. Science, 324: 1554-1556.

McFadden, P.L. & McElhinny, M.W. 1990. Classification of the reversal test in palaeomagnetism. Geophysical Journal International, 103 (3), 725-729.

McRoberts, C.A. and Newton, C.R., 1995. Selective extinction among end-Triassic European bivalves. Geology, 23(2): 102-104.

McRoberts, C.A., Furrer, H., Jones, D.S., 1997. Palaeoenvironmental interpretation of a Triassic–Jurassic boundary section from Western Austria based on palaeoecological and geochemical data. Palaeogeogr. Palaeoclimatol. Palaeoecol., 136, 79– 95.

McRoberts, C.A., Krystyn, L. & Shea, A., 2008, Rhaetian (Late Triassic) Monotis (Bivalvia: Pectinoida) from the eastern Northern Calcareous Alps (Austria) and the end-Norian crisis in pelagic faunas: Palaeontology, v. 51, p. 721–735.

Meyers, P.A., 2014, Why are the $d^{13}C_{org}$ values in Phanerozoic black shales more negative than in modern marine organic matter?: Geochemistry, Geophysiscs, Geosystems, doi: 10.1002/2014GC005305.

Miconnet, P. 1983. La région de Lagonegro (Italie méridionale): évolution géologique d'un bassin dans son cadre alpin. Doctoral dissertation III cicle, Université des Sciences et Techniques de Lille, Lille, France, 185 pp.

Miconnet, P., 1982, Precisions stratigraphiques et tectoniques dans un secteur du Lagonegro (Italie meridionale) : Annales de la Societe Geologique du Nord, v. 102, p. 17–24.

Midwood, A.J., and Boutton, T.W., 1998. Soil carbonate decomposition by acid has little effect on d13C of organic matter.Soil Biol. Biochem., 30, 1301–1307, doi:10.1016/S0038-0717(98)00030-3.

Mock, R. 1980. Field Trip D 'Triassic of the West Carpathians, in Second European conodont symposium' ECOS II. Abhandl. Geol. Bundesanst. 35, 129-144.

Mortensen, J.K and Hulbert, L.J., 1991, A U-Pb zircon age for a Maple Creek gabbro sill, Tatamagouche Creek area, southwest Yukon Territory. In: Radiogenic age and isotopic studies, Report 5, Geological Survey of Canada, Paper 91-2, p. 175-179.

Mostardini, F. & Merlini, S. 1986. Appennino Centro Meridionale - Sezioni Geologiche e Proposta di Modello Strutturale. Memorie della Società Geologica Italiana, 35, 177-202.

Mostler, H., Scheuring, R. & Ulrichs, M. 1978. Zur Mega-, Mikrofauna und Mikroflora der Kossenen Schichten (alpine Obertrias) von Weissloferbach in Tirol unter besonderer Berucksichtigung der in der suessi-und marshi-Zone auftreitenden Conodonten. Osterreichische Akademie der Wissenschaften Erdwissenschaftliche Kommission Schriftenreihe, 4, 141-174.

Muttoni, G., Kent, D.V., Jadoul, F., Olsen, P.E., Rigo, M., Galli, M.T., Nicora, A., 2010. Rhaetian magneto-biostratigraphy from the Southern Alps (Italy): Constraints on Triassic chronology. Palaeogeography, Palaeoclimatology, Palaeoecology, 285, 1–16.

Muttoni, G., Kent, D.V., Olsen, P., Di Stefano, P., Lowrie, W., Bernasconi, S., Martin Hernandez, F., 2004, Tethyan magnetostratigraphy from Pizzo Mondello (Sicily) and correlation to the Late Triassic astrochronological polarity time scale: Geol. Soc. Am. Bull., v. 116, p. 1043-1058.

Muttoni, G., Mazza, M., Mosher, D., Katz, M.E., Kent, D.V., Balini, M., 2014, A Middle–Late Triassic (Ladinian–Rhaetian) carbon and oxygen isotope record from the Tethyan Ocean: Palaeogeography, Palaeoclimatology, Palaeoecology, v. 399, p. 246-259.

Nier A. O., 1938. The isotopic constitution of strontium, barium, bismuth, thallium and mercury. Phys. Rev. 54, 275.

Nikishin, A.M., Ziegler, P.A., Stephenson, R.A., Cloetingh, S.A.P.L., Furne, A.V., Fokin, P.A., Ershov, A.V., Bolotov, S.N., Korotaev, M.V., Alekseev, A.S., Gorbachev, V.I., Shipilov, E.V., Lankreijer, A., Bembinova, E.Y., and Shalimov, I.V., 1996. Late Precambrian to Triassic history of the East European Craton: Dynamics of sedimentary basin evolution. Tectonophysics, 268, 23-63.

Nomade, S., Knight, K.B., Beutel, E., Renne, P.R., Verati, C., Féraud, G., Marzoli, A., Youbi, N., Bertrand, H., 2007. Chronology of the Central Atlantic Magmatic Province: Implications for the Central Atlantic rifting processes and the Triassic-Jurassic biotic crisis. Palaeogeography, Palaeoclimatology, Palaeoecology, 244 (1–4), 326–344.

O'Dogherty, L., Carter, E.S., Dumitrica, P., Goričan, Š., Wever, P.D., Hungerbühler, A., Bandini, A.N. & Takemura, A. 2009. Catalogue of Mesozoic radiolarian genera. Part 1: Triassic. Geodiversitas, 31 (2), 213-270.

Ogg, J.G., 2012. Triassic. In: Gradstein, F.M., Ogg, J.G., Schmitz, M.D., and Ogg, G.M., (eds) The Geologic Time Scale. Elsevier Publ., p. 681-730.

Olsen, P. E., Kent, D. V., Sues, H.-D., Koeberl, C., Huber, H., Montanari, A., Rainforth, E. C., Fowell, S. J., Szajna, M. J., Hartline, B. W., 2002. Ascent of Dinosaurs Linked to an Iridium Anomaly at the Triassic-Jurassic Boundary. Science, 296, 1305-1307.

Orchard, M.J,. 1991, Upper Triassic conodont biochronology and new index species from the Canadian Cordillera: Geological Survey of Canada Bulletin, v. 417, p. 299–335.

Orchard, M.J. & Tozer, E.T. 1997. Triassic conodont biochronology, its calibration with the ammonoid standard, and a biostratigraphic summary for the Western Sedimentary Basin. Bullettin Of Canadian Petroleum Geology, 45 (4), 675-692.

Orchard, M.J., Whalen P.A., Carter E.S. & Taylor H.J. 2007. Latest Triassic conodonts and radiolarian-bearing successions in Baja California Sur. Lucas, S.G. and Spielmann, J.A., eds., 2007, The Global Triassic. New Mexico Museum of Natural History and Science Bulletin 41, 355-365.

Palfy, J., Demeny, A., Haas, J., Carter, E.S., Gorog, A., Halasz, D., Oravecz-Scheffer, A., Hetenyi, M., Marton, E., Orchard, M.J., Ozsvart, P., Veto, I., Zaizon, N., 2007, Triassic-Jurassic boundary events inferred from integrated stratigraphy of the Csovar section, Hungary: Palaeogeography, Palaeoclimatology, Palaeoecology, v. 224, p. 11-33.

Palfy, J., Demeny, A., Haas, J., Carter, E.S., Gorog, A., Halasz, D., Oravecz-Scheffer, A., Hetenyi, M., Marton, E., Orchard, M.J., Ozsvart, P., Veto, I., Zaizon, N., 2007. Triassic-Jurassic boundary events inferred from integrated stratigraphy of the Csovar section, Hungary. Palaeogeography, Palaeoclimatology, Palaeoecology, 224, 11-33.

Palfy, J., Demeny, A., Haas, J., Hetenyi, M., Orchard, M.J., Vetl, I., 2001. Carbon isotope anomaly and other geochemical changes at the Triassic–Jurassic boundary from a marine section in Hungary. Geology, 29, 1047–1050.

Pálfy, J., Kocsis, A.T., 2014, Volcanism of the Central Atlantic magmatic province as the trigger of environmental and biotic changes around the Triassic-Jurassic boundary: Geological Society of America Special Papers, v. 505, p. SPE505-12.

Pallister, J.S., Budahn, J.R., Murchey, B.L., 1989, Pillow basalts of the Angayucham Terrane: Oceanic Plateau and Island Crust Accreted to the Brooks Range: Journal of Geophysical Research, v. 94, p. 15901-15923.

Palmer, A.R. 1983. The decade of North American geology 1983 Geologic time scale. Geology, 11 (9), 503-504.

Palmer, M.R. & Elderfield, H., 1985, Sr isotope composition of sea water over the past 75 Myr: Nature, v. 314, p. 526-528.

Palmer, M.R. and Edmond, J.M., 1989, The Strontium Isotope Budget of the Modern Ocean: Earth and Planetary Science Letters, v. 92, no. 1, p. 11-26, doi: 10.1016/0012-821X(89)90017-4.

Passeri, L., Bertinelli, A. and Ciarapica, G., 2005, Palaeogeographic meaning of the late Triassic–Early Jurassic Lagonegro units: Bollettino Società Geologica Italiana, v. 124, p. 231–245.

Payne, J.L., Lehrmann, D.J., Wei, J., Orchard, M.J., Schrag, D.P., Knoll, A.H., 2004, Large perturbations of the carbon cycle during recovery from the end-Permian extinction: Nature, v. 305, p. 506–509.

Pearson, D.A.B. 1970. Problems of Rhaetian stratigraphy with special reference to the lower boundary of the stage. Quarterly Journal of the Geological Society, 126 (1-4), 125-150.

Pogge von Strandmann, P.A.E., Jenkyns, H.C., Woodfine, R.G., 2013, Lithium isotope evidence for enhanced weathering during Oceanic Anoxic Event 2: Nature Geoscience, v. 6, no. 8, p. 668-672, doi:10.1038/ngeo1875.

Preto, N., Agnini, C., Rigo, M., Sprovieri, M., Westphal, H., 2013, The calcareous nannofossil Prinsiosphaera achieved rock-forming abundances in the latest Triassic of western Tethys: consequences for the $\delta^{13}C$ of bulk carbonate: Biogeosciences, v. 10, p. 6053-6068.

Preto, N., Kustatscher, E., and Wignall, P.B., 2010, Triassic climates—State of the art and perspectives: Palaeogeography, Palaeoclimatology, Palaeoecology, v. 290, p. 1–10, doi:10.1016/j.palaeo.2010.03.015.

Preto, N., Rigo, M., Agnini, C., Bertinelli, A., Guaiumi, C., Borello, S.,Westphal, H., 2012, Triassic and Jurassic calcareous nannofossils of the Pizzo Mondello section: a SEM study: Riv. Ital. Paleontol. Stratigr., v. 118, no. 1, p. 131–141.

Prokoph, A., El Bilali, H., Ernst, R., 2013, Periodicities in the emplacement of large igneous provinces through the Phanerozoic: Relations to ocean chemistry and marine biodiversity evolution: Geoscience Frontiers, v. 4, p. 263-276.

Ramezani, J., Bowring, S.A., Pringle, M.S., Winslow III, F.D., Rasbury, E.T., 2005, The Manicouagan impact melt rock: a proposed standard for the intercalibration of U–Pb and 40Ar/39Ar isotopic systems: Geochim. Cosmochim. Acta Suppl., v. 69, p. A321.

Ramezani, J., Hoke, G.D., Fastovsky, D.E., Bowring, S.A., Therrien, F., Dworkin, S.I., Atchley, S.C., Nordt, L.C., 2011, High precision U-Pb zircon geochronology of the Late Triassic Chinle Formation, Petrified Forest National Park (Arizona, USA): temporal constraints on the early evolution of dinosaurs: Geol. Soc. Am. Bull., v. 123, p. 2142-2159.

Rampino, M.R., and R.B. Stothers, 1988, Flood basalt volcanism during the past 250 million years: Science, v. 241, p. 663-668, doi:10.1126/science.241.4866.663.

Raup, D.M. and Sepkoski, J.J., 1982, Mass extinction in the fossil record: Science, v. 215, p. 1501–1503.

Raven, J., Caldeira, K., Elderfield, H., Hoegh- Guldberg, O., Liss, P., Riebesell, U., Shepherd, J., Turley, C., Watson, A., 2005. Ocean acidification due to increasing atmospheric carbon dioxide, Policy Doc. 12/05, 60 pp., R. Soc., London.

Raymo, M.E., Ruddiman, W.F., Froelich, P.N., 1988, Influence of late Cenozoic mountain building on ocean geochemical cycles: Geology, v. 16, p. 649– 653, doi: 10.1130/0091-7613(1988)016<0649:IOLCMB>2.3.CO;2.

Reggiani, L., Bertinelli, A., Ciarapica, G., Marcucci, M., Passeri, L., Ricci, C. & Rigo, M., 2005, Triassic-Jurassic stratigraphy of the Madonna del Sirino succession (Lagonegro basin, Southern Apennines, Italy): Bollettino Società Geologica Italiana, v. 124, p. 281–291.

Reinhardt, E.G., Blenkinsop, J. & Patterson, R.T., 1998. Assessment of a Sr isotope vital effect (87 Sr/86 Sr) in marine taxa from Lee Stocking Island, Bahamas. Geo-Marine Letters 18, 241–246.

Remane, J. 2003. Chronostratigraphic correlations: their importance for the definition of geochronologic units. Palaeogeography, Palaeoclimatology, Palaeoecology, 196 (1), 7-18.

Renne, P. R., & Basu, A. R., 1991. Rapid eruption of the Siberian Traps flood basalts at the Permo-Triassic boundary. Science, 253(5016), 176-179.

Richoz, S., Krystyn, L., Spotl, C., 2007, Towards a carbon isotope reference curve of the Upper Triassic: New Mexico Museum of Natural History and Science Bulletin, v. 41, p. 366-367.

Rigo, M. and Joachimski, M.M., 2010, Palaeoecology of Late Triassic conodonts: Constraints from oxygen isotopes in biogenic apatite: Acta Palaeontologica Polonica, v. 55, no. 3, p. 471–478.

Rigo, M., Bertinelli, A., Concheri, G., Gattolin, G., Godfrey, L., Katz, M.E., Maron, M., Muttoni, G., Sprovieri, M., Stellin, F., Zaffani, M., 2015, The Pignola-Abriola section (southern Apennines, Italy): a new GSSP candidate for the base of the Rhaetian Stage: Lethaia, doi: 10.1111/let.12145.

Rigo, M., De Zanche, V., Mietto, P., Preto, N. and Roghi, G., 2005, Biostratigraphy of the Calcari con Selce formation: Bollettino Società Geologica Italiana, v. 124, p. 293–300.

Rigo, M., Galli, M.T., Jadoul, F., 2009. Late Triassic biostratigraphic constraints in the Imagna Valley (western Bergamasc Alps, Italy). Albertiana, 37, 39-42.

Rigo, M., Preto, N., Franceschi, M. and Guaiumi, C., 2012b, Stratigraphy of the Carnian-Norian Calcari con Selce Formation in the Lagonegro Basin, Southern Apennines: Rivista Italiana di Paleontologia e Stratigrafia, v. 118, p. 143–154.

Rigo, M., Preto, N., Roghi, G., Tateo, F. & Mietto, P. 2007. A rise in the Carbonate Compensation Depth of western Tethys in the Carnian (Late Triassic): Deep-water evidence for the Carnian Pluvial Event. Palaeogeography, Palaeoclimatology, Palaeoecology, 246, 188-205.

Rigo, M., Preto, N., Roghi, G., Tateo, F. and Mietto, P., 2007, A CCD rise in the Carnian (Upper Triassic) of western Tethys, deep-water equivalent of the Carnian Pluvial Event: Palaeogeography, Palaeoclimatology, Palaeoecology, v. 246, p. 31–182.

Rigo, M., Trotter, J.A., Preto, N., Williams, I.S. 2012, Oxygen isotopic evidence for Late Triassic monsoonal upwelling in the northwestern Tethys: Geology, v. 40; no. 6, p. 515–518, DOI: 10.1130/G32792.1.

Roberts, A. A., J. G. Palacas, and I. C. Frost, 1973. Determination of organic carbon in modern carbonate sediments. J. Sediment. Res., 43, 1157–1159.

Ruhl, M., 2009. Carbon cycle changes during the Triassic-Jurassic transition. PhD thesis.

Ruhl, M., Kurschner, W.M., 2011, Multiple phases of carbon cycle disturbance from large igneous province formation at the Triassic-Jurassic transition: Geology, v. 39, p. 431-434.

Ruhl, M., Kürschner, W.M., Krystyn, L.,2009. Triassic-Jurassic organic carbon isotope stratigraphy of key sections in the western Tethys realm (Austria). Earth and Planetary Science Letters, 281 (3-4). 169-187.

Sala, O.E., Chapin, F.S., III, Armesto, J.J., Berlow, E., Bloomfield, J., Dirzo, R., Huber-Sanwald, E., Huenneke, L.F., Jackson, R.B., Kinzig, A.,Leemans, R., Lodge, D.M., Mooney, H.A., Oesterheld, M., Poff, N.L., Sykes, M.T., Walker, B.H., Walker, M., Wall, D.H., 2000. Global Biodiversity Scenarios for the Year 2100. Science, 287(5459), 1770-1774.

Saunders, A.D., Fitton, J.G., Kerr, A.C., Norry, M.J., and Kent, R.W., 1997, The North Atlantic Igneous Province. In: Mahoney, J.J., and Coffin, M.F. (eds.). Large igneous provinces: Continental, oceanic, and planetary flood volcanism. American Geophysical Union Geophysical Monograph, v. 100, p. 45–93.

Scandone, P., 1967, Studi di geologia lucana: la serie calcareo-silicomarnosa: Bollettino Società Naturalisti Napoli, v. 76, p. 1–175.

Schaller, M.F., Wright, J.D., Kent, D.V., Olsen, P.E., 2012, Rapid emplacement of the Central Atlantic Magmatic Province as a net sink for CO2: Earth and Planetary Science Letters, v. 323–324, p. 27–39.

Schaller,M.F.,Wright, J.D., Kent,D.V., 2011.Atmospheric pCO2 Perturbations Associated with the Central Atlantic Magmatic Province. Science 331 (6023), 1404–1409.

Schlager, W., 1989. Drowning unconformities on carbonate platforms. Spec. Publ.-SEPM 44, 15–25.

Schlanger, S.O. & Jenkyns, H.C. 1976. Cretaceous oceanic anoxic events: causes and consequences. Netherlands Journal of Geosciences/Geologie en Mijnbouw, 55, 179–184.

Schoene, B., Guex, J., Bartolini, A., Schaltegger, U. & Blackburn, T.J., 2010, A correlation between the Triassic-Jurassic boundary mass extinction and flood basalt eruption at the 100-ka level using ID-TIMS U/Pb zircon geochronology: Geology, v. 38, p. 387–390.

Schubert, C.J., and Nielsen, B., 2000. Effects of decarbonation treatments on d13C values in marine sediments.Mar. Chem., 72, 55–59, doi:10.1016/S0304-4203(00)00066-9.

Schuurman, W.M.L., 1979. Aspects of Late Triassic palynology. 3 Palynology of latest Triassic and earliest Jurassic deposits of the northern Limestone Alps in Austria and southern Germany, characterization of the Rhaetian stage in Europe. Review Palaeobotany, Palynology, 27, 29-54.

Self, S., Thordarson, T., Widdowson, M., 2005, Gas fluxes from flood basalt eruptions: Elements, v. 1, p. 283-287.

Sell, B., Ovtcharova, M., Guex, J., Bartolini, A., Jourdan, F., Spangenberg, J.E., Vicente, J.C., Schaltegger, U., 2014, Evaluating the temporal link between the Karoo LIP and climatic–biologic events of the Toarcian Stage with high-precision U–Pb geochronology: Earth and Planetary Science Letters, v. 408, p. 48–56.

Selli, R., 1962, Il Paleogene nel quadro della Geologia dell'Italia Meridionale: Memorie Società Geologica Italiana, v. 3, p. 737–790.

Sengor, A.M.C., Yilmaz, Y. & Sungurlu, O., 1984, Tectonics of the Mediterranean Cimmerides: nature and evolution of the western termination of Palaeo-Tethys: Geological Society, London, Special Publications, v. 17, p. 77–112.

Sephton, M.A., Amor, K., Franchi, I.A., Wignall, P.B., Newton, R., Zonneveld, J.P., 2002, Carbon and nitrogen isotope disturbances and an end-Norian (Late Triassic) extinction event: Geology, v. 30, p. 1119-1122.

Sepkoski, J.J., Jr., 1996. Competition in macroevolution: the double wedge revisited. In E*volutionary Paleobiology* (D. Jablonski, D.H. Erwin and J.H. Lipps, eds), pp. 211–255. Chicago, IL: University of Chicago Press.

Sharma, M., 1997. Siberian traps. Large igneous provinces: Continental, oceanic, and planetary flood volcanism, 273-295.

Silberling, N.J. & Tozer, E.T. 1968. Biostratigraphic classification of the marine Triassic in North America. Geological Society of America Special Papers, 110, 1-56.

Simms, M.J., 2003. Uniquely extensive seismite from the latest Triassic of the United Kingdom: Evidence for bolide impact? Geology, 31, 557-560.

Simms, M.J., Ruffell, A.H., 1989, Synchroneity of climatic change and extinctions in the Late Triassic: Geology, v. 17, p. 265–268.

Simms, M.J., Ruffell, A.H., 1990, Climatic and biotic change in the late Triassic: J. Geol. Soc. (Lond.) v. 147, p. 321–327.

Simms, M.J., Ruffell, A.H., Johnson, A.L.A., 1995, Biotic and climatic changes in the Carnian (Triassic) of Europe and adjacent areas. In: Fraser, N.C., Sues, H.D. (Eds.), In the Shadow of the Dinosaurs. Early Mesozoic Tetrapods. Cambridge Univ. Press p. 352–365.

Slavin, V.I. 1961. Stratigraphic position of the Rhaetian Stage. Sovyetskaya Geologiya, 3, 68-78.

Slavin, V.I. 1963. Au sujet du Rhétian. Bureau Recherches Geoloie et Minieres Memoir, 15, 29-32.

Speranza, F., Minelli, L., Pignatelli, A., Chiappini, M., 2012, The Ionian Sea: the oldest in situ ocean fragment of the world?: Journal of Geophysical Research, v. 117, p. B12101. 1-13., doi:10.1029/2012JB009475

Stampfli, G., Marcoux, J. & Baud, A., 1991, Tethyan margins in space and time: Palaeogeography, Palaeoclimatology, Palaeoecology, v. 87, p. 373–409.

Stampfli, G.M. & Marchant, R.H. 1995. Plate configuration and kinematics in the Alpine region. Accademia Nazionale delle Scienze, Scritti e Documenti, 14, 147-166.

Stampfli, G.M., Mosar, J., De Bono, A., Vavassis, I., 1998, Late Paleozoic, early Mesozoic plate tectonics of the western Tethys: Bullettin od the Geological Society of Greece, v. 32, p. 113-120.

Stampfli, G.M., Vavassis, I., De Bono, A., Rosselet, F., Matti, B. & Bellini, M., 2003, Remnants of the Paleotethys oceanic suture-zone in the western Tethys area: Bollettino della Società Geologica Italiana, Special Volume, no. 2, p. 1-23.

Swart, P.K., 2008, Global synchronous changes in the carbon isotopic composition of carbonate sediments unrelated to changes in the global carbon cycle: Proc. Natl. Acad. Sci., v. 105, no. 37, p. 13741–13745.

Swart, P.K., Eberli, G.P., 2005, The nature of the d13C of periplatform sediments: Implications for stratigraphy and the global carbon cycle: Sedimen Geol, v. 175, p. 115–130.

Tackett, L.S., Kaufman, A.J., Corsetti, F.A., Bottjer, D.J., 2014. Strontium isotope stratigraphy of the Gabbs Formation (Nevada): implications for global Norian–Rhaetian correlations and faunal turnover. Lethaia, 47, 500-511, DOI 10.1111/let.12075.

Tanner L.H., Ciarapica G., Reggiani L., Atudorei V., 2007, Upper Triassic carbon isotope stratigraphy of the Lagonegro Succession, Southern Apennines, Italy: New Mexico Natural History and Science Bullettin, v. 41, p. 406-410.

Tanner, L.H., 2010. The Triassic isotope record. In: Lucas, S.G. (ed.) The Triassic Timescale. Geological Society, London, special publication, 334, 103-118.

Tanner, L.H., Lucas, S.G., Chapman, M.G., 2004, Assessing the record and causes of Late Triassic extinction: Earth Sciences Reviews, v. 65, p. 103-139.

Tanner, L.H., Schiattarella, M. and Di Leo, P., 2006, Carbon isotope record of Upper Triassic strata of the Lagonegro Basin, Southern Apennines, Italy: preliminary results: Mexico Museum of Natural History and Science Bulletin, v. 37, p. 23–28.

Taylor, A.S., Lasaga, A.C., 1999, The role of basalt weathering in the Sr isotope budget of the oceans: Chemical Geology, v. 161, no. 1-3, p. 199-214, doi: 10.1016/S0009-2541(99)00087-X.

Tolan, T.L., Reidel, S.P., Beeson, M.H., Anderson, J.L., Fecht, K.R., and Swanson, D.A., 1989, Revisions to the estimates of the areal extent and volume of the Columbia River Basalt Group.

In: S. Reidel, P. and P. Hooper, R. (eds.). Volcanism and tectonism in the Columbia River flood-basalt province. Geological Society of America, Boulder, p. 1-20.

Tomshin, M.D., Okrugin, A.V., Savvinov, V.T., and Shakhot'ko, L.I., 1997. The Ebe-Khaya dike belt of trachydolerites in the north of the Siberian platform. Russian Geology and Geophysics, 38, 1511-1520.

Tozer, E.T. & Calon, T.J. 1990. Triassic ammonoids from Jabal Safra and Wadi Alwa, Oman, and their significance. Geological Society, London, Special Publications, 49 (1), 203-211.

Tozer, E.T. 1980. Latest Triassic (Upper Norian) ammonoid and Monotis faunas and correlations. Rivista Italiana di Paleontologia e Stratigrafia, 85 (3-4), 843-876.

Tozer, E.T. 1984. The Trias and its ammonoids: The evolution of a time scale. Geological Survey of Canada, Miscellaneous Rep. 35, 171 pp.

Tozer, E.T., 1967, A standard for Triassic time. Geological Survey of Canada, Bulletin, 156, 103 pp.

Trotter, A.J., Williams, S.I., Nicora, A., Mazza, M. and Rigo, M., 2015, Long-term cycles of Triassic climate change: a new d^{18}O record from conodont apatite: Earth and Planetary Science Letters, v. 415, p. 165–174.

van de Schootbrugge, B., Payne, J.L., Tomasovych, A., Pross, J., Fiebig, J., Benbrahim, M., Follmi, K.B., Quan, T.M,. 2008, Carbon cycle perturbation and stabilization in the wake of the Triassic-Jurassic boundary mass extinction event: Geochemistry Geophysics Geosystems, v. 9, p. 1-16.

van Kaam-Peters, H. M. E., S. Schouten, J. W. de Leeuw, and J. S. Sinninghe Damsté, 1997. A molecular and carbon isotope biogeochemical study of biomarkers and kerogen prolysates of the Kimmeridge Clay Facies: Palaeoenvironmental implications. Org. Geochem., 27, 399–422, doi:10.1016/S0146-6380(97)00084-3.

Veizer, J., Ala, K., Azmy, K., Bruckschen, P., Buhl, D., Bruhn, F., Carden, G.A.F., Diener, A., Ebneth, S., Godderis, Y., Jasper, T., Korte, C., Pawellek, F., Podlaha, O.G., Strauss, H., 1999, 87Sr/86Sr, δ13C and δ18O evolution of Phanerozoic seawater: Chem. Geol., v. 161, p. 59–88.

Veizer, J., Buhl, D., Diener, A., Ebneth, S., Podlaha, O.G., Bruckschen, P., Jasper, T., Korte, C., Schaaf, M., Ala, D., Azmy, K., 1997, Strontium isotope stratigraphy: potential resolution and event correlation: Paleogeogr., Paleoclimatol., Paleoecol., v. 132, p. 65–77.

Ward PD, Haggart JW, Carter ES, Wilbur D, Tipper HW, Evans T., 2001. Sudden productivity collapse associated with the Triassic-Jurassic boundary mass extinction. Science, 292, 1148-1151.

Ward, P., Garrison, G., Williford, K.. Kring, D., Goodwin, D., Beattie, M., and McRoberts, C., 2007. The organic carbon isotopic and paleontologicalrecord across the Triassic-Jurassic boundary at the candidate GSSP section at Ferguson Hill, Muller Canyon, Nevada,USA. Palaeogeography, Palaeoclimatology, Palaeoecology, 244 (1-4), 281-289.

Ward, P.D., Garrison, G.H., Haggart, J.W., Kring, D.A., Beattie, M.J., 2004, Isotopic evidence bearing on Late Triassic extinction events, Queen Charlotte Islands, British Columbia, and implications for the duration and cause of the Triassic/Jurassic mass extinction: Earth and Planetary Science Letters, v. 224, p. 589-600.

Ward, P.D., Haggart, J.W., Carter, E.S., Wilbur, D., Tipper, H.W., Evans, T., 2001. Sudden productivity collapse associated with the Triassic-Jurassic boundary mass extinction. Science, 292(5519): 1148-1151.

Whiteside, J. & Ward, P.D. 2011. Ammonoid diversity and disparity track episodes of chaotic carbon cycling during the early Mesozoic. Geology, 39, 99–102.

Whiteside, J.H., Olsen, P.E., Eglinton, T., Brookfield, M.E., and Sambrotto, R.N., 2010, Compound-specific carbon isotopes from Earth's largest flood basalt eruptions directly linked to the end-Triassic mass extinction: PNAS, v. 107, p. 6721–6725.

Wignall, P. B., & Hallam, A., 1992. Anoxia as a cause of the Permian/Triassic mass extinction: facies evidence from northern Italy and the western United States. Palaeogeography, Palaeoclimatology, Palaeoecology, 93(1), 21-46.

Wignall, P.B., 2001. Large igneous provinces and mass extinctions. Earth-Science Reviews, 53, 1–33.

Wignall, P.B., Zonneveld, J.-P., Newton, R.J., Amor, K., Sephton, M.A. & Hartley, S., 2007. The end Triassic mass extinction record of Williston Lake, British Columbia. Palaeogeogr. Palaeoclimatol. Paleoecol., 253, 385–406.

Wood, R., 1999. Reef Evolution. Oxford University Press. 414 pp.

Wotzlaw, J.F., Guex, J., Bartolini, A., Gallet, Y., Krystyn, L., McRoberts, C.A., Taylor, D., Schoene, B. & Schaltegger, U. 2014. Towards accurate numerical calibration of the Late Triassic: high precision U-Pb geochronology constraints on the duration of the Rhaetian. Geology, 42, 571–574.

Yeh, K.Y. & Cheng, Y.N. 1996. An Upper Triassic (Rhaetian) radiolarian assemblage from Busuanga Island, Philippines. Bulletin of the National Museum of Natural Science, Taiwan, 7, 1-43.

Zapfe, H. 1974. Trias in Osterreich. In: Zapfe (Ed.): The stratigraphy of the Alpine Mediterranean Triassic. Schriftenreihe der Erdwissenschaftlichen Kommission, Osterreichische Akademie der Wissenschaften, 2, 245-51.